PhD-FSTC-2018-60
The Faculty of Sciences, Technology and
Communication

Faculty of Applied Sciences
Department of Aerospace and
Mechanical Engineering

DISSERTATION

Defence held on 07/09/2018 in Luxembourg

to obtain the degree of

DOCTEUR DE L'UNIVERSITÉ DU LUXEMBOURG

EN SCIENCES DE L'INGÉNIEUR

AND

DOCTEUR DE L'UNIVERSITÉ DE LIÈGE

EN SCIENCES DE L'INGÉNIEUR

by

Hussein RAPPEL
Born on 22 August 1988 in Tabriz, Iran

MODEL AND PARAMETER IDENTIFICATION THROUGH BAYESIAN INFERENCE IN SOLID MECHANICS

Dissertation defence committee

Dr Ling WU, chairwoman
Research Scientist, Université de Liège
Guest Professor, Vrije Universiteit Brussel

Prof. Stéphane P.A. Bordas, dissertation supervisor
Professor, Université du Luxembourg

Assoc-Prof. Ludovic Noels, dissertation supervisor
Associate Professor, Université de Liège

Prof. Alan Needleman, vice-chairman
Professor, Texas A&M University

Assoc-Prof. Johan P.M. Hoefnagels
Associate Professor, Technische Universiteit Eindhoven

Dr Lars A.A. Beex
Research Scientist, Université du Luxembourg

Model and parameter identification through Bayesian inference in solid mechanics

Thesis by

Hussein Rappel

In partial fulfillment of the requirements
for the degree of

Doctor of Philosophy

University of Luxembourg
Esch-sur-Alzette, Luxembourg

and

University of Liège
Liège, Belgium

September 2018

Model and parameter identification through Bayesian inference in solid mechanics
Thesis by Hussein Rappel

In partial fulfillment of the requirements
for the degree of Doctor of Philosophy

University of Luxembourg
Esch-sur-Alzette, Luxembourg
and
University of Liège
Liège, Belgium
2018

Abstract

Predicting the behaviour of various engineering systems is commonly performed using mathematical models. These mathematical models include application-specific parameters that must be identified from measured data. The identification of model parameters usually comes with uncertainties due to model simplifications and errors in the experimental measurements. Quantifying these uncertainties can effectively improve the predictions as well as the performance of the engineering systems.

Bayesian inference provides a probabilistic framework for quantifying these uncertainties in parameter identification problems. In a Bayesian framework, the user's initial knowledge, which is represented by a probability distribution, is updated by measurement data through Bayes' theorem.

In the first two chapters of this thesis, Bayesian inference is developed for the identification of material parameters in elastoplasticity and viscoelasticity. The effect of the user's prior knowledge is systematically studied with respect to the number of measurements available. In addition, the influence of different types of experiments on the uncertainty is studied.

Since all mathematical models are simplifications of reality, uncertainties of the model itself may also be incorporated. The third chapter of this thesis presents a Bayesian framework for parameter identification in elastoplasticity in which not only the uncertainty of the experimental output is included (i.e. stress measurements), but also the uncertainty of the model and the uncertainty of the experimental input (i.e. strain). Three different formulations for describing the model uncertainty are considered: (1) a random variable which is taken from a normal distribution with constant parameters, (2) a random variable which is taken from a normal distribution with an input-dependent mean, and (3) a Gaussian random process with a stationary covariance function.

In the fourth chapter of this thesis, a Bayesian scheme is proposed to identify material parameter distributions, instead of material parameters. The application in this chapter are random fibre networks, in which the set of material parameters of each fibre is assumed to be a realisation from a material parameter distribution. The fibres behave either elastoplastically or in a perfectly brittle manner. The goal of the identification scheme is to avoid the experimentally demanding task of testing hundreds of constituents. Instead, only 20 fibres are considered.

In addition to their material randomness, the macroscale behaviours of these fibre networks are also governed by their geometrical randomness. Another question aimed to be answered in this chapter is therefore is 'how precise the material randomness needs to be identified, if the geometrical randomness will also influence the macroscale behaviour of these discrete networks'.

Acknowledgments

The research included in this thesis could not have been possible if not for the assistance, patience, and support of many individuals.

First, I would like to thank Prof. Stéphane Bordas who provided this opportunity for me to do this PhD. Throughout the whole period of my PhD Prof. Bordas supported me continuously and he was always available for any discussion, either this discussion was about scientific subjects or future career and life plans. I really appreciate the freedom that he provided for me to do my research in a way that I prefer. He has been patient throughout this PhD, allowed me to make mistakes and corrected me when I went too far off course. I am very happy to know such a humble and supportive person in my life and I know that I can trust him with all his advice as he always wants the best for me.

I am also grateful to my co-supervisor assoc-Prof. Ludovic Noels for his support, guidance, and advice throughout the research specially for the time that I was in Liège. It was so nice to see a person who is as busy as him still tries to learn all details of a new subject.

I am extremely grateful to Dr Lars Beex my daily supervisor with whom I enjoyed a lot doing my research. He accompanied me step by step throughout this PhD, giving me interesting ideas and remarks which always helped me deal with problems and find my way. I also appreciate his humbleness as well as his patience with my perfectionism. There were times that I had asked him to read my manuscript up to 30 times and he always did that without any complaints. Of course, being in contact with a person for every day has its own ups and downs and we were not exceptions. However, I am pretty sure that in any case of discussion whether we both agreed or not he wanted the best for me. I hope we still can continue our collaboration.

I would also like to thank Dr Ling Wu for fruitful discussion and comments as well as her all kind help during my stay in Liège. Furthermore, I thank her for chairing the defence. I am also grateful to Prof. Alan Needleman and assoc-Prof. Johan Hoefnagels for accepting to be my external examiners and travelling to Luxembourg.

I would also like to thank my friend and colleague Dr Paul Hauseux for all his support and help. I would like to give some special thanks to my office mates Dr Satyendra Tomar, Mr Soumianarayanan Vijayaraghavan and Mr Raphaël Bulle. Of course, without a nice and calm environment in my office I would not be able to do my research.

I owe a special note of thanks to Mrs Odile Marois, Mrs Marie Leblanc, Mrs Paula Souza, Ms Catherine Violet and the staff in "Doctoral Education" department without whom I could never do the necessary paper works throughout PhD.

I am also grateful to University of Luxembourg for their financial support of my research. Clearly, without this support I would not be able to do my research.

I also want to acknowledge the anonymous reviewer of my first manuscript on Bayesian inference "Bayesian inference for the stochastic identification of elastoplastic material parameters: Introduction, misconceptions and insights" from whose constructive comments I learnt a lot on probabilistic modelling.

Finally, I would like to extend my deepest gratitude to my parents without whose love, support and understanding I could never have completed this doctoral degree. Words are not enough to thank their sacrifices during my whole life.

Hussein Rappel
Belval, September 2018

Dedicated to my beloved parents

Contents

List of Figures

List of Tables

Glossary

Aleatory uncertainty	The natural randomness of a process, which cannot be reduced.
Conditional probability distribution	Conditional probability distribution $\pi(y\|x)$ provides the plausibility of proposition y, given proposition x.
Copula	A function that joins one dimensional marginal distributions to their joint, multivariate distribution.
Correlation	A general term for the dependence between pairs of random variables.
Correlation coefficient	A measure for the strength of the dependency between pairs of random variables.
Covariance	A measure that shows how two random variables depend on each other.
Covariance matrix	A symmetric matrix in which the off-diagonal elements are covariances of pairs of random variables and the diagonal elements are variances of random variables.
Credible interval (region)	An interval (or a region in the multivariate case) of a distribution in which it is believed the parameters lie with a certain probability.
Cumulative distribution function (CDF)	A distribution that measures the probability that a random variable is less or equal to a given value.
Dependence and independence	Two events are statistically independent if the occurrence of one has no influence on the probability of the occurrence of the other one (i.e. $\pi(x) = \pi(x\|y)$). They are dependent if the occurrence of one has an influence on the probability of the occurrence of the other one (i.e. $\pi(x) \neq \pi(x\|y)$).

Epistemic uncertainty	Uncertainty due to limited data and/or the modeller's limited knowledge about the system.
Event	A set of outcomes of an experiment.
Joint distribution	A multivariate distribution.
Laplace approximation	An approximation of a distribution with a Gaussian distribution centred at MAP.
Likelihood function	If the conditional probability distribution $\pi(y\|x)$ is regarded as a function of x for given fixed y, the function is called a likelihood function. The likelihood describes the plausibility of a parameter, given observation data.
Marginal distribution	The probability distribution of a single variable or a combination of subsets of variables in a multivariate distribution (e.g. $\pi(x)$, $\pi(y)$, $\pi(x, y)$, $\pi(x, z)$ and $\pi(y, z)$, for joint distribution $\pi(x, y, z)$). A marginal distribution is obtained by integrating a multivariate distribution over one or more (but not all) other variables.
Markov chain	A stochastic model to describe a sequence of events in which the probability of each event only depends on the previous event.
Markov chain Monte Carlo (MCMC) methods	A set of techniques to draw samples (i.e. simulate observations) from probability distributions by the construction of a Markov chain.
Maximum a posteriori probability (MAP) point	A point at which the posterior distribution is (globally) maximum.
Mean (expected value)	A measure for the central value of the underlying distribution.
Multivariate distribution	A probability distribution of two or more random variables.
Pearson correlation coefficient	The covariance of two random variables divided by the product of their standard deviations.
Point estimate	A scalar that measures a feature of a population, e.g. the mean value, the MAP point.
Population	The total set of all possible observations that can be made.

Posterior distribution (posterior)	The probability distribution that describes one's knowledge about a random variable or parameter after obtaining new measurements.
Posterior predictive distribution (PPD)	The distribution of unobserved measurements (observations), given the measured (observed) data.
Prior distribution (prior)	The probability distribution that describes one's a-priori knowledge about a random variable or parameter.
Probability	The likelihood (or plausibility) that a certain event occurs.
Probability density function (PDF)	The equation that describes a continuous probability distribution.
Probability distribution	A function that provides the probabilities of the occurrence of various possible outcomes of an experiment.
Random sample	A randomly chosen sample.
Random variable	A variable of which the value depends on the outcome of a random experiment.
Realisation	The value that a random variable takes or the outcome of an experiment after its occurrence.
Sample	A set of observations from a population with the purpose of investigating particular properties of the population.
Standard deviation	A measure for the possible deviation of a random variable from its mean. Large standard deviations indicate large possible differences; and vice versa.
Variance	The standard deviation squared.
Verification (validation) point	A measurement (observation) used to assess the quality of a prediction based on the identified parameters, that is not used for the identification itself.

More definitions on statistical concepts can be found in [3] and [4].

Chapter 1

Introduction

Mathematical models are critical to understand and make predictions about systems arising in the natural, engineering and social sciences. Mathematical models describe systems using mathematical language. They can be used to understand the behaviour of the systems at hand, make predictions and study the importance of different components of the model and of the parameters involved.

Models can therefore be seen and exercised as *descriptive* or *predictive.* In the first case, models help make sense of a large amount of (past) information and to describe underlying phenomena, e.g. the melting of ice caps based on Global positioning system (GPS) measurements. In the latter case, models are used to anticipate events, e.g. predict the weather. In this case, known variables, sometimes called *explicative* are used to explain the behaviour of unknown variables. These two uses of models are not independent, in the sense that past information is typically used to make predictions about the future.

The same mathematical model can be descriptive of a wide variety of systems. For example, the pricing of options can be described with the same model as that of underground water flow. One critical task is therefore to identify the best model and its parameters which is able to describe a system and make associated predictions.

In mechanics of materials, 'mathematical models' used at a given material point are composed of:

1. Governing equations;
2. Constitutive equations;
3. Kinematic equations;
4. Geometrical models;
5. Initial and boundary conditions.

In this thesis, we focus on mathematical models arising in the description and simulation of the mechanical behaviour of engineering materials, i.e. how stresses are related to strains. We therefore focus on constitutive equations and on the identification of the associated parameters.

The identification of material parameters is usually performed by measuring the output of a model for a given input. As illustrated in Fig. 1-1 the description of the system of interest consists of a mathematical model, an input variable (i.e. u), some output (i.e. f) and a parameter set $\mathbf{x}$.

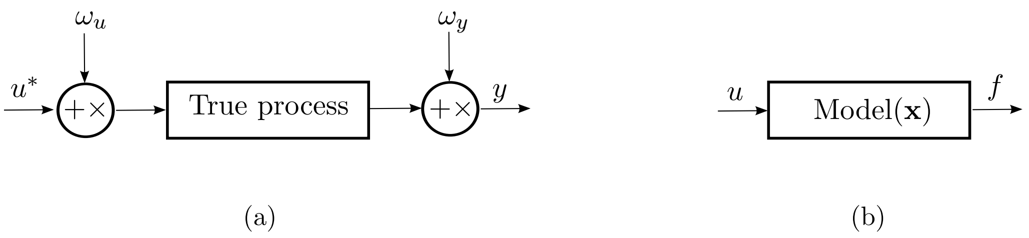

Figure 1-1: Schematic for a true process in an identification problem and its simulation [1]. Note that the input variable in the true process is not necessarily the same as that in the simulation. Furthermore, ω_u and ω_y denote realisations of error in the input and output respectively.

Mathematical models are simplifications of the true phenomena at play and predictions are thus subject to uncertainty, both because of the choice of the model and because of the identification of the associated parameters. Furthermore, experimental measurements (observations) are noisy. The ability to quantify uncertainties provides the user with the ability to assess the importance of certain parameters on quantities of interest and obtain confidence intervals or trust regions, which provides more control on the quality of the simulation outputs.

Uncertainty can be divided into *aleatory* uncertainty and *epistemic* uncertainty. Aleatory uncertainty refers to the natural uncertainty which is irreducible [5]. An example is a 'coin flipping experiment' in which the prediction of the output 'heads' or 'tails' is aleatory. Epistemic uncertainty is due to the fact that the modeller has limited knowledge on the system of interest [5]. This type of uncertainty can be divided into model uncertainty (e.g. solution approximation, modelling simplification, parameter uncertainty) and data uncertainty (e.g. measurement uncertainty). Unlike aleatory uncertainty, epistemic uncertainty is reducible. The task of a statistical identification framework is therefore to quantify these uncertainties.

A probabilistic framework with Bayesian updating gives the possibility to quantify the modelling uncertainties as well as to identify the parameters of the mathematical models. In a Bayesian framework the user's uncertainty about the parameters is represented by probability distributions. From a Bayesian perspective, these probability distributions are not real things but are chosen models, or derived from modelling assumptions, to represent the user's uncertainty about the values of quantities such as model parameters and measurement and model prediction errors. The prior choice for the probability distribution, which incorporates the user's a-priori knowledge about the unknown parameters, is updated by data through Bayes' theorem. The Bayesian inference is used in this thesis as the approach to deal with uncertainties and identification of the parameters of the constitutive equations.

1.1 Parameter identification methods in solid mechanics

1.1.1 Least squares method

We focus here on constitutive models (i.e. the material model) which are used to describe the behaviour of material points. The least squares method (LSM) [6–8] is a common tool for parameter identification. In this approach the summation of the squared differences between the model output and the experimental measurements is considered as an objective function that must be minimised with respect to the parameters in order to determine their most appropriate values. An important characteristic of this approach, which may be considered as a disadvantage, is that the error in the experimental measurements is not considered explicitly. Moreover, the identified parameter values are deterministic.

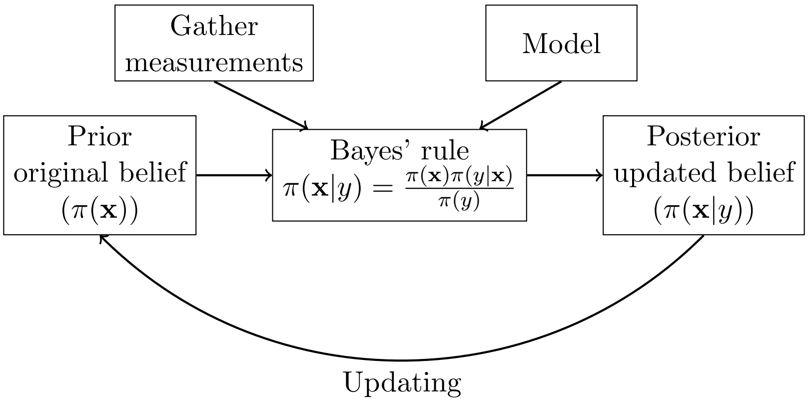

Figure 1-2: Bayesian updating scheme for data modelling. Once the measurements are collected and the model is selected, Bayes' rule is employed to update the user's uncertainty level with new information (measurements). Note that probability distribution $\pi(y|\mathbf{x})$ is the likelihood function and describes the plausibility of obtaining the measurements, given the parameter set $\mathbf{x}$.

1.1.2 Maximum likelihood estimation

Maximum likelihood estimation (MLE) is an approach which estimates the parameters of the model by maximising the likelihood function, which expresses the likelihood to observe a measurement, given parameter set $\mathbf{x}$ [9]. If the likelihood's value for parameter set $\mathbf{x}_1$ is larger than its value for parameter set $\mathbf{x}_2$, $\mathbf{x}_1$ is considered to be more plausible than $\mathbf{x}_2$. More details on likelihood functions and their construction are given in the next chapters. The outcome of MLE is also deterministic but it does explicitly account for the error in the measurements. MLE is employed in various studies for the identification of dynamical systems [10–12] and in solid mechanics [13–15].

1.1.3 Bayesian inference

Bayesian approaches are rigorous probabilistic frameworks for uncertainty quantification and parameter identification. The approaches use probability as their logic [16]. The probability distributions are employed to address uncertainty due to limited information (epistemic uncertainty) or due to inherent randomness (aleatory uncertainty). In Bayesian frameworks, the probability distribution that represents the user's initial belief (about a parameter or model) is updated with the information of the measurements according to Bayes' rule [17].

Fig. 1-2 schematically presents the workings of Bayesian updating. First, we collect the measurements and the model of which its parameters are to be identified. Second, the model and the data are incorporated in the Bayes' rule block and after constructing the likelihood function ($\pi(y|\mathbf{x})$) the prior ($\pi(\mathbf{x})$, i.e. the user's initial belief) is updated. Once the posterior ($\pi(\mathbf{x}|y)$) is obtained for the first measurement, it is used as the prior for the next measurement. Note that the prior describes the user's original belief and the updated belief is described by the posterior. Note furthermore that the definition of the likelihood function is the same as in MLE (i.e. $\pi(y|\mathbf{x})$ describes the plausibility of a measurement set, given the model parameters [18]).

The following points may be considered as some of the advantages of Bayesian inference:

(1) It provides the possibility to combine one's prior knowledge with the measurements.

(2) It provides an $n\%$ credible region in which it is believed the parameter values are present with $n\%$ certainty (where the level of probability n can be adjusted by the user) [19].

(3) Analysing hierarchical models (in which the parameters at one level depend on those at another level) in a Bayesian setting is relatively straightforward [20].

(4) LSM and MLE may result in non-unique parameter values [16]. A Bayesian framework can overcome this issue.

Some of the points of criticism on Bayesian inference are:

(1) It may be hard to define the prior [19]. Sensitivity analyses may alleviate this difficulty however [19].

(2) The resulting posterior can be heavily influenced by the prior [19].

(3) Using Bayesian inference can be computationally expensive for models with a large number of parameters.

More conceptual discussions on Bayesian inference can be found in [19–21].

1.1.4 Markov chain Monte Carlo

Once the posterior is obtained using the Bayes' formula, it can be used to generate possible parameter realisations. Except for some simplistic cases however, it is impossible to perform the corresponding analyses without numerical tools (e.g. calculating mean value, covariance matrix, i.e. a matrix that measures the correlation between the parameters, posterior predictions i.e. calculation of the new measurements based on the current measurements). These statical summaries and analyses can be approximated by drawing mutually independent samples from the posterior distribution [2]. Various types of sampling algorithms are presented in [22], but most often, as in this thesis, Markov chain Monte Carlo (MCMC) algorithms [23, 24] are employed to draw samples from the posterior distribution [25–33].

MCMC techniques were first introduced in physics [34] after the introduction of the Monte Carlo approach by Metropolis and Ulam [35]. In various statistical problems and problems related to Bayesian inference, integration over high-dimensional probability density functions (PDFs) or PDFs that are analytically not tractable needs to be performed (e.g. to determine the mean). Monte Carlo integration [36] is a numerical integration technique in which random point locations are used to integrate functions. The samples in MCMC technique are drawn from the target distribution (here posterior) by running a constructed Markov chain (i.e. a stochastic model for describing a sequence of events in which the probability of each event only depends on the previous event).

An important advantage of MCMC techniques is that they are relatively simple to implement, even if the target distribution is complex [37]. These techniques can furthermore be employed if direct sampling is not possible [38]. The MCMC approach can be slow to converge on the other hand. Difficulties in assessing the chain convergence is another disadvantage of these techniques [39]. Checking the trace plot of the drawn samples and evolution of estimators such as mean value of the approximated distribution are some common approaches of convergence assessment for the MCMC techniques [40]. Note that the chain is supposed to converge to a stationary distribution and not to a deterministic number.

1.2 Aim and novelty

This thesis has two main objectives. First, a Bayesian framework for the identification of material parameters in solid mechanics is presented (elastoplasticity and viscoelasticity are the considered material models). Bayesian inference is not new to identify parameters [41–45], but none of the existing studies consider the effect of uncertainty in the model (model error), as well as that of both the system input and output. Investigating these effects is one of the main novelties of this thesis which is presented in Chapter 4. As mentioned before in Subsection 1.1.3, an important point of criticism on Bayesian inference is the effect of the prior on the resulting posterior. This is therefore carefully studied in Chapters 2 and 3, amongst others with respect to the number of available measurements.

Second, a scheme based on Bayesian inference is presented to not identify material parameters, but to identify parameters of material parameter PDFs if only a limited number of measurements is available. The application of this identification scheme are random fibre networks in which it is assumed that the material parameters of each fibre are realisations from a single PDF. The accuracy of the identification scheme is not only investigated on its own, but also with respect to different levels of geometrical randomness that is present in fibre networks.

1.3 Outline

The outline of this thesis is as follows. In Chapter 2 a relatively gentle introduction of the framework for the identification of elastoplastic material parameters is given. In this chapter we focus on elastoplastic material models because: (1) these models are widely used in the field of solid mechanics, and (2) the class of elastoplastic material models contains both simple (linear elastic) and more complex, nonlinear C_0-continuous responses (elastoplasticity with nonlinear hardening).

Bayesian inference is employed in Chapter 3 to identify material parameters in viscoelasticity. The standard linear solid model is the material model of interest and the experiments of interests are a relaxation test, a constant strain-rate test and a creep test. The objectives of this chapter are: (1) to show the effect of the prior for viscoelasticity, (2) to show the effect of number of measurements, and (3) to show how different types of experiments influence the identified parameters and their uncertainties.

In Chapter 4 the identification of elastoplastic material parameters using Bayesian inference is presented whilst considering both the error in the input (strains) and the output (stresses), as well as the model uncertainty.

In Chapter 5 the Bayesian scheme for the identification of material parameter distributions is presented. The recovered distributions are not only directly compared to the true distributions, but also to the predicted distributions if geometrical randomness is present. Finally, conclusions as well as recommendations for future work are presented in Chapter 6.

Remark 1. *Throughout this thesis all experimental measurements are created numerically, allowing one-to-one comparisons between the true values and identified parameter values.*

Chapter 2

A tutorial on Bayesian inference to identify material parameters in solid mechanics[1]

Abstract

The aim of this chapter is to explain in a relatively easy manner how Bayesian inference can be used to identify material parameters of material models for solids. Bayesian approaches have already been used for this purpose, but most of the literature is not necessarily easy to understand for those new to the field. The reason for this is that most literature focuses either on complex statistical and machine learning concepts or on relatively complex mechanical models. In order to introduce the approach as gently as possible, we only focus on stress-strain measurements coming from uniaxial tensile tests and we only treat elastic and elastoplastic material models. Furthermore, the stress-strain measurements are created artificially in order to allow a one-to-one comparison between the true parameter values and the identified parameter values.

2.1 Introduction

The most commonly used approach to identify parameters of mechanical descriptions for solid materials is to formulate an error function that measures the difference between the model response and the experimental data [45]. This error function is then minimised with respect to the material parameters in order to determine their values. Such an approach provides a deterministic estimate of parameter values, unable to account for the unavoidable uncertainties of each parameter associated with experimental observations.

An alternative, and rather different approach is to use Bayesian inference (BI). Using Bayes' theorem, a probability density function (PDF), the so-called posterior distribution (or the posterior for short) can be formulated as a function of the material parameters of interest. Subsequently, the PDF is analysed to determine relevant summaries, such as the mean of the material parameters, the material properties at which the PDF is maximum (called the 'maximum-a-posteriori-probability' or 'MAP' point) and the covariance matrix (i.e. a matrix that measures the correlation between the parameters). The PDF can only be explored analytically for a limited number of straightforward cases. Hence, numerical methods are commonly employed,

---

[1] Reproduced from: H. Rappel, L.A.A. Beex, J.S. Hale, L. Noels and S.P.A. Bordas, A tutorial on Bayesian inference to identify material parameters in solid mechanics, ready to be submitted.

e.g. Markov chain Monte Carlo (MCMC) techniques [25, 26, 28, 29]. An alternative is to first approximate the PDF (e.g. by a Laplace approximation) and then determine the statistical summaries of the approximated distribution (e.g. mean, MAP point and covariance matrix) [43, 46].

In contrast to deterministic identification approaches, approaches using BI can quite carefully incorporate several uncertainty sources, such as the noises coming from different experimental devices, as well as a possible model uncertainty [47]. On top of that, all parameter values come with their individual uncertainty, that is also measured in terms of the parameter values. This is in contrast to conventional deterministic identification approach which come with one residual as a measure for the full set of parameters, which is obviously not expressed in terms of the parameters themselves. Additionally, BI provides an intrinsic statistical regularisation which makes inverse problems with limited observations solvable [48]. On the other hand, applying Bayes' theorem for material parameter identification does require the measurement noise to be known, i.e. the noise distributions and their parameters must be established, although they can also be treated as unknown parameters that need to be identified and hence, they appear in the posterior. The numerical techniques to analyse the posterior PDFs may furthermore need careful attention.

The developments of BI in the field of parameter identification for mechanical models started with the identification of elastic constants. Isenberg [41] proposed a Bayesian approach for the identification of elastic parameters in 1979. Various researchers subsequently used the framework to identify elastic material parameters based on dynamic responses [42–44]. Lai and Ip [49] used BI to identify the elastic properties of a thin composite plate. Daghia et al. [50] used the Bayesian framework for the dynamic identification of the elastic constants of thick laminated composite plates. Koutsourelakis [51] used Bayesian inference to identify spatially varying elastic material parameters. In 2010, Gogu et al. [45] presented an introduction in the Bayesian approach for the identification of elastic constants, and compared the results with those of a deterministic identification approach. The influence of the prior distributions was however not systematically studied. In another study, Gogu et al. [52] used a Bayesian framework to identify elastic constants in multi-directional laminates.

BI is also used for the parameter identification of nonlinear constitutive models. Muto and Beck [53] and Liu and Au [54] used the approach for parameter identification of hysteretic models, whereas Fitzenz et al. [55] used BI to identify parameters of a creep model of quartz. Most [56] used a Bayesian updating procedure for the parameter identification of an elastoplastic model without hardening (perfect plasticity). Rosić et al. [57] used linear Bayesian updating via polynomial chaos expansion for an elastoplastic system. BI is also employed for the identification of viscoelastic material parameters in [30, 58].

Another study that uses Bayes' theorem to identify material parameters is the work of Nichols et al. [59]. They employed a Bayesian approach to identify the nonlinear stiffness of a dynamic system. Furthermore, Nichols et al. [59] used the method to find the location, size and depth of delamination in a composite beam. Abhinav and Manohar [60] used BI to characterise the dynamic parameters of a structural system with geometrical nonlinearities. The approach is also employed to assess the quality of different models with respect to measured data (i.e. model selection): e.g. hyperelastic constitutive models for soft tissue [61], phenomenological models for tumour growth [62], models for damage progression in composites due to fatigue [63] and fatigue models for metals [64]. Sarkar et al. [40] used the Bayesian method to identify thermodynamical parameters of cementitious materials. BI is also used in the fields of heat transfer and fluid mechanics for inverse problems [26, 65].

Bayesian inversion relies on concepts that may be complex to grasp for those who are only familiar with deterministic inversion methods. The primary objective of this chapter is to show

how Bayesian inference can be applied for the stochastic identification of material parameters. We focus on elastoplastic material models in this chapter for two reasons: (1) they are widely used in the field of mechanics, and (2) the family of elastoplastic material models contains both simple (linear elasticity) and more complex, nonlinear, C_0-continuous responses (linear elasticity-nonlinear hardening) to describe material behaviour. This chapter focuses on results of uniaxial tensile tests in order to be as straightforward as possible. In addition to introducing the general idea of identification approaches based on BI as gently as possible (to our abilities), we also discuss some enhancements, such as not only incorporating the error in the stress, but also incorporating the error in the strain and the uncertainty of the model. Those enhancements are not discussed in much detail, but references to other works are included.

The structure of this chapter is as follows. Section 2.2 briefly discusses the employed material models in this chapter. Section 2.3 discusses the theoretical fundaments behind Bayes' theorem. Furthermore, this section describes a Bayesian approach for the stochastic identification of elastoplastic material parameters, when only the stress measurements include stochastic errors. In Section 2.4, MCMC methods as the numerical techniques to analyse the posterior distribution are explained. In this section, we also explain the posterior predictive distribution (PPD) as an approach for predicting unobserved measurements. In Section 2.5, a considerable number of results are presented. In Section 2.6, some advanced concepts, such as incorporating the error in the strain and the model uncertainty, are discussed. We also briefly discuss how the approach differs if a viscoelastic material model is used instead. In Section 2.7, conclusions are finally presented.

Remark 2. *As mentioned before, we consider stress-strain data coming from uniaxial tensile tests in this chapter. As the force is measured in tensile tests, the measured stress and its error is assumed to be proportional to the measured force and its error (the parameters of its distribution are to be identified using separate calibration experiments). Strain measurements are commonly based either on the clamp displacement or determined using digital image correlation (DIC). In both cases, the parameters of the error distribution of the strain can be determined using calibration experiments.*

Remark 3. *Throughout this chapter bold letters and symbols denote vectors and matrices. Furthermore, capital letters denote random variables.*

2.2 Material models

In this chapter, BI is developed to identify the parameters of four one-dimensional material models: linear elasticity, linear elasticity with perfect plasticity, linear elasticity with linear hardening and linear elasticity with nonlinear hardening. Hardening is considered to be isotropic and associative. For each model, the identification is based on the results of monotonic uniaxial tensile tests. Below, material responses are given for monotonic tensile loading.

2.2.1 Linear elasticity

The linear elastic model assumes a linear relationship between the stress and the strains. In the one dimensional case, this writes:

$$\sigma(\epsilon, \mathbf{x}) = E\epsilon, \tag{2.1}$$

where σ is the stress, ϵ is the strain, $\mathbf{x}$ is the material parameter vector (here $\mathbf{x} = E$) and E is Young's modulus and assumed to be constant in the domain.

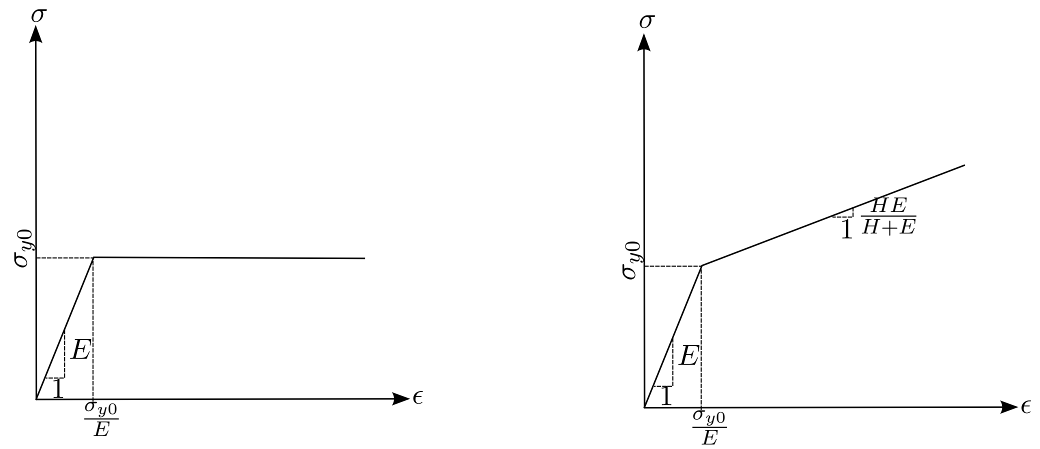

(a) (b)

Figure 2-1: The stress-strain response of (a) linear elastic-perfectly plastic model and (b) linear elastic-linear hardening model during monotonic tension.

2.2.2 Linear elasticity-perfect plasticity

The linear elastic-perfectly plastic model neglects the effect of work hardening, assuming that purely plastic deformation occurs when the stress reaches its yield value. The total strain (ϵ) in this chapter is additively split into an elastic part ϵ_e and a plastic part ϵ_p:

$$\epsilon = \epsilon_e + \epsilon_p, \tag{2.2}$$

and the stress is defined as a function of the elastic strain, ϵ_e:

$$\sigma(\epsilon, \mathbf{x}) = E\epsilon_e = E(\epsilon - \epsilon_p). \tag{2.3}$$

The yield condition at which plastic yielding occurs, is written as:

$$f(\sigma) = |\sigma| - \sigma_{y0} \leq 0, \tag{2.4}$$

where σ_{y0} is the initial yield stress and f is the yield function. Consequently, $\mathbf{x} = \begin{bmatrix} E & \sigma_{y0} \end{bmatrix}^T$.

Furthermore, the flow rule for the plastic strain can be written as:

$$\dot{\epsilon}_p = \dot{\alpha}\frac{\partial f}{\partial \sigma}, \tag{2.5}$$

where α denotes the cumulative plastic strain. Finally, the Kuhn-Tucker conditions [66] must hold:

$$\dot{\alpha} \geq 0, \quad f(\sigma) \leq 0, \quad \dot{\alpha} f(\sigma) = 0. \tag{2.6}$$

The stress-strain response of the linear elastic-perfectly plastic model during monotonic tension can be written as:

$$\sigma(\epsilon, \mathbf{x}) = \begin{cases} E\epsilon & \text{if } \epsilon \leq \frac{\sigma_{y0}}{E} \\ \sigma_{y0} & \text{if } \epsilon > \frac{\sigma_{y0}}{E} \end{cases}. \tag{2.7}$$

Using the Heaviside step function ($h(\cdot)$), Eq. (2.7) can be conveniently expressed as:

$$\sigma(\epsilon, \mathbf{x}) = E\epsilon\bigg(1 - h\Big(\epsilon - \frac{\sigma_{y0}}{E}\Big)\bigg) + \sigma_{y0} h\Big(\epsilon - \frac{\sigma_{y0}}{E}\Big), \tag{2.8}$$

Fig. 2-1(a) presents this response graphically.

2.2.3 Linear elasticity-linear hardening

The linear elastic-linear hardening model is identical to the linear elastic-perfectly plastic model, except for the yield function, which writes:

$$f(\sigma) = |\sigma| - \sigma_{y0} - H\alpha \leq 0, \tag{2.9}$$

where H is the plastic modulus. Hence, $\mathbf{x} = \begin{bmatrix} E & \sigma_{y0} & H \end{bmatrix}^T$.

Consequently, the stress-strain response of the model during monotonic tension writes:

$$\sigma(\epsilon, \mathbf{x}) = \begin{cases} E\epsilon & \text{if } \epsilon \leq \frac{\sigma_{y0}}{E} \\ \sigma_{y0} + H\epsilon_p & \text{if } \epsilon > \frac{\sigma_{y0}}{E} \end{cases}, \tag{2.10}$$

which can again be expressed using the Heaviside step function:

$$\sigma(\epsilon, \mathbf{x}) = E\epsilon\Big(1 - h\Big(\epsilon - \frac{\sigma_{y0}}{E}\Big)\Big) + \Big(\sigma_{y0} + \frac{HE}{H+E}\Big(\epsilon - \frac{\sigma_{y0}}{E}\Big)\Big)h\Big(\epsilon - \frac{\sigma_{y0}}{E}\Big). \tag{2.11}$$

Fig. 2-1(b) shows this response graphically.

2.2.4 Linear elasticity-nonlinear hardening

The linear elastic-nonlinear hardening model also only differs from the linear elastic-perfectly plastic model through the yield function, which writes:

$$f(\sigma) = |\sigma| - \sigma_{y0} - H\alpha^n \leq 0, \tag{2.12}$$

where n is an additional plastic material parameter and hence, $\mathbf{x} = \begin{bmatrix} E & \sigma_{y0} & H & n \end{bmatrix}^T$.

For monotonic uniaxial tension, the stress-strain response can be written as:

$$\sigma(\epsilon, \mathbf{x}) = \begin{cases} E\epsilon & \text{if } \epsilon \leq \frac{\sigma_{y0}}{E} \\ \sigma_{y0} + H\epsilon_p^n & \text{if } \epsilon > \frac{\sigma_{y0}}{E} \end{cases}, \tag{2.13}$$

or using the Heaviside step function:

$$\sigma(\epsilon, \mathbf{x}) = E\epsilon\Big(1 - h\Big(\epsilon - \frac{\sigma_{y0}}{E}\Big)\Big) + \Big(\sigma_{y0} + H\Big(\epsilon - \frac{\sigma(\epsilon, \mathbf{x})}{E}\Big)^n\Big)h\Big(\epsilon - \frac{\sigma_{y0}}{E}\Big). \tag{2.14}$$

Fig. 2-2 shows this stress-strain response.

It is important to note that Eq. (2.14) is an implicit function of the stress ($\sigma(\epsilon, \mathbf{x})$ appears both on the left hand side and right hand side of Eq. (2.14) and cannot analytically be determined if ϵ is known). This is in contrast to the stress-strain expressions of the previous material models for monotonic tension (Eqs. (2.1), (2.8) and (2.11)), which are all explicit functions (i.e. $\sigma(\epsilon, \mathbf{x})$ can analytically be computed when one has ϵ).

2.3 Bayesian inference

2.3.1 Concepts

We start by considering random events A and B, and the discrete probabilities of each event: $\mathrm{P}(a)$ and $\mathrm{P}(b)$. The probability that events A and B both occur, is given by the joint probability,

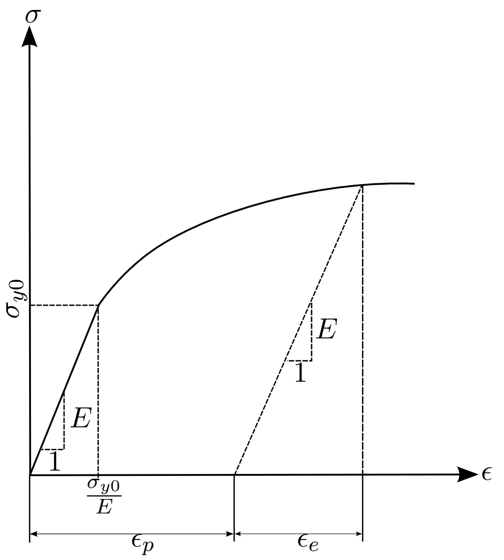

Figure 2-2: The stress-strain response of the linear elastic-nonlinear hardening model during monotonic tension.

$\mathrm{P}(a, b)$, which can be expanded as:

$$\mathrm{P}(a, b) = \mathrm{P}(a|b)\mathrm{P}(b) = \mathrm{P}(b|a)\mathrm{P}(a), \tag{2.15}$$

where $\mathrm{P}(a|b)$ and $\mathrm{P}(b|a)$ are conditional probabilities. Conditional probability $\mathrm{P}(a|b)$ expresses the probability that event A occurs, if it is certain that event B occurs. Using Eq. (2.15), the simplest form of Bayes' theorem can be written as:

$$\mathrm{P}(a|b) = \frac{\mathrm{P}(a)\mathrm{P}(b|a)}{\mathrm{P}(b)}. \tag{2.16}$$

If one regards two continuous random variables $\mathbf{X} \in \mathbb{R}^{n_p}$ and $\mathbf{Y} \in \mathbb{R}^{n_m}$, instead of discrete variables, where $\mathbf{X}$ is a random vector with n_p unknown parameters and $\mathbf{Y}$ a random vector with n_m measurements, Eq. (2.16) can be rewritten in terms of the following probability distribution functions (where π denotes a PDF):

$$\pi(\mathbf{x}|\mathbf{y}) = \frac{\pi(\mathbf{x})\pi(\mathbf{y}|\mathbf{x})}{\pi(\mathbf{y})}, \tag{2.17}$$

where $\pi(\mathbf{x})$, $\pi(\mathbf{y}|\mathbf{x})$ and $\pi(\mathbf{x}|\mathbf{y})$ are referred to as the prior distribution (i.e. the PDF that includes one's prior knowledge), the likelihood function (i.e. the PDF of the observed data $\mathbf{y}$, given unknown parameters $\mathbf{x}$) and the posterior distribution (i.e. the PDF of the unknown parameters $\mathbf{x}$, given the observations $\mathbf{y}$), respectively.

Using the law of total probabilities [67] which relates the marginal probabilities ($\pi(\mathbf{x})$ and $\pi(\mathbf{y})$) to the conditional probabilities ($\pi(\mathbf{y}|\mathbf{x})$), the denominator in Eq. (2.17) can be written as:

$$\pi(\mathbf{y}) = \int_{\mathbb{R}^{n_p}} \pi(\mathbf{x})\pi(\mathbf{y}|\mathbf{x})d\mathbf{x}. \tag{2.18}$$

Since the data ($\mathbf{y}$) is already measured, the denominator in Eq. (2.17) is a constant number, $C \in \mathbb{R}^{+}$. This constant number can be regarded as a normalisation factor that ensures that the integral of the posterior ($\pi(\mathbf{x}|\mathbf{y})$) equals 1:

$$\pi(\mathbf{x}|\mathbf{y}) = \frac{1}{C}\pi(\mathbf{x})\pi(\mathbf{y}|\mathbf{x}). \tag{2.19}$$

Hence, one can rewrite Eq. (2.19) as:

$$\pi(\mathbf{x}|\mathbf{y}) \propto \pi(\mathbf{x})\pi(\mathbf{y}|\mathbf{x}). \tag{2.20}$$

Note that the statistical summaries of the posterior distribution (i.e. the mean, the MAP point and the covariance matrix) do not depend on the absolute posterior, but only on its shape.

In order to obtain the posterior in Eq. (2.20) (i.e. the PDF of the vector of unknown parameters, given the observations $\pi(\mathbf{x}|\mathbf{y})$), the likelihood function ($\pi(\mathbf{y}|\mathbf{x})$) and the prior ($\pi(\mathbf{x})$) need to be formulated. First, the likelihood function is considered.

In order to construct the likelihood function, a noise model has to be formulated and a noise distribution (π_{noise}) has to be determined. For the moment, we assume that the noise distribution is known (including its parameters). The noise model used in this chapter is additive, which is frequently employed, amongst others in [48, 50]. The additive noise model can be written as follows:

$$\mathbf{Y} = \mathbf{f}(\mathbf{X}) + \boldsymbol{\Omega}, \tag{2.21}$$

where $\mathbf{X} \in \mathbb{R}^{n_p}$ denotes again the vector with the unknown material parameters, $\mathbf{Y} \in \mathbb{R}^{n_m}$ the vector with the measured data and $\boldsymbol{\Omega} \in \mathbb{R}^{n_m}$ the noise vector. $\mathbf{f} : \mathbb{R}^{n_p} \to \mathbb{R}^{n_m}$ denotes the material description and is a function of the unknown material parameters ($\mathbf{X}$). Given the realisations $\mathbf{X} = \mathbf{x}$ and $\boldsymbol{\Omega} = \boldsymbol{\omega}$, and assuming that the parameters ($\mathbf{X}$) and the error ($\boldsymbol{\Omega}$) are statistically independent, the likelihood function reads:

$$\pi(\mathbf{y}|\mathbf{x}) = \pi_{\text{noise}}(\mathbf{y} - \mathbf{f}(\mathbf{x})), \tag{2.22}$$

where $\pi_{\text{noise}}(\boldsymbol{\omega})$ is the PDF of the noise (which is assumed to be identified based on separate calibration experiments, see Subsection 2.5.1). Substitution of Eq. (2.22) in Eq. (2.20) yields:

$$\pi(\mathbf{x}|\mathbf{y}) \propto \pi(\mathbf{x})\pi_{\text{noise}}(\mathbf{y} - \mathbf{f}(\mathbf{x})). \tag{2.23}$$

A critical aspect of the Bayesian framework is the selection of the prior distribution ($\pi(\mathbf{x})$) [48] in which *a-priori* knowledge about the parameters is translated in terms of a PDF. The influence of the prior distribution diminishes if the number of observation increases [17], which is considered in more detail in Section 2.5.

Once the posterior is formulated (Eq. (2.23)), the mean parameter values, MAP parameter values and the covariance matrix can be extracted from it. We will use Markov chain Monte Carlo methods for this, since they are the most commonly employed approaches to do so. These techniques are discussed in Subsection 2.4.1. Only for linear elasticity, we analytically analyse the posterior.

Remark 4. *The parameters of the noise distribution can also be treated as unknown parameters that need to be identified. In that case, they appear as variables in the posterior, together with the material parameters. For tensile testers in well-controlled environments however, it is fair to say that the noise distribution and its parameters can be identified using a separate calibration process (see Subsection 2.5.1).*

2.3.2 Application to the material responses during monotonic uniaxial tension

In this subsection, we apply the aforementioned Bayesian framework to the four material responses during monotonic uniaxial tension. Effectively, this means that we replace model $\mathbf{f}(\mathbf{x})$

in Eqs. (2.21) and (2.23) by the four material responses $\sigma(\epsilon, \mathbf{x})$. We will see that the resulting posterior distribution for linear elasticity can be analysed analytically, but the posteriors for the other three material descriptions need to be analysed numerically. The reasons for this is two-fold. First, the other three responses are only C_0-continuous. Second, the linear elastic-nonlinear hardening description is an implicit relation.

Linear elasticity

The only unknown material parameter in the linear elastic model is the Young's modulus (E). Based on Section 2.3, the additive noise model for *a single stress measurement* can be written as follows:

$$Y = E\epsilon + \Omega, \tag{2.24}$$

where Y is the measured stress and Ω is the random variable representing the noise in the stress measurement. We consider the noise distribution to be normal and hence, it can be written as:

$$\pi_{\text{noise}}(\omega) = \frac{1}{\sqrt{2\pi} s_{\text{noise}}} \exp\Big(- \frac{\omega^2}{2 s_{\text{noise}}^2} \Big). \tag{2.25}$$

Using Eq. (2.22), the likelihood function can now be expressed as:

$$\pi(y|E) = \pi_{\text{noise}}(y - E\epsilon) = \frac{1}{\sqrt{2\pi} s_{\text{noise}}} \exp\Big(- \frac{(y - E\epsilon)^2}{2 s_{\text{noise}}^2} \Big). \tag{2.26}$$

Substitution of Eq. (2.26) in Eq. (2.23) then yields the following expression for the posterior:

$$\pi(E|y) \propto \pi(E) \exp\Big(- \frac{(y - E\epsilon)^2}{2 s_{\text{noise}}^2} \Big). \tag{2.27}$$

If we use a prior in the form of a modified normal distribution as follows:

$$\pi(E) \propto \begin{cases} \exp\Big(- \frac{(E - \overline{E})^2}{2 s_E^2} \Big) & \text{if } E \geq 0 \\ 0 & \text{otherwise} \end{cases}, \tag{2.28}$$

the posterior distribution reads:

$$\pi(E|y) \propto \begin{cases} \exp\Big(- \Big[\frac{(E - \overline{E})^2}{2 s_E^2} + \frac{(y - E\epsilon)^2}{2 s_{\text{noise}}^2} \Big] \Big) & \text{if } E \geq 0 \\ 0 & \text{otherwise} \end{cases}, \tag{2.29}$$

where $\overline{E}$ and s_E are the mean and standard deviation of the prior distribution, respectively. Note that the Young's modulus cannot be negative for an actual material, which is taken into account in the prior distribution (Eq. (2.28)).

If we now consider the posterior distribution of the previous measurement to be the prior distribution of the current measurement, the posterior for all n_m measurements can be expressed as:

$$\pi(E|\mathbf{y}) \propto \exp\Big(- \Big[\frac{(E - \overline{E})^2}{2 s_E^2} + \frac{\sum_{i=1}^{n_m} (y_i - E\epsilon_i)^2}{2 s_{\text{noise}}^2} \Big] \Big), \quad E \geq 0, \tag{2.30}$$

where $\pi(E|\mathbf{y}) = \pi(E|y_1, \cdots, y_{n_m})$. Eq. (2.30) can now be written in the following form:

$$\pi(E|\mathbf{y}) \propto \exp\Big(- \frac{(E - \overline{E}_{\text{post}})^2}{2 s_{\text{post}}^2} \Big), \quad E \geq 0, \tag{2.31}$$

where $\overline{E}_{\text{post}}$ and s_{post} are the mean and standard deviation of the posterior distribution, which is again a normal distribution (with the condition $E \geq 0$). Both can be expressed as:

$$\overline{E}_{\text{post}} = \frac{s^2_{\text{noise}}\overline{E}+s^2_E \sum\limits_{i=1}^{n_m} \epsilon_i y_i}{s^2_{\text{noise}}+s^2_E \sum\limits_{i=1}^{n_m} \epsilon_i^2}, \quad s_{\text{post}} = \sqrt{\frac{s^2_{\text{noise}} s^2_E}{s^2_{\text{noise}}+s^2_E \sum\limits_{i=1}^{n_m} \epsilon_i^2}}. \tag{2.32}$$

Hence, it is possible to analytically examine the posterior distribution for linear elasticity if the noise model is additive and the noise distribution as well as the prior distribution are (modified) normal distributions. For the other cases below, we use numerical techniques.

Linear elasticity-perfect plasticity

The parameters to be identified for the linear elastic-perfectly plastic model are the Young's modulus and the initial yield stress, which are stored in the parameter vector $\mathbf{x} = \begin{bmatrix} E & \sigma_{y0} \end{bmatrix}^T$. Since we consider the same experimental equipment and conditions as in the case of linear elasticity (i.e. the measured stresses are still polluted by noise stemming from the same normal distribution and the measured strains are still exact), the same additive noise model applies:

$$Y = \sigma(\epsilon, \mathbf{x}) + \Omega, \tag{2.33}$$

where $\sigma(\epsilon, \mathbf{x})$ is referred to as the theoretical stress and is expressed in Eq. (2.8). Using Eq. (2.25) for the noise distribution, the likelihood function for a single stress measurement reads:

$$\pi(y|\mathbf{x}) = \pi_{\text{noise}}(y - \sigma(\epsilon, \mathbf{x})) = \frac{1}{\sqrt{2\pi} s_{\text{noise}}} \exp\Big(- \frac{(y - \sigma(\epsilon, \mathbf{x}))^2}{2 s^2_{\text{noise}}} \Big), \tag{2.34}$$

or:

$$\pi(y|\mathbf{x}) = \frac{1}{\sqrt{2\pi} s_{\text{noise}}} \exp\left(- \frac{\left(y - E\epsilon\left(1 - h\left(\epsilon - \frac{\sigma_{y0}}{E}\right)\right) - \sigma_{y0} h\left(\epsilon - \frac{\sigma_{y0}}{E}\right)\right)^2}{2 s^2_{\text{noise}}} \right). \tag{2.35}$$

Taking the physical constraints into account that the Young's modulus and the initial yield stress must be nonnegative, the following prior distribution is selected:

$$\pi(\mathbf{x}) \propto \begin{cases} \exp\Big(- \frac{(\mathbf{x}-\overline{\mathbf{x}})^T \mathbf{\Gamma}_{\mathbf{x}}^{-1} (\mathbf{x}-\overline{\mathbf{x}})}{2} \Big) & \text{if } E \geq 0 \text{ and } \sigma_{y0} \geq 0 \\ 0 & \text{otherwise} \end{cases}, \tag{2.36}$$

where $\overline{\mathbf{x}}$ is the mean value vector of the prior distribution and $\mathbf{\Gamma}_{\mathbf{x}}$ is the covariance matrix of the prior. Substitution of Eq. (2.33) and Eq. (2.34) in the reduced variant of Bayes' formula of Eq. (2.23), yields the following posterior distribution for n_m measurements:

$$\pi(\mathbf{x}|\mathbf{y}) \propto \exp\left(- \left[\frac{(\mathbf{x} - \overline{\mathbf{x}})^T \mathbf{\Gamma}_{\mathbf{x}}^{-1} (\mathbf{x} - \overline{\mathbf{x}})}{2} + \frac{\sum\limits_{i=1}^{n_m} \left(y_i - E\epsilon_i \left(1 - h\left(\epsilon_i - \frac{\sigma_{y0}}{E}\right)\right) - \sigma_{y0} h\left(\epsilon_i - \frac{\sigma_{y0}}{E}\right)\right)^2}{2 s^2_{\text{noise}}} \right] \right). \tag{2.37}$$

We again note that the probability of obtaining a negative Young's modulus and yield stress is zero thanks to the selected prior distribution.

It is important to realise that the presence of the Heaviside function in the posterior entails that the posterior cannot be analysed analytically. Hence, the adaptive MCMC approach is employed to analyse the posterior for in Section 2.5.

Linear elasticity-linear hardening

The parameter vector for the linear elastic-linear hardening model reads $\mathbf{x} = \begin{bmatrix} E & \sigma_{y0} & H \end{bmatrix}^T$. Assuming again the same experimental equipment and conditions (and hence, the same noise model and noise distribution), the likelihood function for a single measurement reads:

$$\pi(y|\mathbf{x}) \propto \exp\Bigg(- \frac{\Big(y - E\epsilon\Big(1 - h\Big(\epsilon - \frac{\sigma_{y0}}{E}\Big)\Big) - \Big(\sigma_{y0} + \frac{HE}{H+E}\Big(\epsilon - \frac{\sigma_{y0}}{E}\Big)\Big) h\Big(\epsilon - \frac{\sigma_{y0}}{E}\Big)\Big)^2}{2s_{\text{noise}}^2} \Bigg). \tag{2.38}$$

In addition to the physical constraints for the Young's modulus and the initial yield stress, we also use that plastic modulus H must be nonnegative. The following prior distribution is therefore selected:

$$\pi(\mathbf{x}) \propto \begin{cases} \exp\Big(- \frac{(\mathbf{x}-\overline{\mathbf{x}})^T \mathbf{\Gamma}_{\mathbf{x}}^{-1} (\mathbf{x}-\overline{\mathbf{x}})}{2} \Big) & \text{if } E \geq 0 \text{ and } \sigma_{y0} \geq 0 \text{ and } H \geq 0 \\ 0 & \text{otherwise} \end{cases}. \tag{2.39}$$

Using Bayes' formula, the posterior distribution for n_m measurements reads:

$$\pi(\mathbf{x}|\mathbf{y}) \propto \exp\Bigg(- \Bigg[\frac{(\mathbf{x}-\overline{\mathbf{x}})^T \mathbf{\Gamma}_{\mathbf{x}}^{-1} (\mathbf{x}-\overline{\mathbf{x}})}{2} + \\ \frac{\sum_{i=1}^{n_m} \Big(y_i - E\epsilon_i\Big(1 - h\Big(\epsilon_i - \frac{\sigma_{y0}}{E}\Big)\Big) - \Big(\sigma_{y0} + \frac{HE}{H+E}\Big(\epsilon_i - \frac{\sigma_{y0}}{E}\Big)\Big) h\Big(\epsilon_i - \frac{\sigma_{y0}}{E}\Big)\Big)^2}{2s_{\text{noise}}^2} \Bigg] \Bigg). \tag{2.40}$$

Linear elasticity-nonlinear hardening

The parameter vector for the linear elastic-nonlinear hardening material description is $\mathbf{x} = \begin{bmatrix} E & \sigma_{y0} & H & n \end{bmatrix}^T$. Considering no change of experimental equipment (and hence, the same noise model and noise distribution), the expression for the measured stress again reads as Eq. (2.33), where $\sigma(\epsilon, \mathbf{x})$ is given by Eq. (2.14). It is important to note that in contrast to the previous cases, theoretical stress $\sigma(\epsilon, \mathbf{x})$ is not a closed form expression (see Eq. (2.14)). The likelihood function for a single measurement is:

$$\pi(y|\mathbf{x}) \propto \exp\Big(- \frac{(y - \sigma(\epsilon, \mathbf{x}))^2}{2s_{\text{noise}}^2} \Big), \tag{2.41}$$

where $\sigma(\epsilon, \mathbf{x})$ is numerically determined by solving Eq. (2.14). Choosing the prior distribution in the form of a modified normal distribution as:

$$\pi(\mathbf{x}) \propto \begin{cases} \exp\Big(- \frac{(\mathbf{x}-\overline{\mathbf{x}})^T \mathbf{\Gamma}_{\mathbf{x}}^{-1} (\mathbf{x}-\overline{\mathbf{x}})}{2} \Big) & \text{if } E \geq 0 \text{ and } \sigma_{y0} \geq 0 \text{ and } H \geq 0 \text{ and } n \geq 0 \\ 0 & \text{otherwise} \end{cases}, \tag{2.42}$$

and employing the Bayes' theorem, the posterior distribution for n_m measurements reads:

$$\pi(\mathbf{x}|\mathbf{y}) \propto \exp\left(- \left[\frac{(\mathbf{x} - \overline{\mathbf{x}})^T \mathbf{\Gamma}_{\mathbf{x}}^{-1} (\mathbf{x} - \overline{\mathbf{x}})}{2} + \frac{\sum\limits_{i=1}^{n_m} (y_i - \sigma(\epsilon_i, \mathbf{x}))^2}{2s_{\text{noise}}^2} \right] \right). \tag{2.43}$$

2.4 Numerical procedures

2.4.1 Markov chain Monte Carlo method (MCMC)

Once the posterior is constructed, it needs to be analysed to determine the statistical summaries. For the aforementioned case of linear elasticity, the statistical summaries were established analytically, but for the other cases we need to determine them numerically because they are only C_0-continuous. We will use a Markov chain Monte Carlo (MCMC) technique for this.

MCMC techniques are frequently employed, derivative-free numerical approaches to investigate posteriors [68–70]. They draw samples from the posterior to do so. Below, the fundamental concepts of the Monte Carlo method are discussed, as well as the adaptive Metropolis algorithm to perform the sampling.

Monte Carlo method

The main purpose of the Monte Carlo method is to approximate integrals of the following form:

$$\mathbf{I} = \int_{\mathbb{R}^{n_p}} \mathbf{g}(\mathbf{x}) \pi(\mathbf{x}) d\mathbf{x}, \tag{2.44}$$

where π is the PDF of interest (in our case the posterior) and $\mathbf{g} : \mathbb{R}^{n_p} \to \mathbb{R}^{n_g}$ is an integrable function over $\mathbb{R}^{n_p}$. This integral can be approximated using the following quadrature:

$$\hat{\mathbf{I}} = \frac{1}{n_s} \sum_{i=1}^{n_s} \mathbf{g}(\mathbf{x}_i), \tag{2.45}$$

where $\{\mathbf{x}_i\}_i^{n_s}$ is the set of samples drawn from the PDF of interest (π) and the hat on $\hat{\mathbf{I}}$ represents the numerically approximated equivalent of $\mathbf{I}$. The drawing of samples from π implies that most of the samples are in the domain in which numerical evaluations of π are nonzero. Note that $\hat{\mathbf{I}}$ converges according to [71]:

$$\lim_{n_s \to +\infty} \frac{1}{n_s} \sum_{i=1}^{n_s} \mathbf{g}(\mathbf{x}_i) = \mathbf{I}. \tag{2.46}$$

The numerical approximation of the components of the covariance matrix for $\mathbf{g}(\mathbf{x})$ ($\widehat{\mathbf{\Gamma}}_{\mathbf{g}}$) is [24]:

$$(\widehat{\Gamma}_{\mathbf{g}})_{jk} = \frac{1}{n_s - 1} \sum_{i=1}^{n_s} \Big(g_j(\mathbf{x}_i) - I_j \Big) \Big((g_k(\mathbf{x}_i) - I_k \Big), \; j = 1, 2, \cdots, n_g, \; k = 1, 2, \cdots, n_g. \tag{2.47}$$

The mean of the posterior ($\overline{\mathbf{x}}_{\text{post}}$) can be computed by substituting $\mathbf{g}(\mathbf{x}) = \mathbf{x}$ and $\pi = \pi_{\text{post}}$ in Eq. (2.44), which yields:

$$\overline{\mathbf{x}}_{\text{post}} = \int_{\mathbb{R}^{n_p}} \mathbf{x} \, \pi_{\text{post}}(\mathbf{x}) d\mathbf{x} = \lim_{n_s \to +\infty} \frac{1}{n_s} \sum_{i=1}^{n_s} \mathbf{x}_i. \tag{2.48}$$

Furthermore, the components of the posterior's covariance matrix are approximated as follows:

$$(\widehat{\Gamma}_{\text{post}})_{jk} = \frac{1}{n_s - 1} \sum_{i=1}^{n_s} \Big((x_i)_j - (\overline{x}_{\text{post}})_j \Big) \Big((x_i)_k - (\overline{x}_{\text{post}})_k \Big), \ j = 1, 2, \cdots, n_p, \ k = 1, 2, \cdots, n_p. \tag{2.49}$$

If we assume that a large number of samples is taken (i.e. n_s is large), the MAP point can furthermore be approximated as [71]:

$$\widehat{\mathbf{MAP}} = \underset{\mathbf{x}_{i; i=1,\dots,n_s}}{\operatorname{argmax}} \, \pi(\mathbf{x}_i). \tag{2.50}$$

The essential part of a Monte Carlo procedure is the drawing of admissible samples ($\mathbf{x}_i$). Below, the standard and adaptive Metropolis algorithms are discussed as means to draw samples. The adaptive one is the algorithm used in Section 2.5.

The standard Metropolis-Hastings and the adaptive Metropolis algorithms

The standard Metropolis-Hastings approach is a frequently employed MCMC algorithm [71]. The basic idea of the Metropolis-Hastings algorithm is to explore the PDF of interest by making a random walk across the parameter space $\mathbf{x}$. Considering sample $\mathbf{x}_i$ and its evaluation of the PDF, $\pi(\mathbf{x}_i)$, new sample $\mathbf{x}_p$ is proposed by drawing from a proposal distribution (q in Algorithm 2.1). If the PDF evaluated at the proposed sample ($\pi(\mathbf{x}_p)$) multiplied by the evaluation of the proposal distribution evaluated at $\mathbf{x}_i$, given the proposed sample ($q(\mathbf{x}_i|\mathbf{x}_p)$), is larger than the PDF at the current sample ($\pi(\mathbf{x}_i)$) multiplied by the evaluation of the proposal distribution at the proposed sample given the current sample ($q(\mathbf{x}_p|\mathbf{x}_i)$), the proposed sample is *always* accepted as the new sample. However, if $\pi(\mathbf{x}_p)q(\mathbf{x}_i|\mathbf{x}_p) < \pi(\mathbf{x}_i)q(\mathbf{x}_p|\mathbf{x}_i)$, the proposed sample *may* be accepted based on the ratio of scalar r in Algorithm 2.1. The ratio is compared to a random number generated from a uniform distribution. If the ratio is greater than the random number, the proposed sample is accepted. If the ratio is smaller than the random number, the proposed sample is rejected, and the current sample becomes the new sample. Otherwise, the proposed sample becomes the new sample. The algorithm is repeated for n_s samples.

Algorithm 2.1 The standard Metropolis-Hastings algorithm

```
select the initial sample $\mathbf{x}_0 \in \mathbb{R}^{n_p}$
for $i = 0, 1, 2, ..., n_s - 1$ do
    draw $\mathbf{x}_p \in \mathbb{R}^{n_p}$ from the proposal distribution $q(\mathbf{x}_p|\mathbf{x}_i)$ in Eq. (2.53)
    calculate the ratio $r(\mathbf{x}_i, \mathbf{x}_p) = \min\Big(1, \frac{\pi(\mathbf{x}_p)q(\mathbf{x}_i|\mathbf{x}_p)}{\pi(\mathbf{x}_i)q(\mathbf{x}_p|\mathbf{x}_i)}\Big)$
    ▷ $\pi(\cdot)$ denotes the target distribution (i.e. posterior).
    draw $u \in [0, 1]$ from uniform probability density
    if $r(\mathbf{x}_i, \mathbf{x}_p) \geq u$ then
        $\mathbf{x}_{i+1} = \mathbf{x}_p$
    else
        $\mathbf{x}_{i+1} = \mathbf{x}_i$
    end if
end for
```

In case of a symmetric proposal distribution (as in this chapter), the following relation holds:

$$q(\mathbf{x}_i|\mathbf{x}_p) = q(\mathbf{x}_p|\mathbf{x}_i). \tag{2.51}$$

Consequently, step 4 in Algorithm 2.1 simplifies to:

$$r(\mathbf{x}_i, \mathbf{x}_p) = \min\Big(1, \frac{\pi(\mathbf{x}_p)}{\pi(\mathbf{x}_i)}\Big). \tag{2.52}$$

Note that the Metropolis-Hastings algorithm with a symmetric proposal distribution is commonly called the Metropolis algorithm.

A commonly employed approach to check the stability and convergence of the algorithm is by tracing the generated samples and analysing their characteristics, after the algorithm is finished. The evolution of the mean value and the standard deviation can for instance be checked for convergence [40]. We refer the readers for more information to the review on assessing the convergence of the MCMC by Sinharay [39].

The efficiency of the algorithm is influenced by the initial sample ($\mathbf{x}_0$) and the proposal distribution (q) [48]. The most common proposal distribution for the Metropolis-Hastings algorithm (as employed here) is of the following Gaussian form:

$$q(\mathbf{x}_i|\mathbf{x}_p) = q(\mathbf{x}_p|\mathbf{x}_i) \propto \exp\Big(-\frac{1}{2\gamma^2}\left\|\mathbf{x}_i - \mathbf{x}_p\right\|^2\Big), \tag{2.53}$$

where γ is the parameter that determines the width of the proposal distribution and must be tuned to obtain an efficient and converging algorithm. An efficient starting value is $\gamma = \frac{2.38}{\sqrt{n_p}}$ [72], where n_p is the number of unknown parameters and hence, the dimension of the posterior for the cases presented above.

To overcome the tuning of γ, Haario et al. [73] introduced the adaptive proposal (AP). The AP method updates the width of the proposal distribution, using the existing knowledge of the posterior. The existing knowledge is based on the previous samples. For sample $n_{\mathbf{K}} + 1$, the update employs the following formulation:

$$q(\mathbf{x}_p|\mathbf{x}_i) \sim N(\mathbf{x}_i, \gamma^2\mathbf{R}_{n_{\mathbf{K}}}), \tag{2.54}$$

where $N(\mathbf{x}_i, \gamma^2\mathbf{R}_{n_{\mathbf{K}}})$ denotes a normal distribution with mean $\mathbf{x}_i$ and covariance matrix $\gamma^2\mathbf{R}_{n_{\mathbf{K}}}$, of size $n_p \times n_p$. To establish $\mathbf{R}_{n_{\mathbf{K}}}$, all $n_{\mathbf{K}}$ previous samples are first stored in matrix $\mathbf{K}$ of size $n_{\mathbf{K}} \times n_p$. $\mathbf{R}_{n_{\mathbf{K}}}$, is then computed as:

$$\mathbf{R}_{n_{\mathbf{K}}} = \frac{1}{n_{\mathbf{K}} - 1}\widetilde{\mathbf{K}}^T\widetilde{\mathbf{K}}, \tag{2.55}$$

where $\widetilde{\mathbf{K}} = \mathbf{K} - \mathbf{K}_{\text{mean}}$ and $\mathbf{K}_{\text{mean}}$ reads:

$$\mathbf{K}_{\text{mean}} = \begin{bmatrix}\mathbf{k}_{\text{mean}}\\ \mathbf{k}_{\text{mean}}\\ \vdots \\ \mathbf{k}_{\text{mean}}\end{bmatrix}_{n_{\mathbf{K}} \times n_p}, \tag{2.56}$$

and $\mathbf{k}_{\text{mean}}$ is a row matrix of length n_p which is determined as follows:

$$\mathbf{k}_{\text{mean}} = \frac{1}{i}\left[\sum_{i=1}^{n_{\mathbf{K}}}(K)_{i1} \quad \sum_{i=1}^{n_{\mathbf{K}}}(K)_{i2} \quad \cdots \quad \sum_{i=1}^{n_{\mathbf{K}}}(K)_{in_p}\right]. \tag{2.57}$$

The following relation is used for $N(\mathbf{x}_i, \gamma^2\mathbf{R}_{n_{\mathbf{K}}})$ in this chapter:

$$N(\mathbf{x}_i, \gamma^2\mathbf{R}_{n_{\mathbf{K}}}) \sim \mathbf{x}_i + \frac{\gamma}{\sqrt{n_{\mathbf{K}} - 1}}\widetilde{\mathbf{K}}^T N(0, \mathbf{I}_{n_{\mathbf{K}}}), \tag{2.58}$$

where $\mathbf{I}_{n_\mathbf{K}}$ is the identity matrix of size $n_\mathbf{K} \times n_\mathbf{K}$ and $N(0, \mathbf{I}_{n_\mathbf{K}})$ is the $n_\mathbf{K}$-dimensional normal distribution.

Note that it is computationally inefficient to update the proposal distribution after each new sample is generated. In the numerical examples in this chapter therefore, updating takes place once per 1000 sample generations. Algorithm 2.2 shows the Metropolis-Hastings algorithm with the symmetric AP proposal (Eq. (2.58)) that is employed here.

Algorithm 2.2 The Metropolis algorithm with AP proposal

```
select the initial sample $\mathbf{x}_0 \in \mathbb{R}^{n_p}$ and set $\gamma = \frac{2.38}{\sqrt{n_p}}$
for $i = 0, 1, 2, ..., n_s - 1$ do
    draw $\mathbf{x}_p \in \mathbb{R}^{n_p}$ from the proposal distribution $q(\mathbf{x}_p|\mathbf{x}_i)$ in Eq. (2.58)
    calculate the ratio $r(\mathbf{x}_i, \mathbf{x}_p) = \min\Big(1, \frac{\pi(\mathbf{x}_p)}{\pi(\mathbf{x}_i)}\Big)$
    ▷ $\pi(\cdot)$ denotes the target distribution (i.e. posterior).
    draw $u \in [0, 1]$ from uniform probability density
    if $r(\mathbf{x}_i, \mathbf{x}_p) \geq u$ then
        $\mathbf{x}_{i+1} = \mathbf{x}_p$
    else
        $\mathbf{x}_{i+1} = \mathbf{x}_i$
    end if
    per 1000 samples
        update matrix $\widetilde{\mathbf{K}}$
end for
```

2.4.2 Posterior predictive distribution (PPD)

Once the posterior is established, the posterior predictive distribution can be used to predict new measurements, given the current measurements. A comparison between the newly generated measurements and the current (yet observed) measurements may then indicate if a different model and/or prior need to be used. For instance, if the envelope of the new measurements differs substantially from the envelope of the current measurements, the current measurements are unlikely to be generated using the current model and/or prior and the user may want to select a new model and/or prior.

Considering measurements $\mathbf{y} = \begin{bmatrix} y_1 & \cdots & y_{n_m} \end{bmatrix}^T$, the posterior predictive distribution of new measurement y^{new} for new strain ϵ^{new}, given the current measurements, reads [16]:

$$\pi(y^{\text{new}}|\mathbf{y}, \boldsymbol{\epsilon}, \epsilon^{\text{new}}) = \int_{\mathbb{R}^{n_p}} \pi(y^{\text{new}}|\mathbf{x}, \epsilon^{\text{new}}) \pi(\mathbf{x}|\mathbf{y}, \boldsymbol{\epsilon}) d\mathbf{x}, \tag{2.59}$$

where $\boldsymbol{\epsilon} = \begin{bmatrix} \epsilon_1 & \cdots & \epsilon_{n_m} \end{bmatrix}^T$ is the vector of the strains at which stresses $\mathbf{y}$ were measured. Note that we have so far neglected $\boldsymbol{\epsilon}$ in the notation.

Computing the integral in Eq. (2.59) is usually challenging for high dimensional problems. However, the Monte Carlo Markov chain can be employed to draw samples from the PPD for a new measurement (y^{new}), given measurement vector $\mathbf{y}$. This can be achieved by employing a sampling procedure twice. First, samples are drawn from the posterior distribution for the parameters, given the measurements ($\pi(\mathbf{x}|\mathbf{y}, \boldsymbol{\epsilon})$). Note that this is already performed during the numerical analysis of the posterior and hence, if those samples are saved, this procedure does not have to be applied again. Second, the i^{th} sample is replaced in $\pi(y^{\text{new}}|\mathbf{x}_i, \epsilon^{\text{new}})$, which is subsequently used to generate a sample for new measurement y_i^{new}.

2.5 Examples

All formulations derived in the previous section are investigated below. The effect of the prior distribution on the posterior distribution is studied, as well as the ability of the current formulations to recover a material parameter distribution when they are taken from a specific distribution. Also, BI's ability to recover correlations between different material parameters is exposed. First however, we will identify the noise distribution and its parameters.

2.5.1 Noise distribution

To determine the noise distribution and its parameters, two sets of 'calibration experiments' can be performed. First, a test is performed without any specimen. The stress-strain measurements of this test are shown in Fig. 2-3(a). It shows that the PDF of the noise in the 'stress measurements' is a normal distribution with a zero mean and a standard deviation of s_{noise}.

Second, the evolution of the noise distribution (including its parameters) is determined. To this purpose, a tensile test is performed on a calibration specimen (of which the Young's modulus is known). The artificially generated results are presented in Fig. 2-3(b). The mean stress value varies linearly with the strain. Standard deviation s_{noise} remains the same however.

Thus, the 'calibration measurements' indicate that an additive noise model can be used and the stresses are polluted by realisations coming from a normal noise distribution with standard deviation s_{noise}. Now, we will employ BI to identify the Young's modulus of the linear elastic model.

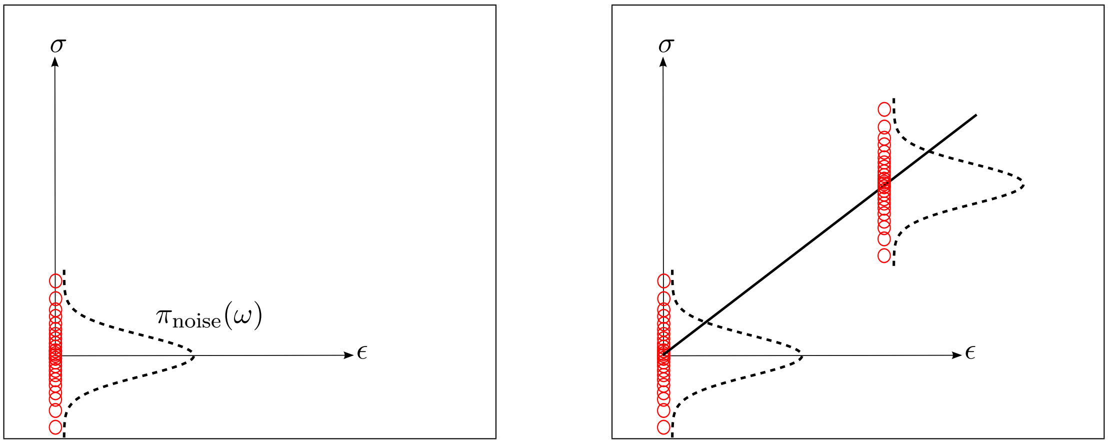

(a) Fitted noise distribution

(b) The shifted noise distribution

Figure 2-3: Schematic of the stress-strain measurements (red circles) of the 'calibration experiments', including the noise distributions (dashed). The theoretical stress-strain relation (which is exact for the calibration experiments) is presented as a solid line in the diagram on the right.

2.5.2 Linear elasticity

Identification of the Young's modulus In the first example, a specimen with a Young's modulus of 210 GPa is considered, which is to be identified. 'calibration experiments' were performed and the noise in the stress follows the normal distribution of Eq. (2.25) with $s_{\text{noise}} = 0.01$ GPa. For only one stress measurement of $y = 0.1576$ GPa with corresponding strain $\epsilon = 7.25 \times 10^{-4}$, the posterior distribution is calculated using Eq. (2.31). Selecting the prior distribution as in Eq. (2.28) with mean $\overline{E} = 150$ GPa and a relatively large standard deviation of $s_E = 50$ GPa, the posterior reads:

$$\pi(E|y) \propto \exp\Big(-\tfrac{(E-\overline{E}_{\text{post}})^2}{2s_{\text{post}}^2}\Big), \quad E \geq 0, \tag{2.60}$$

where $\overline{E}_{\text{post}} = 212.6486$ GPa and $s_{\text{post}} = 13.2964$ GPa.

Fig. 2-4 shows this posterior distribution, as well as the prior distribution and the value predicted by the least squares method, for one and five measurements. Fig. 2-5 presents the linear elastic responses for one and for ten measurements. The figure also shows the stress-strain responses using Young's moduli drawn from the 95% credible region (i.e. the region that contains 95% of the posterior) of the posterior as well as the posterior predictions. One can see that envelope associated with the 95% credible region is narrower than the 95% prediction interval. Note that the 95% prediction interval is obtained using the posterior predictive distribution and its upper and lower bounds read:

$$\text{prediction bounds} = \overline{\text{PPD}} \pm 2s_{\text{PPD}}, \tag{2.61}$$

where $\overline{\text{PPD}}$ denotes the mean of posterior predictive distribution for the new measurement (i.e. y^{new} in (2.59)) and s_{PPD} denotes its standard deviation.

Two points can be observed in Fig. 2-4. First, the strain at which a measurement is made has a strong influence on the posterior. This can be observed by comparing the posterior of Fig. 2-4(a) with that in Fig. 2-4(b) for only one measurement (the distribution in red, denoted by $\pi(E|y_1)$). The latter distribution is significantly wider and its MAP point is relatively distant from the specimen's Young's modulus. Hence, a measurement made at a comparatively large strain reduces the width of the posterior distribution (i.e. reduces the uncertainty).

The second remark is that for an increasing number of measurements, the posterior becomes narrower and the MAP point moves closer to the specimen's Young's modulus.

By comparing the MAP point for a single measurement in Fig. 2-4(b) ($\overline{E}_{\text{post}} = 207.2821$ GPa) with the result of the least squares method for the same measurement ($E_{\text{ls}} = 210.2216$ GPa), one can notice the effect of the selected prior distribution. One interpretation of this is that the least squares method gives a more accurate result than BI (although this depends the selected prior), as the result of the least squares method is closer to the specimen's Young's modulus than the MAP point determined using BI. On the other hand, the result determined using the least squares method is not the actual Young's modulus of the specimen (210 GPa), whereas the posterior distribution of BI does include this value. Furthermore, the MAP point and mean value of BI, come with an uncertainty in terms of the parameter value itself. This can be considered as an advantage if one wants to include this uncertainty, instead of including one deterministic value.

The main point is that BI cannot be directly compared to the least squares method, because contrary to the latter, BI results in a posterior probability distribution that represents the probability of each possible value to occur.

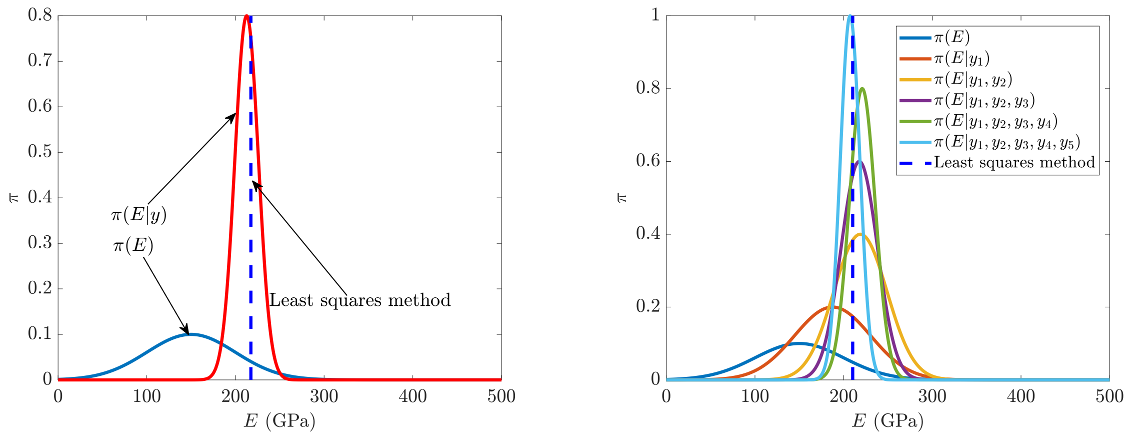

(a) One observation (b) Five successive observations

Figure 2-4: Linear elasticity: The prior, the posterior and the value predicted by least squares method for one measurement (a) and five measurements (b). The distributions are not normalised. The strain at which a measurement is made has a considerable influence on the posterior. This can be observed when the posterior of (a) ($\pi(E|y)$, red line) is compared to the posterior of (b), if only the first measurement is considered ($\pi(E|y_1)$, red line). An increase of the number of measurements results in narrower posteriors, with their MAP estimates closer to the true Young's modulus.

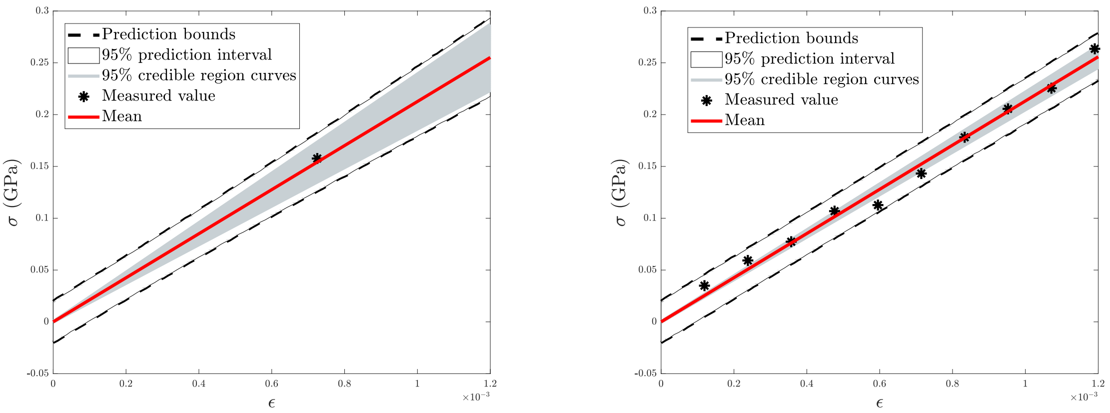

(a) One observation (b) Ten observations

Figure 2-5: Linear elasticity: The measurements, the posterior prediction and the stress-strain curves created using the posterior and mean for (a) one measurement and (b) ten measurements. The envelope associated with the 95% credible region is narrower than the 95% prediction interval.

The influence of the prior Now, we will study the effect of the prior distribution on the MAP point (which is the same as the mean value for the normal posteriors in this subsection). In Fig. 2-6 the MAP points are shown as a function of the mean and the standard deviation of the prior. The MAP points are presented for different numbers of measurements. As can be seen, an increase of the number of measurements results in a flatter surface, which means that the influence of the prior distribution decreases.

Recovering material heterogeneity A last important point to show using the linear elastic model is BI's ability (or inability for the current formulation) to capture the intrinsic heterogeneity of the material parameters. The question here is thus if BI is able to recover the distribution of the Young's modulus if several specimens are tested and their Young's moduli are taken from a specific underlying distribution. To this end, 25 specimens are considered of which the

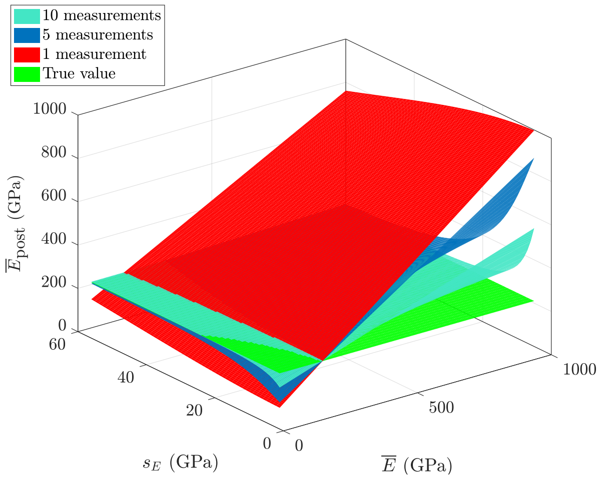

Figure 2-6: Linear elasticity: The influence of the prior (i.e. the mean value and the standard deviation) on the resulting MAP point for different numbers of measurements. Increasing the number of the measurements results in a flatter surface which indicates a decreasing influence of the prior distribution.

Young's moduli are taken from a normal distribution with a mean value of 210 GPa and a standard deviation of 10 GPa (blue curve in Fig. 2-7). For each specimen ten measurements are made. The same noise model and noise distribution are applied.

The resulting posterior is presented by the red curve in Fig. 2-7, which is a (modified) normal distribution with $\overline{E}_{\text{post}} = 215.3971$ GPa and $s_{\text{post}} = 0.8561$ GPa. The posterior is substantially narrower than the distribution of the specimens' Young's moduli and hence, using the BI formulations of this chapter, the material heterogeneity cannot be captured. This entails that the width of the posterior distributions (represented by s_{post} in this subsection) is only a measure of the uncertainty of the MAP points and the mean value and not of the material heterogeneity.

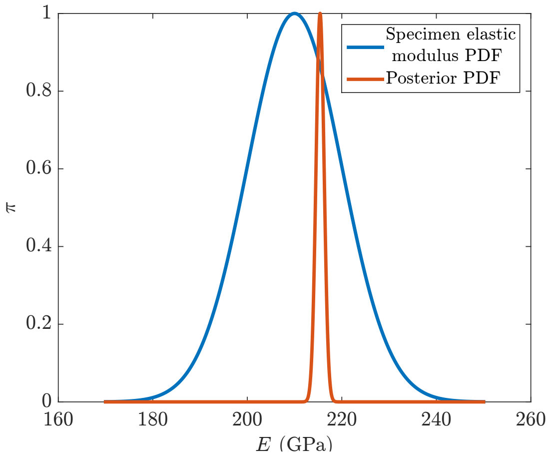

Figure 2-7: Linear elasticity: The distribution of the specimens' Young's moduli and the resulting posterior. The PDFs are not normalised. The current formulation is clearly not able to recover the material heterogeneity. To be able to recover the material heterogeneity, one needs to consider both the intrinsic uncertainty of the material parameters as well as that of the measurements.

2.5.3 Linear elasticity-perfect plasticity

Identification of the material parameters In the first example of this subsection, a linear elastic-perfectly plastically behaving specimen is considered with Young's modulus $E = 210$ GPa and yield stress $\sigma_{y0} = 0.25$ GPa. Twelve measurements are generated by employing the same noise distribution as in the previous subsection. The prior distribution of Eq. (2.36) is furthermore selected with the following mean vector and covariance matrix:

$$\overline{\mathbf{x}} = \begin{bmatrix} 200 \\ 0.29 \end{bmatrix} \text{ GPa}, \ \boldsymbol{\Gamma}_{\mathbf{x}} = \begin{bmatrix} 2500 & 0 \\ 0 & 2.7778 \times 10^{-4} \end{bmatrix} \text{GPa}^2. \tag{2.62}$$

Consequently, the posterior of Subsection 2.3.2 is of the form of Eq. (2.37), which is investigated by the MCMC approach given in Subsection 2.4.1. Running the chain for 10^4 samples whilst burning the first 3000 samples (i.e. the first 3000 samples are not used to determine the mean, the covariance matrix and the MAP estimate) yields:

$$\widehat{\overline{\mathbf{x}}}_{\text{post}} = \begin{bmatrix} 208.9859 \\ 0.2578 \end{bmatrix} \text{ GPa}, \ \widehat{\boldsymbol{\Gamma}}_{\text{post}} = \begin{bmatrix} 29.807 & 4.1064 \times 10^{-4} \\ 4.1064 \times 10^{-4} & 1.5067 \times 10^{-5} \end{bmatrix} \text{ GPa}^2, \tag{2.63}$$

and

$$\widehat{\mathbf{MAP}} = \begin{bmatrix} 208.4475 \\ 0.2578 \end{bmatrix} \text{ GPa}, \tag{2.64}$$

where the hat sign $\widehat{(\cdot)}$ denotes the numerical approximation.

Fig. 2-8(a) shows the samples generated by the adaptive MCMC approach which are used to approximate the posterior distribution. The domains presented in Fig. 2-8(b) show which of the measurements are included in the purely elastic part and which fall within the elastoplastic part. These discrete domains are a result of the C_0-continuity of Eq. (2.8). In domain 'a' (in which no samples are generated by the adaptive MCMC approach), all the measurements are considered to be in the elastoplastic part. In domain 'b' on the other hand, the first measurement (the one with the smallest strain) is considered to be in the purely elastic part and the others remain in the elastoplastic part. Continuing like this, in domain 'c' the second measurement is also considered to be in the purely elastic part. Finally, in domain 'm' all measurements are considered to fall within the elastoplastic domain. Based on Fig. 2-8(b) the MAP point is clearly located in the domain in which the first six measurements are considered to be in the purely elastic part and the remaining in the elastoplastic part.

The 95% credible region is shown together with the posterior distribution in Fig. 2-9(a). The possible stress-strain responses inside the credible region as well as the posterior predictions are presented in Fig. 2-9(b). The posterior distribution seems to be roughly of an elliptical shape with its primary axes almost along the E-axis and σ_{y0}-axis. This entails that the correlation between the two material parameters is not significant. One has to notice though, that the assumed prior is uncorrelated. In other words, the prior covariance matrix ($\boldsymbol{\Gamma}_{\mathbf{x}}$) is diagonal. It is therefore interesting to investigate the influence of the off-diagonal term of the prior covariance matrix on the posterior covariance matrix. In Fig. 2-10, this influence is graphically presented for the three terms of the posterior covariance matrix (note that both the prior covariance matrix and the posterior covariance matrix are symmetric). It seems that an increase of $(\Gamma_{\mathbf{x}})_{12}$ leads to some decreasing trend for $(\widehat{\Gamma}_{\text{post}})_{11}$ and some increasing trend for $(\widehat{\Gamma}_{\text{post}})_{12}$. However, it is difficult to assess whether or not these trends can be considered as meaningful.

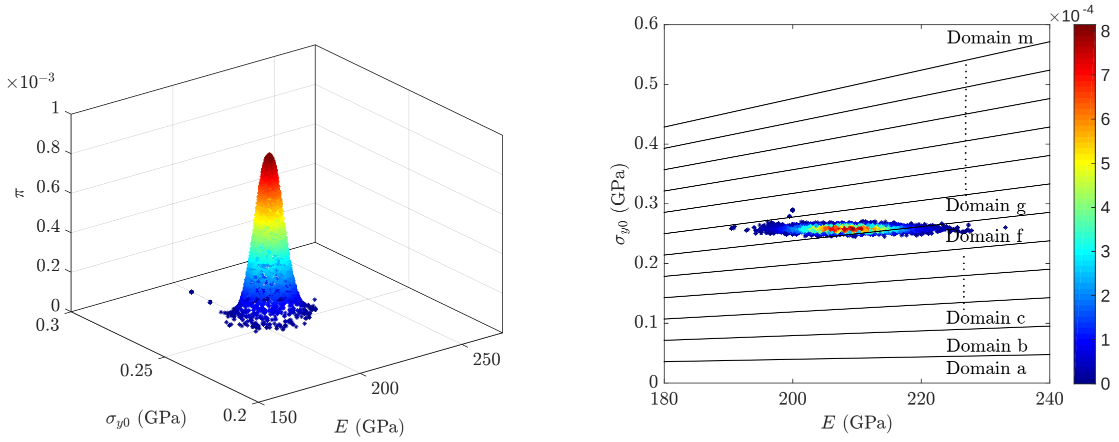

(a) Samples generated by the adaptive MCMC approach

(b) Samples generated by the adaptive MCMC approach (top view) including different domains

Figure 2-8: Linear elasticity-perfect plasticity: Two different views of the samples generated by the adaptive MCMC approach to approximate the posterior. The colours represent the value of the posterior, which in the left image is also shown along the z-axis. In Fig. 2-8(b) several domains are shown. Each of these domains corresponds to a region for which the number of measurements considered to be in the purely elastic part is constant (e.g. zero in domain a and one in domain b).

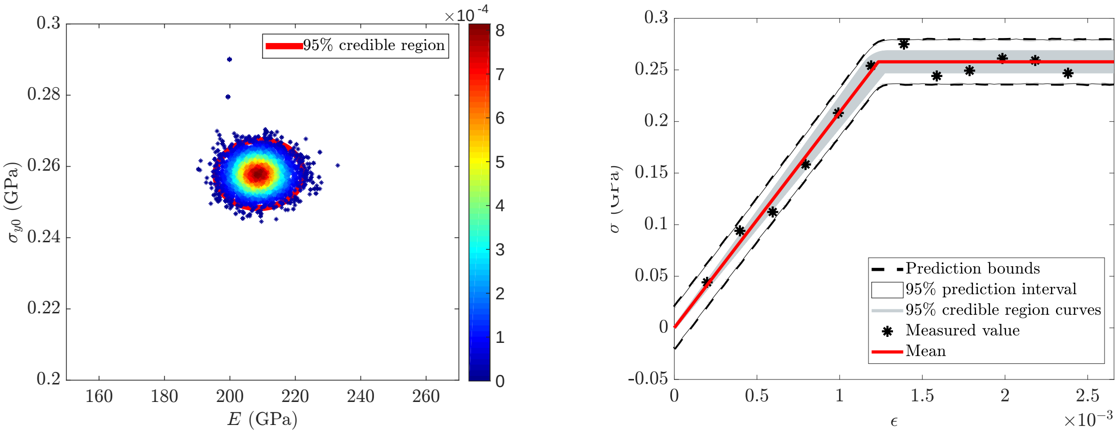

(a) The 95% credible region

(b) The measurements, the posterior prediction and the stress-strain curves

Figure 2-9: Linear elasticity-perfect plasticity: The 95% credible region and the posterior distribution (a), the measurements, the posterior prediction and the stress-strain curves created using the 95% credible region of the posterior (b).

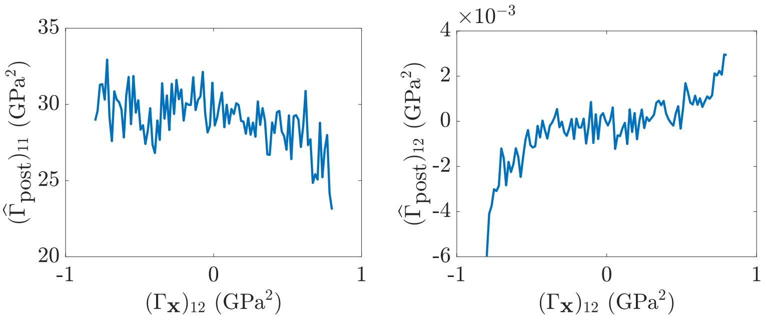

(a) Effect of $(\Gamma_{\mathbf{x}})_{12}$ on $(\widehat{\Gamma}_{\text{post}})_{11}$ (b) Effect of $(\Gamma_{\mathbf{x}})_{12}$ on $(\widehat{\Gamma}_{\text{post}})_{12}$

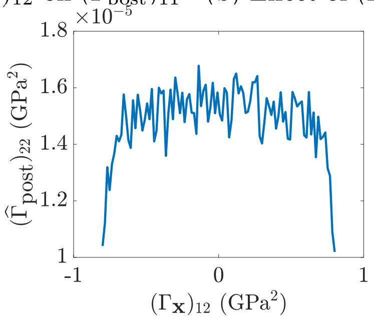

(c) Effect of $(\Gamma_{\mathbf{x}})_{12}$ on $(\widehat{\Gamma}_{\text{post}})_{22}$

Figure 2-10: Linear elasticity-perfect plasticity: Effect of the off-diagonal component of the prior's covariance matrix on the posterior's covariance matrix. It seems that an increase of $(\Gamma_{\mathbf{x}})_{12}$ leads to a decreasing trend of $(\widehat{\Gamma}_{\text{post}})_{11}$ and a increasing trend of $(\widehat{\Gamma}_{\text{post}})_{12}$. However, it is difficult to assess whether or not a true trend is present in these results.

The influence of the prior on the correlation between the material parameters

The next example focuses on the ability of the current formulation to capture a correlation between the Young's modulus and the initial yield stress when they are correlated. To this end, ten specimens are considered of which the material parameters are governed by a normal distribution with the following mean vector and covariance matrix:

$$\overline{\mathbf{x}}_{\text{spc}} = \begin{bmatrix} 210 \\ 0.25 \end{bmatrix} \text{ GPa}, \ \mathbf{\Gamma}_{\text{spc}} = \begin{bmatrix} 100 & 10^{-4} \\ 10^{-4} & 1.1111 \times 10^{-4} \end{bmatrix} \text{GPa}^2. \tag{2.65}$$

For each specimen, twelve measurements are made. Using the same prior as in the previous example (see Eq. (2.62)) and the adaptive MCMC approach for 10^4 samples whilst burning the first 3000 samples, yields:

$$\widehat{\overline{\mathbf{x}}}_{\text{post}} = \begin{bmatrix} 211.1077 \\ 0.2519 \end{bmatrix} \text{ GPa}, \ \widehat{\mathbf{\Gamma}}_{\text{post}} = \begin{bmatrix} 5.5373 & -8.396 \times 10^{-4} \\ -8.396 \times 10^{-4} & 1.8174 \times 10^{-6} \end{bmatrix} \text{ GPa}^2. \tag{2.66}$$

The MAP point is given by:

$$\widehat{\mathbf{MAP}} = \begin{bmatrix} 210.5923 \\ 0.2521 \end{bmatrix} \text{ GPa}. \tag{2.67}$$

These results show that the correlation of the posterior is not the same as that of the distribution of the actual material. This corresponds closely with the observation that the formulations in this chapter are unable to capture any of the intrinsic uncertainty of the material parameters. Fig. 2-11 shows the effect of the off-diagonal component of the prior's covariance matrix ($\boldsymbol{\Gamma}_{\mathbf{x}}$) on the components of the posterior's covariance matrix ($\boldsymbol{\Gamma}_{\text{post}}$). Again, no real trends can be observed.

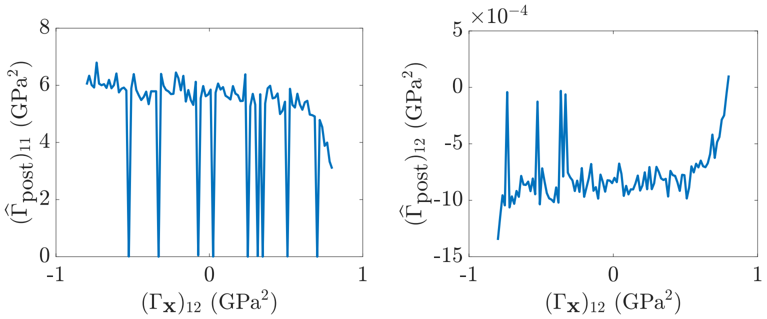

(a) Effect of $(\Gamma_{\mathbf{x}})_{12}$ on $(\widehat{\Gamma}_{\text{post}})_{11}$ (b) Effect of $(\Gamma_{\mathbf{x}})_{12}$ on $(\widehat{\Gamma}_{\text{post}})_{12}$

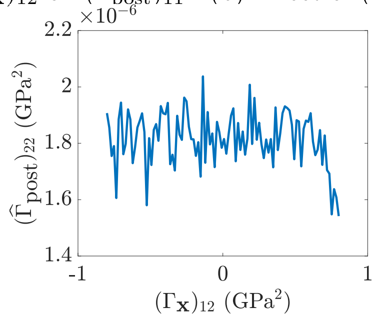

(c) Effect of $(\Gamma_{\mathbf{x}})_{12}$ on $(\widehat{\Gamma}_{\text{post}})_{22}$

Figure 2-11: Linear elasticity-perfect plasticity: Effect of the off-diagonal components of the prior's covariance matrix on the posterior's covariance matrix if the measurements are generated from ten specimens with their material parameters drawn from a normal distribution given in Eq. (2.65). No real trends can be observed.

2.5.4 Linear elasticity-linear hardening

Identification of the material parameters This subsection deals with the Bayesian formulation for the linear elastic-linear hardening material description. A specimen with Young's modulus $E = 210$ GPa, initial yield stress $\sigma_{y0} = 0.25$ GPa and plastic modulus $H = 50$ GPa is regarded. Twelve measurements are created by employing the same noise distribution as in the previous subsection. The prior distribution is given by Eq. (2.39) with the following properties:

$$\overline{\mathbf{x}} = \begin{bmatrix} 200 \\ 0.29 \\ 60 \end{bmatrix} \text{ GPa}, \; \boldsymbol{\Gamma}_{\mathbf{x}} = \begin{bmatrix} 2500 & 0 & 0 \\ 0 & 2.7778 \times 10^{-4} & 0 \\ 0 & 0 & 100 \end{bmatrix} \text{GPa}^2. \tag{2.68}$$

The adaptive MCMC algorithm for 10^4 samples whilst burning the first 3000 samples yields:

$$\widehat{\overline{\mathbf{x}}}_{\text{post}} = \begin{bmatrix} 207.4586 \\ 0.2533 \\ 55.9187 \end{bmatrix} \text{ GPa}, \widehat{\boldsymbol{\Gamma}}_{\text{post}} = \begin{bmatrix} 36.5642 & -1.2746 \times 10^{-2} & -3.7886 \\ -1.2746 \times 10^{-2} & 4.0359 \times 10^{-5} & -2.6218 \times 10^{-2} \\ -3.7886 & -2.6218 \times 10^{-2} & 66.8214 \end{bmatrix} \text{GPa}^2, \tag{2.69}$$

and

$$\widehat{\mathbf{MAP}} = \begin{bmatrix} 206.9528 \\ 0.2548 \\ 55.2838 \end{bmatrix} \text{ GPa}. \tag{2.70}$$

Fig. 2-12 shows the generated samples by the adaptive MCMC approach in the $E - \sigma_{y0} - H$ space, including the projections on the $E - \sigma_{y0}$, $E - H$ and $\sigma_{y0} - H$ planes.

The 95% credible region is presented in Fig. 2-13(a) and the stress-strain responses associated with it, as well as the posterior prediction are shown in Fig. 2-13(b).

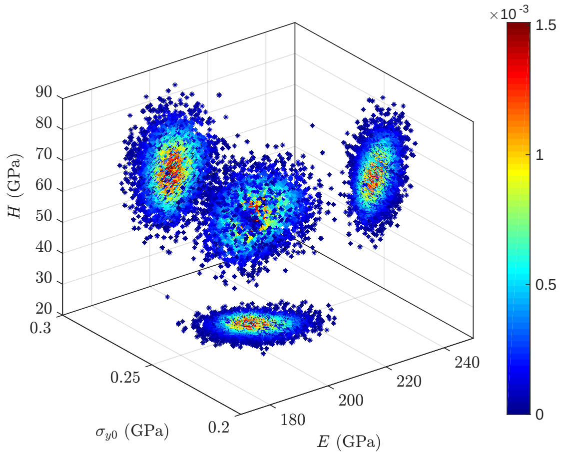

Figure 2-12: Linear elasticity-linear hardening: Samples generated by the adaptive MCMC approach to approximate the posterior distribution and its projection on the three planes.

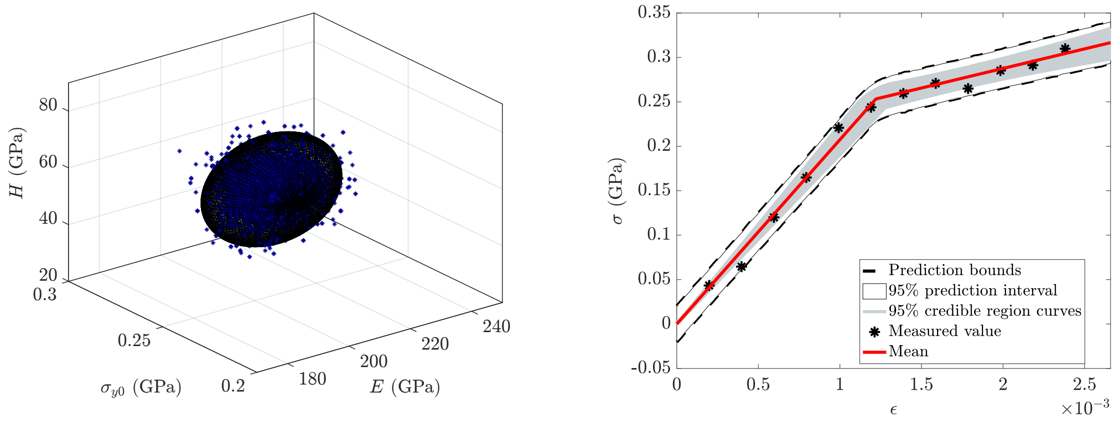

(a) The 95% credible region

(b) The measurements, the posterior prediction and the stress-strain curves

Figure 2-13: Linear elasticity-linear hardening: The 95% credible region and the posterior distribution (a) and the measurements, the posterior prediction and the stress-strain curves associated with the 95% credible region (b).

2.5.5 Linear elasticity-nonlinear hardening

Identification of the material parameters In this subsection, twelve measurements are generated using $E = 210$ GPa, $\sigma_{y0} = 0.25$ GPa, $H = 2$ GPa, $n = 0.57$ (which are to be identified) and the same noise distribution as in the previous subsections. The prior distribution is selected in the form of Eq. (2.42) with the following mean vector and covariance matrix:

$$\overline{\mathbf{x}} = \begin{bmatrix} 200 \\ 0.29 \\ 2.5 \\ 0.57\ \text{GPa}^{-1} \end{bmatrix} \text{GPa},\ \boldsymbol{\Gamma}_{\mathbf{x}} = \begin{bmatrix} 2500 & 0 & 0 & 0 \\ 0 & 2.7778 \times 10^{-4} & 0 & 0 \\ 0 & 0 & 0.1111 & 0 \\ 0 & 0 & 0 & 0.0025\ \text{GPa}^{-2} \end{bmatrix} \text{GPa}^2. \quad (2.71)$$

Running the adaptive MCMC approach for 10^4 samples and burning the first 3000 samples yields:

$$\widehat{\overline{\mathbf{x}}}_{\text{post}} = \begin{bmatrix} 210.444 \\ 0.254 \\ 2.1937 \\ 0.5988\ \text{GPa}^{-1} \end{bmatrix} \text{GPa},$$

$$\widehat{\boldsymbol{\Gamma}}_{\text{post}} = \begin{bmatrix} 24.3496 & -8.1743 \times 10^{-3} & 0.1501 & -2.2095 \times 10^{-3}\ \text{GPa}^{-1} \\ -8.1743 \times 10^{-3} & 9.5238 \times 10^{-5} & -6.8472 \times 10^{-4} & 1.8694 \times 10^{-4}\ \text{GPa}^{-1} \\ 0.1501 & -6.8472 \times 10^{-4} & 9.5319 \times 10^{-2} & 5.4179 \times 10^{-3}\ \text{GPa}^{-1} \\ -2.2095 \times 10^{-3}\text{GPa}^{-1} & 1.8694 \times 10^{-4}\ \text{GPa}^{-1} & 5.4179 \times 10^{-3}\ \text{GPa}^{-1} & 1.0629 \times 10^{-3}\ \text{GPa}^{-2} \end{bmatrix} \text{GPa}^2, \quad (2.72)$$

and

$$\widehat{\mathbf{MAP}} = \begin{bmatrix} 210.0794 \\ 0.2536 \\ 2.198 \\ 0.5978\ \text{GPa}^{-1} \end{bmatrix} \text{GPa}. \quad (2.73)$$

The stress-strain responses associated with the 95% credible region of the posterior and the posterior prediction are presented in Fig. 2-14.

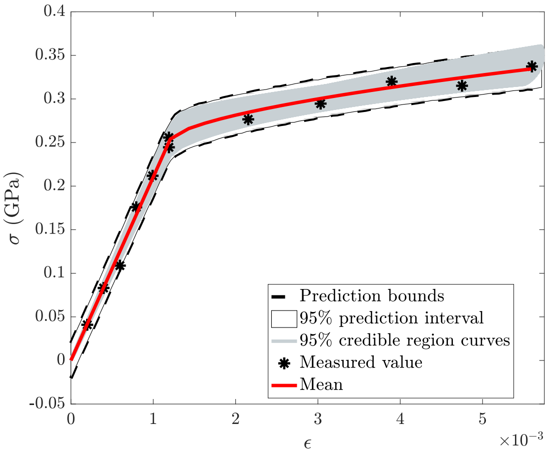

Figure 2-14: Liner elasticity-nonlinear hardening: The measurements, the stress-strain curves associated with the 95% credible region and the posterior prediction.

2.6 Additional concepts for parameter identification from uniaxial tensile results

In the previous sections, we have introduced BI for the identification of elastic and elastoplastic parameters. The formulation of the framework was relatively basic. In this section, we will discuss, without too many details, some changes to the framework if (1) a viscoelastic model is considered instead, (2) not only the stress measurements are uncertain, but also the strain measurements, and (3) the model itself is uncertain as well.

2.6.1 Viscoelasticity

Viscoelasticity differs from the aforementioned elastoplasticity by its rate-dependency (whilst no plastic deformation occurs). Consequently, the rate-dependency must be identified, besides one or more stiffness parameters. The rate at which uniaxial tensile tests are performed thus comes into play. On the other hand, the mechanical responses are C_1-continuous, which results in C_1-continuous posteriors. This may be considered as more straightforward to treat with MCMC approaches than the posteriors of the aforementioned elastoplastic descriptions.

Instead of performing uniaxial tensile tests at a constant rate, one may also choose to use (uniaxial) relaxation tests or creep tests. In a relaxation test, a user-selected displacement (i.e. strain) is enforced as fast as possible in the beginning of the test and then kept constant. The result of this is a stress-time response. In a creep test, a user-selected force (i.e. stress) is prescribed as fast as possible in the beginning of the test and then kept constant. The result of this is a strain-time response. In relaxation and creep tests, the stress-strain response for the material descriptions in this chapter must be replaced by a stress-time response or a strain-time response. As these are both C_1-continuous, their posteriors are also C_1-continuous and hence, the MCMC algorithm to explore them is easier to implement than for elastoplasticity.

The study of Rappel et al. [30] shows that the effect of the prior on the mean and MAP point in viscoelasticity is larger than for elastoplasticity. The influence is especially larger for the damping parameter. Although an increase of the number of measurements decreases the influence of the prior, its influence on the damping parameter remains recognisable. The uncertainty level of the identified parameter values is furthermore substantially larger if uniaxial tensile tests at constant strain-rates are used than if relaxation or creep tests are used. More detailed information can be found in [30].

2.6.2 Noise in both stress and strain

The additive noise model when both the stresses and strains are contaminated by stochastic noise, can be expressed as follows:

$$\begin{cases} Y = \sigma(\epsilon, \mathbf{x}) + \Omega_y \\ \epsilon^* = \epsilon + \Omega_{\epsilon^*} \end{cases}, \tag{2.74}$$

where ϵ^* denotes the measured strain, ϵ the theoretical strain, Ω_y the error of the stress measurement and Ω_{ϵ^*} the error of the strain measurement. Because the information from both the measured stress and the measured strain is used here, Bayes' formula for multiple variables must be employed [74]:

$$\pi(\mathbf{x}|y, \epsilon^*) = \frac{\pi(\mathbf{x})\pi(\epsilon^*)\pi(y|\mathbf{x}, \epsilon^*)}{\pi(\epsilon^*)\pi(y|\epsilon^*)}. \tag{2.75}$$

Since the denominator in Eq. (2.75) is a constant number, the equation above can be written as:

$$\pi(\mathbf{x}|y, \epsilon^*) \propto \pi(\mathbf{x})\pi(y|\mathbf{x}, \epsilon^*). \tag{2.76}$$

The likelihood function, $\pi(y|\mathbf{x}, \epsilon^*)$, must be determined by integration (over ϵ [17]), because $\pi(y|\mathbf{x}, \epsilon)$ can be determined directly, but $\pi(y|\mathbf{x}, \epsilon^*)$ not. To this end, we write:

$$\pi(y|\mathbf{x}, \epsilon^*) = \int_0^a \pi(y|\mathbf{x}, \epsilon)\pi(\epsilon|\epsilon^*)d\epsilon, \tag{2.77}$$

where a denotes the physical upper bound of the tensile tester (i.e. the ratio of the original length of the specimen and the maximum distance that the clamps can move). Using Eq. (2.74), one can express conditional probabilities $\pi(y|\mathbf{x}, \epsilon)$ and $\pi(\epsilon|\epsilon^*)$ as follows:

$$\begin{cases} \pi(y|\mathbf{x}, \epsilon) = \pi_y(y - \sigma(\epsilon, \mathbf{x})) \\ \pi(\epsilon|\epsilon^*) = \pi_{\epsilon^*}(\epsilon^* - \epsilon) \end{cases}, \tag{2.78}$$

where $\pi_y(\omega_y)$ and $\pi_{\epsilon^*}(\omega_{\epsilon^*})$ are the noise distributions of the errors in the stress measurements and the strain measurements, respectively. For n_m independent measurements, we write:

$$\pi(\mathbf{y}|\mathbf{x}, \boldsymbol{\epsilon}^*) = \prod_{i=1}^{n_m} \pi(y_i|\mathbf{x}, \epsilon_i^*), \tag{2.79}$$

where $\mathbf{y} = \begin{bmatrix} y_1 & \cdots & y_{n_m} \end{bmatrix}^T$ is the vector of n_m stress measurements, $\boldsymbol{\epsilon}^* = \begin{bmatrix} \epsilon_1^* & \cdots & \epsilon_{n_m}^* \end{bmatrix}^T$ is the vector of measured strains and $\pi(y_i|\mathbf{x}, \epsilon_i^*)$ is given in Eq. (2.77). Further details on the resulting likelihoods for different material models is presented in [32].

We show now a simple example for linear elasticity with one measurement point, given by $y = 0.1576$ GPa and $\epsilon^* = 7.25 \times 10^{-4}$. It is furthermore assumed that both noise distribution are normal distributions with a zero mean and $s_y = 0.01$ GPa and $s_{\epsilon^*} = 0.0001$ for the noise in stress and the noise in the strain, respectively.

In Fig. 2-15 the posteriors are shown if only the noise in the stress measurement is considered and if the noise in the stress measurement as well as in the strain measurement is considered. The prior is also presented, which is in form of Eq. (2.28) with mean $\overline{E} = 150$ GPa and standard deviation $s_E = 50$ GPa. Not only is the posterior for the double uncertainty case wider than the other one, it is also asymmetric.

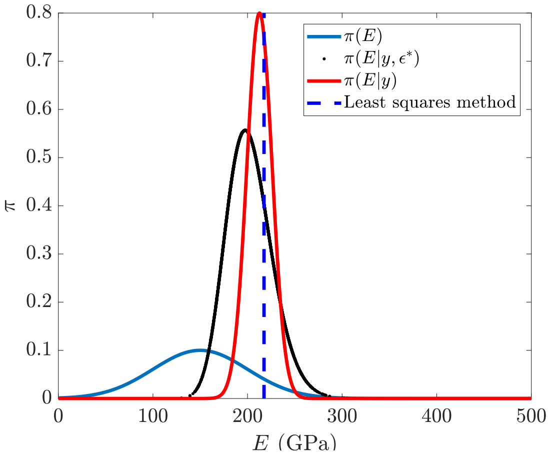

Figure 2-15: Noise in the stress and strain: The prior and posterior when both the stress and the strain are corrupted by noise (black dots), the posterior when only the stress is contaminated (red) and the value predicted by the least squares method (blue dashed). The posterior for the case with noise in the stress and strain is wider than the posterior for the case with noise in the stress only. Note furthermore that the posterior if only the noise in the stress is considered is a (modified) normal distribution (symmetric), but the posterior if both noises are incorporated neither is a (modified) normal distribution, nor is it symmetric.

Fig. 2-16 shows the posterior predictions for the same case, except that ten measurements are considered. One can see that incorporating the error results in a wider envelope that includes more validation points. Note that the validation points are only used to assess the quality of the predictions based on the identified material parameter (i.e. E) and not for identification of the material parameter.

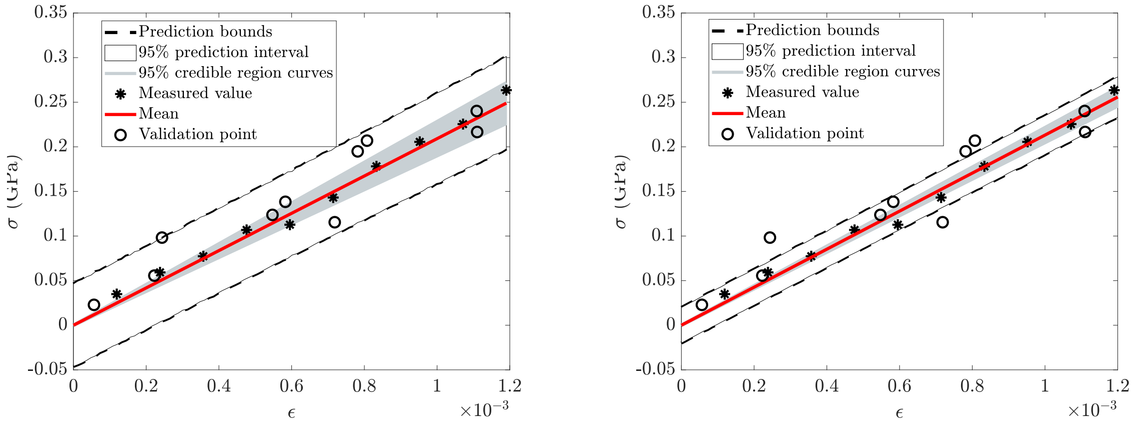

(a) Uncertainty in both the stress and the strain measurements

(b) Uncertainty in the stress only

Figure 2-16: Noise in the stress and strain: The measurements, the validation points, the posterior prediction and the stress-strain curves associated with the 95% credible region of the posterior for (a) noise in the stress and the strain and (b) noise in the stress only. One can see that the uncertainty is larger for the case with noise in the stress and strain, than that for the case with noise in the stress only. Consequently, the posterior predictions if both the noise in the stress and strain is incorporated, includes more validation points.

Incorporating not only the error in the stress, but also the error in the strain often results in a larger uncertainty (wider posterior) and consequently, the posterior prediction interval encompasses more measurement data. More information can be found in [32].

2.6.3 Model uncertainty

So far in this chapter, the modelling error (model uncertainty) has not been incorporated. However, no model is completely correct and model uncertainty as an error source may be incorporated. A framework able to do so was developed by Kennedy and O'Hagan [47] (the 'KOH' framework). In this framework, the difference between theoretical model response $\sigma(\epsilon, \mathbf{x})$ and true response σ_{true} is written as an additive uncertainty term [75]:

$$Y = \sigma_{\text{true}} + \Omega, \tag{2.80}$$

with

$$\sigma_{\text{true}} = \sigma(\epsilon, \mathbf{x}) + d(\epsilon, \mathbf{x}_d), \tag{2.81}$$

where $d(\epsilon, \mathbf{x}_d)$ denotes the model uncertainty, which can be assumed to depend on the input (i.e. strain ϵ here), and $\mathbf{x}_d$ denotes the parameter vector of the model uncertainty. Assuming that both the form and parameters of the noise distribution of the stress measurements are known, the likelihood function now reads:

$$\pi(y|\mathbf{x}, \mathbf{x}_d) = \pi_{\text{noise}}(y - \sigma(\epsilon, \mathbf{x}) - d(\epsilon, \mathbf{x}_d)). \tag{2.82}$$

Note that we have not incorporated the error in the strain measurements for simplicity. Readers are referred to [32] for the case that the error in the strain also is considered.

Using Eqs. (2.23) and (2.82), the posterior distribution for a single measurement can be written as:

$$\pi(\mathbf{x}, \mathbf{x}_d|y) \propto \pi(y|\mathbf{x}, \mathbf{x}_d)\pi(\mathbf{x})\pi(\mathbf{x}_d). \tag{2.83}$$

For several independent measurements, the final likelihood function is the product of the likelihood function for each measurement:

$$\pi(\mathbf{y}|\mathbf{x}, \mathbf{x}_d) = \prod_{i=1}^{n_m} \pi_{\text{noise}}(y_i - \sigma(\epsilon_i, \mathbf{x}) - d(\epsilon_i, \mathbf{x}_d)). \tag{2.84}$$

After establishing the posterior, the posterior needs to be sampled numerically (see Subsection 2.4.1) in order to obtain the statistical summaries (e.g. mean value, MAP point or covariance matrix). Note that the posterior distribution of Eq. (2.83) is a joint distribution of $\mathbf{x}$ and $\mathbf{x}_d$. In order to sample the marginal distribution of each parameter (e.g. the Young's modulus), one only needs to consider the samples of that specific parameter in the joint posterior distribution (i.e. Eq.(2.83)) and ignore those of the other parameters [22].

Various formulations have been employed in different studies to express the model uncertainty term given in Eq. (2.81). Probably the simplest way is to represent the model uncertainty using a single deterministic variable [76]. It can also be described by a deterministic, input-dependent function [15]. Another way to express this uncertainty is to describe it by a random variable coming from a normal distribution and include the parameters of this distribution in the posterior distribution [32, 75, 76]. The parameters of the normal distribution from which the model uncertainty is originating can also be input-dependent functions (i.e. strain) [32, 75]. The model uncertainty can also be represented as a Gaussian process [47, 77, 78]. Some more formulations to describe model uncertainty can be found in [75].

As an example here, we consider a nonlinear curve (i.e. dashed line in Fig. 2-17(a)) as our true material response whilst the material response uses linear elasticity. Thirty measurements are generated artificially (see Fig. 2-17(a)). Model uncertainty is described by a random variable coming from a normal distribution with constant parameters and hence, the mean and standard deviation of this normal distribution appear as parameters in the posterior.

The marginal posteriors of the Young's modulus are presented in Fig. 2-17(b). One can observe that the incorporation of model uncertainty in this example results in a wider posterior distribution that includes the true value, although its MAP point is located further away from the true value. If the error in the strain is incorporated as well, the posterior at the true value increases even more.

The posterior predictions for these three cases are shown in Fig. 2-18. Incorporating model uncertainty clearly results in a wider prediction interval. If both the error in the strain and model uncertainty are incorporated however, the prediction interval becomes even wider and all measurement points and validation points are present within its bounds.

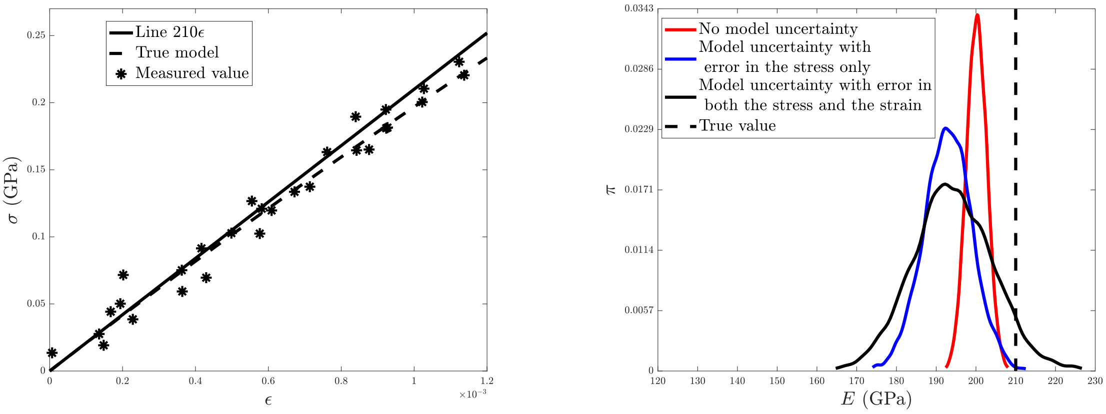

(a) True curve

(b) Marginal posteriors of Young's modulus

Figure 2-17: Model uncertainty: (a) The true stress-strain curve from which the measurements are generated, as well as the linear stress-strain curve with the true Young's modulus. (b) The marginal posterior distribution of the Young's modulus with no model uncertainty (red curve), with model uncertainty and error in the stress (blue curve) and with model uncertainty and error in both the stress and the strain measurements (black curve). Incorporating model uncertainty results in a posterior distribution that includes the true Young's modulus. In case the error in the strain is considered as well, the probability at the true Young's modulus increases even further.

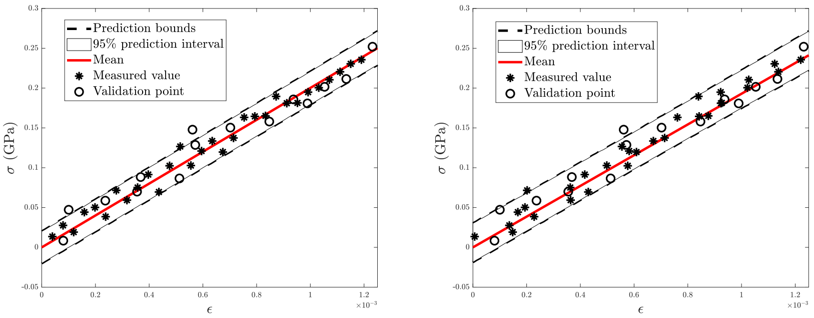

(a) Error in the stress

(b) Error in the stress and model uncertainty

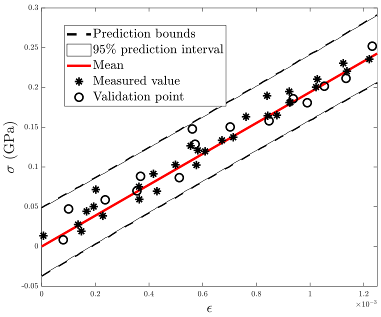

(c) Errors in the stress and strain and model uncertainty

Figure 2-18: Model uncertainty: The measurements, validation points and the posterior predictions. One can see that if model uncertainty is considered, the prediction interval becomes wider. Furthermore, only if model uncertainty as well as the errors in both the stress and the strain measurements are incorporated, all measured and validation points are inside the prediction interval.

2.7 Conclusions

Bayesian inference (BI) can be used to identify the parameters of a material model from experimental measurements. Unlike deterministic identification approaches (e.g. the standard least squares method), which result in a single value for each parameter, the result of BI is a parameter distribution. The parameter distribution is based on (1) a-priori knowledge about the parameters and (2) the acquired measurement data. Although the parameter distribution provides knowledge about the uncertainty of the parameters, it still assumes that only one parameter set is to be identified. This point has been addressed in an example given in Section 2.5.

Although BI has been employed in various studies for parameter identification, most may not be straightforward to understand for those who are new to the subject. In this chapter, we have aimed to explain BI in a basic manner. For this purpose, a number of Bayesian inference formulations are presented to identify elastic and elastoplastic material parameters from uniaxial tensile results. Elastic and elastoplastic material models are chosen for two reasons: (1) they are widely used in solid mechanics and (2) they include the most simple material behaviour (linear elasticity), as well as increasingly complex descriptions such as linear elasticity-nonlinear hardening, which entails C_0-continuous, implicit responses.

The following conclusions can be made based on the examples given in Section 2.5:

(1) The results of BI cannot directly be compared to those of the least squares method, since the result of BI is a distribution and that of the least squares method is a single value.

(2) If one wants to compare the two nevertheless, point estimators such as the mean and MAP point can be compared to the results of the least squares method. It is shown in Fig. 2-6 that the selected prior distribution may significantly influence the results. Fig. 2-6 also shows that the influence of the prior decreases significantly if the number of measurements increases.

(3) The standard deviations and correlations of the material parameters established using the ‘standard’ BI formulations presented in this chapter, do *not* reflect the heterogeneity of the material parameters. In other words, they are *not* representative for the standard deviations and correlations of the intrinsic material parameter distributions, but only for the level of uncertainty. The reason is that the formulations in this chapter still assume that a unique set of parameter values is the solution of the identification problem.

Chapter 3

Bayesian inference to identify parameters in viscoelasticity[1]

Abstract

This chapter discusses Bayesian inference (BI) as an approach to identify parameters in viscoelasticity. The aims are (i) to show that the prior has a substantial influence for viscoelasticity, (ii) to show that this influence decreases for an increasing number of measurements and (iii) to show how different types of experiments influence the identified parameters and their uncertainties. The standard linear solid model is the material description of interest and a relaxation test, a constant strain-rate test and a creep test are the tensile experiments focused on. The experimental data are artificially created, allowing us to make a one-to-one comparison between the input parameters and the identified parameter values. Besides dealing with the aforementioned aims, we believe that this chapter forms a comprehensible start for those interested in applying BI in viscoelasticity.

3.1 Introduction

A frequently employed approach to identify model parameters from a set of experimental data is the least squares method (LSM, see e.g. [8]). The standard LSM formulates the squared difference between the measured data and the model response in terms of the parameters of interest and minimises this difference with respect to the parameters of interest. Those parameters that minimise the difference are the resulting parameter values. The residual is a measure for how well the response fits the measurement data, but does not give insight in the uncertainty of the identified parameter values.

Some enhanced LSM formulations incorporate the statistical information of the measurement noise, in contrast to the standard LSM [79, 80]. Linearised approximations are however needed to extract the most probable parameter values and the covariance (i.e. a measure that shows how the random variables depend on each other). These approaches furthermore assume that the measurement noise is symmetrically distributed with a constant variance. In other words, they assume that the noise is independent of the measured value and that a particular positive noise realisation is equally possible as a negative realisation of the same magnitude [81].

Bayesian inference (BI) can be used to formulate an alternative identification approach, which may account for the fact that only a limited number of measurement data is available.

---

[1] Reproduced from: H. Rappel, L.A.A. Beex and S.P.A. Bordas, Bayesian inference to identify parameters in viscoelasticity, Mechanics of Time-Dependent Materials, 22 (2), (2018) 221-258.

It achieves this by incorporating an *a-priori* assumption on the parameter values. In practise, this entails that the user has to specify a prior distribution (i.e. the prior). The influence of this prior distribution can influence the identified parameter values significantly, but its influence decreases for an increasing number of measurement data [61, 82].

An intermediate result of BI is a probability density function (PDF) in terms of the parameters of interest, called the posterior distribution (or the posterior). Once the posterior distribution is established, its statistical characteristics need to be evaluated, e.g. the mean, the covariance matrix and the parameter values at which the PDF is maximum (called the 'maximum-a-posteriori-probability' or 'MAP' point). Most often, numerical methods like Markov chain Monte Carlo [25, 26] are necessary to extract the statistical characteristics from the posterior distribution. For posteriors with C_2-continuity, Laplace approximations can be applied to evaluate the quantities of the interest. The posterior is then approximated by a Gaussian distribution [43, 46].

The application of BI to identify (elastic) material parameters was started by Isenberg [41], to the best of our knowledge. For two decades afterwards, BI was not used for material parameter identification. When the developments started again, it was amongst others used for the identification of elastic constants from dynamic responses [42–44, 50, 60], the elastic constants of composite and laminate plates [49, 50, 52, 59] and spatially varying elastic constants [51]. An introduction to identify Young's moduli using BI is presented in [45].

Approaches based on BI are also used to identify material parameters in elastoplasticity. Some examples are the studies of Fitzenz et al. [55], Muto and Beck [53], Most [56], Rosić et al. [57] and Liu and Au [54]. Rappel et al. [82] have recently written an introduction of how BI can be employed for elastoplastic models. In an another study, Sarkar et al. [40] used the Bayesian approach to identify thermodynamical parameters of cementitious materials.

These days, BI is also used as an approach to evaluate the quality of different mechanical models with respect to each other, to which is referred as 'model selection'. Some examples are the studies of Madireddy et al. [61] for hyperelastic constitutive models for tissue, Oden et al. [62] for phenomenological models for tumour growth, Chiachío et al. [63] for models of damage progression in composites due to fatigue, and Babuška et al. [64] for fatigue descriptions of metals. Model selection is however out of the scope of this chapter.

BI is also used to identify viscoelastic parameters. Zhang et al. [83] used BI to characterise the Young's modulus of a viscoelastic polymer layer in a laminated structure. Their work includes a validation. Mehrez et al. [84] employed BI to identify the viscoelastic properties of aged and unaged asphalt. Miles et al. [85] applied BI to characterise the viscoelastic parameters of a dielectric elastomer undergoing finite deformation. Hernandez et al. [58] employed the Bayesian approach for the probabilistic identification of five viscoelastic parameters. Zhao and Pelegri [86] used BI together with a finite element model to identify the time constant of a Voigt-based tissue model. All mentioned studies (except [86]) are based on actual experimental data. Kenz et al. [87] compared asymptotic theory, bootstrapping, and Bayesian estimation for a viscoelastic wave propagation model. Also in this study, experimental data was used (for a homogeneous tissue-mimicking gel).

None of the mentioned BI studies for viscoelasticity have focused on the influence of the prior distribution however. Furthermore, none of them have investigated the influence of the number of measurement data. Except for Zhao and Pelegri [86] none of the studies for viscoelasticity are able to compare the resulting values with the input values. Finally, none of the aforementioned studies have compared the estimated parameter values for different types of tests (e.g. relaxation test, constant strain rate test and creep test). Hence, BI was used in the past to identify viscoelastic parameters, but if other prior distributions were selected, the number of measurements were different or other tests were used, the results of the aforementioned

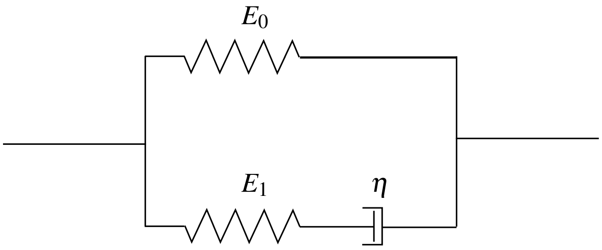

Figure 3-1: The one-dimensional spring-dashpot representation of the SLS model.

studies would be different.

The aim of this chapter is to show how viscoelastic parameters identified by BI are dependent on the selected prior distribution, the number of measurement data and the type of test. The standard linear solid (SLS) model is the employed viscoelastic description and a tensile relaxation test, a tensile constant strain-rate test and the creep test are the experiments of interest. The measurements are generated artificially, including the noise realisations. This allows us to compare the identified values with the input values and with the LSM values, in a controlled and thorough manner. In order to investigate if better parameter values are obtained by different types of tests, the values identified based on different tests are also compared to each other.

The structure of the chapter is as follows. Section 3.2 briefly discusses the SLS model. Section 3.3 presents the theoretical fundamentals of BI, the final expression of the posterior distribution for the SLS model and the three types of experiments. Section 3.4 discusses the MCMC method to numerically extract the most probable parameter values from the posterior distribution (including the associated covariances). Section 3.5 briefly discusses the LSM and genetic optimisation as the minimisation approach to find the parameter values identified by LSM. Section 3.6 presents the examples. This chapter is closed with some conclusions (Section 3.7).

3.2 Material model

Viscoelasticity can be used to describe the stress-strain-time relation of time-dependent materials. These materials show both viscous and elastic behaviour under deformation [88]. Well-known viscoelastic material models are the Maxwell model, the Kelvin-Voigt model, the standard linear solid (SLS) model and the generalised Maxwell model [88]. As the goal of this chapter is to identify the parameters of the SLS model, the remainder of this section considers this description.

The SLS model describes stress-relaxation and creep phenomena in viscoelastic systems with only one rate-dependent parameter [89]. In one dimension, the model can schematically be represented using two springs and a dashpot (see Fig. 3-1).

For uniaxial tension, the stress-strain-time relation of the SLS can be described by the following differential equation [90]:

$$\sigma + \frac{\eta}{E_1}\frac{\partial \sigma}{\partial t} = E_0\epsilon + (E_0 + E_1)\frac{\eta}{E_1}\frac{\partial \epsilon}{\partial t}, \tag{3.1}$$

where σ is the stress, ϵ is the strain, $\frac{\partial}{\partial t}$ denotes the derivative with respect to time, E_0 is the stiffness of the parallel spring, E_1 is the stiffness of the spring in series with the dashpot and η is the viscosity of the dashpot (see Fig.3-1).

In a tensile relaxation experiment in which strain ϵ_0 is applied infinitely fast and then kept constant, the stress-time relation during relaxation resulting from Eq. (3.1) reads:

$$\sigma(\mathbf{x}, t) = E_0\epsilon_0 + E_1\epsilon_0 \exp\big(- \frac{E_1 t}{\eta}\big), \tag{3.2}$$

where $\mathbf{x} = \begin{bmatrix} E_0 & E_1 & \eta \end{bmatrix}^T$ is the parameter vector. Fig. 3-2 shows the relaxation behaviour of Eq. (3.2) schematically.

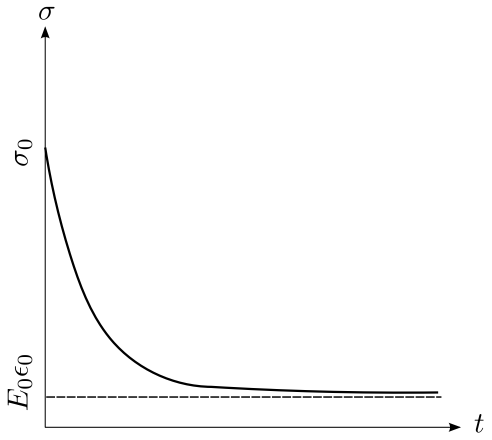

Figure 3-2: A schematic stress-time curve for one-dimensional stress relaxation of the SLS model. It is assumed that applied strain ϵ_0 is prescribed infinitely fast, resulting in $\sigma_0 = E_0\epsilon_0 + E_1\epsilon_0$.

For a constant strain-rate experiment in tension, in which the specimen is elongated with a constant strain-rate $\dot{\epsilon}_0$, the stress-time relation reads:

$$\sigma(\mathbf{x}, t) = E_0\dot{\epsilon}_0 t + \eta\dot{\epsilon}_0\Big(1 - \exp\big(- \frac{E_1 t}{\eta}\big)\Big). \tag{3.3}$$

The stress-time response of the constant strain-rate test is shown in Fig. 3-3 schematically.

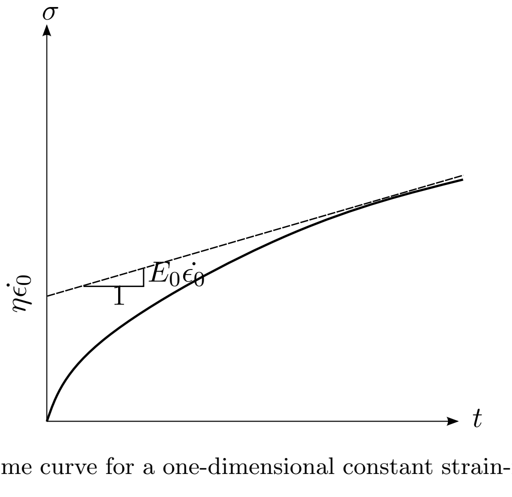

Figure 3-3: A schematic stress-time curve for a one-dimensional constant strain-rate test of the SLS model. The applied strain-rate is $\dot{\epsilon}_0$.

In a creep test in tension a constant tensile stress σ_0 is applied to the specimen infinitely fast, which is then kept constant. Strain is the quantity that is measured in this experiment.

The strain-time relation for a creep test of the SLS model reads:

$$\epsilon(\mathbf{x},t) = \frac{\sigma_0}{E_0} + \sigma_0\Big(\frac{1}{E_0+E_1} - \frac{1}{E_0}\Big)\exp\big(-\frac{E_0 E_1 t}{\eta(E_0+E_1)}\big). \tag{3.4}$$

Fig. 3-4 shows the behaviour of Eq. (3.4) schematically.

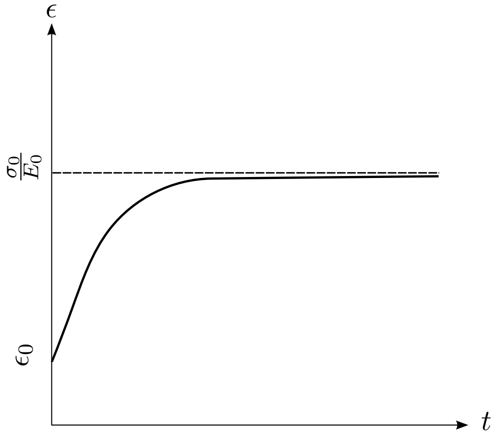

Figure 3-4: A schematic strain-time curve for a one-dimensional creep test in tension of the SLS model. It is assumed that the constant stress σ_0 is applied infinitely fast and then remains constant. The initial strain is $\epsilon_0 = \frac{\sigma_0}{E_0+E_1}$.

3.3 Bayesian inference

Identification approaches based on BI are less common than those based on the LSM. An intermediate result of Bayesian approaches is a probability density function (PDF) for the parameters to be identified (the so-called ‘posterior distribution’ or ‘posterior’). The posterior includes one’s prior knowledge about the parameters, as a PDF (the so-called ‘prior distribution’ or ‘prior’). Numerical techniques are most often required to extract the mean, the variance and MAP point from the posterior. In this chapter, MCMC is employed for this, which is discussed in Section 3.4.

This section focuses on the fundamentals of BI for continuous events (Subsection 3.3.1) and BI for the specific application to the SLS model and the tensile uniaxial relaxation, constant strain-rate and creep tests (Subsection 3.3.2).

Throughout this section capital letters denote random variables and bold ones denote vectors *and* matrices. An important issue for this chapter is to recognise that we only consider a statistical noise in the measured output, not in the experimental input. We thus consider the time measurements to be exact. In [82] and [32], we have treated double uncertainties however.

3.3.1 Fundamentals of Bayesian inference

Bayes’ theorem

Consider two continuous random variables $\mathbf{X} \in \mathbb{R}^n$ and $\mathbf{Y} \in \mathbb{R}^k$ with associated PDFs $\pi(\mathbf{x})$ and $\pi(\mathbf{y})$. Joint probability density function $\pi(\mathbf{x},\mathbf{y})$ expresses the probability that *both* $\mathbf{x}$ and $\mathbf{y}$ occur. This joint PDF can be expanded as:

$$\pi(\mathbf{x},\mathbf{y}) = \pi(\mathbf{x})\pi(\mathbf{y}|\mathbf{x}) = \pi(\mathbf{y})\pi(\mathbf{x}|\mathbf{y}), \tag{3.5}$$

where $\pi(\mathbf{y}|\mathbf{x})$ and $\pi(\mathbf{x}|\mathbf{y})$ are conditional PDFs. Conditional PDF $\pi(\mathbf{x}|\mathbf{y})$ expresses the probability that $\mathbf{x}$ occurs, if it is certain that $\mathbf{y}$ occurs. Using Eq. (3.5), the simplest form of Bayes' theorem can be written as:

$$\pi(\mathbf{x}|\mathbf{y}) = \frac{\pi(\mathbf{x})\pi(\mathbf{y}|\mathbf{x})}{\pi(\mathbf{y})}. \tag{3.6}$$

If we now consider $\mathbf{x}$ to be the vector with n identifiable parameters and $\mathbf{y}$ to be the vector with k measurements, then $\pi(\mathbf{x})$, $\pi(\mathbf{y}|\mathbf{x})$ and $\pi(\mathbf{x}|\mathbf{y})$ are the prior distribution (i.e. the PDF that represents the original belief or prior knowledge), the likelihood function (i.e. the PDF of the measured data $\mathbf{y}$, given unknown parameters $\mathbf{x}$) and the posterior distribution (i.e. the PDF of unknown parameters $\mathbf{x}$, given measured data $\mathbf{y}$). Furthermore, $\pi(\mathbf{y})$ is called the evidence and can be calculated using the law of total probabilities [67] as follows:

$$\pi(\mathbf{y}) = \int_{\mathbb{R}^n} \pi(\mathbf{x})\pi(\mathbf{y}|\mathbf{x})d\mathbf{x}. \tag{3.7}$$

As the measured data ($\mathbf{y}$) is already known after the experiment, the evidence in Eq. (3.6) ($\pi(\mathbf{y})$) is a constant number ($C \in \mathbb{R}^+$). It can thus be considered as a normalisation factor that ensures that the integral of the posterior ($\pi(\mathbf{x}|\mathbf{y})$) equals 1.

As the MAP point, the mean and the covariance matrix of the posterior are independent of this normalisation factor, it suffices to rewrite Eq. (3.6) as follows:

$$\pi(\mathbf{x}|\mathbf{y}) \propto \pi(\mathbf{x})\pi(\mathbf{y}|\mathbf{x}). \tag{3.8}$$

Eq. (3.8) is the expression for the posterior in which we are interested. Based on Eq. (3.8) it may be clear that in order to obtain the posterior distribution ($\pi(\mathbf{x}|\mathbf{y})$), one needs to define the prior ($\pi(\mathbf{x})$) and the likelihood function ($\pi(\mathbf{y}|\mathbf{x})$). The prior is the PDF that expresses one's *a-priori* knowledge. It can have a significant influence on the estimated MAP point, mean value and covariance matrix if the number of measurement data is small (see e.g. [48, 82] and the results section of this chapter). On the other hand, if the number of measurement data is large, the influence of the prior decreases [61].

Likelihood function

In order to construct the likelihood function, one needs to formulate the noise model (i.e. the uncertainty model) and determine the type of noise distribution (π_{noise}), including its parameters. This is often based on a calibration procedure of the experimental equipment. The most common noise model in the literature is the additive noise model, in which the noise distribution is independent of the theoretical model ($f(\mathbf{x}, t)$ in Fig. 3-5). Consequently, the noise only shifts around the theoretical model (see Fig. 3-5 again).

The additive noise model is also employed in this chapter. For a consideration of other types of noise models, the readers are referred to [48].

Given $\mathbf{X} \in \mathbb{R}^n$ as the vector with the parameters to be identified, $\mathbf{Y} \in \mathbb{R}^k$ as the vector with the measurements, $\mathbf{\Omega} \in \mathbb{R}^k$ as the noise vector, $\mathbf{f} : \mathbb{R}^n \to \mathbb{R}^k$ as the model dependent on the unknown parameters and using the additive noise model, one can write the relation between the measurements and the noise (i.e. the error in the measurements) as follows:

$$\mathbf{Y} = \mathbf{f}(\mathbf{X}) + \mathbf{\Omega}. \tag{3.9}$$

It can be noted that the measurements, $\mathbf{Y}$, are made at a specific experimental input $\mathbf{t}$. In the *relaxation* and *constant strain-rate* tests, the *stress* measurements ($\mathbf{Y}$) can be recognised

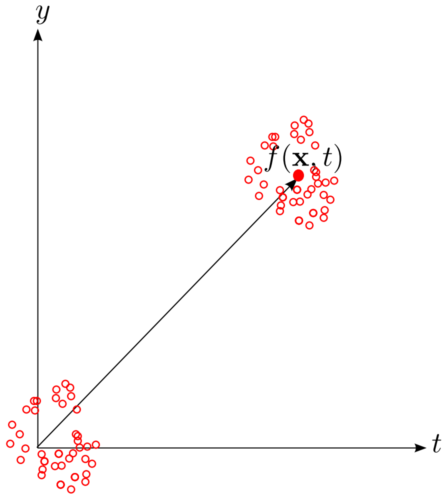

Figure 3-5: Schematic of additive noise. The noise around the known theoretical response $f(\mathbf{x},t)$ is independent of $f(\mathbf{x},t)$ [2]. In this representation, an error in the time measurements is included as well.

as the experimental output and the *strain* measurements for the *creep* test. The experimental input can be recognised as the time at which each stress or strain measurement is made ($\mathbf{t}$). In Eq. (3.9) we should thus have written $\mathbf{f}(\mathbf{X}|\mathbf{t})$. We have however chosen not to do this in order to simplify the notation.

If realisation $\mathbf{X} = \mathbf{x}$ is given for Eq. (3.9), the only random variable on the right-hand side is noise vector ($\boldsymbol{\Omega}$). Assuming that the noise vector and the unknown parameters are statistically independent, the noise distribution is the likelihood function:

$$\pi(\mathbf{y}|\mathbf{x}) = \pi_{\text{noise}}(\mathbf{y} - \mathbf{f}(\mathbf{x})), \tag{3.10}$$

where $\pi_{\text{noise}}(\boldsymbol{\omega})$ is the noise PDF (based on calibration experiments, see Subsection 3.6.1) and $\boldsymbol{\Omega} = \boldsymbol{\omega}$ is the noise realisation. Substituting Eq. (3.10) in Eq. (3.8) yields the posterior:

$$\pi(\mathbf{x}|\mathbf{y}) \propto \pi(\mathbf{x})\pi_{\text{noise}}(\mathbf{y} - \mathbf{f}(\mathbf{x})). \tag{3.11}$$

Once the posterior is established, one can calculate the statistical quantities of interest (e.g. the MAP point, the mean and the covariance matrix).

3.3.2 Bayesian inference for the uniaxial tensile relaxation, constant strain-rate and creep tests

In this subsection, we will employ the theory of the previous subsection to construct the posterior for the one-dimensional SLS model and our experiments of interest in uniaxial tension.

The parameters of the SLS model to be identified are E_0, E_1 and η. Hence, the parameter vector thus reads $\mathbf{x} = \begin{bmatrix} E_0 & E_1 & \eta \end{bmatrix}^T$.

First we start with the relaxation test, in which the model ($\mathbf{f}(\mathbf{X})$ in Eq. (3.9)) is given by Eq. (3.2) for one measurement. Employing these relations and considering only one measurement point (measurement point i), Eq. (3.9) reads:

$$y_i = E_0\epsilon_0 + E_1\epsilon_0 \exp\Big(-\frac{E_1 t_i}{\eta}\Big) + \omega_i, \tag{3.12}$$

where y_i is the measured stress, t_i is the time at which y_i is measured and ω_i originates from realisation $\Omega = \omega_i$.

To identify the statistical distribution of the measurement noise, calibration experiments must be performed (discussed in Subsection 3.6.1). For now we assume that these calibration experiments have exposed that a normal distribution with standard deviation S_{noise} can be used:

$$\pi_{\text{noise}}(\omega) = \frac{1}{\sqrt{2\pi}S_{\text{noise}}}\exp\Big(-\frac{\omega^2}{2S_{\text{noise}}^2}\Big), \tag{3.13}$$

where $\Omega = \omega$ is a realisation for the noise drawn from the distribution given by Eq. (3.13).

Using Eqs. (3.10) and (3.12) the likelihood function for measurement point i reads:

$$\pi(y_i|\mathbf{x}) = \pi_{\text{noise}}(y_i - E_0\epsilon_0 - E_1\epsilon_0\exp\big(-\frac{E_1t_i}{\eta}\big)) = \\ \frac{1}{\sqrt{2\pi}S_{\text{noise}}}\exp\Bigg(-\frac{\Big(y_i - E_0\epsilon_0 - E_1\epsilon_0\exp\big(-\frac{E_1t_i}{\eta}\big)\Big)^2}{2S_{\text{noise}}^2}\Bigg). \tag{3.14}$$

The next step is to choose the prior distribution ($\pi(\mathbf{x})$). As the material parameters cannot be negative, a modified normal distribution is selected:

$$\pi(\mathbf{x}) \propto \begin{cases} \exp\Big(-\frac{(\mathbf{x}-\overline{\mathbf{x}}_{\text{prior}})^T\mathbf{\Gamma}_{\text{prior}}^{-1}(\mathbf{x}-\overline{\mathbf{x}}_{\text{prior}})}{2}\Big) & \text{if } E_0 \geq 0 \text{ and } E_1 \geq 0 \text{ and } \eta \geq 0 \\ 0 & \text{otherwise} \end{cases}, \tag{3.15}$$

where $\overline{\mathbf{x}}_{\text{prior}}$ and $\mathbf{\Gamma}_{\text{prior}}$ are the mean vector and the covariance matrix of the prior, respectively. The values in $\overline{\mathbf{x}}_{\text{prior}}$ and $\mathbf{\Gamma}_{\text{prior}}$ must be selected by the user. After all, they are assumptions (as is the shape of the priori distribution).

Substituting Eqs. (3.3.2) and (3.15) in Eq. (3.8) yields the posterior for measurement point i as follows:

$$\pi(\mathbf{x}|y_i) \propto \exp\Bigg(-\Bigg[\frac{(\mathbf{x}-\overline{\mathbf{x}}_{\text{prior}})^T\mathbf{\Gamma}_{\text{prior}}^{-1}(\mathbf{x}-\overline{\mathbf{x}}_{\text{prior}})}{2} + \\ \frac{\Big(y_i - E_0\epsilon_0 - E_1\epsilon_0\exp\big(-\frac{E_1t_i}{\eta}\big)\Big)^2}{2S_{\text{noise}}^2}\Bigg]\Bigg). \tag{3.16}$$

Since the posterior for measurement point i can serve as the prior for measurement point $i+1$, the posterior for k measurement points reads:

$$\pi(\mathbf{x}|\mathbf{y}) \propto \exp\Bigg(-\Bigg[\frac{(\mathbf{x}-\overline{\mathbf{x}}_{\text{prior}})^T\mathbf{\Gamma}_{\text{prior}}^{-1}(\mathbf{x}-\overline{\mathbf{x}}_{\text{prior}})}{2} + \\ \frac{\sum_{i=1}^{k}\Big(y_i - E_0\epsilon_0 - E_1\epsilon_0\exp\big(-\frac{E_1t_i}{\eta}\big)\Big)^2}{2S_{\text{noise}}^2}\Bigg]\Bigg), \tag{3.17}$$

where $\pi(\mathbf{x}|\mathbf{y}) = \pi(\mathbf{x}|y_1, y_2, \cdots, y_k)$.

For the constant strain-rate test the only change is the employed model ($\mathbf{f}(\mathbf{X})$ in Eq. (3.9)) which is given by Eq. (3.3). Hence, for the same noise distribution (Eq. (3.13)) and the prior given in Eq. (3.15), the posterior distribution for k stress measurements reads:

$$\pi(\mathbf{x}|\mathbf{y}) \propto \exp\Bigg(- \Bigg[\frac{(\mathbf{x}-\overline{\mathbf{x}}_{\text{prior}})^T \mathbf{\Gamma}_{\text{prior}}^{-1} (\mathbf{x}-\overline{\mathbf{x}}_{\text{prior}})}{2} + \frac{\sum_{i=1}^{k} \Big(y_i - E_0 \dot{\epsilon_0} t_i - \eta \dot{\epsilon_0} \Big(1 - \exp\big(- \frac{E_1 t_i}{\eta}\big)\Big)\Big)^2}{2S_{\text{noise}}^2} \Bigg]\Bigg), \tag{3.18}$$

where $\dot{\epsilon_0}$ is the constant applied strain-rate and $\pi(\mathbf{x}|\mathbf{y}) = \pi(\mathbf{x}|y_1, y_2, \cdots, y_k)$.

As was mentioned previously the output for the creep test ($\mathbf{Y}$ in Eq. (3.9)) is the strain measurements. The model $\mathbf{f}(\mathbf{X})$ for this case is given by Eq. (3.4). We furthermore assume that the noise distribution is of the same for as for the previous two cases (Eq. (3.13)). Hence, using Eqs. (3.4), (3.11), (3.13) and (3.15) the final form of the posterior for the creep test with k strain measurements reads:

$$\pi(\mathbf{x}|\mathbf{y}) \propto \exp\Bigg(- \Bigg[\frac{(\mathbf{x}-\overline{\mathbf{x}}_{\text{prior}})^T \mathbf{\Gamma}_{\text{prior}}^{-1} (\mathbf{x}-\overline{\mathbf{x}}_{\text{prior}})}{2} + \frac{\sum_{i=1}^{k} \Big(y_i - \frac{\sigma_0}{E_0} - \sigma_0 \Big(\frac{1}{E_0+E_1} - \frac{1}{E_0}\Big) \exp\big(- \frac{E_0 E_1 t_i}{\eta(E_0+E_1)}\big)\Big)^2}{2S_{\text{noise}}^2} \Bigg]\Bigg), \tag{3.19}$$

where y_i is the measured strain at time t_i, $\mathbf{x}$ is the parameter vector $\begin{bmatrix} E_0 & E_1 & \eta \end{bmatrix}^T$ and σ_0 is the constant applied tensile stress.

Now the posterior is established for all three cases (relaxation, constant strain-rate and creep test), we will use the MCMC approach to identify the mean parameter values, the parameter values at which the posterior is maximum (i.e. the ‘MAP’ point) and the covariance matrix of the posterior. The covariance matrix is a measure for the possible spread of the parameter values, as well as how each parameter value depends on the others.

3.4 Markov chain Monte Carlo method (MCMC)

After establishing the posterior, one needs to determine the statistical properties of the posterior, such as the MAP point, the mean and the covariance matrix. These statistical quantities can be found analytically for straightforward cases, but often the use of a numerical technique cannot be avoided. One such a technique is Markov chain Monte Carlo sampling [68–70]. MCMC techniques are based on drawing samples from a target distribution (here the posterior) and numerically approximating the quantities of interest (e.g. the mean). Below, the Monte Carlo method and the adaptive Metropolis algorithm are discussed as means to obtain appropriate samples.

3.4.1 Monte Carlo method

The main goal of the Monte Carlo approach is to numerically approximate integrals of the following form:

$$\mathbf{I} = \int_{\mathbb{R}^n} \mathbf{g}(\mathbf{x})\pi(\mathbf{x})d\mathbf{x}, \tag{3.20}$$

where π is the target distribution (here posterior) and $\mathbf{g} : \mathbb{R}^n \to \mathbb{R}^k$ is an integrable function over $\mathbb{R}^n$. Having a set of samples $\{\mathbf{x}_i\}_i^N$ drawn from target PDF $\pi(\mathbf{x})$, the integral $\mathbf{I}$ can be numerically approximated as follows:

$$\hat{\mathbf{I}} = \frac{1}{N}\sum_{i=1}^{N} \mathbf{g}(\mathbf{x}_i), \tag{3.21}$$

where $\hat{\mathbf{I}}$ represents the numerical approximation of $\mathbf{I}$. Note that $\hat{\mathbf{I}}$ converges as follows [71]:

$$\lim_{N\to+\infty} \frac{1}{N}\sum_{i=1}^{N} \mathbf{g}(\mathbf{x}_i) = \mathbf{I}. \tag{3.22}$$

The numerical approximation of the components of the covariance matrix for $\mathbf{g}(\mathbf{x})$ ($\widehat{\boldsymbol{\Gamma}}_{\mathbf{g}}$) reads [24]:

$$(\widehat{\Gamma}_{\mathbf{g}})_{jm} = \frac{1}{N}\sum_{i=1}^{N} \Big(g_j(\mathbf{x}_i) - I_j\Big)\Big((g_m(\mathbf{x}_i) - I_m\Big), \; j = 1, 2, \cdots, k, \; m = 1, 2, \cdots, k. \tag{3.23}$$

In our case, we substitute $\mathbf{g}(\mathbf{x}) = \mathbf{x}$ and $\pi = \pi_{\text{post}}$ in the previous equations in order to obtain the following relation for the mean of the posterior:

$$\overline{\mathbf{x}}_{\text{post}} = \int_{\mathbb{R}^n} \mathbf{x}\pi_{\text{post}}(\mathbf{x})d\mathbf{x} = \lim_{N\to+\infty} \frac{1}{N}\sum_{i=1}^{N} \mathbf{x}_i. \tag{3.24}$$

The components of the covariance matrix of the posterior ($\widehat{\boldsymbol{\Gamma}}_{\text{post}}$) are furthermore approximated as follows:

$$(\widehat{\Gamma}_{\text{post}})_{jm} = \frac{1}{N}\sum_{i=1}^{N} \Big((x_i)_j - (\overline{x}_{\text{post}})_j\Big)\Big((x_i)_m - (\overline{x}_{\text{post}})_m\Big), \; j = 1, 2, \cdots, k, \; m = 1, 2, \cdots, k. \tag{3.25}$$

Assuming that the number of the drawn samples is large (i.e. N is large), the MAP point can be approximated as follows [71]:

$$\widehat{\mathbf{MAP}} = \underset{\mathbf{x}_{i;i=1,\ldots,N}}{\text{argmax}} \; \pi(\mathbf{x}_i). \tag{3.26}$$

In next subsection the standard and adaptive Metropolis algorithms are discussed as means to obtain appropriate samples. The adaptive Metropolis algorithm is employed in this chpater as the sampling approach.

3.4.2 The standard Metropolis algorithm

The Metropolis-Hastings approach is an often employed technique for sampling [71]. Its goal is to explore the target PDF (i.e. the posterior) by making a random walk through parameter space $\mathbf{x}$. The procedure accomplishes this by basing each new sample on the previous sample.

We start by the consideration of sample $\mathbf{x}_i$. The posterior is evaluated for this sample (resulting in $\pi_{\text{post}}(\mathbf{x}_i)$). Subsequently, a new sample $\mathbf{x}_p$ is proposed using a proposal distribution (q in Algorithm 3.1). If the value of the PDF at the proposed sample multiplied by the evaluation of the proposal distribution evaluated at $\mathbf{x}_i$, given the proposed sample ($q(\mathbf{x}_i|\mathbf{x}_p)$), is larger than the PDF at the current sample ($\pi(\mathbf{x}_i)$) multiplied by the evaluation of the proposal distribution at the proposed sample given the current sample ($q(\mathbf{x}_p|\mathbf{x}_i)$), the proposed sample will be accepted as the new sample. Otherwise, the sample will be accepted *or* rejected, based on the ratio r in Algorithm 3.1 and its comparison with a random number generated from a uniform PDF. If the ratio is less than the random number drawn from the uniform distribution, the proposed sample is rejected. If the ratio is larger, it is accepted. Algorithm 3.1 shows the standard Metropolis-Hastings algorithm in practice.

Algorithm 3.1 The standard Metropolis-Hastings algorithm

```
 1: select the initial sample $\mathbf{x}_0 \in \mathbb{R}^n$
 2: for $i = 0, 1, 2, ..., N-1$ do
 3:     draw $\mathbf{x}_p \in \mathbb{R}^n$ from the proposal distribution $q(\mathbf{x}_p|\mathbf{x}_i)$ in Eq. (3.29)
 4:     calculate the ratio $r(\mathbf{x}_i, \mathbf{x}_p) = \min\Big(1, \frac{\pi(\mathbf{x}_p)q(\mathbf{x}_i|\mathbf{x}_p)}{\pi(\mathbf{x}_i)q(\mathbf{x}_p|\mathbf{x}_i)}\Big)$
        ▷ $\pi(\cdot)$ denotes the target distribution (i.e. posterior).
 5:     draw $u \in [0, 1]$ from uniform probability density
 6:     if $r(\mathbf{x}_i, \mathbf{x}_p) \geq u$ then
 7:         $\mathbf{x}_{i+1} = \mathbf{x}_p$
 8:     else
 9:         $\mathbf{x}_{i+1} = \mathbf{x}_i$
10:     end if
11: end for
```

For a symmetric proposal distribution (i.e. transition kernel, q in Algorithm 3.1), one can write:

$$q(\mathbf{x}_i|\mathbf{x}_p) = q(\mathbf{x}_p|\mathbf{x}_i). \tag{3.27}$$

Using Eq. (3.27), line 4 of the algorithm can then be rewritten as:

$$r(\mathbf{x}_i, \mathbf{x}_p) = \min\Big(1, \frac{\pi(\mathbf{x}_p)}{\pi(\mathbf{x}_i)}\Big). \tag{3.28}$$

The convergence and stability of the algorithm can be checked by focusing for instance on the evolution of the mean value and the covariance matrix as a function of the number of the drawn samples [40]. The approximated distribution converges to the posterior if the approximated statistical quantities remain the same for an increase of the number of samples.

Factors that influence the efficiency of the algorithm are the proposal distribution (q) and the initial sample ($\mathbf{x}_0$) [48]. The most common proposal distribution for the Metropolis-Hastings algorithm (as employed in this chapter) is a normal distribution:

$$q(\mathbf{x}_i|\mathbf{x}_p) = q(\mathbf{x}_p|\mathbf{x}_i) \propto \exp\Big(-\frac{1}{2\gamma^2}\left\|\mathbf{x}_i - \mathbf{x}_p\right\|^2\Big), \tag{3.29}$$

where γ is the standard deviation, which can be tuned to increase the efficiency. In the work of Gelman et al. [72], $\gamma = \frac{2.38}{\sqrt{n}}$ is given as an efficient starting value, where n is the dimension of the posterior (i.e. the number of unknown parameters).

3.4.3 The adaptive Metropolis algorithm

The adaptive proposal (AP) is introduced by Haario et al. [73] to automatically tune γ and by doing so, increase the efficiency of the Metropolis algorithm. AP bases its updates on the knowledge of the posterior, gathered from previously drawn samples. The proposal distribution in the adaptive Metropolis algorithm reads:

$$q(\mathbf{x}_p|\mathbf{x}_i) \sim N(\mathbf{x}_i, \gamma^2\mathbf{R}_i), \tag{3.30}$$

where $N(\mathbf{x}_i, \gamma^2\mathbf{R}_i)$ denotes a normal distribution with mean $\mathbf{x}_i$ and covariance matrix $\gamma^2\mathbf{R}_i$, of size $n \times n$. γ is the initially selected standard deviation and $\mathbf{R}_i$ is updated based on the previous samples. Matrix $\mathbf{R}_i$ is established by first storing all i previous samples in matrix $\mathbf{K}$ of size $i \times n$. $\mathbf{R}_i$ is then computed as:

$$\mathbf{R}_i = \frac{1}{i-1}\widetilde{\mathbf{K}}^T\widetilde{\mathbf{K}}, \tag{3.31}$$

where $\widetilde{\mathbf{K}} = \mathbf{K} - \mathbf{K}_{\text{mean}}$ and $\mathbf{K}_{\text{mean}}$ reads:

$$\mathbf{K}_{\text{mean}} = \begin{bmatrix} \mathbf{k}_{\text{mean}} \\ \mathbf{k}_{\text{mean}} \\ \vdots \\ \mathbf{k}_{\text{mean}} \end{bmatrix}_{i\times n}, \tag{3.32}$$

with $\mathbf{k}_{\text{mean}}$ as a $1 \times n$ vector of the following form:

$$\mathbf{k}_{\text{mean}} = \frac{1}{i}\begin{bmatrix} \sum\limits_{j=1}^{i}(K)_{j1} & \sum\limits_{j=1}^{i}(K)_{j2} & \cdots & \sum\limits_{j=1}^{i}(K)_{jn} \end{bmatrix}. \tag{3.33}$$

In terms of $\widetilde{\mathbf{K}}$, one can rewrite the proposal distribution as follows:

$$N(\mathbf{x}_i, \gamma^2\mathbf{R}_i) \sim \mathbf{x}_i + \frac{\gamma}{\sqrt{i-1}}\widetilde{\mathbf{K}}^T N(0, \mathbf{I}_i), \tag{3.34}$$

where $\mathbf{I}_i$ is the identity matrix of size $i \times i$ and $N(0, \mathbf{I}_i)$ denotes an i-dimensional normal distribution. In this chapter, the proposal distribution is updated once per thousand samples, as it is inefficient to update the proposal distribution too often. Algorithm 3.2 shows the Metropolis-Hastings algorithm with the symmetric AP proposal (Eq. (3.34)).

3.5 Least squares method and genetic minimisation

3.5.1 The least squares method

The LSM is based on measuring the squared difference between the measurement data and the response of the model for the same experiment. Consequently, the squared difference is a function of the parameters to be identified. In order to obtain the parameter values that give the best model response for the measurement data, the squared difference is minimised with respect to the parameters. Those parameter values that minimise the squared difference are

Algorithm 3.2 The Metropolis-Hastings algorithm with symmetric AP proposal

```
select the initial sample $\mathbf{x}_0 \in \mathbb{R}^n$ and set $\gamma = \frac{2.38}{\sqrt{n}}$
for $i = 0, 1, 2, ..., N-1$ do
    draw $\mathbf{x}_p \in \mathbb{R}^n$ from the proposal distribution $q(\mathbf{x}_p|\mathbf{x}_i)$ in Eq. (3.34)
    calculate the ratio $r(\mathbf{x}_i, \mathbf{x}_p) = \min\Big(1, \frac{\pi(\mathbf{x}_p)}{\pi(\mathbf{x}_i)}\Big)$
    ▷ $\pi(\cdot)$ denotes the target distribution (i.e. posterior).
    draw $u \in [0,1]$ from uniform probability density
    if $r(\mathbf{x}_i, \mathbf{x}_p) \geq u$ then
        $\mathbf{x}_{i+1} = \mathbf{x}_p$
    else
        $\mathbf{x}_{i+1} = \mathbf{x}_i$
    end if
    per 1000 samples
        update matrix $\widetilde{\mathbf{K}}$
end for
```

the identified values. The difference that remains at the identified values (i.e. the residual) is a measure for how well the model fits the experimental data.

The squared difference $J(\mathbf{x}|\mathbf{y})$ for the one-dimensional SLS model and relaxation experiment in tension is:

$$J(\mathbf{x}|\mathbf{y}) = \frac{1}{2}\sum_{i=1}^{k}\Big(y_i - E_0\epsilon_0 - E_1\epsilon_0\exp\big(-\frac{E_1 t_i}{\eta}\big)\Big)^2, \tag{3.35}$$

In contrast to the Bayesian formulation, the noise distribution does not require to be known explicitly in the standard LSM of Eq. (3.35). This saves calibration efforts. It does however entail two assumptions about the noise: (1) it assumes an additive noise model and (2) it assumes that the noise is symmetrically distributed.

The parameter values that give the best match between the measurement data and the model response are denoted by $\mathbf{x}_{\text{LSM}}$. The squared difference must be minimised to obtain them. We are thus interested in the following:

$$\mathbf{x}_{\text{LSM}} = \text{argmin}_{\mathbf{x}}\ J(\mathbf{x}|\mathbf{y}), \tag{3.36}$$

where $\text{argmin}_{\mathbf{x}}$ gives us the values of $\mathbf{x}$ that minimise $J(\mathbf{x}|\mathbf{y})$.

3.5.2 Genetic optimisation

Numerous approaches can be employed to tackle the minimisation problem of Eq. (3.36). In this chapter, we employ genetic optimisation (GO). GO has the advantage that no initial guess is required. Instead, it searches for the optimum in a domain. This may be considered convenient for identification problems, because an appropriate initial guess for the parameters is not always trivial to choose. Another advantage is that GO finds the optimum in an entire, even it contains several local optima [91]. A particular advantage compared to the Newton-Raphson method is that GO is entirely derivative-free. Hence, no issues with the conditioning of Hessians occur (i.e. a squared matrix of second-order partial derivatives of a scalar valued function) [91].

The derivative-free character of GO entails some clear advantages as discussed above, but it also makes GO substantially slower than optimisation approaches using derivatives [92]. This can make the approach computationally prohibitive for large optimisation problems. For the case in this chapter however, this is not an issue, because the model is an equation (Eqs. (3.2) and (3.36)) and only three parameters are to be identified.

The GO algorithm for the problem defined in Eq. (3.36) starts with the seeding of numerous vectors in the parameter space. In fact, we start with 1000 vectors, given by $E_0 \in \{0.5, 1.5556, \cdots, 10\}$, $E_1 \in \{0.5, 1, \cdots, 5\}$ and $\eta \in \{50, 63.3333, \cdots, 170\}$. The squared difference (J) is computed for each of these vectors, and they are ranked based on their squared difference. The first 100 with the smallest squared difference are subsequently used to create new vectors, whilst the other ones are ignored. Each of the first 100 vectors will randomly choose 10 other vectors out of these 100 vectors (which may include the same vector more than once). With each partner vector j, vector i creates a new vector v, of which the values are established as follows:

$$E_0^v = (r_1^{E_0} E_0^i + (1 - r_1^{E_0}) E_0^j) r_2^{E_0}, \tag{3.37}$$

$$E_1^v = (r_1^{E_1} E_1^i + (1 - r_1^{E_1}) E_1^j) r_2^{E_1}, \tag{3.38}$$

and

$$\eta^v = (r_1^{\eta} \eta^i + (1 - r_1^{\eta}) \eta^j) r_2^{\eta}, \tag{3.39}$$

where $r_1^{E_0}$, $r_1^{E_1}$ and r_1^{η} are independently chosen from a uniform distribution in domain $[0, 1]$ and $r_2^{E_0}$, $r_2^{E_1}$ and r_2^{η} are independently chosen from a uniform distribution in domain $[0.95, 1.05]$.

For the newly created vectors, the squared difference is computed and the newly created vectors are ranked, together with the old vectors, based on their squared difference. Those 100 with the smallest squared difference (this can include old and new vectors) are then again used to create new vectors and the process is repeated for 50 generations.

3.6 Results

This section presents the results of the Bayesian framework for the SLS model. The main points we focus on are how the number of measurement points affects the results and the influence of the prior, and how the three different tests influence the results. However, we start with the calibration of the measurement noise for the relaxation experiment.

3.6.1 Noise calibration

In this subsection, we briefly discuss a procedure to identify the noise model, the noise distribution and its parameters. The noise is artificially created and hence, this subsection only aims to outline a procedure of how to identify the noise. The noise here is generated using an additive noise model and a normal distribution with a zero mean and $S_{\text{noise}} = 0.5$ MPa. The aim here is thus to find this back. We only focus on the identification of the noise in the relaxation test, because the procedure is principally the same for the other two tests (note that the output y for the creep test is the measured strain).

We start with a test without specimens. The stress-time measurements of these tests show that the noise in the stress behaves according to a normal distribution with a zero mean and a standard deviation S_{noise} (see Fig. 3-6(a)). No noise in the time is observed.

Now we would like to know if this distribution depends on the measured stress. Therefore, relaxation tests on a calibration specimen (of which parameters E_0, E_1 and η are known) are performed. Some schematic results are shown in Fig. 3-6(b). The results show that the noise distribution does not evolve and only shifts with the exact response of the calibration specimen (shown by the bold black curve in Fig. 3-6(b)).

The artificially created calibration experiments show that the additive model can be used to describe the uncertainty and a normal distribution with a zero mean and a standard deviation of S_{noise} pollutes the stress measurements.

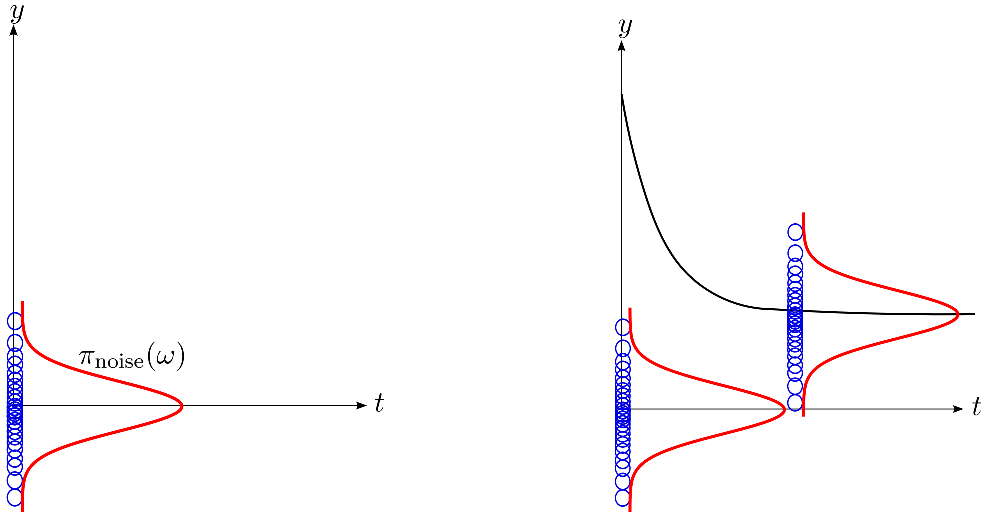

(a) The results of the 'calibration tests' without specimen

(b) The results of the 'calibration tests' with calibration specimen, together with those without specimen

Figure 3-6: Schematic of the stress-time measurements (blue circles) of the 'calibration tests', including the noise distributions (red curves). The stress-time relation of the calibration specimen is presented by the bold black curve in (b). The noise distribution shifts to the curve of the calibration sample, meaning that the additive noise model can be used to describe the uncertainty.

3.6.2 Identification of the SLS parameters using the relaxation test and two measurements

Bayesian inference

In this section we consider a relaxation experiment in tension on a specimen with $E_0 = 3.9455$ MPa, $E_1 = 2.9636$ MPa and $\eta = 136.8035$ MPa.s. The noise distribution is furthermore identified in Subsection 3.6.1. The standard deviation of this normal distribution is identified as $S_{\text{noise}} = 0.5$ MPa.

In the first example, we consider only two measurements: $y_1 = 4.1598$ MPa and $y_2 = 1.9220$ MPa, measured at $t_1 = 10$ s and $t_2 = 80$ s, respectively. The measurements are made in the fast decaying part of the stress-time response (i.e. the nonasymptotic part of the curve in Fig. 3-2). The prior is chosen to follow Eq. (3.15) with the following mean and covariance matrix:

$$\overline{\mathbf{x}}_{\text{prior}} = \begin{bmatrix} 5.5 \\ 2 \\ 110 \text{ s} \end{bmatrix} \text{ MPa}, \ \mathbf{\Gamma}_{\text{prior}} = \begin{bmatrix} 1 & 0 & 0 \\ 0 & 0.4444 & 0 \\ 0 & 0 & 400 \text{ s}^2 \end{bmatrix} \text{MPa}^2. \tag{3.40}$$

This yields a posterior in the form of Eq. (3.3.2). We run an MCMC chain of 10^4 samples and we 'burn' the first 3000 samples (meaning that the first 3000 samples are not used to determine the mean, the covariance matrix and the MAP estimate). The result of this reads:

$$\overline{\mathbf{x}}_{\text{post}} = \begin{bmatrix} 4.7082 \\ 2.4488 \\ 106.9068 \text{ s} \end{bmatrix} \text{ MPa}, \ \boldsymbol{\Gamma}_{\text{post}} = \begin{bmatrix} 0.3253 & -0.0573 & -1.4514 \text{ s} \\ -0.0573 & 0.3487 & 0.3816 \text{ s} \\ -1.4514 \text{ s} & 0.3816 \text{ s} & 373.7074 \text{ s}^2 \end{bmatrix} \text{ MPa}^2, \tag{3.41}$$

and

$$\mathbf{MAP} = \begin{bmatrix} 4.6841 \\ 2.3969 \\ 106.6689 \text{ s} \end{bmatrix} \text{ MPa}. \tag{3.42}$$

Fig. 3-7 shows the samples drawn by the adaptive MCMC approach and their projections on the planes $E_0 - E_1$, $E_1 - \eta$ and $\eta - E_0$. Fig. 3-8 shows the 95% credible region (i.e. the region that contains 95% of the posterior, approximated by an ellipsoid) and the associated stress-time responses. The wide credible region is partially caused by the large standard deviation of the noise distribution ($S_{\text{noise}} = 0.5$ MPa).

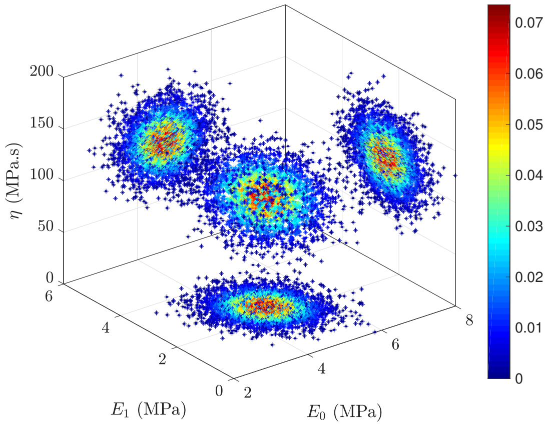

Figure 3-7: Samples drawn by the adaptive MCMC approach to approximate the posterior distribution. The projections of the samples on three planes are also presented.

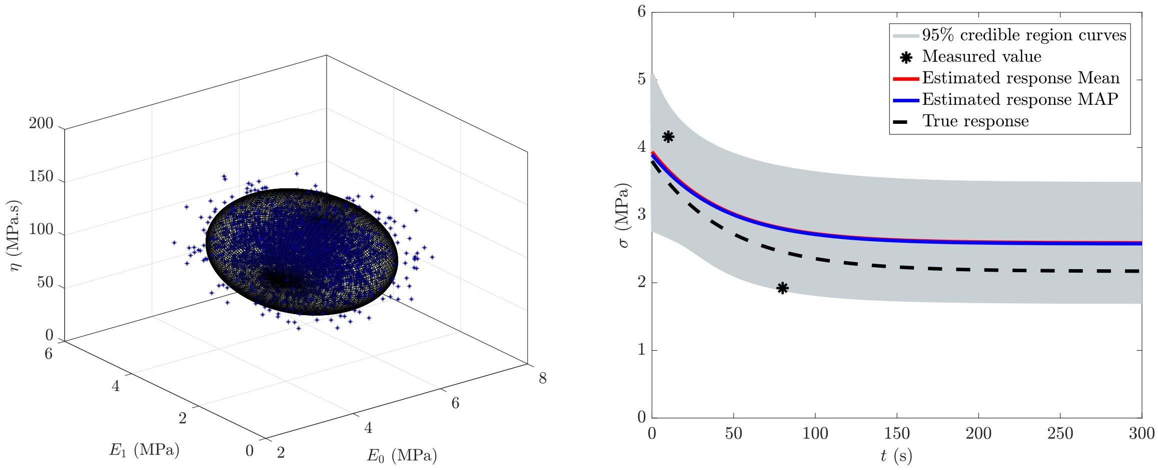

(a) The 95% credible region

(b) The measurements and the stress-time curves

Figure 3-8: The 95% credible region of the posterior distribution (a) and the stress-time response associated with the 95% credible region, together with the two measurements, the true response, the response associated with the mean and the response associated with the MAP point (b). The 95% credible region (approximated by an ellipsoid) contains 95% of the posterior. Note that the responses associated with the mean and the MAP point are practically on top of each other.

The prior in BI may have a significant effect on the posterior for a small number of measurements (as is the case here). To illustrate this influence, we now change the mean of the prior, while keeping the covariance matrix of the prior constant. The following covariance matrix is used for the prior:

$$\mathbf{\Gamma}_{\text{prior}} = \begin{bmatrix} 1 & 0 & 0 \\ 0 & 0.4444 & 0 \\ 0 & 0 & 277.7778 \text{ s}^2 \end{bmatrix} \text{MPa}^2. \tag{3.43}$$

Figs. 3-9 to 3-11 show that the mean value of a particular parameter in the posterior mostly depends on the mean value of that same parameter in the prior (e.g. $\overline{E}_1^{\text{post}}$ depends mostly on the selected value of $\overline{E}_1^{\text{prior}}$). For $\overline{E}_0^{\text{post}}$ however, $\overline{E}_0^{\text{prior}}$ and $\overline{E}_1^{\text{prior}}$ both have an influence.

$\overline{\eta}^{\text{post}}$ almost entirely depends on $\overline{\eta}^{\text{prior}}$. This is caused by the fact that η has relatively the smallest influence on the stress-time relation. After all, E_0 is responsible for the plateau stress and E_1 (together with E_0) is responsible for the initial stress at the start of the relaxation (see Fig. 3-2). Parameters η and E_1 are however together responsible for the time scale at which the initial stress relaxes to the plateau stress (see Eq. (3.2)). Consequently, the sensitivity of the stress-time relation is the smallest for η of the three parameters.

Fig. 3-12 shows the effect of the mean of the prior on the diagonal components of the posterior ($\mathbf{\Gamma}_{\text{post}}$). The results show that the mean of the prior only affects $(\Gamma_{\text{post}})_{33}$ in a systematic manner. An increasing $\overline{\eta}^{\text{prior}}$ leads to an increase of $(\Gamma_{\text{post}})_{33}$, whereas an opposite effect can be observed for $\overline{E}_0^{\text{prior}}$ and $\overline{E}_1^{\text{prior}}$.

The effect of the selected mean of the prior on the off-diagonal components of the $\mathbf{\Gamma}_{\text{post}}$ is shown in Fig. 3-13. The prior's mean hardly has a systematic influence on the off-diagonal components.

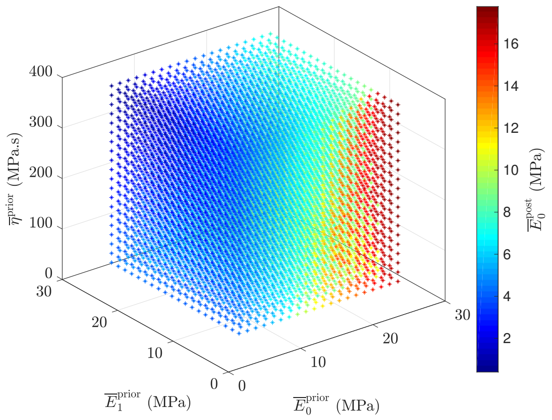

Figure 3-9: The mean value of E_0 of the posterior ($\overline{E}_0^{\text{post}}$) as a function of the mean values of the prior ($\overline{E}_0^{\text{prior}}$, $\overline{E}_1^{\text{prior}}$ and $\overline{\eta}^{\text{prior}}$). $\overline{E}_0^{\text{post}}$ is mostly dependent on the selected value of $\overline{E}_0^{\text{prior}}$ and $\overline{E}_1^{\text{prior}}$, whereas $\overline{\eta}^{\text{prior}}$ has substantially less influence.

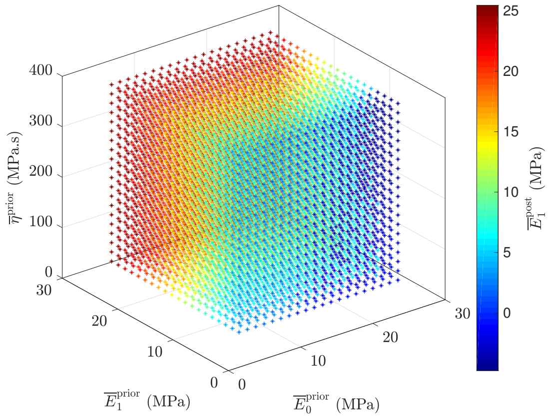

Figure 3-10: The mean value of E_1 of the posterior ($\overline{E}_1^{\text{post}}$) as a function of the mean values of the prior ($\overline{E}_0^{\text{prior}}$, $\overline{E}_1^{\text{prior}}$ and $\overline{\eta}^{\text{prior}}$). $\overline{E}_1^{\text{post}}$ is mostly dependent on the selected value of $\overline{E}_1^{\text{prior}}$, compared to $\overline{E}_0^{\text{prior}}$ and $\overline{\eta}^{\text{prior}}$.

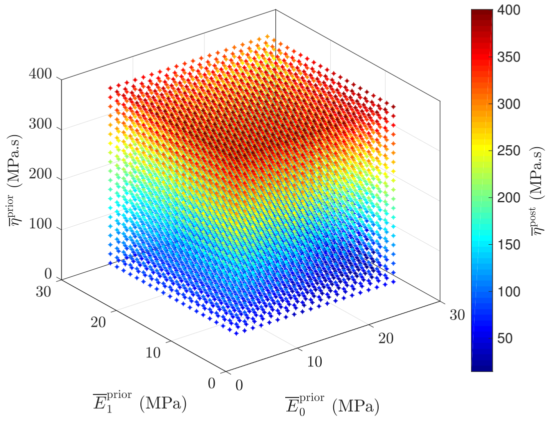

Figure 3-11: The mean value of η of the posterior ($\overline{\eta}^{\text{post}}$) as a function of the mean values of the prior ($\overline{E}_0^{\text{prior}}$, $\overline{E}_1^{\text{prior}}$ and $\overline{\eta}^{\text{prior}}$). $\overline{\eta}^{\text{post}}$ depends highly on the selected value of $\overline{\eta}^{\text{prior}}$, compared to the values of $\overline{E}_0^{\text{prior}}$ and $\overline{E}_1^{\text{prior}}$.

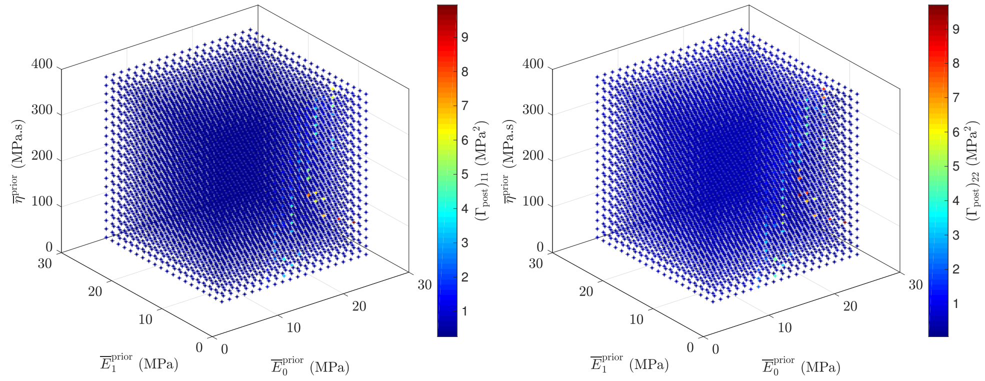

(a) Effect of $\overline{\mathbf{x}}_{\text{prior}}$ on $(\Gamma_{\text{post}})_{11}$ (b) Effect of $\overline{\mathbf{x}}_{\text{prior}}$ on $(\Gamma_{\text{post}})_{22}$

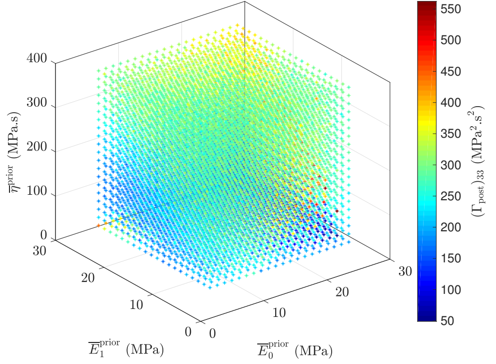

(c) Effect of $\overline{\mathbf{x}}_{\text{prior}}$ on $(\Gamma_{\text{post}})_{33}$

Figure 3-12: The effect of the mean of the prior on the diagonal components of the posterior's covariance matrix. Only $(\Gamma_{\text{post}})_{33}$ is systematically influenced by the mean of the prior.

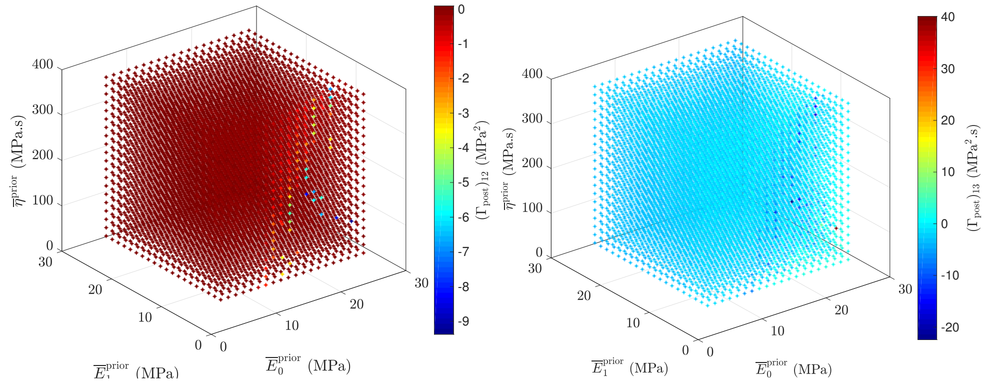

(a) Effect of $\overline{\mathbf{x}}_{\text{prior}}$ on $(\Gamma_{\text{post}})_{12}$ (b) Effect of $\overline{\mathbf{x}}_{\text{prior}}$ on $(\Gamma_{\text{post}})_{13}$

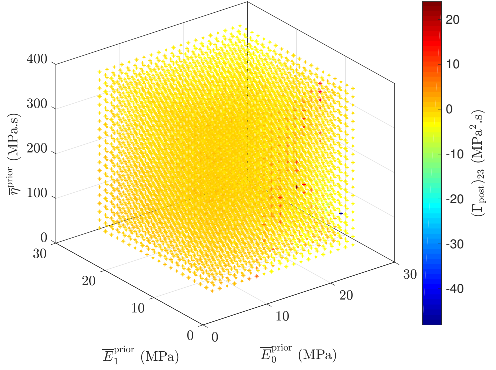

(c) Effect of $\overline{\mathbf{x}}_{\text{prior}}$ on $(\Gamma_{\text{post}})_{23}$

Figure 3-13: The effect of the mean of the prior on the off-diagonal components of the posterior's covariance matrix. The prior's mean does not seem to have a systematic influence.

Now we will look at the effect of the prior's covariance matrix on the posterior. We will keep the mean of the prior constant in this exercise. To investigate the effect of the prior's covariance matrix, the modified normal distribution given in Eq. (3.15) is selected with following mean:

$$\overline{\mathbf{x}}_{\text{prior}} = \begin{bmatrix} 6 \\ 3 \\ 110\text{ s} \end{bmatrix} \text{ MPa}, \tag{3.44}$$

We have chosen this prior's mean, because it is located relatively far from $\overline{\mathbf{x}}_{\text{prior}} = \begin{bmatrix} 0 & 0 & 0 \end{bmatrix}^T$ so that we can investigate the influence of relative large components of the prior's covariance matrices.

Figs. 3-14 to 3-16 show the effect of the different diagonal components of the prior covariance matrix ($(\Gamma_{\text{prior}})_{11}$, $(\Gamma_{\text{prior}})_{22}$ and $(\Gamma_{\text{prior}})_{33}$) on the mean of the posterior. The results show that $\overline{E}_0^{\text{post}}$ mostly depends on $(\Gamma_{\text{prior}})_{11}$ and for an increase of $(\Gamma_{\text{prior}})_{11}$, the influence on $\overline{E}_0^{\text{post}}$ decreases. $\overline{E}_1^{\text{post}}$ is hardly influenced by $(\Gamma_{\text{prior}})_{33}$. All components of the prior's covariance matrix are of influence on $\overline{\eta}^{\text{post}}$.

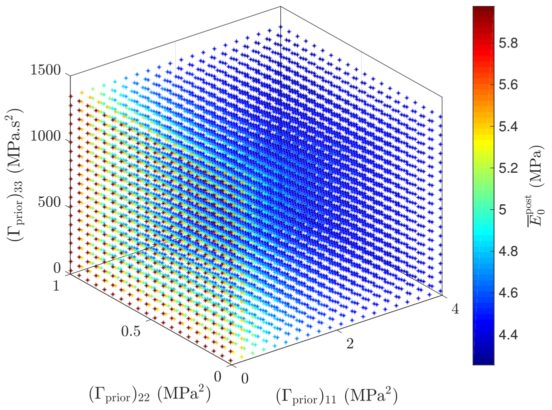

Figure 3-14: The effect of $\mathbf{\Gamma}_{\text{prior}}$ on $\overline{E}_0^{\text{post}}$. Except for $(\Gamma_{\text{prior}})_{11}$, the diagonal components of the prior's covariance matrix hardly have an influence on $\overline{E}_0^{\text{post}}$.

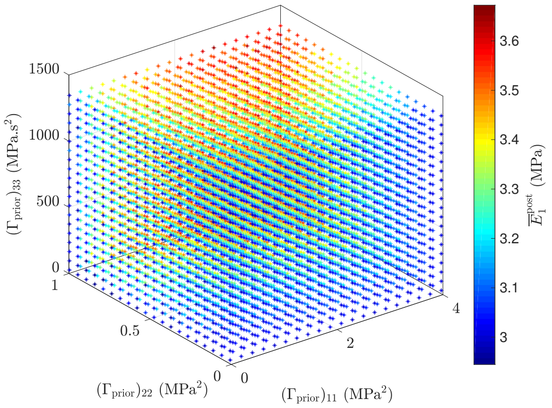

Figure 3-15: The effect of $\mathbf{\Gamma}_{\text{prior}}$ on $\overline{E}_1^{\text{post}}$. $\overline{E}_1^{\text{post}}$ is influenced by $(\Gamma_{\text{prior}})_{11}$ and $(\Gamma_{\text{prior}})_{22}$, but not by $(\Gamma_{\text{prior}})_{33}$.

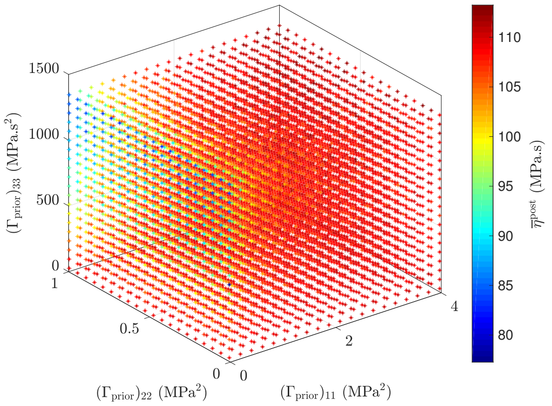

Figure 3-16: The effect of $\mathbf{\Gamma}_{\text{prior}}$ on the estimated value for $\overline{\eta}^{\text{post}}$. All diagonal components of the prior's covariance matrix are of influence.

The effect of the prior's covariance matrix on the components of the posterior's covariance matrix $\mathbf{\Gamma}_{\text{post}}$ is shown in Figs. 3-17 and 3-18. The diagonal components of the posterior's covariance matrix clearly depend mostly on their equivalents in the prior's covariance matrix. For the off-diagonal components Fig. 3-18 shows that $(\Gamma_{\text{post}})_{12}$ is mostly influenced by $(\Gamma_{\text{prior}})_{11}$ and $(\Gamma_{\text{prior}})_{22}$. $(\Gamma_{\text{post}})_{13}$ depends on all diagonal components, and $(\Gamma_{\text{post}})_{23}$ is influenced by $(\Gamma_{\text{prior}})_{22}$ and $(\Gamma_{\text{prior}})_{33}$.

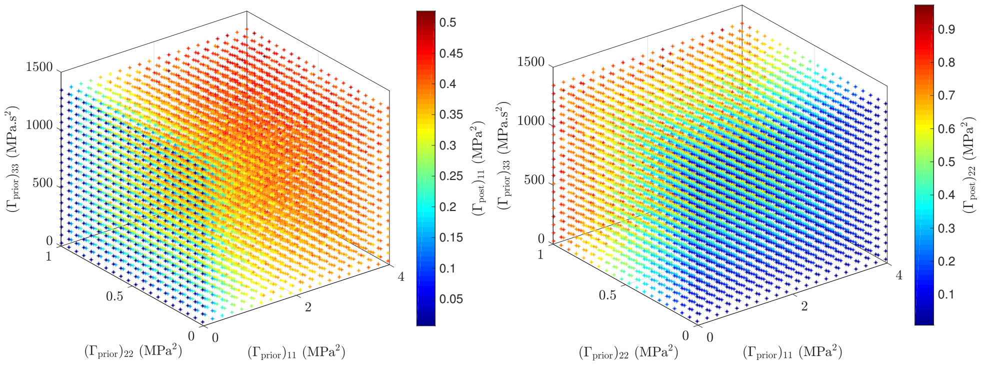

(a) Effect of $\mathbf{\Gamma}_{\text{prior}}$ on $(\Gamma_{\text{post}})_{11}$ (b) Effect of $\mathbf{\Gamma}_{\text{prior}}$ on $(\Gamma_{\text{post}})_{22}$

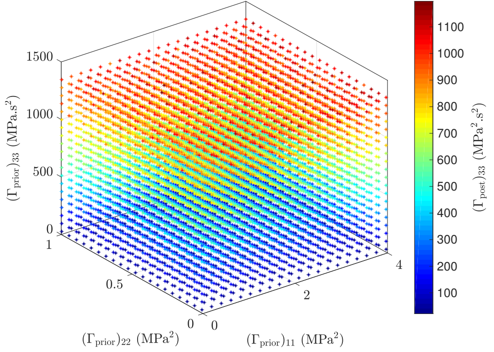

(c) Effect of $\mathbf{\Gamma}_{\text{prior}}$ on $(\Gamma_{\text{post}})_{33}$

Figure 3-17: The effect of $\mathbf{\Gamma}_{\text{prior}}$ on the diagonal components of the posterior's covariance matrix. Each diagonal component is mostly dependent on its equivalent in the prior covariance matrix.

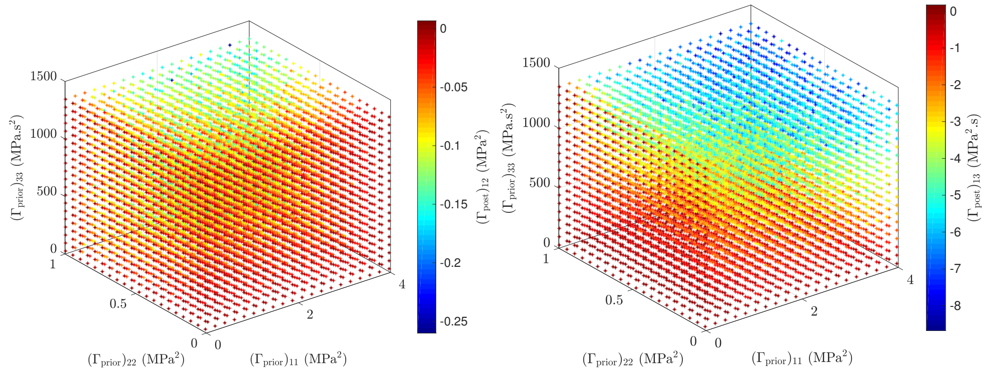

(a) Effect of $\mathbf{\Gamma}_{\text{prior}}$ on $(\Gamma_{\text{post}})_{12}$ (b) Effect of $\mathbf{\Gamma}_{\text{prior}}$ on $(\Gamma_{\text{post}})_{13}$

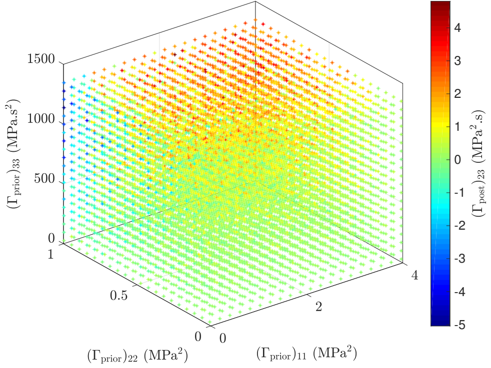

(c) Effect of $\mathbf{\Gamma}_{\text{prior}}$ on $(\Gamma_{\text{post}})_{23}$

Figure 3-18: The effect of $\mathbf{\Gamma}_{\text{prior}}$ on the off-diagonal components of the posterior's covariance matrix. $(\Gamma_{\text{post}})_{12}$ is mostly influenced by $(\Gamma_{\text{prior}})_{11}$ and $(\Gamma_{\text{prior}})_{22}$. $(\Gamma_{\text{post}})_{13}$ depends on all diagonal components and $(\Gamma_{\text{post}})_{23}$ is influenced by $(\Gamma_{\text{prior}})_{22}$ and $(\Gamma_{\text{prior}})_{33}$.

Least squares method

As the number of parameters to be identified is three and we only have two measurements, the minimisation of the objective function in the LSM ($J(\mathbf{x}|\mathbf{y})$ in Eqs. (3.35) and (3.36)) is ill-posed. This means that no unique solution to the minimisation problem of Eq. (3.32) exists. Consequently, a wide range of parameter sets can be obtained. Fig. 3-19 shows some possible curves generated based on the results of running the GO routine described in Subsection 3.5.2 several times. Note that the various curves obtained for the LSM do not represent any uncertainty as the curves created using the 95% credible region in the Bayesian approach. The bounds between which any possible curve of the LSM is located are presented by the two blue curves in Fig. 3-19.

Hence, for two measurements a large difference between the Bayesian approach and the LSM occurs. After all, the LSM case is ill-posed, whereas the prior in BI regularises the Bayesian framework.

3.6.3 Identification of the SLS parameters using the relaxation test and more than two measurements

In the next example, we add another three measurements to the two measurements of the previous subsection and investigate how this influences the results of the Bayesian framework as well as those of the LSM. The modified normal distribution given in Eq. (3.15) with the mean and covariance matrix given in Eq. (3.40) is selected as the prior distribution. Running

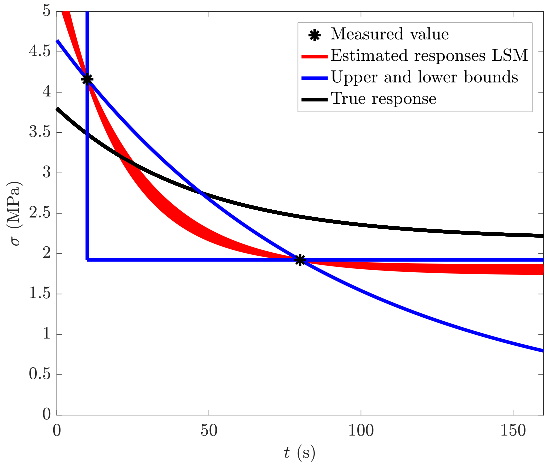

Figure 3-19: Different curves (red) associated with the parameters identified by the LSM due to ill-posedness. All the curves are made for the same measurements and each time that the LSM is applied as an identification approach the identified values lead to a different curve. However, in the Bayesian approach the problem is regularised by the prior and hence, it is not ill-posed. Note that the estimated responses by the LSM do not represent any uncertainty.

the MCMC chain for 10^4 samples, whilst burning the first 3000 samples, yields:

$$\overline{\mathbf{x}}_{\text{post}} = \begin{bmatrix} 4.8354 \\ 2.4069 \\ 109.7946\ \text{s} \end{bmatrix} \text{ MPa},\ \boldsymbol{\Gamma}_{\text{post}} = \begin{bmatrix} 0.1453 & -0.0328 & -1.4935\ \text{s} \\ -0.0328 & 0.3392 & 0.6262\ \text{s} \\ -1.4935\ \text{s} & 0.6262\ \text{s} & 361.5418\ \text{s}^2 \end{bmatrix} \text{ MPa}^2, \tag{3.45}$$

and

$$\mathbf{MAP} = \begin{bmatrix} 4.8463 \\ 2.4558 \\ 110.6589\ \text{s} \end{bmatrix} \text{ MPa}. \tag{3.46}$$

The values identified by the LSM are:

$$\mathbf{x}_{\text{LSM}} = \begin{bmatrix} 4.1156 \\ 4.6433 \\ 199.5536\ \text{s} \end{bmatrix} \text{ MPa}. \tag{3.47}$$

Comparing Eqs. (3.45), (3.47) and the true values, one can see that the errors of E_1^{LSM} and η^{LSM} are larger than of $\overline{E}_1^{\text{post}}$ and $\overline{\eta}^{\text{post}}$. This is thanks to the prior knowledge used in the Bayesian framework. One should however note that if the number of measurements is small, the selection of the prior's mean far from the true values and small components for the prior's covariance matrix would lead to a larger error. After all, the Bayesian framework aims to account for the fact that only a limited number of measurement points are available by incorporating a prior distribution. It is therefore questionable if a direct comparison between the LSM results and the posterior's mean and MAP point is truly valid at all.

The stress-time curves associated with the 95% credible region are given in Fig. 3-20. Increasing the number of measurements clearly leads to a narrower credible region (i.e. a smaller uncertainty, cf. Fig. 3-8(b)).

To study the effect of the prior's mean on the posterior's mean, we again show the posterior's

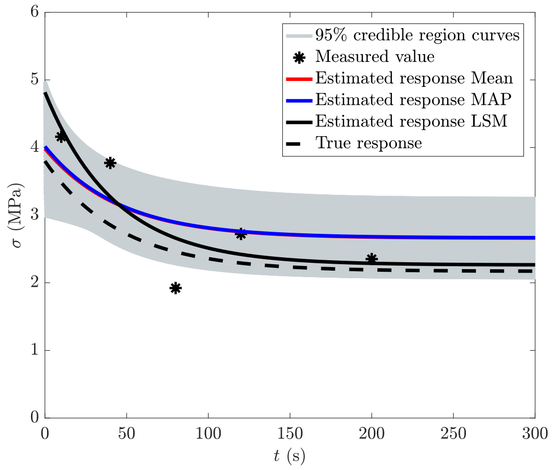

Figure 3-20: The stress-time curves for the relaxation test with five measurements. Increasing the number of the measurements leads to a narrower region (cf. Fig. 3-8(b)). This means that the uncertainty decreases as the number of measurements increases. Note that the responses associated with the mean and the MAP point are almost on top of each other.

mean values as functions of the prior's mean, see Fig. 3-21. Comparing Fig. 3-21 with 3-9 shows that an increasing number of measurements results in a smaller dependency of $\overline{E}_0^{\text{post}}$ on $\overline{\mathbf{x}}_{\text{prior}}$. This is also true for $\overline{E}_1^{\text{post}}$ and η^{post}, but this cannot well be observed by comparing Figs. 3-21 and 3-9.

In the next example the number of measurements is increased to ten. Assuming the same prior distribution given in Eq. (3.15) with $\overline{\mathbf{x}}_{\text{prior}}$ and $\mathbf{\Gamma}_{\text{prior}}$ given in Eq. (3.40) the mean, covariance matrix and MAP point read:

$$\overline{\mathbf{x}}_{\text{post}} = \begin{bmatrix} 4.6381 \\ 2.4154 \\ 107.4595 \text{ s} \end{bmatrix} \text{ MPa}, \ \mathbf{\Gamma}_{\text{post}} = \begin{bmatrix} 0.0812 & -0.0143 & -1.4925 \text{ s} \\ -0.0143 & 0.3043 & 0.8244 \text{ s} \\ -1.4925 \text{ s} & 0.8244 \text{ s} & 359.5813 \text{ s}^2 \end{bmatrix} \text{ MPa}^2, \tag{3.48}$$

and

$$\mathbf{MAP} = \begin{bmatrix} 4.6507 \\ 2.4299 \\ 106.5064 \text{ s} \end{bmatrix} \text{ MPa}. \tag{3.49}$$

The estimated values using the LSM are:

$$\mathbf{x}_{\text{LSM}} = \begin{bmatrix} 4.4661 \\ 3.9303 \\ 121.0358 \text{ s} \end{bmatrix} \text{ MPa}. \tag{3.50}$$

Fig. 3-22 shows the associated stress-time curves. As the number of measurements is increased compared to the previous examples, the responses associated with the 95% credible region become more localised (i.e. the uncertainty decreases, cf. Figs. 3-8(b) and 3-21).

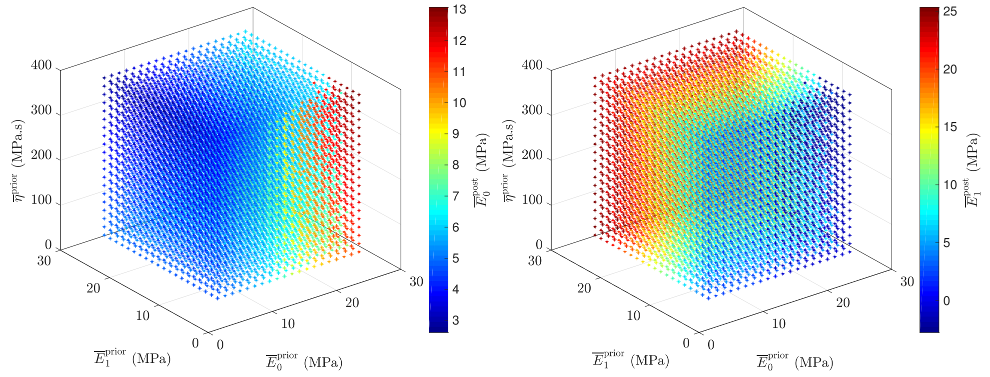

(a) Effect of $\overline{\mathbf{x}}_{\rm prior}$ on $\overline{E}_0^{\rm post}$ (b) Effect of $\overline{\mathbf{x}}_{\rm prior}$ on $\overline{E}_1^{\rm post}$

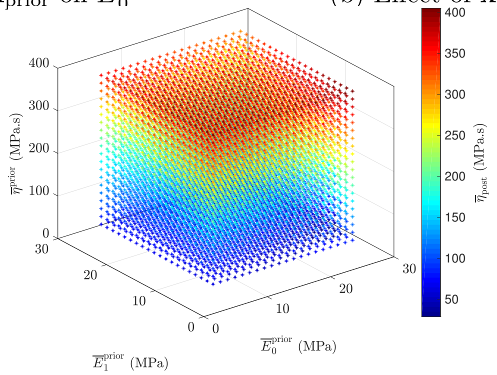

(c) Effect of $\overline{\mathbf{x}}_{\rm prior}$ on $\overline{\eta}^{\rm post}$

Figure 3-21: The effect of $\overline{\mathbf{x}}_{\rm prior}$ on $\overline{\mathbf{x}}_{\rm post}$ for five measurements. An increase of the number of measurements results in a smaller dependency of $\overline{E}_0^{\rm post}$ on $\overline{\mathbf{x}}_{\rm prior}$. This is also the case for $\overline{E}_1^{\rm post}$ and $\overline{\eta}^{\rm post}$, but this is more difficult to observe by comparing this figure with Fig. 3-9.

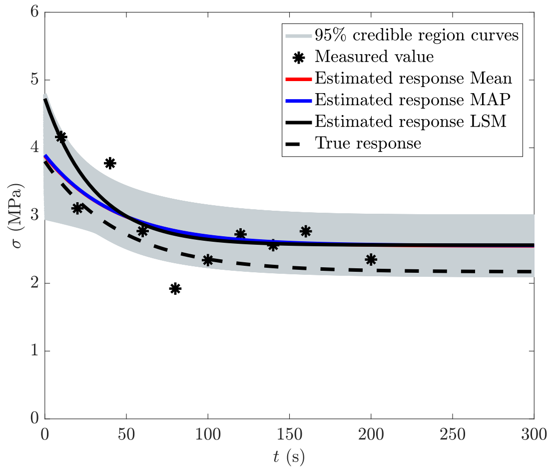

Figure 3-22: The stress-time curves for the relaxation experiment with ten measurements. Increasing the number of measurements leads to a narrower region (cf. Figs. 3-8(b) and 3-21). This means that the uncertainty decreases as the number of measurements increases. Note that the responses associated with the mean and the MAP point are practically on top of each other.

The effect of prior's mean on $\overline{\mathbf{x}}_{\rm post}$ is shown in Fig. 3-23. Comparing Fig. 3-23 with Figs. 3-9, 3-10, 3-11 and 3-21, it is clear that the prior's mean has again less influence on the posterior's mean. This is most obvious for $\overline{E}_0^{\rm post}$.

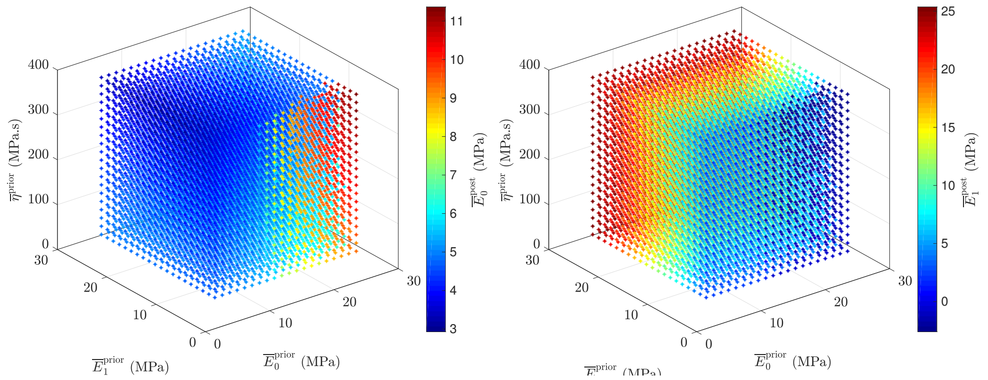

(a) Effect of $\overline{\mathbf{x}}_{\text{prior}}$ on $\overline{E}_0^{\text{post}}$ (b) Effect of $\overline{\mathbf{x}}_{\text{prior}}$ on $\overline{E}_1^{\text{post}}$

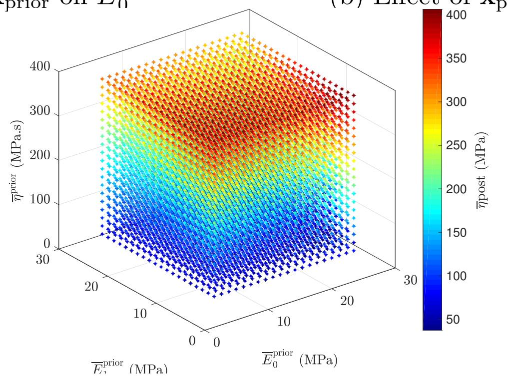

(c) Effect of $\overline{\mathbf{x}}_{\text{prior}}$ on $\overline{\eta}^{\text{post}}$

Figure 3-23: The effect of the prior's mean ($\overline{\mathbf{x}}_{\text{prior}}$) on $\overline{E}_0^{\text{post}}$, $\overline{E}_1^{\text{post}}$ and $\overline{\eta}^{\text{post}}$ for ten measurements. The effect of the prior's mean becomes less significant, especially for $\overline{E}_0^{\text{post}}$. For $\overline{E}_1^{\text{post}}$ and $\overline{\eta}^{\text{post}}$ one can observe that an increase in the number of measurements decreases the prior's effect.

3.6.4 Identification of the SLS parameters when the measurements are created by the generalised Maxwell model using the relaxation test

In the final example for the relaxation test, we study the results of the Bayesian approach and the LSM when the measurements are generated using the generalised Maxwell model with three spring-dashpots in series (instead of only one as in the SLS model). The model is shown schematically in Fig. 3-24. We take $E_0 = 4$ MPa, $E_1 = 3$ MPa, $E_2 = 2.5$ MPa, $E_3 = 2$ MPa, $\eta = 140$ MPa.s, $\eta_2 = 110$ MPa.s and $\eta_3 = 100$ MPa.s. The same noise distribution is considered as in the previous examples ($S_{\text{noise}} = 0.5$MPa). The modified normal distribution given in Eq. (3.15) is selected as the prior distribution with $\overline{\mathbf{x}}_{\text{prior}}$ and $\mathbf{\Gamma_{prior}}$ given in Eq. (3.40). Running the MCMC chain for 10^4 sample and burning the first 3000 samples yields:

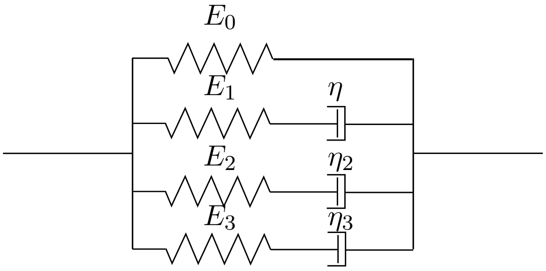

Figure 3-24: Schematic representation of the generalised Maxwell model with three spring-dashpots in series.

$$\overline{\mathbf{x}}_{\text{post}} = \begin{bmatrix} 4.5290 \\ 3.4806 \\ 122.3883 \text{ s} \end{bmatrix} \text{ MPa}, \ \boldsymbol{\Gamma}_{\text{post}} = \begin{bmatrix} 0.0810 & -0.0175 & -1.7183 \text{ s} \\ -0.0175 & 0.2714 & 1.9272 \text{ s} \\ -1.7183 \text{ s} & 1.9272 \text{ s} & 300.6031 \text{ s}^2 \end{bmatrix} \text{ MPa}^2, \tag{3.51}$$

and

$$\mathbf{MAP} = \begin{bmatrix} 4.5352 \\ 3.4771 \\ 122.9158 \text{ s} \end{bmatrix} \text{ MPa}. \tag{3.52}$$

The identified values by the LSM are:

$$\mathbf{x}_{\text{LSM}} = \begin{bmatrix} 3.3702 \\ 9.9743 \\ 306.8281 \text{ s} \end{bmatrix} \text{ MPa}. \tag{3.53}$$

In Fig. 3-25 all associated stress-time responses are presented. The LSM response is clearly closer to the true response, than the responses associated with the mean and the MAP of the Bayesian framework. The prior distribution clearly also has a substantial influence for this case.

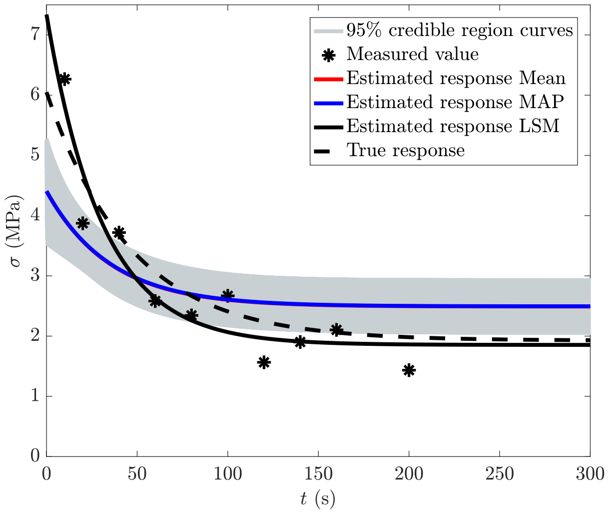

Figure 3-25: The stress-time response for the SLS model when ten measurement points are created using the generalised Maxwell model. The response identified by the LSM is significantly closer to the true response than the responses associated with the mean and the MAP point of the Bayesian framework. Hence, also in this case the prior has a significant influence in the Bayesian framework. Note that the responses associated with the mean and the MAP point are on top of each other.

3.6.5 Comparison with the constant strain-rate test and the creep test

In this subsection we compare the results for the relaxation test to the results for the constant strain-rate test and the creep test. To make our comparison is as 'fair' as possible, we try to keep every condition as similar to the relaxation test with five measurements. This means amongst others that we also consider five measurements in the constant strain-rate test and the creep test and that we again try to find the same parameter values back (E_0 = 3.9455 MPa, E_1 = 2.9636 MPa and η = 136.8035MPa.s). In the following two subsections we explain how we try to keep the other conditions as similar as possible. The comparison of the results is presented in Subsection 3.6.5.

Set-up of the constant strain-rate test

In the constant strain-rate test, strain-rate $\dot{\epsilon_0}$ is chosen such that the maximum stress that will occur is the same as the maximum stress occurring in the relaxation test. Consequently, the following expression to determine the applied strain-rate:

$$\dot{\epsilon_0} = \frac{(E_0 + E_1)\epsilon_0}{E_0 t_{\mathrm{exp}} + \eta\Big(1 - \exp\big(-\frac{E_1 t_{\mathrm{exp}}}{\eta}\big)\Big)}, \tag{3.54}$$

where $t_{\mathrm{exp}} = 300$ s and represents the duration of the relaxation test as well as that of the constant strain-rate test. The strain applied in the relaxation test is represented by ϵ_0.

Note that the reason to choose $\dot{\epsilon_0}$ according to Eq. (3.54) is to have the same order of magnitude for the stresses in both tests. In this way, the noise distribution (for which we again use a normal distribution with zero mean and $S_{\mathrm{noise}} = 0.5$ MPa) has approximately the same influence in both tests. Furthermore, we assume that the noise realisation for each measurement at time t_i in the constant strain-rate test is the same as the noise realisation at the same time in the relaxation test. In this way, the noise realisations have approximately the same influence in both tests.

Set-up of the creep test

The noise distribution in the creep test is again chosen to be in the form of Eq. (3.13). As the quantity measured in a creep test is the strain however, the standard deviation of the noise distribution (i.e. S_{noise} in Eq. (3.13)) must be re-defined such that a 'fair' comparison can be made between the results of the previous two tests and the creep test. For this reason, the standard deviation of the noise distribution in the creep test, $S_{\mathrm{noise}}^{\mathrm{creep}}$ is chosen as follows:

$$S_{\mathrm{noise}}^{\mathrm{creep}} = \frac{S_{\mathrm{noise}}^{\mathrm{relaxation}} \epsilon_{\mathrm{max}}^{\mathrm{creep}}}{\sigma_{\mathrm{max}}^{\mathrm{relaxation}}}, \tag{3.55}$$

where $S_{\mathrm{noise}}^{\mathrm{relaxation}}$ is the standard deviation of the noise in the relaxation test, $\epsilon_{\mathrm{max}}^{\mathrm{creep}}$ is the maximum strain occurring in the creep test and $\sigma_{\mathrm{max}}^{\mathrm{relaxation}}$ is the maximum stress that has occurred in the relaxation test. Using Eqs. (3.2) and (3.4) $\epsilon_{\mathrm{max}}^{\mathrm{creep}}$ and $\sigma_{\mathrm{max}}^{\mathrm{relaxation}}$ are calculated as follows:

$$\epsilon_{\mathrm{max}}^{\mathrm{creep}} = \frac{\sigma_0}{E_0} + \sigma_0\Big(\frac{1}{E_0 + E_1} - \frac{1}{E_0}\Big)\exp\big(-\frac{E_0 E_1 t_{\mathrm{exp}}^{\mathrm{creep}}}{\eta(E_0 + E_1)}\big), \tag{3.56}$$

and

$$\sigma_{\mathrm{max}}^{\mathrm{relaxation}} = (E_0 + E_1)\epsilon_0, \tag{3.57}$$

where $t_{\mathrm{exp}}^{\mathrm{creep}}$ represents the duration of the creep test.

Furthermore, a comparison between Eqs. (3.2), (3.3) and (3.4) shows that the coefficient in the exponent of the strain-time expression for the creep test (i.e. $\frac{E_0 E_1}{\eta(E_0+E_1)}$) is smaller than the one in the strain-time expressions for the other two tests (i.e. $\frac{E_1}{\eta}$). This entails that more time is required in the creep test to achieve the same amount of relaxation as in the previous two tests. Consequently, the experiment duration for the creep test is scaled as $t_{\mathrm{exp}}^{\mathrm{creep}} = \frac{(E_0+E_1)}{E_0} t_{\mathrm{exp}}^{\mathrm{relaxation}}$. $t_{\mathrm{exp}}^{\mathrm{relaxation}}$ refers here to the duration of the relaxation test (here $t_{\mathrm{exp}}^{\mathrm{relaxation}} = 300$ s and $t_{\mathrm{exp}}^{\mathrm{creep}} = 525.3403$ s).

Table 3.1: The estimated values of the posterior's mean, MAP and components of the covariance matrix for the three experiments.

Estimated value	Relaxation test	Constant strain-rate test	Creep test
$\overline{E}_0^{\text{post}}$ (MPa)	4.8354	4.9115	3.9047
$\overline{E}_1^{\text{post}}$ (MPa)	2.4069	2.0435	1.7861
$\overline{\eta}^{\text{post}}$ (MPa.s)	109.7946	109.0151	105.7801
E_0^{MAP} (MPa)	4.8463	4.8448	3.8569
E_1^{MAP} (MPa)	2.4558	1.9383	1.7678
η^{MAP} (MPa.s)	110.6589	107.4682	106.1140
$(\Gamma_{\text{post}})_{11}$ (MPa^2)	0.1453	0.3548	0.0748
$(\Gamma_{\text{post}})_{22}$ (MPa^2)	0.3392	0.4562	0.4173
$(\Gamma_{\text{post}})_{33}$ (MPa^2.s^2)	361.5418	398.6452	420.1033
$(\Gamma_{\text{post}})_{12}$ (MPa^2)	-0.0328	-0.0302	-0.0121
$(\Gamma_{\text{post}})_{13}$ (MPa^2.s)	-1.4935	-1.9472	-0.9538
$(\Gamma_{\text{post}})_{23}$ (MPa^2.s)	0.6262	0.2432	-0.8297

Because we scale the duration of the creep test, we also scale the time at which each measurement is made as $t_i^{\text{creep}} = \frac{(E_0+E_1)}{E_0} t_i^{\text{relaxation}}$. t_i^{creep} refers here to the time at which measurement i is made in the creep test and $t_i^{\text{relaxation}}$ refers to the time at which the same measurement is made in the relaxation test.

Using Eq. (3.55) the standard deviation of the noise distribution in the creep test is determined as $S_{\text{noise}} = 0.0724$. Note that σ_0 in Eq. (3.4) is chosen such that the final strain in the creep test is the same as the strain applied in the relaxation test (i.e. ϵ_0 in Eq. (3.2)). Additionally, we assume that noise realisation i in the creep test (ω_i^{creep}) has the same probability to occur as noise realisation i in the relaxation test ($\omega_i^{\text{relaxation}}$). This entails that we scale each noise realisation as follows:

$$\omega_i^{\text{creep}} = \omega_i^{\text{relaxation}} \frac{S_{\text{noise}}^{\text{creep}}}{S_{\text{noise}}^{\text{relaxation}}}. \tag{3.58}$$

Comparison of results

In this subsection we present the results of both the constant strain-rate test and the creep test and compare them with each other and those of the relaxation test. The prior for the two new tests is the same as we used for the relaxation test with five measurements (using Eq. (3.15) with the mean and covariance matrix in Eq. (3.40)). The MCMC chain is again run for 10^4 sample and we have burnt the first 3000 samples. Table 3.1 shows the estimated values of each parameter and each component of the posterior's covariance matrix ($\mathbf{\Gamma}_{\text{post}}$) for the three tests.

Comparing the values given in Table 3.1 with each other and the real values (i.e. $E_0 =$ 3.9455 MPa, $E_1 = 2.9636$ MPa and $\eta = 136.8035$ MPa.s), one can see that the identified parameter values for the three tests are all approximately of the same accuracy. The relaxation and constant strain-rate test overestimate the value of E_0, whereas the creep test identifies this value accurately. However, the creep test underestimates the value of E_1 substantially more than the other two tests. This is not very surprising since this results from the fact that the stress is measured in the relaxation and constant strain-rate test and that the strain is measured in the creep test. The posteriors' means and MAPs for the different tests in Table 3.1 cannot well be compared to begin with, since we only consider five measurements and one prior.

More interesting are the results for the uncertainty of E_0. After all, the values of $(\Gamma_{\text{post}})_{11}$

vary with a factor of five for the three tests. The difference between the uncertainty of E_0 of the relaxation test and the constant strain-rate test can be explained based on comparing the stress-time relations for both tests (see Eqs. (3.2) and (3.3)). If t approaches infinity in the relaxation test ($t \to +\infty$), an horizontal asymptote occurs ($\sigma = E_0\epsilon_0$) which depends only on E_0. In the constant strain-rate test however, an oblique asymptote occurs (i.e. $E_0\dot{\epsilon_0}t+\eta\dot{\epsilon_0}$) which depends on two parameters (E_0 and η). This means if $t \to \infty$, a measurement in the relaxation test only provides information about E_0, but in the constant strain-rate test this measurement gives information about E_0 and η. Consequently, E_0 is determined with more certainty in the relaxation test than in the constant strain-rate test. Furthermore, at the beginning of the relaxation test information is directly obtained for E_0 and E_1, whereas the constant strain-rate does not provide any information at time $t = 0$ s. The same reasoning can be used for the creep test as well. Unlike the stress-time relation for the relaxation test however, the one for the creep test is a combination of homographic and exponential functions. For this reason we obtain a different value for $(\Gamma_{\text{post}})_{11}$ in the creep test.

Figs. 3-26 and 3-27 present the stress-time responses and the strain-time responses of the constant strain-rate test and the creep test, respectively. The curves associated with 95% credible region are generated using the points from region which contain 95% of the posterior (approximated by an ellipsoid).

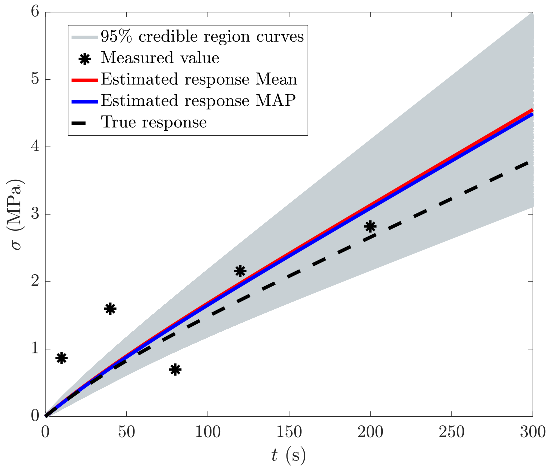

Figure 3-26: The stress-time curves for the constant strain-rate test with five measurements. The measurements are made using the same noise distribution as in Subsection 3.6.2. Furthermore, it is assumed that the noise realisation for each measurement at time t_i in the constant strain-rate test is the same as the noise realisation at the same time in the relaxation test. Note that the associated curves with the mean and MAP point are practically on top of each other.

In the remainder of this subsection we investigate the effect of prior's mean $\overline{\mathbf{x}}_{\text{prior}}$ on the results. For this exercise, the prior's covariance matrix is kept constant (i.e. the covariance matrix given in Eq. (3.40)).

Fig. 3-28 shows the effect of $\overline{\mathbf{x}}_{\text{prior}}$ on $\overline{E}_0^{\text{post}}$ for the relaxation, constant strain-rate and creep test. It can be observed that $\overline{E}_0^{\text{post}}$ depends least on $\overline{\mathbf{x}}_{\text{prior}}$ for the relaxation test. It can also be observed that $\overline{E}_0^{\text{post}}$ depends only on $\overline{E}_0^{\text{prior}}$ for the creep test, whereas it depends on $\overline{E}_0^{\text{prior}}$ and $\overline{E}_1^{\text{prior}}$ in the other two tests. Note that a possible reason for the different influence of the prior in the creep test is the type of function for its stress-time relation (Eq. (3.4) is a combination of homographic and exponential function of parameters).

Now we investigate the effect of the prior's mean on the estimated values. The prior's covariance matrix is again kept constant for this. The influence of the prior's mean on the

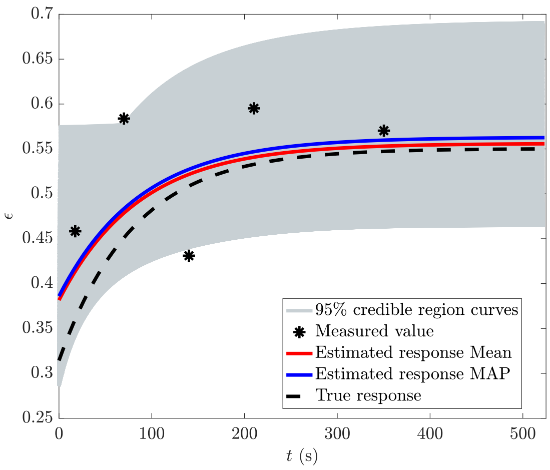

Figure 3-27: The strain-time curves for the creep test with five measurements. The measurements are generated using a normal distribution with zero mean and a standard deviation given by Eq. (3.55). To ensure that the same amount of relaxation occurs as in the other two tests, the time at which each measurement is made is scaled according to $t_i^{\text{creep}} = \frac{(E_0+E_1)}{E_0} t_i^{\text{relaxation}}$.

estimated values is very similar to that for the relaxation test, except for $(\Gamma_{\text{post}})_{11}$, $(\Gamma_{\text{post}})_{33}$, $(\Gamma_{\text{post}})_{13}$ and $(\Gamma_{\text{post}})_{23}$. In Fig. 3-29 the effect of $\overline{\mathbf{x}}_{\text{prior}}$ on $(\Gamma_{\text{post}})_{11}$ is presented. Only for the creep test an actual trend can be observed.

Fig. 3-30 indicates that the effect of $\overline{\mathbf{x}}_{\text{prior}}$ on the estimated value of $(\Gamma_{\text{post}})_{33}$ for the relaxation test, whereas it is the smallest for the constant strain-rate test.

Figs. 3-31 and 3-32 show the effect of $\overline{\mathbf{x}}_{\text{prior}}$ on $(\Gamma_{\text{post}})_{13}$ and $(\Gamma_{\text{post}})_{23}$ for the three tests employed in this chapter. The estimated value of $(\Gamma_{\text{post}})_{13}$ does not depends on $\overline{\mathbf{x}}_{\text{prior}}$ for the constant strain-rate test, whereas a dependency can be observed for the other two tests. Furthermore, for $(\Gamma_{\text{post}})_{23}$ we can only see a dependency for the relaxation test. The values estimated for $(\Gamma_{\text{post}})_{12}$ using the three tests are independent of the mean of the prior, although the value change for each test.

Investigating the effect of the mean of the prior on the estimated values for the parameters and components of the posterior's covariance matrix shows that the constant strain-rate test is less sensitive to the prior's mean compared to the two other tests. This can be due to the existence of the term $\eta\dot{\epsilon}_0$ that does not vanish for $t \to \infty$ (see Eq. (3.3)), whereas a constant remains for the other two tests. The nature of the different tests therefore seems to have a considerable influence on the results.

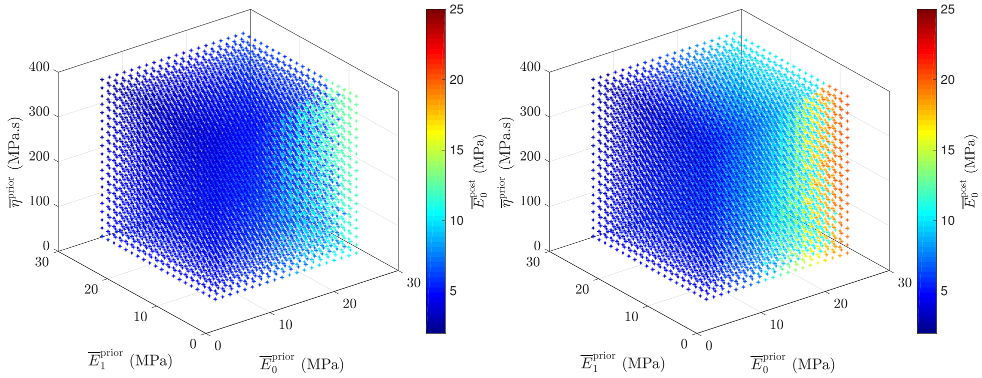

(a) The relaxation test (b) The constant strain-rate test

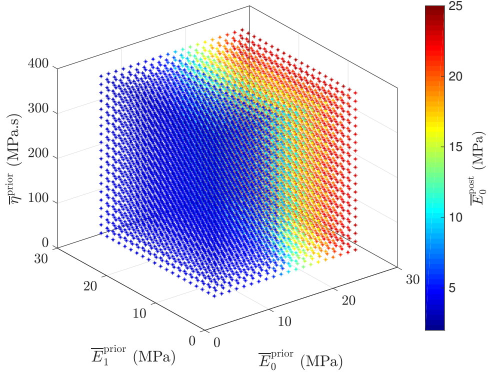

(c) The creep test

Figure 3-28: The effect of $\overline{\mathbf{x}}_{\text{prior}}$ on $\overline{E}_0^{\text{post}}$ for the three tests. $\overline{E}_0^{\text{post}}$ depends least on the prior for the relaxation test. $\overline{E}_0^{\text{post}}$ depends only on $\overline{E}_0^{\text{prior}}$ for the creep test, whereas it depends on $\overline{E}_0^{\text{prior}}$ and $\overline{E}_1^{\text{prior}}$ in the other two tests.

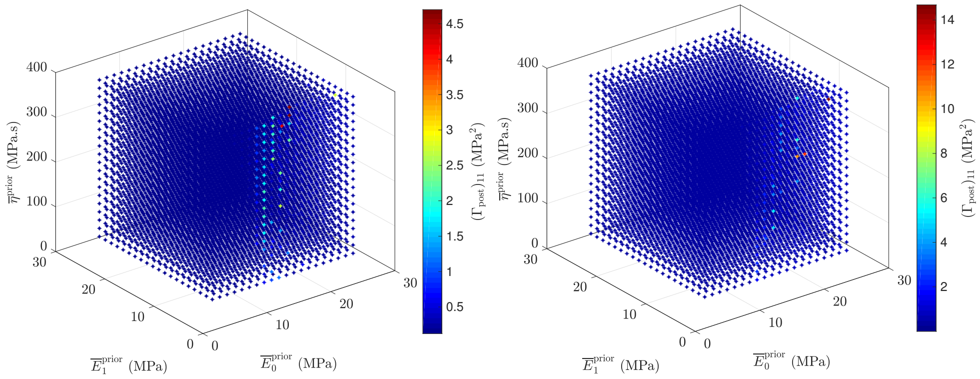

(a) The relaxation test (b) The constant strain-rate test

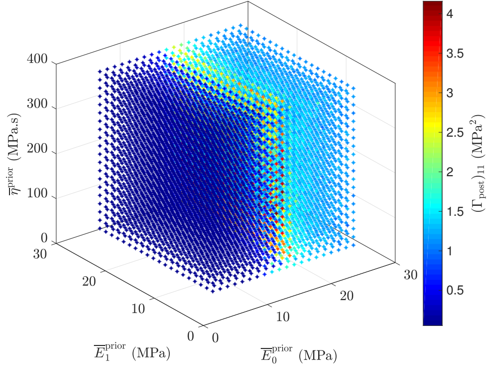

(c) The creep test

Figure 3-29: The effect of $\overline{\mathbf{x}}_{\text{prior}}$ on $(\Gamma_{\text{post}})_{11}$. Only for the creep test a trend can be distinguished.

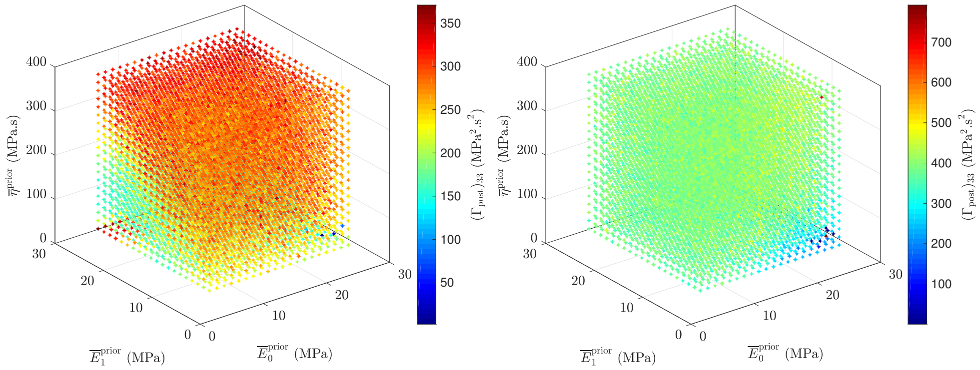

(a) The relaxation test (b) The constant strain-rate test

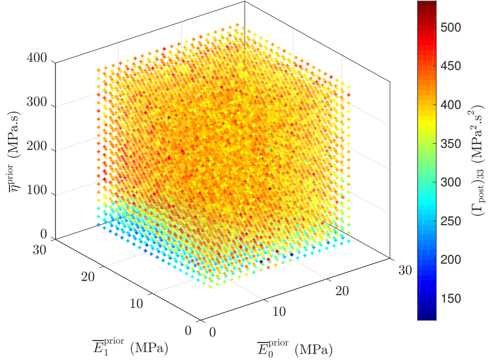

(c) The creep test

Figure 3-30: The effect of $\overline{\mathbf{x}}_{\text{prior}}$ on $(\Gamma_{\text{post}})_{33}$. The influence for the relaxation test is most significant, whereas almost no influence can be observed for the constant strain-rate test.

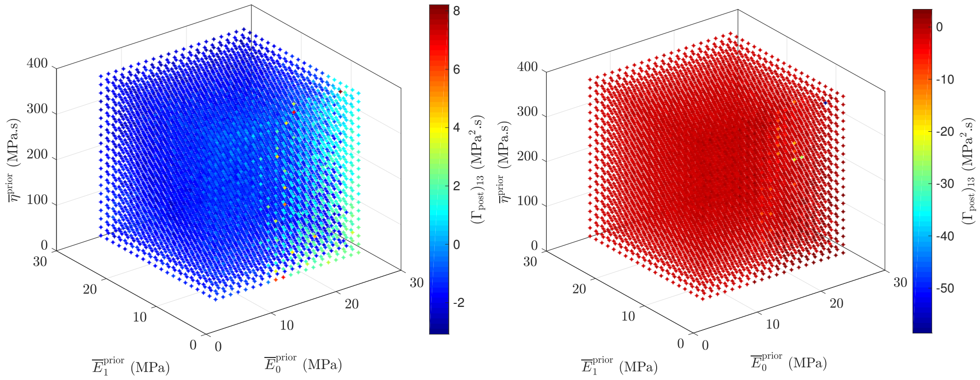

(a) The relaxation test (b) The constant strain-rate test

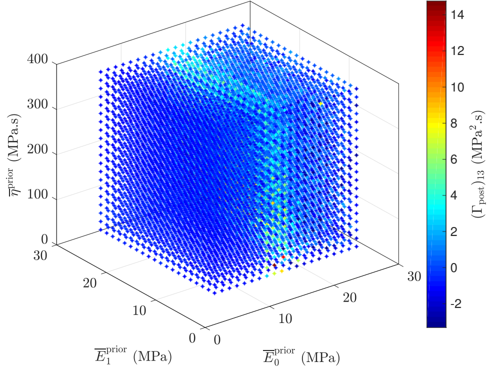

(c) The creep test

Figure 3-31: The effect of $\overline{\mathbf{x}}_{\mathrm{prior}}$ on $(\Gamma_{\mathrm{post}})_{13}$ for the three employed tests. Unlike the constant strain-rate test, the estimated value for $(\Gamma_{\mathrm{post}})_{13}$ is function of the mean of the prior for the two other tests.

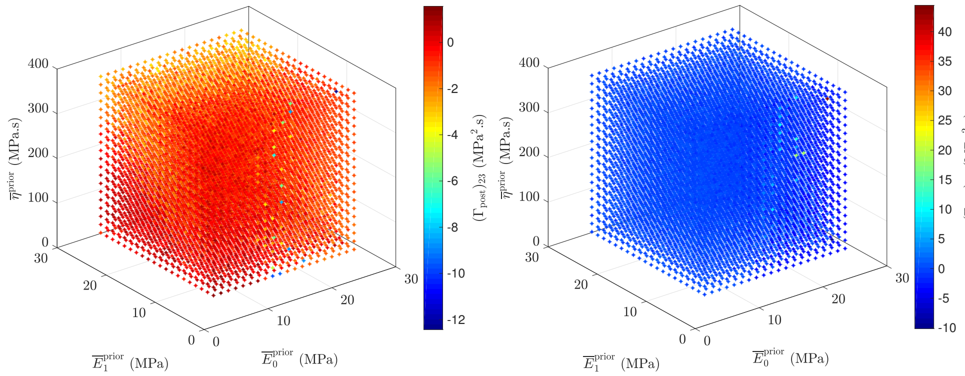

(a) The relaxation test (b) The constant strain-rate test

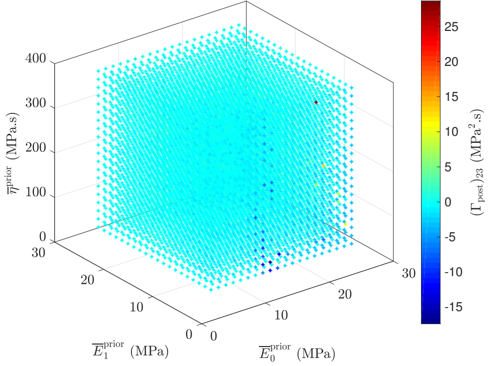

(c) The creep test

Figure 3-32: The effect of $\overline{\mathbf{x}}_{\text{prior}}$ on $(\Gamma_{\text{post}})_{23}$ for the three employed tests. Except for the relaxation test, the other tests are independent of the prior's mean.

3.7 Conclusions

In this chapter Bayesian inference is used to identify parameters in viscoelasticity. The model focused on was the standard linear solid model and the experiments of interest were a relaxation test, a constant strain-rate test and a creep test in tension. We have investigated four issues. First, the influence of the number of measurements on the parameter values and their uncertainty was investigated. Second, the identified parameter values were compared to those identified by the least squares method (LSM) for the relaxation test. Thirdly, three different types of experiments were considered in order to study how they affect the results. Finally, the sensitivity on the prior distribution was investigated for all the aforementioned cases.

The obtained results allow us to draw four conclusions:

1. The prior has a substantially larger effect on the identified values (i.e. the mean and the MAP) in viscoelasticity than in elastoplasticity. The influence on the damping parameter is especially large. The reason for the prior's substantial influence in viscoelasticity compared to elastoplasticity is that no clear domains can be distinguished in viscoelasticity, whereas two domains are present in elastoplasticity (in which an elastic and elastoplastic domain can be distinguished).

2. An increase of the number of measurement points reduces the influence of the prior, but the influence on the damping parameter is still substantially present. If only two measurement points are present furthermore, the LSM has no unique solution but the prior in the Bayesian framework regularises this case such that it becomes unique.

3. For the relaxation test with more than two measurements, the stress-time responses associated with the LSM results are practically always closer to the true responses than the responses associated with the mean and MAP values identified by the Bayesian framework. It is however questionable if this means that the LSM is 'better' than the Bayesian framework. After all, the Bayesian framework incorporates the assumption that other measurements could have been made as well (incorporated in the prior). Furthermore, the Bayesian framework treats the parameters as random variables and consequently, the parameter values come with a credible region. This is not the case for the LSM. In other words, if one desires to propagate the uncertainty of the parameters in a predictive model, the standard LSM gives no estimate for the interval of a particular parameter. The Bayesian framework is however able to do this, including the dependency on the other parameters.

4. The use of BI has enabled us to distinguish that the uncertainty of the identified parameter values resulting from the constant strain-rate test is substantially larger than those resulting from the relaxation test and the creep test. This can be explained by the fact that asymptotic behaviour occurs in the relaxation and creep test, for which only one parameter is responsible. Consequently, the uncertainty of this parameter is relatively small and because of that, the uncertainties of the other parameters are also relatively small compared to those resulting from the constant strain-rate experiment. The results however show that this does not mean that the influence of the prior is larger.

The Bayesian identification approach and the LSM both have their advantages and disadvantages to identify material parameters. BI incorporates a regularisation that makes cases with few measurements solvable, which cannot be solved using the standard formulation of the LSM. An result of BI, which cannot be obtained using the standard LSM, is that the parameters come with uncertainties. This is essential for the propagation of uncertainties in mechanical predictions. On the other hand, the prior information in BI can also significantly influence the results negatively. Probably, it will always remain a matter of taste to prefer one method above the other. In case of a small number of measurements and obtaining an uncertainty however, BI seems to be unavoidable.

Chapter 4

Identifying elastoplastic parameters with Bayes' theorem considering double error sources and model uncertainty[1]

abstract

We discuss Bayesian inference for the identification of elastoplastic material parameters. In addition to errors in the stress measurements, which are commonly considered, we also consider errors in the strain measurements. Since a difference between the model and the experimental data may still be present if the data is not contaminated by noise, we also incorporate the possible error of the model itself. The three formulations to describe model uncertainty in this chapter are: (1) a random variable which is taken from a normal distribution with constant parameters, (2) a random variable which is taken from a normal distribution with an input-dependent mean, and (3) a Gaussian random process with a stationary covariance function. Our results show that incorporating model uncertainty often, but not always, improves the results. If the error in the strain is considered as well, the results improve even more.

4.1 Introduction

A frequent approach for the identification of material parameters in solid mechanics is the least squares method (LSM; see [8]), in which the squared difference between the experimental output and the model response is minimised with respect to the material parameters. The result of such an approach is a deterministic estimate of the parameter values. A true insight in the certainty of each identified parameter value lacks however, as only a single residual forms the measure for the quality of the ensemble of identified values. Although some advanced formulations of LSM incorporate statistical information [79, 80], they assume that the measurement error is symmetrically distributed. For nonlinear models furthermore, linearised approximations are required to estimate the parameter distributions [81].

An alternative approach is the Bayesian approach which allows accounting for modelling uncertainty and the statistical noises of the experimental devices [16]. The result of Bayesian

---

[1] Reproduced from: H. Rappel, L.A.A. Beex, L. Noels and S.P.A. Bordas, Identifying elastoplastic parameters with Bayes theorem considering double error sources and model uncertainty, Probabilistic Engineering Mechanics (2018). `https://doi.org/10.1016/j.probengmech.2018.08.004`

inference (BI) is a probability density function (PDF) as a function of the parameters of interest. This PDF is called the posterior distribution in Bayesian terminology. Once the posterior distribution is obtained, statistical summaries of the posterior such as mean, the value at which the posterior PDF is maximal (i.e. the 'maximum-a-posteriori-probability' or 'MAP' point) and the covariance matrix need to be evaluated. With the exception of a few cases, numerical frameworks need to be employed for this. Markov chain Monte Carlo (MCMC) techniques [25, 26, 28, 29] are probably the most frequently employed approaches for sampling PDFs.

Bayesian inference (BI) was used in various previous studies to identify material parameters. The earliest work known to the authors is that of Isenberg [41], in which it was used to identify elastic parameters in 1979. In other works, this framework was employed to identify elastic material parameters based on dynamic responses [42–44]. BI was also used to identify the elastic constants of composite laminates in [49, 50, 52, 59]. Spatially varying elastic parameters were furthermore identified using BI by Koutsourelakis [51]. An introduction to identify Young's moduli employing Bayesian inference can be found in [45].

Elastoplastic parameters were also identified using BI. Parameters in linear elasticity-perfect plasticity were identified by Most [56], while Bayesian updating via a polynomial chaos expansion for an elastoplastic system was considered by Rosić et al. [57]. In addition to elastoplastic material models, Bayesian updating procedures were employed to identify material parameters of hysteretic models [53, 54] and other nonlinear material models such as viscoelasticity and creep [30, 55, 58].

In none of the aforementioned studies, the fact that the model itself may not be perfectly equipped to capture the experimental measurements was considered. A framework that can deal with this was nevertheless introduced by Kennedy and O'Hagan [47] in 2001, which is currently known as the 'KOH' framework and was employed in [51, 76, 77, 93–95]. Another issue that has received little attention in previous studies is that not only the output (e.g. the stress measurements) can be polluted by statistical noise, but the input as well (e.g. the strain measurements).

The aim of this chapter is to present a Bayesian identification framework for elastoplasticity that can treat uncertainties in both the output and the input, whilst also accounting for model uncertainty. The framework is constructed to deal with experimental data coming from monotonically increasing, uniaxial tensile tests. Output errors (the noise in the stress measurements) are commonly considered in identification approaches using BI, but input errors (i.e. the errors in the strains) seem to remain untreated in Bayesian identification approaches. They may be worthwhile to include, because of the use of clamp displacement as a measure to derive strains often overestimates the measured strains due to slip in the clamps. Even if digital image correlation (DIC) is employed to determine strains, errors may be included due to the finite accuracy of (1) the applied pixel patterns, (2) the finite resolution of the images, and (3) the algorithms of the DIC software, which come with different user-selected parameters (such as the size of facets) and finite minimisation residuals.

Bayesian updating including uncertainties in both output and input was yet employed in [96] for linear dynamic systems and was aimed at identifying modal parameters. The framework uses the assumption that the posterior can be approximated as a Gaussian distribution at the MAP point, which may be considered as a limitation. Studies in other fields can also be found that treat two error sources [97–102], but those studies effectively employ linear regression.

The KOH framework to address model uncertainty was furthermore not employed in any of the aforementioned studies. Model uncertainty can be incorporated in several ways in the KOH framework. The simplest way is to describe it with a constant variable, which is to be identified [76]. One can also use a random variable and treat the parameters of the random variable's distribution as unknown parameters that need to be identified as well (and hence, they appear in the posterior) [75, 76]. Instead of incorporating a deterministic variable, one can include a function of which the parameters are deterministic [15]. One can also include a random variable and assume its distribution's parameters to be dependent on the input [75]. Model uncertainty can also be represented by a Gaussian process [47, 77, 78]. More information on different ways to incorporate model uncertainty can be found in [75].

In this chapter, we investigate the effect of three model uncertainty formulations (i.e. a correction of the uniaxial material response in terms of the strain from ideal elasticity or elastoplasticity equations) on the parameter identification in elasticity and elastoplasticity: (1) a random variable which is assumed to come from a normal distribution with constant parameters, (2) a random variable which is assumed to come from a normal distribution with a mean that depends on the input (i.e. the strain) and (3) a Gaussian process with a zero mean and a stationary covariance function. On top of that, we also investigate how the incorporation of the input error influences the results.

The structure of the chapter is as follows. Section 4.2 briefly discusses the expressions of the considered material models for uniaxial, monotonic tension. In Section 4.3, the main concepts of Bayesian frameworks for parameter identification are presented. In Section 4.4, the employed model uncertainty functions are elaborated, including the corresponding likelihood functions. Section 4.5 presents the Bayesian approaches that incorporate both the measurements errors in the stresses and in the strains, as well as the model uncertainty. Examples are presented in Section 4.6. The measurement data in this section are artificially generated, so that we can compare the parameter distributions with the true values. Finally, this chapter is closed with conclusions (Section 4.7).

Remark 5. *Throughout this chapter bold capital letters and symbols denote matrices and bold normal letters and symbols are vectors or columns.*

4.2 Material model

In this section we present the stress-strain relations of the considered material models for monotonic uniaxial tensile tests. The material models presented in this section are: linear elasticity, linear elasticity with perfect plasticity and linear elasticity with linear hardening.

4.2.1 Linear elasticity

In linear elasticity, the stress-strain relation is described fully linearly. This relation can be written as follows for uniaxial tension:

$$\sigma(\epsilon, \mathbf{x}) = E\epsilon, \tag{4.1}$$

where σ is the stress, ϵ is the strain and $\mathbf{x}$ is the vector containing the material parameters, which here only consists of Young's modulus E.

4.2.2 Linear elasticity-perfect plasticity

In a linear elastic-perfectly plastic material model, the elastic response is again described linearly in terms of the elastic strain. Plastic deformation occurs without hardening when the stress reaches yield stress σ_{y0}. The stress-strain relationship for monotonic, uniaxial tension can be written as follows:

$$\sigma(\epsilon, \mathbf{x}) = \begin{cases} E\epsilon & \text{if } \epsilon \leq \frac{\sigma_{y0}}{E} \\ \sigma_{y0} & \text{if } \epsilon > \frac{\sigma_{y0}}{E} \end{cases}, \tag{4.2}$$

where $\mathbf{x} = \begin{bmatrix} E & \sigma_{y0} \end{bmatrix}^T$.

4.2.3 Linear elasticity-linear hardening

Unlike the linear elastic-perfectly plastic model, work hardening is included in the linear elastic-linear hardening model. In other words, the stress continues to increase (linearly) when plastic deformation takes place. The stress-strain relation for this model during monotonic, uniaxial tensions reads as:

$$\sigma(\epsilon, \mathbf{x}) = \begin{cases} E\epsilon & \text{if } \epsilon \leq \frac{\sigma_{y0}}{E} \\ \sigma_{y0} + \frac{HE}{H+E}\left(\epsilon - \frac{\sigma_{y0}}{E}\right) & \text{if } \epsilon > \frac{\sigma_{y0}}{E} \end{cases}, \tag{4.3}$$

where H is the hardening modulus and hence, $\mathbf{x} = \begin{bmatrix} E & \sigma_{y0} & H \end{bmatrix}^T$.

4.3 Bayesian parameter identification

In this section some concepts of Bayesian inference are explained. First, a rather standard Bayesian framework for parameter identification is presented. Subsequently, we present a Bayesian approach that incorporates a generalised model error term in the KOH framework. The parametrised formulations for the employed model errors and their corresponding likelihood functions are presented in Section 4.4 in more detail.

4.3.1 Bayesian inference fundamentals

Let $\mathbf{y} = \begin{bmatrix} y_1 & \cdots & y_{n_m} \end{bmatrix}^T$ be a vector of n_m measurements and let $\mathbf{x}$ be a vector of n_p parameters which are to be identified. Using the Bayes' theorem, one can write:

$$\pi(\mathbf{x}|\mathbf{y}) = \frac{\pi(\mathbf{x})\pi(\mathbf{y}|\mathbf{x})}{\pi(\mathbf{y})}, \tag{4.4}$$

where $\pi(\mathbf{x})$ is the prior distribution (i.e. the PDF that represents one's assumed prior knowledge about the parameters, e.g. the fact that the Young's modulus cannot be smaller than zero), $\pi(\mathbf{y}|\mathbf{x})$ is the likelihood function (i.e. the PDF that measures the likelihood that measurements $\mathbf{y}$ are observed, given a set of parameter values $\mathbf{x}$), $\pi(\mathbf{x}|\mathbf{y})$ is the posterior distribution (i.e. the PDF that describes the chance to obtain parameters $\mathbf{x}$, given the measurements $\mathbf{y}$) and $\pi(\mathbf{y})$ is called evidence. As the measured data ($\mathbf{y}$) are already known and hence, $\mathbf{y}$ are not variables in the posterior ($\pi(\mathbf{x}|\mathbf{y})$), the evidence is a constant number ($\pi(\mathbf{y}) = C \in \mathbb{R}^+$) that does not depend on the parameters. Consequently, Eq. (4.4) behaves as follows:

$$\pi(\mathbf{x}|\mathbf{y}) \propto \pi(\mathbf{x})\pi(\mathbf{y}|\mathbf{x}). \tag{4.5}$$

Since the statistical quantities of interest, such as the mean, covariance and MAP point, are the same for Eq. (4.4) as for Eq. (4.5), it is sufficient to deal with Eq. (4.5). Next, we will discuss likelihood function $\pi(\mathbf{y}|\mathbf{x})$ in the presence of a general model error term.

4.3.2 Likelihood function

We denote the stress-strain response to be modelled by $\sigma(\epsilon, \mathbf{x})$. In the KOH framework, the relation between a stress measurement and the model response is written as [75]:

$$y = \sigma_{\text{true}} + \omega_y, \tag{4.6}$$

with

$$\sigma_{\text{true}} = \sigma(\epsilon, \mathbf{x}) + d(\epsilon), \tag{4.7}$$

where ω_y denotes the error in the stress measurement (output error), which is considered to be a realisation from the PDF that we call here the stress noise distribution. Furthermore, d represents the model uncertainty which can be assumed to be dependent on the input (i.e. strain ϵ here). Assuming that we know the form of the noise distribution, the likelihood function for a deterministic model uncertainty reads:

$$\pi(y|\mathbf{x}, \mathbf{x}_d, \mathbf{x}_{\omega_y}) = \pi_{\omega_y}(y - \sigma(\epsilon, \mathbf{x}) - d(\epsilon)), \tag{4.8}$$

where $\mathbf{x}_d$ is the parameter vector of the model uncertainty and $\mathbf{x}_{\omega_y}$ is the vector of parameters of the stress noise distribution. Often, the stress noise distribution is assumed to be a Gaussian distribution with $s^2_{\omega_y}$ variance and zero mean. Frequently, the parameters for both the model uncertainty (d) and the stress noise distribution (i.e. s_{ω_y} for the Gaussian distribution with zero mean) are unknown and consequently, they must also be identified, i.e. they appear as variables in the posterior. As uniaxial tensile tests are generally performed in well-controlled tensile testers of which the noise of the load cell can be rather straightforwardly calibrated, we assume that the stress noise distribution and its parameters can be defined through a noise calibration process.

Using Eqs. (4.5) and (4.8), the posterior distribution for a single measurement can be written as:

$$\pi(\mathbf{x}, \mathbf{x}_d|y) \propto \pi(\mathbf{x})\pi(\mathbf{x}_d)\pi_{\omega_y}(y - \sigma(\epsilon, \mathbf{x}) - d(\epsilon)), \tag{4.9}$$

where $\pi(\mathbf{x})$ and $\pi(\mathbf{x}_d)$ are the prior PDFs for the model parameters and the model uncertainty parameters, respectively. Clearly, we have assumed here that the probabilities of the model parameters and of the model uncertainty are independent ($\pi(\mathbf{x}, \mathbf{x}_d) = \pi(\mathbf{x})\pi(\mathbf{x}_d)$). Furthermore, $\pi(\mathbf{x}, \mathbf{x}_d|y)$ is the joint PDF for $\mathbf{x}$ and $\mathbf{x}_d$. For the case of n_m independent measurements, the final likelihood function is a product of the likelihood functions for each output y_i (coming with input ϵ_i):

$$\pi(\mathbf{y}|\mathbf{x}, \mathbf{x}_d) = \prod_{i=1}^{n_m} \pi_{\omega_y}(y_i - \sigma(\epsilon_i, \mathbf{x}) - d(\epsilon_i)). \tag{4.10}$$

Once the posterior is established, one can employ numerical sampling techniques to approximate the posterior's statistical summaries (e.g. mean value, MAP point or covariance matrix). In this chapter the adaptive Metropolis algorithm [73] is employed to sample the posterior.

4.4 Model uncertainty

In Section 4.3, Bayesian inference for a general model uncertainty was discussed. In this section, we present the likelihood functions for the three formulations of model uncertainty ($d(\epsilon)$), see Eq. (4.7). As mentioned before, these three formulations are: (1) a random variable coming from a normal distribution with a constant mean and variance, (2) a random variable which comes from a normal distribution with a constant variance and a mean which is a polynomial function in terms of the input (the strain), and (3) a Gaussian random process with a stationary covariance function.

Important to realise again is that the stress noise distribution is described by a normal distribution with zero mean and $s^2_{\omega_y}$ variance, i.e. $\omega_y \sim N(0, s^2_{\omega_y})$. As mentioned before, we assume that s_{ω_y} is known (see Subsection 4.6.1).

4.4.1 Random variable coming from a normal distribution with constant parameters

In the first case, we describe the difference between the material model and the true response as realisations from a normal distribution with mean $\overline{d}$ and variance s_d^2, i.e. $N(\overline{d}, s_d^2)$. $\overline{d}$ and s_d^2 are unknown and must be identified by the Bayesian updating process. Prior knowledge about them can be incorporated in the prior distribution. The likelihood function for n_m measurements, previously expressed in Eq. (4.10), can now be written as:

$$\pi(\mathbf{y}|\mathbf{x}, \mathbf{x}_\mathrm{d}) = N(\boldsymbol{\sigma}(\boldsymbol{\epsilon}, \mathbf{x}) + \overline{d}\mathbf{1}_{n_m}, (s_{\omega_y}^2 + s_\mathrm{d}^2)\mathbf{I}_{n_m}), \tag{4.11}$$

where $\boldsymbol{\sigma}(\boldsymbol{\epsilon}, \mathbf{x})$ is the vector of model responses for each input $\begin{bmatrix}\sigma(\epsilon_1, \mathbf{x}) & \cdots & \sigma(\epsilon_{n_m}, \mathbf{x})\end{bmatrix}^T$, $\mathbf{1}_{n_m}$ is the unit vector of size $n_m \times 1$, $\mathbf{I}_{n_m}$ is the identity matrix of size $n_m \times n_m$ and $\mathbf{x}_d$ is the parameter vector for the model uncertainty i.e. $\mathbf{x}_d = \begin{bmatrix}\overline{d} & s_d\end{bmatrix}^T$. Eq. (4.11) clearly shows that this model uncertainty adds a correction to the mean and increases the likelihood's variance by s_d^2.

4.4.2 Random variable coming from a normal distribution with an input dependent mean

In the second case, we describe the difference between the model response and the true response as a random variable, that originates from a normal distribution of which the mean is a function of the input. We use polynomial functions to describe the relation between the mean and the input, $\overline{d}(\epsilon) = \sum_{l=0}^{L} a_l \epsilon^l$, resulting in $L+2$ model uncertainty parameters: $\mathbf{x}_d = \begin{bmatrix}a_0 & a_1 & \cdots & a_L & s_d\end{bmatrix}^T$. Consequently, the likelihood function reads as:

$$\pi(\mathbf{y}|\mathbf{x}, \mathbf{x}_\mathrm{d}) = N(\boldsymbol{\sigma}(\boldsymbol{\epsilon}, \mathbf{x}) + \overline{\mathbf{d}}(\boldsymbol{\epsilon}), (s_{\omega_y}^2 + s_\mathrm{d}^2)\mathbf{I}_{n_m}), \tag{4.12}$$

where $\overline{\mathbf{d}}(\boldsymbol{\epsilon}) = \begin{bmatrix}\overline{d}(\epsilon_1) & \cdots & \overline{d}(\epsilon_{n_m})\end{bmatrix}^T$. Note that increasing the polynomial order can lead to model nonidentifiability [75].

4.4.3 Gaussian process with a stationary covariance function

In the work by Kennedy and O'Hagan [47], model uncertainty was described by a Gaussian process [103], entailing that the error between the model and the true response is nonlocal in terms of the strain (i.e. the input). Following [47] and [78] describing a Gaussian process (GP) with a zero mean, we write:

$$d \sim \mathrm{GP}(0, \lambda^2 c(\cdot, \cdot|\psi)), \tag{4.13}$$

where c is the squared exponential correlation function:

$$c(\epsilon_i, \epsilon_j|\psi) = \exp\Big(-\frac{(\epsilon_i - \epsilon_j)^2}{2\psi^2}\Big), \tag{4.14}$$

where λ^2 denotes the variance and ψ the length scale, yielding $\mathbf{x}_d = \begin{bmatrix}\lambda & \psi\end{bmatrix}^T$. ϵ_i and ϵ_j are furthermore two input values which may be the same ($i, j \in \{1, \cdots, n_m\}$). Note that the zero mean in the Gaussian process implies that no bias is included that increases the chance for $d(\epsilon)$

to be positive or negative. The likelihood function now reads:

$$\pi(\mathbf{y}|\mathbf{x}, \mathbf{x}_\mathrm{d}) = N(\boldsymbol{\sigma}(\boldsymbol{\epsilon}, \mathbf{x}), \mathbf{\Gamma}_\mathrm{GP} + s^2_{\omega_y}\mathbf{I}_{n_m}), \tag{4.15}$$

where

$$\mathbf{\Gamma}_\mathrm{GP} = \begin{bmatrix} \lambda^2 c(\epsilon_1, \epsilon_1|\psi) & \cdots & \lambda^2 c(\epsilon_1, \epsilon_{n_m}|\psi) \\ \vdots & \ddots & \vdots \\ \lambda^2 c(\epsilon_{n_m}, \epsilon_1|\psi) & \cdots & \lambda^2 c(\epsilon_{n_m}, \epsilon_{n_m}|\psi) \end{bmatrix}. \tag{4.16}$$

Eq. (4.16) clearly shows that the errors in the stress measurements are correlated in a GP. This implies that the updating procedure is not done by a multiplication operator as in Eq. (4.10). Instead, we consider **y** to be a realisation from a multivariant Gaussian distribution with non-zero off-diagonal components (unlike the cases in Subsections 4.4.1 and 4.4.2, in which the covariance matrix of the likelihood function only has non-zero components on its diagonal).

4.5 Model uncertainty and noise in the strain

In the previous sections, we have assumed that the strain measurements are perfect (i.e. they are not polluted by noise). In this section, we reformulate the framework such that it can also treat errors in the strain. The errors in the stress and in the strain are assumed to be independent of each other, as the devices to measure the forces and strains or clamp displacements are independent of each other (e.g. if a load cell and digital image correlation are used). We first give the general likelihood function in case model uncertainty and the noise in the strain is incorporated. Then, we specify the likelihood functions for the three material descriptions for monotonically increasing uniaxial tension, if only the error in the noise is incorporated. Subsequently, we include model uncertainty for the three material descriptions.

4.5.1 General likelihood function

In this subsection, a general likelihood function is presented that incorporates model uncertainty as well as the input error (and the output error obviously). As mentioned in Subsection 4.3.2, the experimental output in the KOH framework [47] can be written as follows:

$$y = \sigma(\epsilon, \mathbf{x}) + d(\epsilon) + \omega_y. \tag{4.17}$$

We now assume that each strain measurement, ϵ^*, is also polluted by some statistical error, ω_{ϵ^*}, in an additive manner:

$$\epsilon^* = \epsilon + \omega_{\epsilon^*}, \tag{4.18}$$

where ϵ is the true strain. Similar to the error in the stress measurements, we assume that the strain errors are realisations from a Gaussian distribution with a zero mean and variance $s^2_{\omega_{\epsilon^*}}$. Using Bayes' theorem, we can now write:

$$\pi(\mathbf{x}, \mathbf{x}_d, \epsilon|y, \epsilon^*) = \frac{\pi(y|\mathbf{x}, \mathbf{x}_d, \epsilon)\pi(\epsilon|\epsilon^*)\pi(\mathbf{x})\pi(\mathbf{x}_d)\pi(\epsilon^*)}{\pi(y|\epsilon^*)\pi(\epsilon^*)}, \tag{4.19}$$

or

$$\pi(\mathbf{x}, \mathbf{x}_d, \epsilon|y, \epsilon^*) \propto \pi(y|\mathbf{x}, \mathbf{x}_d, \epsilon)\pi(\epsilon|\epsilon^*)\pi(\mathbf{x})\pi(\mathbf{x}_d). \tag{4.20}$$

The joint distribution of the material parameter vector $\mathbf{x}$ and model uncertainty parameter vector $\mathbf{x}_d$ reads:

$$\pi(\mathbf{x}, \mathbf{x}_d|y, \epsilon^*) \propto \int_0^b \pi(y|\mathbf{x}, \mathbf{x}_d, \epsilon)\pi(\epsilon|\epsilon^*)d\epsilon \; \pi(\mathbf{x})\pi(\mathbf{x}_d), \tag{4.21}$$

where b denotes the physical upper bound of the tensile tester (i.e. the ratio of the original length of the specimen and the maximum distance that the clamps can displace). Assuming again that the noise distributions for both the stress and strain measurements are known Eq. (4.21) for a deterministic model uncertainty reads:

$$\pi(\mathbf{x}, \mathbf{x}_d|y, \epsilon^*) \propto \int_0^b \pi_{\omega_y}(y - \sigma(\epsilon, \mathbf{x}) - d(\epsilon))\pi_{\omega_{\epsilon^*}}(\epsilon^* - \epsilon)d\epsilon \; \pi(\mathbf{x})\pi(\mathbf{x}_d), \tag{4.22}$$

where π_{ω_y} denotes the noise distribution for a stress measurement and $\pi_{\omega_{\epsilon^*}}$ denotes the noise distribution for a strain measurement. Note again that one may assume a form for both noise distributions and then treat the parameters of both distributions as unknowns, which are to be identified together with the material parameters and the model uncertainty parameters in the Bayesian updating procedure. However, we assume that these parameters can be identified using a calibration procedure (see Subsection 4.6.1).

For n_m measurements, the posterior reads:

$$\pi(\mathbf{x}, \mathbf{x}_d|\mathbf{y}, \boldsymbol{\epsilon}^*) \propto \underbrace{\int_0^b \cdots \int_0^b}_{n_m} \pi(\mathbf{y}|\mathbf{x}, \mathbf{x}_d, \boldsymbol{\epsilon})\pi(\boldsymbol{\epsilon}|\boldsymbol{\epsilon}^*)d\boldsymbol{\epsilon}\pi(\mathbf{x})\pi(\mathbf{x}_d), \tag{4.23}$$

where $\mathbf{y} = \begin{bmatrix} y_1 & \cdots & y_{n_m} \end{bmatrix}^T$, $\boldsymbol{\epsilon}^* = \begin{bmatrix} \epsilon_1^* & \cdots & \epsilon_{n_m}^* \end{bmatrix}^T$. We furthermore use now $\pi(\boldsymbol{\epsilon}|\boldsymbol{\epsilon}^*) = N(0, s^2_{\omega_{\epsilon^*}}\mathbf{I}_{n_m})$. $\mathbf{I}_{n_m}$ is the identity matrix of size $n_m \times n_m$. In case of n_m independent measurements, the posterior reads:

$$\pi(\mathbf{x}, \mathbf{x}_d|\mathbf{y}, \boldsymbol{\epsilon}^*) \propto \prod_{i=1}^{n_m} \int_0^b \pi_{\omega_y}(y_i - \sigma(\epsilon, \mathbf{x}) - d(\epsilon))\pi_{\omega_{\epsilon^*}}(\epsilon_i^* - \epsilon)d\epsilon \; \pi(\mathbf{x})\pi(\mathbf{x}_d). \tag{4.24}$$

The integrals in Eqs. (4.21)-(4.24) are either numerically approximated (e.g. using Monte Carlo integration [23]) or analytically determined (see next subsection).

4.5.2 The likelihood function considering input error

Linear elasticity

In case of linear elasticity during monotonically increasing, uniaxial tension, Eq. (4.1) provides the model response, whilst the model uncertainty in Eq. (4.22) is ignored for now. Considering that $\omega_y \sim N(0, s^2_{\omega_y})$ and $\omega_{\epsilon^*} \sim N(0, s^2_{\omega_y})$, the likelihood function for a single measurement reads:

$$\pi(y|\mathbf{x}, \epsilon^*) = \frac{1}{2\pi s_{\omega_y} s_{\omega_{\epsilon^*}}} \int_0^b \exp\Big(- \Big[\frac{(y - E\epsilon)^2}{2s^2_{\omega_y}} + \frac{(\epsilon^* - \epsilon)^2}{2s^2_{\omega_{\epsilon^*}}}\Big]\Big) d\epsilon. \tag{4.25}$$

By computing the integral in Eq. (4.25) analytically, it can be rewritten as follows:

$$\pi(y|\mathbf{x}, \epsilon^*) = \frac{\sqrt{p_3}}{2\sqrt{2\pi} s_{\omega_y} s_{\omega_{\epsilon^*}}} \exp\Big(- \frac{p_2 - p_1^2}{2p_3}\Big) \Big[\text{erf}\Big(\frac{b - p_1}{\sqrt{2p_3}}\Big) - \text{erf}\Big(\frac{-p_1}{\sqrt{2p_3}}\Big)\Big], \tag{4.26}$$

where erf(·) is the error function [104] and p_1, p_2 and p_3 are formulated as follows:

$$p_1 = \frac{E\, y s_{\omega_{\epsilon^*}}^2 + s_{\omega_y}^2 \epsilon^*}{E^2 s_{\omega_{\epsilon^*}}^2 + s_{\omega_y}^2},\ p_2 = \frac{s_{\omega_y}^2 (\epsilon^*)^2 + s_{\omega_{\epsilon^*}}^2 y^2}{E^2\ s_{\omega_{\epsilon^*}}^2 + s_{\omega_y}^2},\ p_3 = \frac{(s_{\omega_y} s_{\omega_{\epsilon^*}})^2}{E^2\ s_{\omega_{\epsilon^*}}^2 + s_{\omega_y}^2}. \tag{4.27}$$

In case of n_m measurements, $\pi(\mathbf{y}|\mathbf{x}, \boldsymbol{\epsilon}^*)$ is obtained using the product in Eq. (4.24).

Linear elasticity-perfect plasticity

The only change for linear elasticity-perfect plasticity compared to linear elasticity is the material model. Substituting Eq. (4.2) in Eq. (4.22) yields:

$$\begin{aligned}\pi(y|\mathbf{x}, \epsilon^*) = \frac{1}{2\sqrt{2\pi} s_{\omega_y} s_{\omega_{\epsilon^*}}} \Bigg(& \sqrt{p_3} \exp\Big(- \frac{p_2 - p_1^2}{2p_3}\Big) \Big[\operatorname{erf}\Big(\frac{\frac{\sigma_{y0}}{E} - p_1}{\sqrt{2p_3}}\Big) - \operatorname{erf}\Big(\frac{-p_1}{\sqrt{2p_3}}\Big)\Big] + \\ & s_{\omega_{\epsilon^*}} \exp\Big(- \frac{(y - \sigma_{y0})^2}{2s_{\omega_y}^2}\Big) \Big[\operatorname{erf}\Big(\frac{\epsilon^* - \frac{\sigma_{y0}}{E}}{\sqrt{2} s_{\omega_{\epsilon^*}}}\Big) - \operatorname{erf}\Big(\frac{\epsilon^* - b}{\sqrt{2} s_{\omega_y}}\Big)\Big], \end{aligned} \tag{4.28}$$

where p_1, p_2 and p_3 are again given by Eq. (4.27).

Linear elasticity-linear hardening

For linear elasticity-linear hardening, the unknown parameters are $\mathbf{x} = \begin{bmatrix} E & \sigma_{y0} & H \end{bmatrix}^T$. Again substituting Eq. (4.3) in Eq. (4.22) results in the following likelihood function for a single measurement:

$$\begin{aligned}\pi(y|\mathbf{x}, \epsilon^*) = \frac{1}{2\sqrt{2\pi} s_{\omega_y} s_{\omega_{\epsilon^*}}} \Bigg(& \sqrt{p_3} \exp\Big(- \frac{p_2 - p_1^2}{2p_3}\Big) \Big[\operatorname{erf}\Big(\frac{\frac{\sigma_{y0}}{E} - p_1}{\sqrt{2p_3}}\Big) - \operatorname{erf}\Big(\frac{-p_1}{\sqrt{2p_3}}\Big)\Big] + \\ & \frac{1}{\sqrt{p_1^*}} \exp\Big(- \frac{p_1^* p_3^* - p_2^{*2}}{2p_1^*}\Big) \Big[\operatorname{erf}\Big(\frac{\sqrt{p_1^*} a - \frac{p_2^*}{\sqrt{p_1^*}}}{\sqrt{2}}\Big) - \operatorname{erf}\Big(\frac{\frac{\sigma_{y0}\sqrt{p_1^*}}{E} - \frac{p_2^*}{\sqrt{p_1^*}}}{\sqrt{2}}\Big)\Big], \end{aligned} \tag{4.29}$$

where p_1, p_2 and p_3 are again given by Eq. (4.27) and p_1^*, p_2^* and p_3^* are expressed as follows:

$$\begin{aligned} p_1^* &= \frac{\left(\frac{HE}{H+E}\right)^2}{s_{\omega_y}^2} + \frac{1}{s_{\omega_{\epsilon^*}}^2},\ p_2^* = \frac{(y - \sigma_{y0}) \frac{HE}{H+E} + \left(\frac{HE}{H+E}\right)^2 \frac{\sigma_{y0}}{E}}{s_\sigma^2} + \frac{\epsilon^*}{s_{\omega_{\epsilon^*}}^2}, \\ p_3^* &= \frac{(y - \sigma_{y0})^2 + 2(y - \sigma_{y0}) \frac{HE}{H+E} \frac{\sigma_{y0}}{E} + \left(\frac{HE}{H+E}\right)^2 \left(\frac{\sigma_{y0}}{E}\right)^2}{s_{\omega_y}^2} + \frac{(\epsilon^*)^2}{s_{\omega\epsilon^*}^2}. \end{aligned} \tag{4.30}$$

In the following subsection we present the formulations of the likelihood functions if model uncertainty is incorporated as well.

4.5.3 The likelihood function considering input error and model uncertainty

Adding input-dependent model uncertainty renders even the likelihood function of the linear elastic material model impossible to analyse analytically. Consequently, we employ Monte Carlo integration to numerically approximate the integral of Eq. (4.21). $\pi(\mathbf{y}|\mathbf{x}, \mathbf{x}_d, \boldsymbol{\epsilon})$ for all formulations of model uncertainty are given in Eqs. (4.11), (4.12) and (4.15).

Note that in the case of the GP, the components of the measurement vector $\mathbf{y}$ are correlated. This means that updating, according to the multiplication operation in Eq. (4.24), is not possible. Instead, we consider that measurement vector $\mathbf{y}$ is a realisation from a multivariant Gaussian distribution with non-zero off-diagonal components. In this case, Eq. (4.23) is used to construct the posterior.

4.6 Examples

This section presents some examples of the Bayesian framework for the elastic and elastoplastic material models and uniaxial tensile data. The main points we aim to investigate are: (1) the influence of incorporating the input error, (2) the influence of incorporating the three types of model uncertainty and (3) the influence of incorporating both the input error and model uncertainty.

For this purpose the measurements are generated numerically using responses which deviate from the constitutive responses. Next, Bayesian inference is used to identify the parameters of the material models given in Section 4.2. To investigate the effect of incorporating the input error and model uncertainty on the identification results, posteriors and posterior predictions are furthermore presented for various cases and compared with the true parameter values and measurements. However, we first start with the calibration of the two measurement noises for uniaxial tensile tests. Note that all results are obtained using the adaptive Metropolis method for 5×10^4 samples, whilst burning the first 1.5×10^4 samples.

4.6.1 Noise calibration

We start the noise calibration procedure by acquiring measurement data without the use of actual specimens. Stress-strain measurements as schematically presented in Fig. 4-1 are typical results. They show that both noises can be represented as individual normal distributions with zero means and their own variance. In this chapter we have assumed $s_{\omega_y} = 0.01$ GPa and $s_{\omega_{\epsilon^*}} = 5 \times 10^{-5}$.

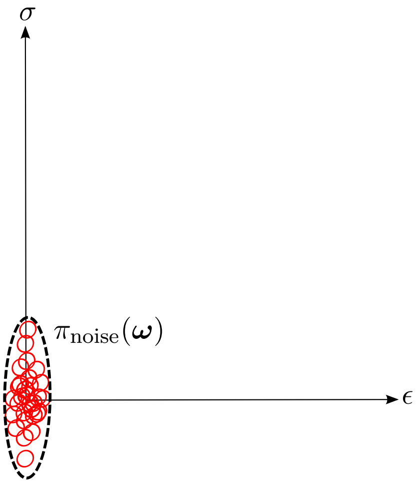

Figure 4-1: Schematic of the stress-strain measurements (red circles) of the 'noise calibration experiments', including an isoline if both noise distributions would be represented by a bivariate normal distribution (dashed).

4.6.2 Linear elasticity

Input error

In the first example, the added value of including the strain error is investigated for linear elasticity. The measurement data are originating from the following non-linear expression:

$$\sigma(\epsilon, a, E) = \frac{E\epsilon}{1 + \frac{\epsilon}{a}}, \tag{4.31}$$

where $E = 210$ GPa and $a = 0.015$. 20 measurements are generated using the same noise distributions as identified in the previous subsection. Parameter a in Eq. (4.31) is chosen such that the difference between the non-linear expression used to generate the measurements and its linear approximation in the neighbourhood of $\epsilon = 0$ (i.e. $\sigma = 210\epsilon$) is not too large (see Fig. 4-2(a)). We consider the following prior for the Young's modulus:

$$\pi(E) \propto \begin{cases} \exp\left(- \frac{(E - \overline{E}_{\text{prior}})^2}{2 s^2_{\overline{E}_{\text{prior}}}} \right) & \text{if } E \geq 0 \\ 0 & \text{otherwise} \end{cases}, \tag{4.32}$$

with $\overline{E}_{\text{prior}} = 150$ GPa and $s_{\overline{E}_{\text{prior}}} = 50$ GPa.

Fig. 4-2(b) presents the marginal posterior PDF of the Young's modulus for the case in which the output error alone is included (red curve) and for the case in which both the output and input errors are included (blue curve). Incorporating both error sources clearly results in a wider posterior. However, none of the resulting posteriors contains true value $E = 210$ GPa. The posterior mean and variance are given in Table 4.1.

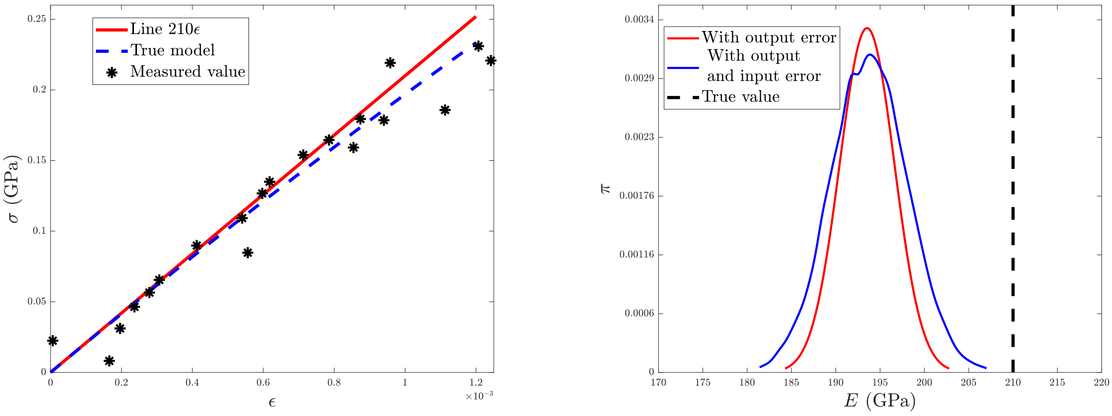

(a) (b)

Figure 4-2: Linear elasticity: (a) The experimental data generated for the first example, including the curve from which the data points are generated and its approximation in the neighbourhood of $\epsilon = 0$. One can see that parameter a is chosen such that the difference between line 210ϵ and the true model is not large for small strains. (b) The marginal posterior PDF of the Young's modulus if the stress error alone is incorporated (red curve) and if the stress and strain errors are incorporated (blue curve). Considering both errors results in a wider distribution of the Young's modulus, but none of the distributions contain the true value.

The posterior predictions are shown in Fig. 4-3. One can observe that incorporating both error sources results in a wider envelope. This wider envelope includes more measurements, meaning that incorporating both error sources results in a more likely result.

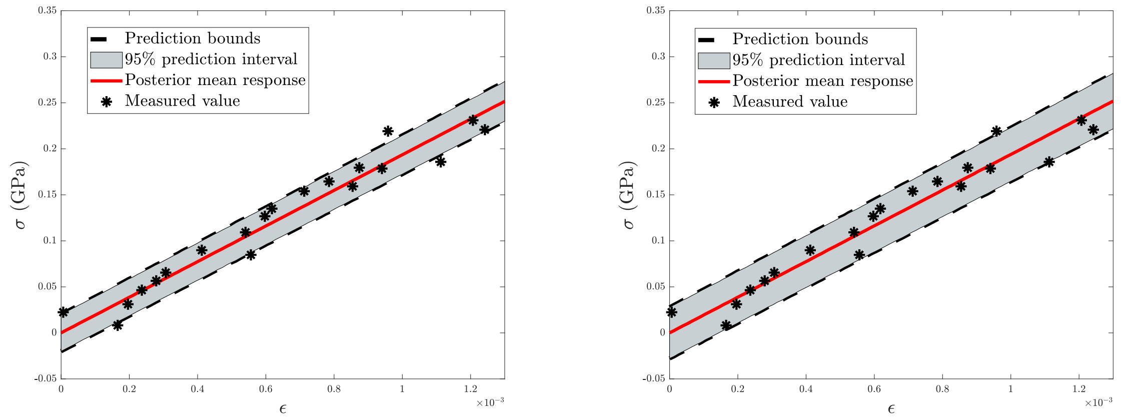

(a) Error in the stress measurements only

(b) Error in both the stress and strain measurements

Figure 4-3: Linear elasticity: The measurements, the posterior mean response and the posterior predictions. One can observe that the incorporation of both error sources results in a wider envelope, thereby including more measurements.

Input error and model uncertainty

The effect of model uncertainty on the resulting posterior is studied now. First, we only include the case with output error but without input error. The prior used for the Young's modulus is the same mentioned previously. For the case in which model uncertainty is considered as a random variable coming from a Gaussian distribution with an input-dependent mean, we consider the following expression for its mean:

$$\overline{d}(\epsilon) = a_0 + a_1\epsilon + a_2\epsilon^2. \tag{4.33}$$

In case model uncertainty is modelled as a random variable, either coming from a Gaussian distribution with constant parameters or coming from a Gaussian distribution with an input-dependent mean, infinitely wide uniform distributions are used as prior distributions for the model uncertainty parameters ($\mathbf{x}_d$). However, for the case in which model uncertainty is described as a Gaussian process with a stationary covariance function, we have considered the following prior distributions for the model uncertainty parameters ($\mathbf{x}_d = \begin{bmatrix}\lambda & \psi\end{bmatrix}^T$):

$$\pi(\lambda) \propto \begin{cases} \exp\Big(-\frac{(\lambda-\overline{\lambda}_{\text{prior}})^2}{2s^2_{\overline{\lambda}_{\text{prior}}}}\Big) & \text{if } \lambda \geq 0 \\ 0 & \text{otherwise} \end{cases}, \tag{4.34}$$

and,

$$\pi(\psi) \propto \begin{cases} \exp\Big(-\frac{(\psi-\overline{\psi}_{\text{prior}})^2}{2s^2_{\overline{\psi}_{\text{prior}}}}\Big) & \text{if } \psi \geq 1.578 \times 10^{-5} \\ 0 & \text{otherwise} \end{cases}, \tag{4.35}$$

where $\overline{\lambda}_{\text{prior}} = 0.025$ GPa, $s_{\overline{\lambda}_{\text{prior}}} = 0.0083$ GPa, $\overline{\psi}_{\text{prior}} = 0.0006$ and $s_{\overline{\psi}_{\text{prior}}} = 0.0003$.

It must be noted that if infinitely wide uniform distributions are used for the model uncertainty parameters of the Gaussian process, the MCMC algorithm fails to converge. Using the fact that the model uncertainty function ($d(\epsilon)$) is a smooth function, we have chosen the mean of the prior for the length scale parameter ($\overline{\psi}_{\text{prior}}$) to be half of the maximum occurring strain. The standard deviation is chosen to be relatively large. To prevent negative length scale parameters and length scale parameters smaller than the minimum distance between two consecutive strains to be realised from the prior distribution, we have set a lower bound on the prior distribution. We have chosen the value of the mean of the variance of the GP ($\overline{\lambda}_{\text{prior}}$ in Eq. (4.34)) as 10% of the maximum occurring stress and the standard deviation such that 99.7% of the realisations coming from the prior distribution remain below 20% of the maximum occurring stress. A lower bound is also included (Eq. (4.34)).

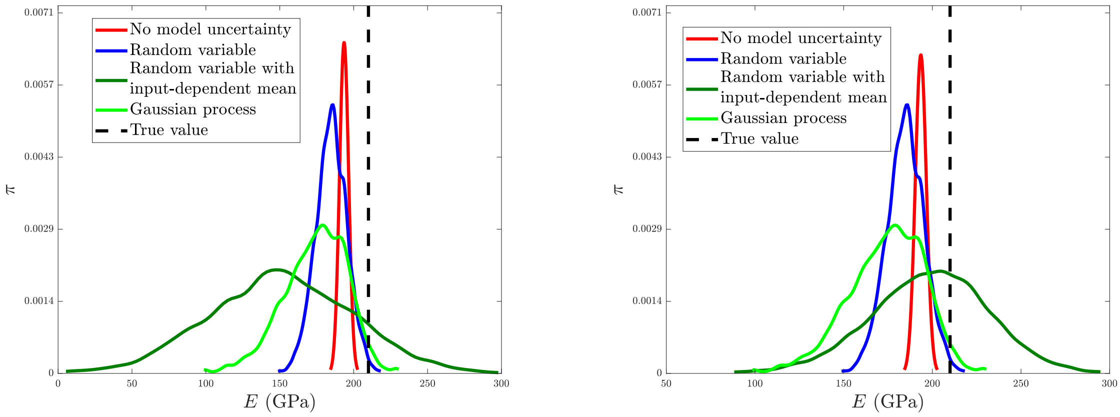

(a) (b)

Figure 4-4: Linear elasticity: Marginal posteriors for the Young's modulus for different types of model uncertainty. (a) The mean for model uncertainty as a random variable coming from a Gaussian distribution with input-dependent mean, is given by Eq. (4.33). One can observe that incorporating any of the model uncertainties results in wider posterior distributions. Although the MAP point moves further away from the true value for all model uncertainty cases, all their posteriors include the true value, whereas the posterior for the case without model uncertainty does not include the true value. It must furthermore be noted that the posterior for the case in which model uncertainty is treated as a random variable coming from a Gaussian distribution with an input-dependent mean, is practically the same as the prior of the Young's modulus. (b) The same marginal posteriors as in (a), except that the case in which model uncertainty is modelled as a random variable coming from a normal distribution with an input-dependent mean, Eq. (4.36) is used for the mean instead of Eq. (4.33). One can see that the MAP point has moved considerably closer to the true value. This can be caused by the fact that the true stress-strain behaviour given in Eq. (4.31) is not highly nonlinear and the difference between $\sigma(\epsilon, a, E)$ in Eq. (4.31) and linear elasticity ($E\epsilon$) can rather accurately be represented by the remaining terms of a Taylor expansion for $\sigma(\epsilon, a, E)$.

Fig. 4-4(a) shows that the incorporation of model uncertainty increases the widths of the posteriors, such that the true value is possible to be generated from it. On the other hand, the MAP point (point estimator) when model uncertainty is not incorporated is closer to the true value than all the other posteriors' MAP points.

An important point to mention here is that in case model uncertainty is incorporated as a random variable coming from a normal distribution with an input-dependent mean, the marginal posterior PDF is approximately the same as the prior of the Young's. The reason for this is the linear term that is present in the input-dependent mean ($a_1\epsilon$ in Eq. (4.33)), which is also present in the model ($E\epsilon$). If we ignore the linear term and instead use the following expression for the input-dependent mean:

$$\overline{d}(\epsilon) = a_0 + a_2\epsilon^2, \tag{4.36}$$

we obtain the PDF presented in Fig. 4-4(b). The figure shows that the marginal posterior includes the true value of the Young's modulus. The MAP point has furthermore moved substantially closer to the true value. This can be caused by the fact that the true response (Eq. (4.31)) is not highly nonlinear and hence, its difference with the linear approximation (here $E\epsilon$) can be rather accurately described by a remaining terms of the Taylor expansion of the true model.

The posterior predictions for the three kinds of model uncertainty are presented in Figs. 4-5(a), 4-5(c) and 4-5(e). The diagrams show that if model uncertainty is considered as a random variable coming from a normal distribution, either with constant parameters or an input-dependent mean, more measurements are included in the envelope than if model uncertainty is represented by a Gaussian process. By comparing Figs. 4-3 and 4-5(e) furthermore, it becomes clear that more measurement data is present in the posterior prediction's envelope if both errors in the stress and strain are considered than if model uncertainty is considered as a Gaussian process without input error. This can be caused by the fact that, although the posterior is wider, the mean and MAP point are further from the true value if model uncertainty is described by a Gaussian process (see Fig. 4-4(a) and Table 4.1).

The effect of treating the input error as well as incorporating model uncertainty is presented in Fig. 4-6 for the marginal posteriors. Note that we have used the same priors as before. One can see that the posteriors become wider if the input error is incorporated, except for the Gaussian process. That posterior has however changed such that the true value is less in its tail, than if the input error is not incorporated.

The posterior predictions for all three model uncertainties if the input error is also considered are shown in Figs. 4-5(b), 4-5(d) and 4-5(f). One can see that for both cases in which model uncertainty is a random variable, the posterior mean responses move closer to the measurement data. In case model uncertainty is considered as a Gaussian process, including the input error results in a wider envelope that includes more data (cf. Figs. 4-5(e) and 4-5(f)). Also the only data point not present in the envelope is still closer to the envelope if the input error is considered. The numerical values for the marginal posteriors mean, MAP point and standard deviation are given in Table 4.1.

4.6.3 Linear elasticity-perfect plasticity

For linear elasticity, we have shown that considering the error in the strain and model uncertainty leads to wider marginal posteriors of the Young's modulus (except if model uncertainty is treated as a Gaussian process). This can generally be considered as an improvement, because either the true value was present inside the wider distributions or the MAP point has moved towards the true value. In this subsection, we will consider linear elasticity-perfect plasticity.

In the next example, we generate the measurements using the following expression:

$$\sigma(\epsilon, \mathbf{x}_{\text{true}}) = \begin{cases} \frac{E\epsilon}{1+\frac{\epsilon}{a}} & \text{if } \epsilon \leq 0.0012 \\ \sigma_{y0} + H\Big(\epsilon - \frac{\sigma(\epsilon,\mathbf{x})}{E}\Big)^m & \text{if } \epsilon > 0.0012 \end{cases}, \tag{4.37}$$

where $\mathbf{x}_{\text{true}} = \begin{bmatrix} E & a & \sigma_{y0} & H & m \end{bmatrix}^T$. Thirty measurements are generating with $E = 210$ GPa, $a = 0.015$, $\sigma_{y0} = 0.2333$ GPa, $H = 2$ GPa, $m = 0.57$, $s_{\omega_y} = 0.01$ GPa and $s_{\omega_{\epsilon^*}} = 5\times10^{-5}$, which are shown in Fig. 4-8. The parameters to be identified in linear elasticity-perfect plasticity are obviously Young's modulus E and yield stress σ_{y0}. The same prior as in Eq. (4.32) is used for Young's modulus and the yield stress's prior reads similarly:

$$\pi(\sigma_{y0}) \propto \begin{cases} \exp\Big(-\frac{(\sigma_{y0}-\overline{\sigma}_{y0_{\text{prior}}})^2}{2s^2_{\overline{\sigma}_{y0_{\text{prior}}}}}\Big) & \text{if } \sigma_{y0} \geq 0 \\ 0 & \text{otherwise} \end{cases}, \tag{4.38}$$

where $\overline{\sigma}_{y0_{\text{prior}}} = 0.25$ GPa and $s_{\overline{\sigma}_{y0_{\text{prior}}}} = 0.025$ GPa.

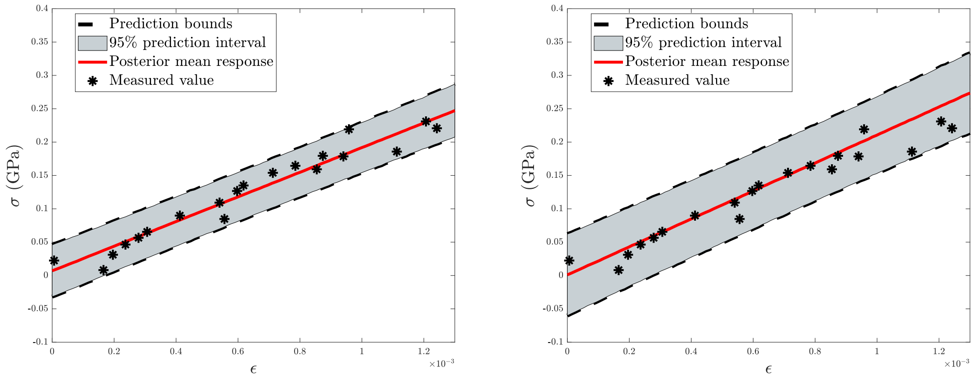

(a) (b)

Normal distribution with constant parameters

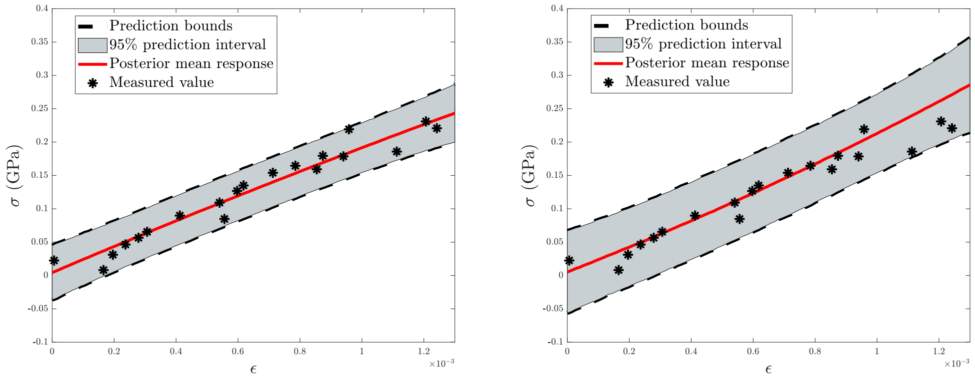

(c) (d)

Normal distribution with an input-dependent mean

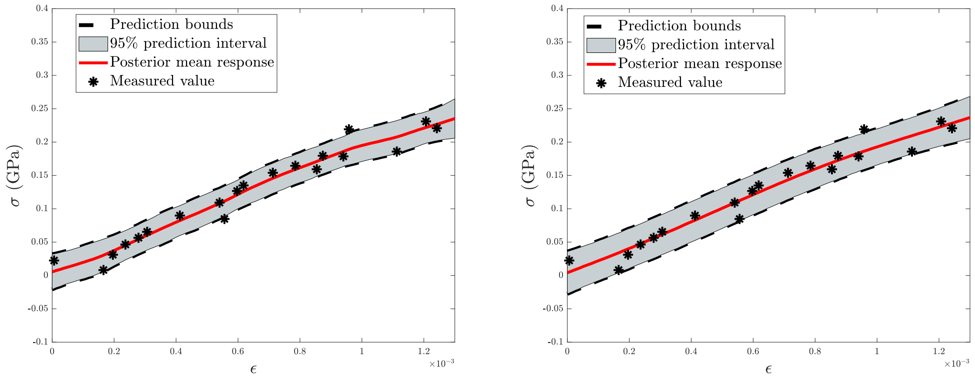

(e) (f)

Gaussian process

Figure 4-5: Linear elasticity: The measurements, the posterior mean responses and the posterior predictions. Left: without input error and right: including input error. One can see that if model uncertainty is described by a random variable coming from a normal distribution either with constant parameters or an input-dependent mean, more measurements are present inside the posterior's predictions interval than if a Gaussian process is considered. In case model uncertainty is a Gaussian process furthermore, one can see that including the input error results in more measurements to be present inside the posterior prediction bounds (cf. Figs. 4-5(e) and 4-5(f)).

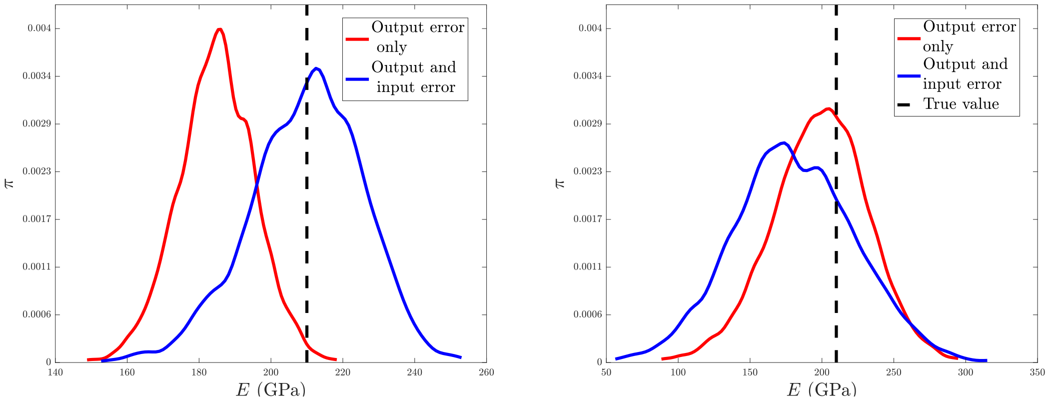

(a) Normal distribution with constant parameters

(b) Normal distribution with an input-dependent mean

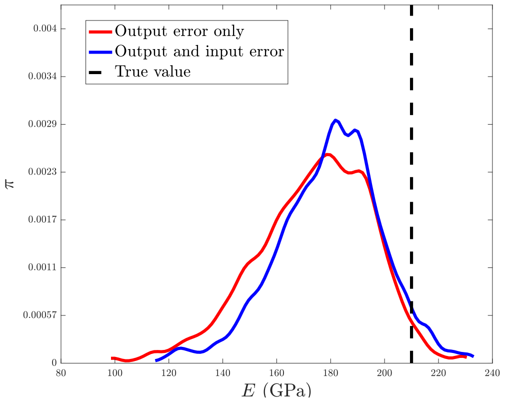

(c) Gaussian process

Figure 4-6: Linear elasticity: Marginal posteriors of the Young's modulus for three kinds of model uncertainty including input error. One can see that if model uncertainty is described by a random variable coming from a normal distribution (either with constant parameters or an input-dependent mean) the marginal posterior becomes wider if the input error is incorporated. In case model uncertainty is represented by a Gaussian process, the marginal posterior gets slightly narrower.

Table 4.1: Linear elasticity: The numerical values of the mean, the MAP point and the standard deviation of the marginal posterior PDFs of the Young's modulus for all considered cases.

Model uncertainty	Mean (GPa)	MAP (GPa)	Standard deviation (GPa)
Error in the stress only			
None	193.5201	193.5201	3.0861
Random variable from a normal distribution with constant parameters	184.7892	185.6223	10.7162
Random variable from a normal distribution with an input-dependent mean	198.3326	209.6297	33.5192
Gaussian process with a stationary covariance function	173.8981	191.6519	21.5282
Error in the stress and strain			
None	193.7848	193.6629	4.3032
Random variable from a normal distribution with constant parameters	209.7249	208.3623	15.9041
Random variable from a normal distribution with an input-dependent mean	180.6751	187.1383	42.6510
Gaussian process with a stationary covariance function	179.6355	184.3772	19.4364

We separately consider the error in the stress, the errors in both the stress and the strain, and the errors in both the stress and the strain as well as model uncertainty. For the case in which model uncertainty is treated as a random variable coming from a normal distribution with an input-dependent mean, we use the relation of Eq. (4.33). Furthermore, the prior distributions of the covariance function's parameters for the Gaussian process ($\mathbf{x}_d = \begin{bmatrix}\lambda & \psi\end{bmatrix}^T$) are given by Eqs. (4.38) and (4.39) with $\overline{\lambda}_{\text{prior}} = 0.03$ GPa, $s_{\overline{\lambda}_{\text{prior}}} = 0.01$ GPa, $\overline{\psi}_{\text{prior}} = 0.0028$ and $s_{\overline{\psi}_{\text{prior}}} = 9.3333 \times 10^{-4}$. The lower bound for length scale parameter ψ is set to 2.89×10^{-6}.

Figs. 4-7(a) and 4-7(b) show that all marginal posterior PDFs of the Young's modulus contain the true value, but adding model uncertainty results in a higher probability at the true value. This is especially true if a Gaussian process is used to describe model uncertainty. One can furthermore see in Fig. 4-7(b) that only adding the error in the strain has a negligible effect on the marginal posterior PDF of the yield stress. This is due to the fact that the plastic domain in linear elasticity-perfect plasticity is not dependent on the strain at all. Furthermore, one can see that if model uncertainty is described by a random variable coming from a normal distribution with constant parameters, the marginal posterior of the yield stress does not include the true value. The marginal posteriors with model uncertainty and the error in the stress only are presented in Figs. 4-7(c) and 4-7(d) for comparison.

The posterior predictions are shown in Fig. 4-8. This figure shows that adding model uncertainty results in posterior predictions that encompass all measurement data. Note that if model uncertainty is a random variable coming from a normal distribution with constant parameters (Fig. 4-8(c)), no hardening can be observed and hence, adding model uncertainty increases the width of the prediction interval. It can furthermore be observed that the measurements are closer to the posterior mean responses if model uncertainty is input-dependent (see Figs. 4-8(d) and 4-8(e)).

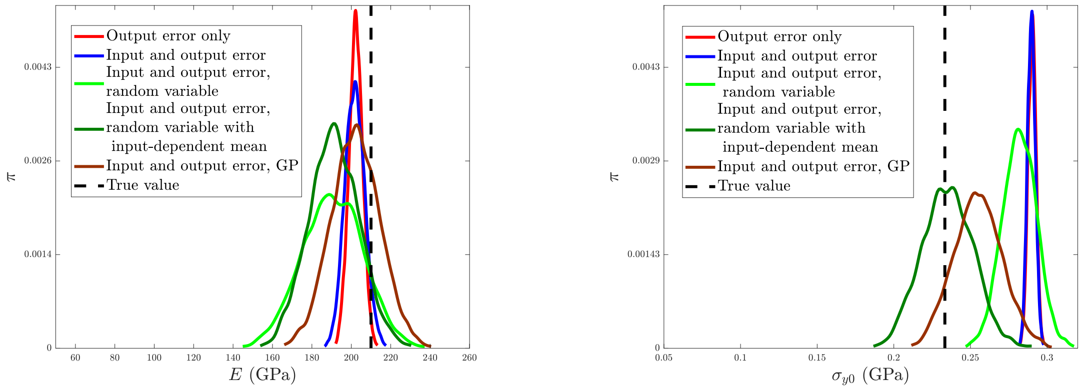

(a) Young's modulus (b) Yield stress

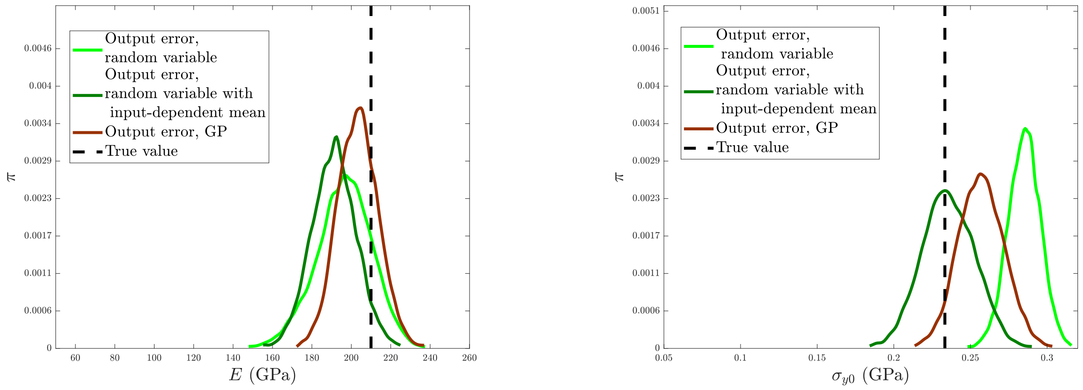

(c) Young's modulus (d) Yield stress

Figure 4-7: Linear elasticity-perfect plasticity: The Young's modulus (left) and the yield stress (right) in case the input error is incorporated (top) and ignored (bottom). One can see that the posterior of the Young's modulus improves substantially by incorporating the input error and even more by incorporating any of the three model uncertainties. The posteriors of the yield stress are not improved by considering the input error and only improve substantially if a type of model-uncertainty is incorporated that is input-dependent. The reason is that the yield stress does not depend on the strain.

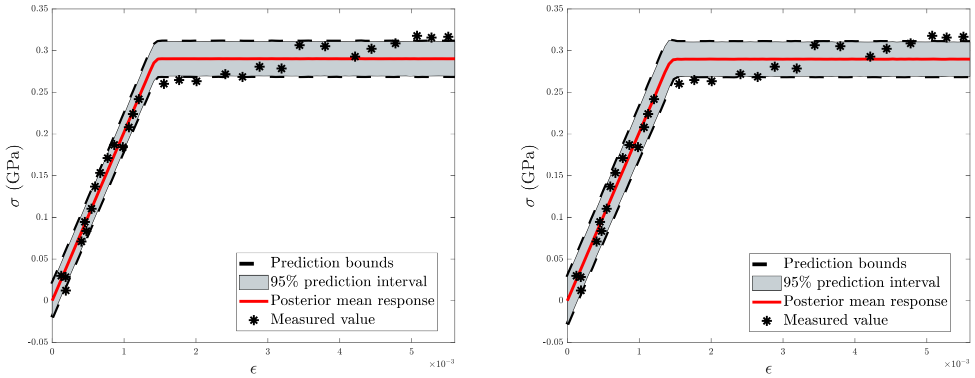

(a) Error in the stress only (b) Error in both the stress and the strain

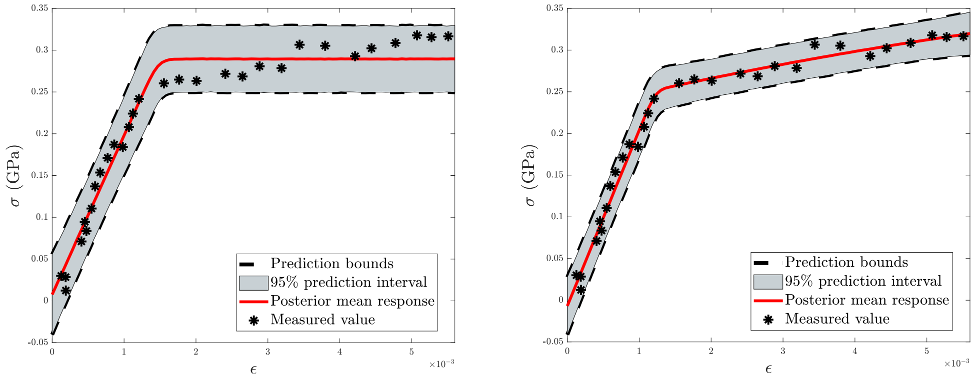

(c) Normal distribution with constant parameters (d) Normal distribution with an input-dependent mean

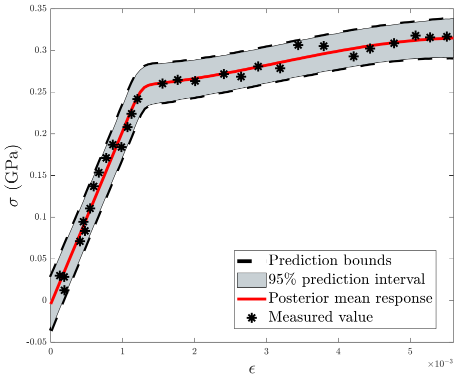

(e) Gaussian process

Figure 4-8: Linear elasticity-perfect plasticity: The measurements, the posterior mean responses and the posterior predictions. One can see that considering any type of model uncertainty results in all measurement data to be present in the posterior prediction bounds. For the case in which model uncertainty is a random variable coming from a normal distribution with constant parameters, no hardening effect can be observed and hence, adding model uncertainty increases the width of the prediction interval. In the other two cases of model uncertainty, hardening can be observed. In case model uncertainty is input-dependent furthermore((d) and (e)), the measurement data is closer to the posterior mean responses.

In this subsection, we have presented some typical examples for linear elasticity-perfect plasticity, whereby we have generated the measurement data using relations that are not too different from the model response of interest. This has allowed us to compare the identified distributions with the true values. However, the measurement data may deviate considerably more from the model response. In the next subsection, we present examples for linear elasticity-linear hardening. Because the deviation between the curves used to generate the data and the model response is so significant, we will not be able to compare the distributions with true values. Instead, we will only investigate the posterior predictions.

4.6.4 Linear elasticity-linear hardening

In this subsection, we have initially generated 30 measurements using the following curve:

$$\sigma(\epsilon, a, \epsilon_{\max}) = a\sqrt{\epsilon_{\max}^2 - (\epsilon_{\max} - \epsilon)^2}, \tag{4.39}$$

where $a = 50$ GPa, $0 \leq \epsilon \leq \epsilon_{\max}$ and $\epsilon_{\max} = 0.0056$. Similar as in the previous subsection, output and input noise was generated using $s_{\omega_y} = 0.01$ GPa and $s_{\omega_{\epsilon^*}} = 5 \times 10^{-5}$ (see Fig. 4-9 for the measurements). The linear elastic-linear hardening model is used as the material description. This entails that we want to identify Young's modulus E, yield stress σ_{y0} and hardening modulus H. The same prior distributions as in Eqs. (4.32) and (4.38) are used for the Young's modulus and yield stress with $\overline{E}_{\text{prior}} = 100$ GPa, $s_{\overline{E}_{\text{prior}}} = 50$ GPa, $\overline{\sigma}_{y0} = 0.25$ GPa and $s_{\overline{\sigma}_{y0}} = 0.05$ GPa. The prior for the hardening modulus reads:

$$\pi(H) \propto \begin{cases} \exp\Big(-\frac{(H-\overline{H}_{\text{prior}})^2}{2s_{\overline{H}_{\text{prior}}}^2}\Big) & \text{if } H \geq 0 \\ 0 & \text{otherwise} \end{cases}, \tag{4.40}$$

where $\overline{H}_{\text{prior}} = 30$ GPa and $s_{\overline{H}_{\text{prior}}} = 15$ GPa. In case model uncertainty is described by a random variable coming from a normal distribution with an input-dependent mean, the relation of Eq. (4.33) is used for the mean. Furthermore, the prior distributions of the covariance function's parameters for the Gaussian process are given in Eqs. (4.34) and (4.35) with $\overline{\lambda}_{\text{prior}} = 0.03$ GPa, $s_{\overline{\lambda}_{\text{prior}}} = 0.01$ GPa, $\overline{\psi}_{\text{prior}} = 0.0028$ and $s_{\overline{\psi}_{\text{prior}}} = 9.3333 \times 10^{-4}$. The lower limit for length scale parameter ψ is set to 2.5×10^{-5}.

The posterior predictions are presented in Fig. 4-9. Two main issues can be observed. (1) By comparing Figs. 4-9(a) and 4-9(b), it can be noticed that including the error in the strain results in a wider prediction interval. This is especially true for the initial part of the response in which the model response is only governed by elasticity. This is due to the fact that the Young's modulus is larger than the stiffness during elastoplastic deformation (i.e. $\frac{HE}{H+E}$ in Eq.(4.3)). (2) Considering model uncertainties furthermore results in wide posterior prediction envelopes, which consequently include almost all measurement and verification points. Only for the case in which model uncertainty is represented by a random variable coming from a normal distribution with constant parameters, two verification points are not present within the bounds. One should note however, that in the cases in which model uncertainty is input-dependent, the model uncertainty is so dominant that the two linear regimes in the model response (the elastic regime and the elastoplastic regime) cannot be recognised anymore.

It is also worth to mention that in case the difference between the constitutive model (here linear elasticity-linear hardening) and the true response used to generate the measurements (here Eq. (4.39)) is large, the influence of incorporating model uncertainty is larger than that of incorporating the error in the strain. Incorporating the error in the strain, if model uncertainty is to be incorporated, can still have a positive influence however, as we have presented for linear elasticity.

In the examples in which linear elasticity and linear elasticity-perfect plasticity were considered, we were able to compare not just the posterior predictions with the measurement data, but also the marginal posteriors with the true values. In case of linear elasticity-linear hardening, it is not possible to compare the marginal posteriors with the true values, because the material model and the true response do not share any parameters. In the case of linear elasticity-linear hardening therefore, we have introduced and will introduce verification points in order to compare the posterior predictions in more detail. In Fig. 4-9, we have shown verification points inside the domain of the measured strains. Now, we will add verification data outside the strain domain and investigate the posterior predictions for the verification points outside the initial strain domain.

Instead of 30 measurements, we now consider 20 measurements, polluted by noise coming from the aforementioned noise distributions. All priors and their parameters remain the same, except that the covariance function's parameters for the Gaussian process are set to $\overline{\lambda}_{\text{prior}} = 0.026$ GPa, $s_{\overline{\lambda}_{\text{prior}}} = 0.0087$ GPa, $\overline{\psi}_{\text{prior}} = 0.0018$ and $s_{\overline{\psi}_{\text{prior}}} = 0.0006$. The lower limit for length scale parameter ψ is set to 2.5×10^{-5}.

The posterior predictions are shown in Fig. 4-10, together with the measurement and verification data. It can be observed that all verification data are inside the posterior predictions' bounds if model uncertainty is described by a random variable coming from a normal distribution with constant parameters or by a Gaussian process. In case model uncertainty is described by a Gaussian process furthermore, the uncertainty is substantially larger than if a random variable coming from a normal distribution with constant parameters is used. This can be due to the fact that the Gaussian process assumes the measurements to be correlated, and hence, the larger the distance from the measured data, less information is available and a larger spread is observed. It can furthermore be observed that the smallest number of verification data is present inside the posterior prediction's bounds if model uncertainty is represented by a normal distribution with an input-dependent mean. It must be noted though, that if another relation for the mean would be selected, the posterior predictions would differ.

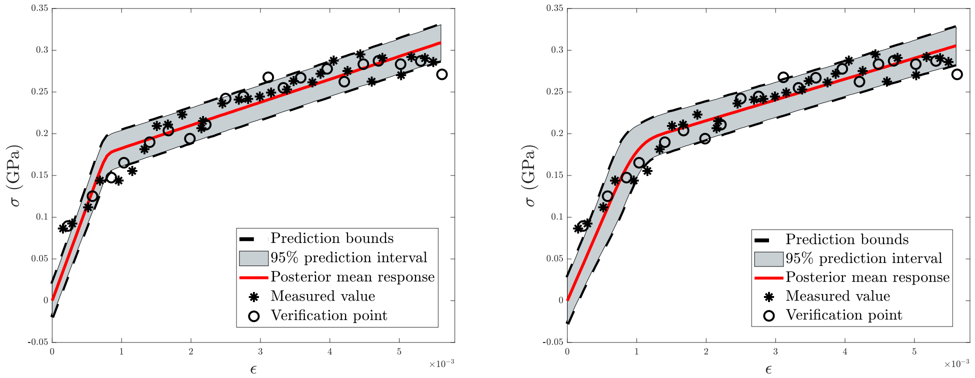

(a) Error in the stress only

(b) Error in both the stress and the strain

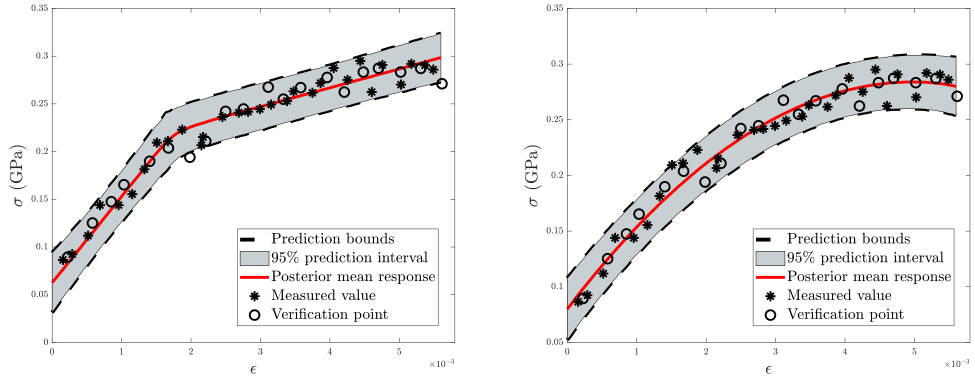

(c) Normal distribution with constant parameters

(d) Normal distribution with an input-dependent mean

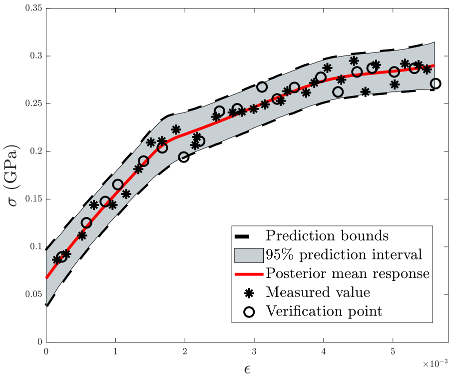

(e) Gaussian process

Figure 4-9: Linear elasticity-linear hardening: The measurements, the verification points, the posterior mean responses and the posterior predictions. Note that for all cases in which model uncertainty is incorporated, the error in the strain is also incorporated. One can see that considering model uncertainty results in more measurements to be present inside the bounds of the posterior predictions. For the cases in which model uncertainty is input-dependent the model uncertainty is so dominant that the two linear regimes in the model response (the elastic regime and the elastoplastic regime) cannot be recognised anymore.

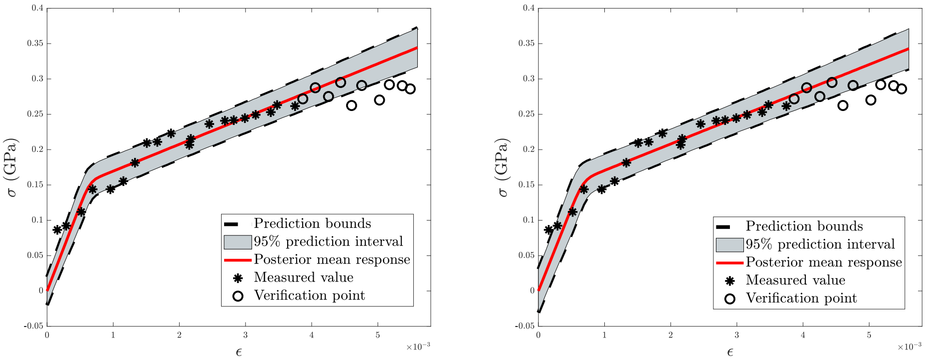

(a) Error in the stress only (b) Error in both the stress and the strain

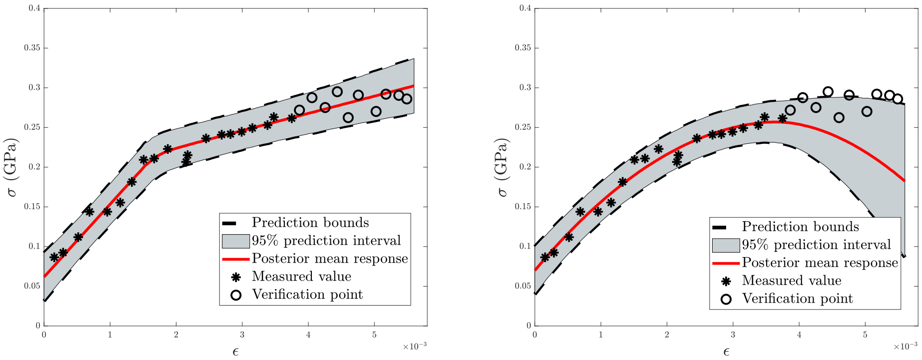

(c) Normal distribution with constant parameters (d) Normal distribution with an input-dependent mean

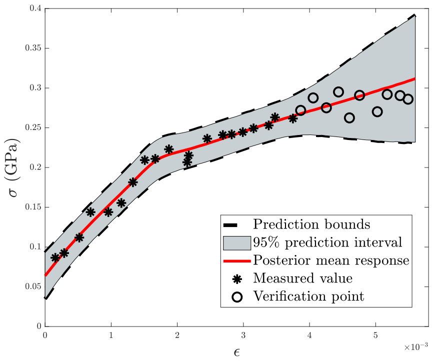

(e) Gaussian process

Figure 4-10: Linear elasticity-linear hardening: The measurements, the verification points, the posterior mean responses and the posterior predictions. Note that for all cases in which model uncertainty is incorporated, the error in the strain is also incorporated. One can see that considering model uncertainty results in more measurements to be located inside the bounds of the posterior predictions. It can be observed that all verification data are inside the posterior predictions' bounds if model uncertainty is described by a random variable coming from a normal distribution with constant parameters or by a Gaussian process. In case model uncertainty is described by a Gaussian process furthermore, the uncertainty is substantially larger than if a random variable coming from a normal distribution with constant parameters is used. This can be due to the fact that the Gaussian process assumes the measurements to be correlated, and hence, the larger the distance from the measured data, less information is available and a larger spread is observed. It can furthermore be observed that the smallest number of verification data is present inside the posterior prediction's bounds if model uncertainty is represented by a normal distribution with an input-dependent mean. It must be noted though, that if another relation for the mean would be selected, the posterior predictions would differ.

4.7 Conclusions

In this chapter, we have formulated a Bayesian approach that considers the output error (the error in the stress), the input error (the error in the strain) and the uncertainty of the model in order to identify parameters in elasticity and elastoplasticity from monotonically increasing uniaxial tensile tests. We have treated three types of model uncertainty: (1) a random variable coming from a normal distribution with constant parameters, (2) a random variable coming from a normal distribution with an input-dependent mean and (3) a Gaussian process with a stationary covariance function.

We have applied the identification approach to linear elasticity, linear elasticity-perfect plasticity and linear elasticity-linear hardening. The measurement data were artificially generated, allowing us to compare the parameter distributions with the true values for linear elasticity and linear elasticity-perfect plasticity, because the material models and the true responses, used to generate the measurement data, shared parameters. For linear elasticity-linear hardening the difference between the true response, used to generate the measurement data, and the material model response was so significant that no parameters were shared by the two. Consequently, we have only used posterior predictions to assess the quality of the results.

The results for linear elasticity show that incorporating any of the three model uncertainty formulations results in wider marginal posterior distributions of the Young's modulus. Consequently, the chance that the posterior distributions include the true value increases. Incorporating model uncertainty also results in wider posterior prediction intervals, which therefore contain more measurements.

If, in addition to model uncertainty, the error in the strain is also incorporated the marginal posterior (distribution) of the Young's modulus becomes even wider. The exception is the case in which model uncertainty is described by a Gaussian process (with a stationary covariance function). The posterior becomes narrower in this case, but the evaluation of the posterior at the true value is nevertheless larger. In other words, the true value has a higher chance to be realised from the posterior.

Incorporating the error in the strain (input error), as well as model uncertainty, also results in wider posterior prediction intervals, which are therefore more likely to contain the measurement data. If model uncertainty is described by a Gaussian process however, the posterior prediction interval does not become wider, but still contains more measurements than if the input error is not included.

Our results generally show that incorporating both model uncertainty and the input error has a favourable influence on the identified parameters and the posterior predictions, compared to only incorporating model uncertainty or only incorporating the input error. If the difference between the true response (used to generate the measurements) and the response of the material model increases however, the added value of incorporating the input error as well reduces substantially.

Chapter 5

Estimating fibres' material parameter distributions from limited data with the help of Bayesian inference[1]

abstract

Numerous materials are essentially structures of discrete fibres, yarns or struts. Considering these materials at their discrete scale, one may distinguish two types of intrinsic randomness that affect the structural behaviours of these discrete structures: geometrical randomness and material randomness. Identifying the material randomness is an experimentally demanding task, because many small fibres, yarns or struts need to be tested, which are not easy to handle. To avoid the testing of hundreds of constituents, this chapter proposes an identification approach that only requires a few dozen of constituents to be tested (we use twenty to be exact). The identification approach is applied to artificially generated measurements, so that the identified values can be compared to the true values. Another question this chapter aims to answer is how precise the material randomness needs to be identified, if the geometrical randomness will also influence the macroscale behaviour of these discrete networks. We therefore also study the effect of the identified material randomness to that of the actual material randomness for three types of structures; each with an increasing level of geometrical randomness.

5.1 Introduction

Of all materials important for industry and society, some important ones are essentially discrete mesostructures and microstructures. Some examples are paper materials, open-cell metal foams, dry-woven fabrics and electrospun scaffolds. The mechanical behaviours of such materials are often described using computational models in which each fibre, yarn or strut is represented by a series of springs or beams. Examples are the works of Kulachenko and Uesaka [105], Persson and Isaksson [106], Wilbrink et al. [107], Beex et al. [108], and Bosco et al. [109] for paper materials, the works Badiche et al. [110] and Jung et al. [111] for open-cell metal foams, the works of Gao et al. [112] and Beex et al. [113] for dry-woven fabrics and the work of Argento et al. [114] for elecrospun scaffolds.

---

[1] Reproduced from: H. Rappel and L.A.A. Beex, Estimating fibres' material parameter distributions from limited data with the help of Bayesian inference, submitted to European Journal of Mechanics-A/Solids.

A substantial amount of these discrete structures are intrinsically stochastic, which may be important to incorporate in their associated discrete models (see e.g. Sastry et al. [115], Wang et al. [116], Bronkhorst [117], Hatami-Marbini and Picu [118], Picu [119], Shahsavari and Picu [120] and Ban et al. [121]). Two types of stochastic aspects may be distinguished: stochastic geometries and stochastic mechanical behaviours of the base materials. Identifying both types of randomness is experimentally demanding because the structures and constituents are small.

Identifying stochastical geometries often involves the scanning of the structures with micro-CT scanners. An image analysis algorithm is then commonly applied, aiming to distinguish the individual fibres, yarns or struts in order to provide information such as their lengths, cross-sectional areas and orientations (e.g. Le et al. [122], Latil et al. [123], Sencu et al. [124]). Especially in order to distinguish the constituents in densely packed, small-scale structures, these algorithms need to be rather complex.

Some works that experimentally show and discuss stochastic aspects of the base materials of discrete constituents are the work of Seth and Page [125] for paper materials and the work of Jung et al. [126] for open-cell metal foams. These studies show that a substantial difference in the mechanical behaviour can be observed between one constituent and another, but they do not present the actual distributions from which these behaviours are realisations. A possible reason for the fact that material parameter distributions are commonly not presented is that it requires the testing of a substantial number of fibres, yarns or struts, which are not easy to handle due to their small size.

The first aim of this chapter is therefore to propose a scheme that enables one to identify material parameter distributions using only a limited number of fibres, yarns or struts. We demonstrate the scheme for 20 constituents to be precise. The scheme assumes that all constituents can be described by the same material model and that the set of material parameters of each constituent is a realisation from some probability density function (PDF). For now, the scheme thus assumes that the material parameters are constant inside each constituent and the aim is to identify the parameters of the material parameter PDF. We apply the scheme to synthetically created measurements so that we can compare the identified values with the true ones.

The identification scheme requires four steps to be performed. First, fibres, yarns of struts need to be harvested and experimentally tested.

Second, the material parameters need to be identified separately for each constituent. We assume that the experimental tests are conducted in a well-controlled environment and hence, plenty of measurements are available for each tested constituent. Thanks to the abundance of available stress-strain data, the identification of the material parameters of each constituent is performed using the least squares method (LSM), in which an objective function in terms of the material parameters is minimised in order to determine their most appropriate values.

Third, univariate PDFs (i.e. single variable PDFs) are selected for each type of material parameter. The parameters of each univariate PDF are then identified based on the material parameter values identified in the previous step. The parameters of each univariate PDF are identified using Bayesian inference (BI), because not enough observations are available to allow a deterministic identification approach (we only have 20 observations). BI includes a regularisation that makes this separate identification problem well-posed.

Fourthly, the univariate PDFs together with their identified parameters are collected in one joint PDF, in which possible correlations between the univariate PDFs are incorporated. Mathematically combining the univariate PDFs is based on copulas, which come with their own parameter(s). Since again only 20 observations are available, the use of a deterministic approach for the identification of the copula parameters can be challenging and hence, we resort again to BI.

Bayesian frameworks treat observations as realisations from a probability model and their output are probability distributions in terms of the model parameters. Initially, assumed parameter distributions need to be specified, which are then updated by inferring the observations. The result of this is again a probability distribution, which represents the user's uncertainty about the model parameters. This final PDF is called the posterior (distribution), whereas the initially assumed PDF is called the prior (distribution). In order to obtain statistical summaries of the posterior (e.g. at which parameter values the PDF is maximum) numerical frameworks are commonly employed.

Various studies can be found in which BI is used to identify material parameters. Examples that have focused on the identification of elastic material parameters are the works of Isenberg [41], Alvin [42], Beck and Katafygiotis [43], Marwala and Sibusiso [44], Gogu et al. [45], Koutsourelakis [51], Lai and Ip [49], Daghia et al. [50], Nichols et al. [59] and Gogu et al. [52]. Studies that have focused on the identification of elastoplastic parameters include the works of Most [56] and Rappel et al. [32]. BI is also used to identify material parameters of hysteretic models [53, 54] and other nonlinear material models such as viscoelasticity and creep [30, 31, 55, 58].

As mentioned before, the univariate PDFs of each material parameter are coupled in one joint PDF by the use of copulas in this chapter. Copulas are defined as functions that link the joint cumulative distribution function (CDF) and the univariate CDFs. They allow us to include the dependencies of several random variables on each other, resulting in a single multivariate distribution for all the material parameters.

Most often the parameters of the joint distribution (i.e. the parameters of univariate PDFs, as well as those of the copula) are identified by a two step identification scheme. Genest et al. [127] approximated the parameters of univariate distributions by empirical distribution (i.e. a nonparametric estimator of the CDF for a random variable) and used a maximum likelihood approach [22] to identify the parameters of the copula. Hürlimann [128] and Roch and Alegre [129] also employed a two step scheme, but with a maximum likelihood approach in both steps. Silva and Lopes [130] employed a full Bayesian approach for the identification of all unknown parameters in one step. However, the number of observations in their work is large compared to that in this chapter. Silva and Lopes also presented a comparison between one and two step methods, which showed a negligible difference between the point estimators of the one step scheme and the two step scheme.

Besides proposing the aforementioned identification scheme, this chapter also aims to answer the question of how accurate the material parameter PDF needs to be identified, if some level of geometrical randomness is present. To this purpose, we consider three types of virtual structures, each with an increasing level of geometrical randomness, and assess their macroscopic behaviour if the actual PDF is used and if the identified PDF is used. We investigate this for two responses of the base material: a damage model and an elastoplastic model. Geometrically linear Euler-Bernoulli beams are used to discretise the constituents in the virtual structures in a 2D setting.

The outline of this chapter is as follows. Section 5.2 briefly discusses the material models. In Section 5.3, we discuss the identification scheme. In Section 5.4 we detail the generation and treatment of the virtual structures. In Section 5.5 we present some results, which are subdivided in those of the identification scheme itself and in how the distributions influence the macroscale behaviour of random network models. Finally, we present our conclusions (Section 5.6).

5.2 Material models

In this section, we briefly introduce the two material models that are used throughout this chapter. It is sufficient to express them in one dimension and without the use of the Poisson's ratio, because the identification scheme is applied to uniaxial (monotonically increasing) tensile tests and the virtual experiments use two-dimensional beam descriptions without shear deformation.

5.2.1 Damage

The first material model describes a linear elastic response until a failure strain is reached. When this failure strain is reached anywhere in the constituent (in the tensile tests considered in the identification scheme) or in a beam that represents a part of the constituent (in the virtual experiments), it fails entirely. No load will thus be transferred from that point onwards.

The Cauchy stress, σ, is expressed as follows in this material model:

$$\sigma = \big(1 - D(\kappa)\big)E\epsilon, \tag{5.1}$$

where D denotes the damage variable, which is a function of history variable κ. E denotes the Young's modulus and ϵ the linear strain.

We express the damage variable in terms of history variable κ as follows:

$$D(\kappa) = \begin{cases} 0 & \text{if } \kappa < \epsilon_f \\ 1 & \text{if } \kappa \geq \epsilon_f \end{cases}, \tag{5.2}$$

where ϵ_f denotes the failure strain. The following loading function and the Karush-Kuhn-Tucker (KKT) conditions [66] ensure that κ takes the largest strain value in a constituent or beam and that damage is irreversible:

$$g = \tilde{\epsilon} - \kappa, \tag{5.3}$$

with

$$\tilde{\epsilon} = \max_{\vec{x}} \big|\epsilon(\vec{x})\big|, \tag{5.4}$$

where $\vec{x}$ denotes the location vector to any material point in a constituent or beam. The KKT conditions read:

$$\dot{\kappa} \geq 0, \quad g \leq 0, \quad \dot{\kappa} g = 0. \tag{5.5}$$

It may be clear that in a monotonically increasing, uniaxial tensile test performed on a constituent, the strain is constant. Consequently, Eq. (5.4) can be simplified to:

$$\tilde{\epsilon} = \epsilon. \tag{5.6}$$

The stress-strain response during a monotonically increasing, uniaxial tensile test can then be written as:

$$\sigma = \begin{cases} E\epsilon & \text{if } \epsilon < \epsilon_f \\ 0 & \text{if } \epsilon \geq \epsilon_f \end{cases}. \tag{5.7}$$

5.2.2 Elastoplasticity

Second, we consider an elastoplastic material model with isotropic, linear hardening. In this material description, the linear strain, ϵ, is additively split in an elastic strain, ϵ_e, and a plastic strain, ϵ_p:

$$\epsilon = \epsilon_e + \epsilon_p. \tag{5.8}$$

The Cauchy stress, σ, is expressed as follows:

$$\sigma = E\epsilon_e. \tag{5.9}$$

The yield function reads:

$$f = \sqrt{\sigma^2} - \sigma_{y0} - H\tilde{\epsilon}_p, \tag{5.10}$$

where $\tilde{\epsilon}_p$ denotes the cumulative plastic strain, σ_{y0} the initial yield stress and H the plastic modulus. The relation between a change of the plastic strain and that of the cumulative plastic strain furthermore reads:

$$\dot{\epsilon}_p = \dot{\tilde{\epsilon}}_p \frac{\partial f}{\partial \sigma} = \dot{\tilde{\epsilon}}_p \, \mathrm{sgn}(\sigma), \tag{5.11}$$

where sgn$(\cdot)$ denotes the sign function. The following KKT conditions finalise the material model:

$$\dot{\tilde{\epsilon}}_p \geq 0, \quad f \leq 0, \quad f\dot{\tilde{\epsilon}}_p = 0. \tag{5.12}$$

It may be clear that the stress-strain relation during monotonically increasing, uniaxial tension for this material model reads:

$$\sigma = \begin{cases} E\epsilon & \text{if } \epsilon < \frac{\sigma_{y0}}{E} \\ \sigma_{y0} + \frac{EH}{E+H}(\epsilon - \frac{\sigma_{y0}}{E}) & \text{if } \epsilon \geq \frac{\sigma_{y0}}{E} \end{cases}. \tag{5.13}$$

5.3 Identification scheme

In this section we detail the scheme to identify the parameters of the probability density function (PDF) from which it is assumed the material parameters of each specimen (i.e. tested constituent) are coming. First, the concept of the framework is discussed. Subsequently, the basics of Bayesian inference are discussed. Then, copulas are discussed as the mathematical tool to combine two or more univariate PDFs in one joint PDF. Finally, the two steps of the scheme in which BI and copulas are used are discussed in more detail.

5.3.1 Concept

The aim of the identification scheme is to experimentally test a relatively small number of fibres, yarns or struts and from those test results (i.e. stress-strain data), obtain the parameters of the material parameter PDF. We will achieve this by subdividing the identification problem in four steps, which are to be performed consecutively. These steps are discussed below and schematically illustrated in Fig. 5-1.

Step 1: Experimentally test individual constituents

First, some fibres, yarns or struts must be harvested and tested experimentally. We assume that 20 fibres are harvested and that these are separately tested in tension in a well-controlled environment. We thus obtain 20 stress-strain curves, which are necessary for the next step.

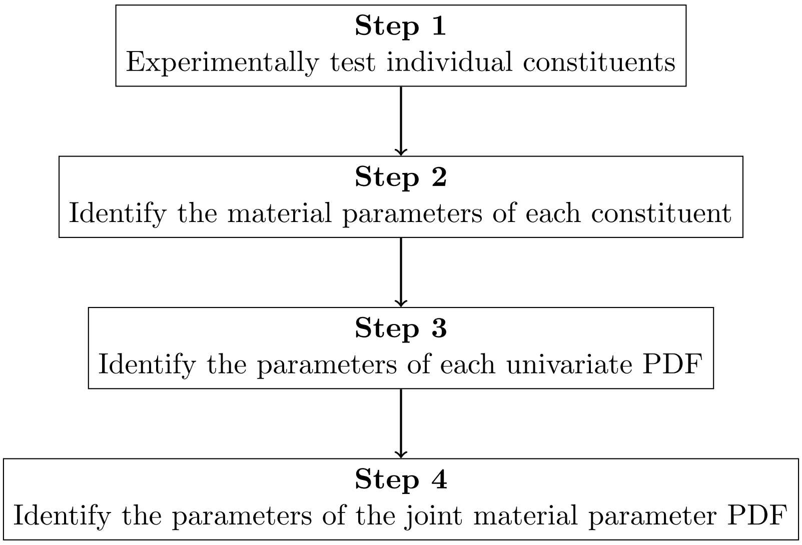

Figure 5-1: The steps of the identification scheme.

Step 2: Identify the material parameters of each constituent
Based on the stress-strain data obtained in the previous step, a material model must be selected in the current step and its parameters are separately identified for each constituent. We assume that a large number of stress-strain data is gathered during each test such that a deterministic identification approach based on the minimisation of an objective function is possible, i.e. the least squares method (LSM). The final result of the current step is thus a set of material parameters for each constituent. If we for instance assume the damage model of the previous section, we obtain 20 Young's moduli and 20 failure strains: two material parameters for each constituent. The material parameters of each constituent are necessary for the next step.

Step 3: Identify the parameters of each univariate PDF
In the third step, we select a univariate PDF for each type of material parameter (e.g. normal or beta distributions [22]) and identify the parameters of each univariate PDF separately. If we again assume the damage model of the previous section, we thus obtain two univariate PDFs: one for the Young's modulus and one for the failure strain. As 20 observations (e.g. 20 Young's moduli) are not sufficient to identify the parameters of a univariate distribution deterministically, we employ Bayes' theorem to enable the use of assumed knowledge, which regularises the identification problem of the current step. The use of Bayes' theorem effectively means that a distribution of the univariate PDF's parameters is assumed and this distribution is updated by inferring each observation. We thus start the identification problem of the current step with the assumption of a distribution of the PDFs' parameters and the final result of BI is also a distribution in terms of the PDF's parameters (albeit corrected for the observations). We then use a numerical framework (Markov chain Monte Carlo, MCMC techniques) to explore the distribution of the univariate PDF's parameters to find their point estimates [48] (e.g. the mean vectors or MAP vectors). These point estimates are then considered as the identified parameter set of each univariate PDF, which are necessary for the fourth step.

Step 4: Identify the parameters of the joint material parameter PDF
In the last step, we take the univariate PDFs (including their identified parameters) and couple them together to form a single, joint PDF. The coupling of the univariate PDFs allows the incorporation of correlations and is mathematically performed here using a so-called copula.

Different copula formulations can be distinguished and hence, the user has to select one. Since each copula comes with its own parameters, the identification problem in this fourth step thus aims to identify the copula parameters. Important to realise is that we again do not have enough information to employ a deterministic identification approach to identify the copula's parameters. Once more, we employ Bayes' theorem, requiring us to define an assumed PDF in terms of the copula parameters and inferring this PDF with the 20 observations. The resulting posterior needs to be numerically explored in order to determine the point estimates that represent the identified copula parameters.

It is worth mentioning that in principle the entire identification procedure can be performed in a single identification framework that is entirely based on Bayes' theorem. As the number of observations is small however, the MCMC algorithm (to numerically explore the final PDF in order to determine the point estimates) will not converge. Since we choose to obtain a joint PDF, we subdivide the identification approach into several identification problems. It is furthermore not very useful to consider the identification problem of Step 2 in a stochastic manner, because if we assume that a large number of stress-strain data for each constituent is available and the number of constituents is small, the uncertainty stemming from Step 2 is substantially small compared to the uncertainty stemming from Steps 3 and 4.

It is also worth noting that some clear assumptions are made in Steps 3 and 4: (i) the type of univariate PDFs (Step 3), (ii) the initially assumed distributions of the parameters of the univariate PDFs (Step 3), (iii) the type of copula (Step 4) and (iv) the initially assumed PDFs of the copula parameters (Step 4). The error induced by these assumptions cannot be evaluated to the best of the authors' knowledge, because few observations are available. If the number of tested constituents tends to infinity however, the error in the identified parameter values approximates zero (if the same PDFs and copula is selected as used to generate the material parameters).

5.3.2 Bayesian inference

Bayesian inference (BI) is a procedure in which one fits a probability model to a set of data. The result of BI is a PDF (the so-called posterior). Assuming that $\mathbf{z} = \begin{bmatrix} z_1 & \cdots & z_{n_o} \end{bmatrix}^T$ denotes a vector of n_o observations and $\mathbf{p}$ a vector of n_p parameters which are to be identified, Bayes' formula reads:

$$\pi(\mathbf{p}|\mathbf{z}) = \frac{\pi(\mathbf{p})\pi(\mathbf{z}|\mathbf{p})}{\pi(\mathbf{z})} = \frac{1}{k}\pi(\mathbf{p})\pi(\mathbf{z}|\mathbf{p}), \tag{5.14}$$

where $\pi(\mathbf{p})$ denotes the prior PDF (i.e. the PDF that represents one's assumed prior knowledge about the parameters, e.g. the fact that the Young's modulus cannot be smaller than zero), $\pi(\mathbf{z}|\mathbf{p})$ denotes the likelihood function (i.e. the PDF that measures the likelihood that measurements $\mathbf{z}$ are observed, for a given set of parameter values $\mathbf{p}$), $\pi(\mathbf{p}|\mathbf{z})$ denotes the posterior PDF (i.e. the PDF that describes the probability to obtain parameters $\mathbf{p}$, for the given set of observations $\mathbf{z}$) and $\pi(\mathbf{z})$ is called the evidence. Since $\mathbf{z}$ is known, the evidence is a constant number ($\pi(\mathbf{z}) = k \in \mathbb{R}^+$), which is thus independent of the parameters (i.e. the variables of interest). Since $\pi(\mathbf{z}) = k$, it suffices to write Eq. (5.14) as follows:

$$\pi(\mathbf{p}|\mathbf{z}) \propto \pi(\mathbf{p})\pi(\mathbf{z}|\mathbf{p}), \tag{5.15}$$

because the statistical summaries of the posterior, such as the mean, the MAP (i.e. the 'maximum-a-posteriori-probability' or the parameter values at which the posterior is maximal) and the covariance matrix (i.e. the matrix that measures the correlation between the parameters), are independent of scaling factor $\frac{1}{k}$.

Once the posterior is established, the statistical summaries of the posterior need to be determined. With the exception of a few cases, numerical frameworks need to be employed for this. Markov chain Monte Carlo (MCMC) techniques [24] are frequently employed to draw samples from the posterior PDF. The drawn samples can be used to approximate statistical summaries and predict new observations. Readers are referred to [16, 31] for more details.

5.3.3 Copulas

Nelsen [131] defines copulas as functions that join one dimensional marginal distributions to their joint, multivariate distribution. These functions are tools to model the dependencies of several random variables. We will discuss them in some more detail in this subsection.

Let $\mathbf{P} = \begin{bmatrix} P_1 & \cdots & P_n \end{bmatrix}^T$ be a random vector with joint cumulative distribution function (CDF) Π, and Π_i be the marginal univariate CDF of P_i. According to Sklar's theorem [132], an n-dimensional copula C exists such that:

$$\Pi(p_1, \cdots, p_n) = C(\Pi_1(p_1), \cdots, \Pi_n(p_n)). \tag{5.16}$$

The joint PDF can then be obtained by differentiating Eq. (5.16) with respect to the random variables as follows:

$$\pi(p_1, \cdots, p_n) = c(\Pi_1(p_1), \cdots, \Pi_n(p_n)) \prod_{i=1}^{n} \pi_i(p_i), \tag{5.17}$$

where $c(u_1, \cdots, u_n) = \frac{\partial C(u_1, \cdots, u_n)}{\partial u_1 \cdots \partial u_n}$ with $u_i = \Pi_i(p_i)$ and $\pi_i(p_i)$ denotes the i^{th} marginal PDF.

Various types of copulas can be used to describe the dependencies of random variables [130], but we restrict ourselves to the Gaussian one. This entails that we write:

$$C(\mathbf{u}|\mathbf{\Gamma}_C) = \Phi_n(\Phi^{-1}(u_1), \cdots, \Phi^{-1}(u_n)|\mathbf{\Gamma}_C), \tag{5.18}$$

where again $u_i = \Pi_i(p_i)$, and $\mathbf{\Gamma}_C \in [-1, 1]^{n \times n}$ denotes the covariance matrix containing correlation parameters. These correlation parameters are called Pearson's ρ and each one is a measure for the linear relationship between two random variables [133]. Furthermore, $\Phi(\tilde{p})$ denotes the standard Gaussian CDF (i.e. $\tilde{p} \sim N(0, 1) = \frac{1}{\sqrt{2\pi}}\exp(-\frac{\tilde{p}^2}{2})$) and $\Phi_n(\tilde{\mathbf{p}}|\mathbf{\Gamma}_C)$ denotes the joint CDF of a multivariate Gaussian distribution with a zero mean vector and covariance matrix $\mathbf{\Gamma}_C$ (i.e. $\tilde{\mathbf{p}} \sim N_n(0, \mathbf{\Gamma}_C)$ with $\tilde{\mathbf{p}} = \begin{bmatrix} \tilde{p}_1 & \cdots & \tilde{p}_n \end{bmatrix}^T$). [134] writes the density of the Gaussian copula as follows:

$$c(\mathbf{u}|\mathbf{\Gamma}_C) = \frac{1}{\sqrt{|\mathbf{\Gamma}_C|}}\exp\Big(-\frac{1}{2}\begin{bmatrix} \Phi^{-1}(u_1) & \cdots & \Phi^{-1}(u_n) \end{bmatrix} \times (\mathbf{\Gamma}_C^{-1} - \mathbf{I}) \times \begin{bmatrix} \Phi^{-1}(u_1) & \cdots & \Phi^{-1}(u_n) \end{bmatrix}^T\Big), \tag{5.19}$$

where $|\cdot|$ denotes the determinant and $\mathbf{I}$ the $n \times n$ identity matrix.

5.3.4 Details of Step 3

In this subsection and the next, we return to Steps 3 and 4 of the identification scheme and present them in more detail in the light of the previous discussions on BI and the Gaussian copula. In the current subsection, we focus on Step 3, meaning that we focus on how we use BI to identify the parameters of a univariate PDF based on 20 observations.

Let us assume that we have tested 20 constituents and identified the n_p types of material parameters for each constituent. We store the identified values of the first type of material parameters in a vector of length 20, $\overline{\mathbf{p}}_1$, the identified values of the second type of material parameters in a vector of the same length, $\overline{\mathbf{p}}_2$, and repeat this until we obtain n_p vectors of length 20.

In the current step, we separately focus on each type of material parameter, assume that they are realisations from some univariate PDF and identify the parameters of that univariate PDF. This means that we can now express Bayes' theorem for the material parameter of type i as follows:

$$\pi_{\text{post}}(\mathbf{p}_{i\text{PDF}}|\overline{\mathbf{p}}_i) \propto \pi_{\text{prior}}(\mathbf{p}_{i\text{PDF}})\pi_{\text{like}}(\overline{\mathbf{p}}_i|\mathbf{p}_{i\text{PDF}}), \tag{5.20}$$

where $\mathbf{p}_{i\text{PDF}}$ denote the parameters of the univariate PDF associated with the i^{th} type of material parameter and $\overline{\mathbf{p}}_i$ denote the observations for the current identification problem (e.g. if the i^{th} type of material parameter is the Young's modulus, $\overline{\mathbf{p}}_i$ contains the 20 Young's moduli identified in Step 2). The prior PDF is thus denoted by $\pi_{\text{prior}}(\mathbf{p}_{i\text{PDF}})$ and must be defined by the user. The posterior is denoted by $\pi_{\text{post}}(\mathbf{p}_{i\text{PDF}}|\overline{\mathbf{p}}_i)$. Likelihood function $\pi_{\text{like}}(\overline{\mathbf{p}}_i|\mathbf{p}_{i\text{PDF}})$ can straightforwardly be formulated using the product of the univariate PDF that is selected by the user:

$$\pi_{\text{post}}(\mathbf{p}_{i\text{PDF}}|\overline{\mathbf{p}}_i) \propto \pi_{\text{prior}}(\mathbf{p}_{i\text{PDF}}) \prod_{j=1}^{20} \pi_{\text{uni}}\Big((\overline{\mathbf{p}}_i)_j|\mathbf{p}_{i\text{PDF}}\Big), \tag{5.21}$$

where $(\overline{\mathbf{p}}_i)_j$ denotes the j^{th} component of vector $\overline{\mathbf{p}}_i$ (e.g. the j^{th} Young's modulus) and π_{uni} denotes the univariate PDF that must be selected by the user. The point estimates of all n_p posteriors are numerically estimated using MCMC techniques and are stored in n_p vectors $\overline{\mathbf{p}}_{1\text{PDF}}, \cdots, \overline{\mathbf{p}}_{n_p\text{PDF}}$.

Note that in principle the lengths of different vectors $\overline{\mathbf{p}}_{i\text{PDF}}$ may vary, since a different univariate PDF can be selected for each type of material parameter and each univariate PDF can come with its own number of parameters.

5.3.5 Details of Step 4

In the fourth step of the identification scheme, we take all the material parameters identified in Step 2 (stored in vectors $\overline{\mathbf{p}}_1, \cdots, \overline{\mathbf{p}}_{n_p}$, and for the ease of notation collect them in $\overline{\mathbf{p}}$) and the univariate PDFs including their parameters identified in Step 3 (stored in vectors $\overline{\mathbf{p}}_{1\text{PDF}}, \cdots, \overline{\mathbf{p}}_{n_p\text{PDF}}$ and for the ease of the notation collect them in $\overline{\mathbf{p}}_{\text{PDF}}$) and couple them with an assumed copula C, which comes with copula parameters $\boldsymbol{\rho}$. Hence, the aim of the current step is to identify the parameters in $\boldsymbol{\rho}$, which is of length $\frac{n_p(n_p-1)}{2}$ because the covariance matrix in a Gaussian copula is written as:

$$\boldsymbol{\Gamma}_C = \begin{bmatrix} 1 & \rho_{12} & \cdots & \cdots & \rho_{1n_p} \\ & 1 & \cdots & \cdots & \rho_{2n_p} \\ & \text{sym} & \ddots & \ddots & \vdots \\ & & & 1 & \rho_{(n_p-1)n_p} \\ & & & & 1 \end{bmatrix}, \tag{5.22}$$

where all values ρ_{ij} are stored in $\boldsymbol{\rho}$.

We can now express Bayes' theorem for the identification problem of the current step as follows:

$$\pi_{\text{post}}(\boldsymbol{\rho}|\overline{\mathbf{p}}, \overline{\mathbf{p}}_{\text{PDF}}) \propto \pi_{\text{prior}}(\boldsymbol{\rho})\pi_{\text{like}}(\overline{\mathbf{p}}|\overline{\mathbf{p}}_{\text{PDF}}, \boldsymbol{\rho}), \tag{5.23}$$

where we can decompose the likelihood function multiplicatively in terms of the joint PDF as follows:

$$\pi_{\text{like}}(\overline{\mathbf{p}}|\overline{\mathbf{p}}_{\text{PDF}}, \boldsymbol{\rho}) = \prod_{i=1}^{20} \pi_{\text{joint}}\Big((\overline{\mathbf{p}}_1)_i, \cdots, (\overline{\mathbf{p}}_{n_p})_i|\overline{\mathbf{p}}_{\text{PDF}}, \boldsymbol{\rho}\Big), \tag{5.24}$$

where the material parameters of the i^{th} tested specimen are denoted by $(\overline{\mathbf{p}}_1)_i, \cdots, (\overline{\mathbf{p}}_{n_p})_i$ (e.g. the i^{th} Young's modulus and failure strain) and the joint PDF for this specimen can be expressed as follows:

$$\begin{aligned} &\pi_{\text{joint}}\Big((\overline{\mathbf{p}}_1)_i, \cdots, (\overline{\mathbf{p}}_{n_p})_i|\overline{\mathbf{p}}_{\text{PDF}}, \boldsymbol{\rho}\Big) = \\ &\quad c\Big(\Pi_{\text{uni}1}\big((\overline{\mathbf{p}}_1)_i|\overline{\mathbf{p}}_{1\text{PDF}}\big), \cdots, \Pi_{\text{uni}n_p}\big((\overline{\mathbf{p}}_{n_p})_i|\overline{\mathbf{p}}_{n_p\text{PDF}}\big)|(\boldsymbol{\Gamma}_C|\boldsymbol{\rho})\Big) \prod_{j=1}^{n_p} \pi_{\text{uni}j}\big((\overline{\mathbf{p}}_j)_i|\overline{\mathbf{p}}_{j\text{PDF}}\big). \end{aligned} \tag{5.25}$$

The only remaining issues are to select a prior and subsequently, to determine the point estimates of the posterior using an MCMC algorithm [24].

5.4 Structural network models

As mentioned before, the accuracy of the identification scheme may not have a substantial effect on macroscopic network responses, if some form of geometrical randomness is also of influence. To investigate this, we use three types of two-dimensional network models; each with an increasing level of geometrical randomness. In this section, we detail the geometrical generation of the structural models, their discretisations, and the solution schemes associated with the two employed material models.

5.4.1 Geometries

The numerical network experiments in the results section are all performed on specimens resembling a dog-bone (see Fig. 5-2). The only boundary conditions prescribed are displacements in vertical direction, except for the first node on the bottom-left corner for which the displacement in horizontal direction restrained as well. The cross-sectional shape of all discrete constituents is square, with the orientation of one edge of the square in out-of-plane direction. The cross-sectional dimensions are 1×1 mm^2.

In the first type of geometry, the discrete constituents are infinitely long (whilst still respecting the dog-bone shape), they are equally spaced (by parameter h in horizontal direction) and they are oriented with an angle of $\theta = 45°$ or $\theta = 135°$. A typical geometry is schematically presented in Fig. 5-3(a). Each 'lane' in the structure is entirely taken by a single constituent. We will refer to this type of network as type A.

In the second type of geometry, the discrete constituents are all of a finite length. The length of each constituent is sampled from a uniform distribution with bounds $l_{\min}$ and $l_{\max}$. If a constituent crosses the specimen's borders, it is cut. If a constituent is entirely located outside the specimen, it is ignored. Instead of an exact orientation of $\theta = 45°$ or $\theta = 135°$, their orientation is sampled from a uniform distribution with bounds $45° - \frac{1}{2}w_\theta$ and $45° + \frac{1}{2}w_\theta$

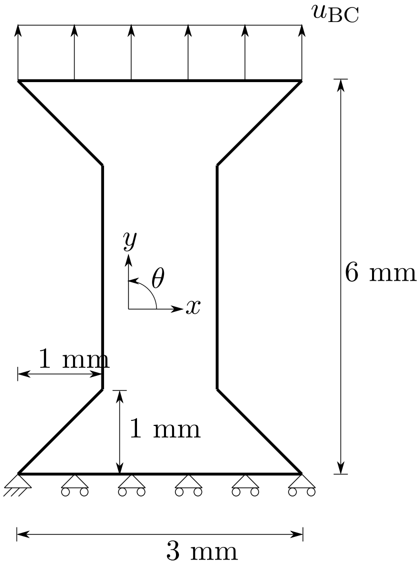

Figure 5-2: The shape, dimensions and boundary conditions of the specimens in the virtual experiments.

or $135° - \frac{1}{2}w_\theta$ and $135° + \frac{1}{2}w_\theta$. The average distance between two constituents in horizontal direction is again set by parameter h. The horizontal location of the centre of gravity of the first constituents of each 'lane' is randomly taken from a uniform distribution with bounds $3\ \mathrm{mm} - l_{\max}$ and $3\ \mathrm{mm} + l_{\max}$ and their vertical location is then fully determined by the fact that its 'lane' is set. The centres of gravities of the subsequent constituents in the same 'lane' are then located such that they exactly touch the beginning or the ends of the other constituents in that 'lane'. Subsequently, the centre of gravity of each constituent is relocated to a position that is sampled from a bivariate, uncorrelated uniform distribution with bounds $x_c - \frac{1}{2}h_c$, $x_c + \frac{1}{2}h_c$, $y_c - \frac{1}{2}h_c$, and $y_c + \frac{1}{2}h_c$, where x_c and y_c denote the horizontal and vertical locations of the original centre of gravity, respectively. A typical geometry resulting from this generation is presented in Fig. 5-3(b). We will refer to this type of network as type B.

In the third and last type of geometry (in Fig. 5-3(c)), the length of the discrete constituents is again sampled from a uniform distribution with bounds $l_{\min}$ and $l_{\max}$. Their centres of gravity are randomly located in a rectangle of $(3\ \mathrm{mm} + 2l_{\max}) \times (6\ \mathrm{mm} + 2l_{\max})$, with the specimen centred in it. Their orientation is completely random (i.e. their orientation is sampled from a uniform distribution with bounds 0° and 180°). If constituents cross the specimen's border, they are cut, and they are ignored if they are located entirely outside the specimen. We will refer to this type of network as type C.

5.4.2 Discretisations

After the geometries are created, each constituent is discretised by a series of two dimensional, geometrically linear, Euler-Bernoulli beams. If a constituent is not connected to any of the other constituent or if it is not connected to any of the specimen's edges to which boundary conditions are applied via other constituents, it is not discretised and hence, ignored. One beam is used for each constituent segment that is connected to two consecutive constituents. The beams are completely unified at their nodes, entailing perfect connections between the constituents.

If the length of the smallest beam in the network is substantially small compared to the longest beam in the network, the stiffness matrix may become ill-posed. To avoid this problem, the length of the largest beam is measured and all beams that are smaller than 1% of the

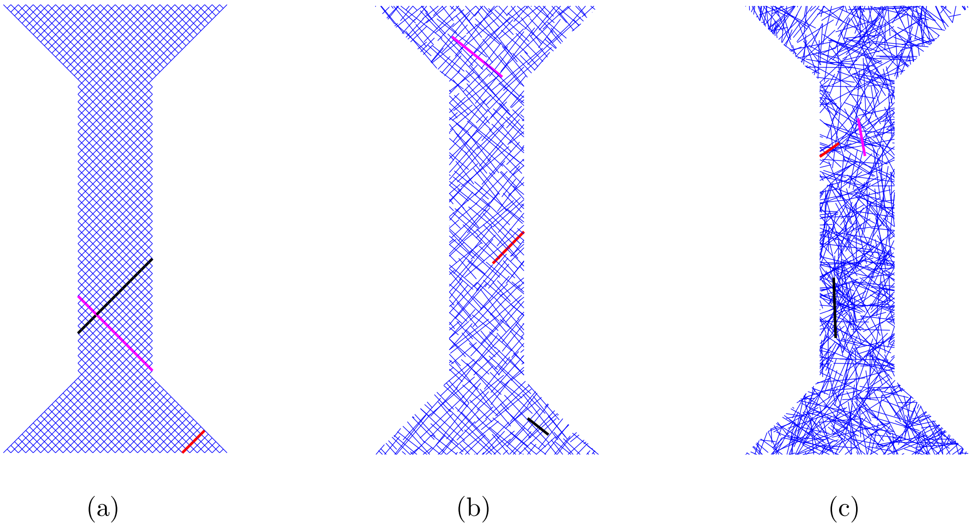

(a) (b) (c)

Figure 5-3: Schematic illustrations of the three types of networks. A few constituents are highlighted. The horizontal distance between the constituents in the type A and type B networks is $h = 0.1$ mm. The type B network is furthermore characterised by $l_{\min} = 0.3$ mm, $l_{\max} = 0.9$ mm, $w_\theta = 15^\circ$ and $h_c = 0.04$ mm. The type C network geometry is characterised by $l_{\min} = 0.3$ mm, $l_{\max} = 0.9$ mm and by the fact that 2000 fibres are generated in domain $(3 \text{ mm} + 2l_{\max}) \times (6 \text{ mm} + 2l_{\max})$ with the specimen centred in it.

longest beam are removed and their nodes are unified. This process may involve more than two nodes at the same location. Finally, all beams that are only connected to one other beam are removed because they will not contribute to the structural response. A typical result of this discretisation strategy is shown in Fig. 5-4(b), together with the geometry in Fig. 5-4(a).

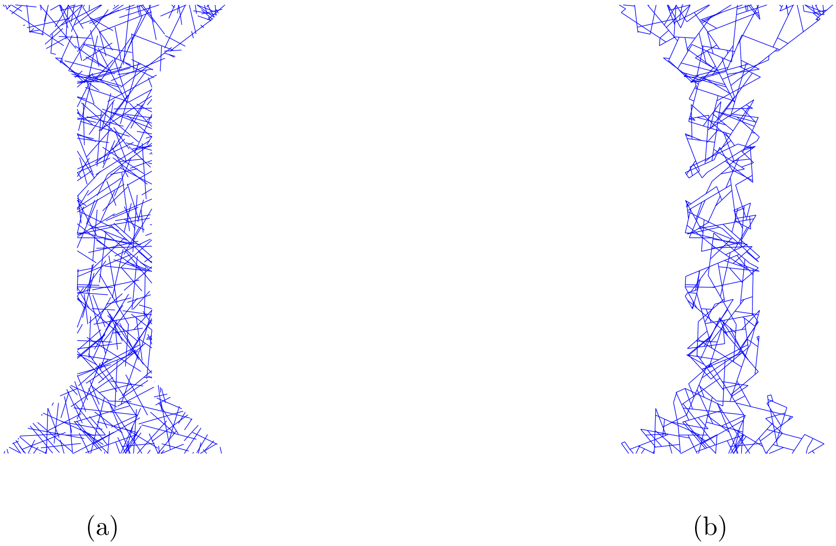

(a) (b)

Figure 5-4: A type C network geometry (a) and its beam discretisation (b). Note that we have used a significantly coarse network so that the effect of the discretisation can easily be observed.

5.4.3 Solution schemes

In this subsection, we briefly discuss the solution schemes for the EB beam network models associated with the two material models.

Damage

Solving the network model with the linear elastic-brittle fracture description starts with the application of an arbitrary value for u_{BC} in Fig. 5-2. After solving the linear system that results from this, we calculate in which of the beams the ratio between the occurring strain and the failure strain is the largest. This largest ratio will not equal one, but it should be at the moment that the beam fails. Since the material model is linear, we can scale this ratio directly to determine at which value of u_{BC} the beam fails. Similarly, we can also scale the reaction forces. After we have determined this, we remove the contributions of the failed beam to the stiffness matrix and again prescribe a value of u_{BC} and determine which of the beams is next to fail and at which value of u_{BC} and the reaction forces this would occur. We repeat this procedure until the sum of the reaction forces equals zero. This simple solution procedure is possible (instead of a true arc-length approach) due to the linearity of the model.

Eq. (5.4) states that the largest absolute strain occurring in a beam determines the value of κ and hence, the damage value for the entire beam. The maximisation problem of Eq. (5.4) is solved in a straightforward manner, because the largest absolute strain in a 2D EB beam occurs at the periphery of the beam, at its beginning or at its end. Consequently, we only need to determine the strain at four locations per beam; two at the beginning and two at the end of each beam (left in Fig. 5-5).

Elastoplasticity

The network models using the elastoplastic material model are solved in a manner that is standard for elastoplasticity (e.g. using return mapping and the consistent tangent stiffness). We therefore do not detail them. The only issue worth mentioning is that we only use four integration points per beam in order to save computational efforts. These integration points are located at the centres of four equally sized, rectangular subdomains as shown on the right in Fig. 5-5.

One may argue that these network models are far from perfect. We could for instance have used more integration points per beam for the elastoplastic material model. We also do not account for the fact that plasticity will lead to some form of localisation. We furthermore use cross-sectional dimensions that are too large to allow the use of geometrically linear EB beams. As the purpose of the virtual experiments in the next section is to compare the influence of the identified parameter distributions relative to the true parameter distributions if geometrical randomness is also present however, this comparison remains valid.

5.5 Results

This section presents the results for the identification scheme proposed in Section 5.3 as well as the results that show the effect of the different material parameter PDFs on the macroscale behaviour of the random network models. We start with the results of the parameter identification scheme.

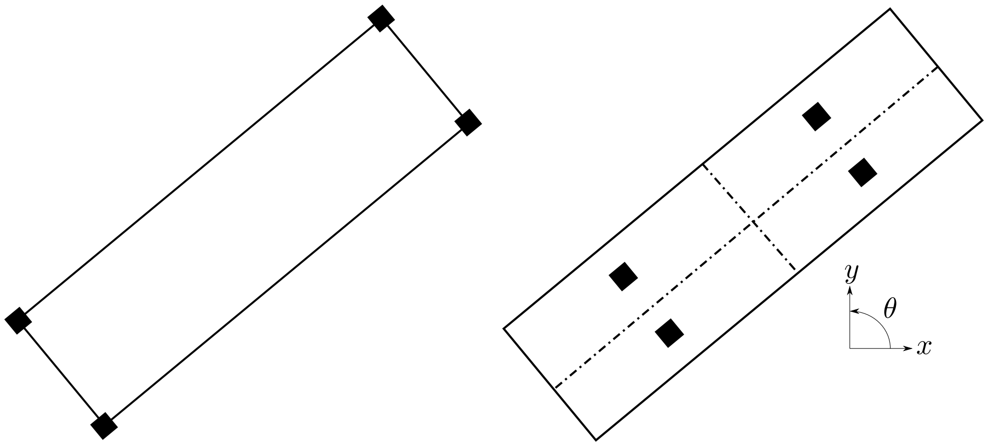

Figure 5-5: Left: the four locations at which the maximum strain in a $2D$ EB beam may occur (black squares). Right: the locations of the four integration points in a beam for the elastoplastic model (black squares).

5.5.1 Identification of the material parameter PDFs

In all results presented, we omit Steps 1 and 2 of the identification procedure and only consider Steps 3 and 4. This can be justified by assuming that an abundance of stress-strain measurements is obtained in Step 1, which makes the deterministic identification of the material parameters in Step 2 highly accurate.

We produce synthetic material parameters from two multivariate PDFs that are to be identified: one bivariate PDF for the damage model (in which Young's modulus E and failure strain ϵ_f are the material parameters) and a trivariate PDF for the elastoplastic model (in which Young's modulus E, initial yield stress σ_0 and hardening modulus H are the material parameters). We will refer to these PDFs as the 'true' PDFs. We draw 20 sets of material parameters from each true PDF. These sets of material parameters are considered to be the output of Step 2 and the observations in Step 3 (i.e. $\overline{\mathbf{p}}_i$).

Damage

In case of damage, we assume that the true bivariate PDF uses two univariate marginal PDFs which are four-parameter beta distributions of the following form:

$$\pi_{\text{uni}i}(p_i|\mathbf{p}_{i\text{PDF}}) = \frac{(p_i - a_{1i})^{\alpha_i - 1}(a_{2i} - p_i)^{\beta_i - 1}}{(a_{2i} - a_{1i})^{\alpha_i + \beta_i - 1} B(\alpha_i, \beta_i)}, \; i = E \text{ and } \epsilon_f \tag{5.26}$$

where p_i denotes the material parameter (either E or ϵ_f), α_i and β_i denote the shape parameters of the univariate PDF and a_{1i} and a_{2i} the lower and upper bounds, respectively. Furthermore, $B(\cdot, \cdot)$ denotes the beta function. The two univariate PDFs are joined together with a Gaussian copula. The values that we have chosen for the true PDF are presented in Table 5.2, whilst the true PDF is graphically presented in Fig. 5-6(a).

Now we continue with the actual identification. We first need to assume the type of univariate marginal PDFs and copula. We choose to work with the same types as for the true PDF (i.e. both univariate marginal PDFs are four-parameter beta distributions and the copula is Gaussian), so that we can compare the identified values with true ones.

In addition to selecting the univariate PDFs and copula to be identified, we also need to select the priors for their parameters. It is important to realise that we only have a small number of observations (20), which easily makes the MCMC algorithm, used to explore the posterior PDF, fail to converge if non-informative priors are selected. We therefore need to select rather informative priors. This can easily be justified for the lower and upper bounds (a_1 and a_2) by the fact that one generally knows the type of base material. We have furthermore used the mean value and the standard deviation of the observations to construct the prior for the shape parameters (α and β). (Note that both the mean value and the standard deviation of the four-parameter beta distribution are functions of α, β, a_1 and a_2.)

The priors assigned to the parameters of the univariate marginal PDFs are in the following form:

$$\pi((\mathbf{p}_{i\text{PDF}})_j) \propto \begin{cases} \exp\Big(-\frac{(p_{i\text{PDF}})_j - \overline{(\mathbf{p}_{i\text{PDF}})_j^{\text{prior}}})^2}{2s^2_{(\mathbf{p}_{i\text{PDF}})_j}}\Big) & \text{if } (\mathbf{p}_{i\text{PDF}})_j \geq 0 \\ 0 & \text{otherwise} \end{cases}, \tag{5.27}$$

where $(\mathbf{p}_{i\text{PDF}})_j$ denotes the j^{th} parameter of the univariate marginal PDF for the i^{th} type of material parameter. In other words, j refers to α, β, a_1 or a_2 and i to E or ϵ_f. Furthermore, $\overline{(\mathbf{p}_{i\text{PDF}})_j^{\text{prior}}}$ and $s_{(\mathbf{p}_{i\text{PDF}})_j}$ are the prior's mean value and standard deviation, respectively. We assume the prior for the copula parameter (i.e. $\rho_{E\epsilon_f}$) to be in the same form:

$$\pi(\rho_{E\epsilon_f}) \propto \begin{cases} \exp\Big(-\frac{(\rho_{E\epsilon_f} - \overline{\rho}_{E\epsilon_f}^{\text{prior}})^2}{2s^2_{\rho_{E\epsilon_f}}}\Big) & \text{if } -1 < \rho_{E\epsilon_f} < 1 \\ 0 & \text{otherwise} \end{cases}. \tag{5.28}$$

The chosen values for the means and standard deviations are presented in Table 5.1.

Table 5.1: Damage: the chosen values for the parameters that define the assigned priors.

$\overline{\alpha}_E^{\text{prior}}$	2	$\overline{\alpha}_{\epsilon_f}^{\text{prior}}$	3	$\overline{\rho}_{E\epsilon_f}^{\text{prior}}$	0.9
s_{α_E}	1	$s_{\alpha_{\epsilon_f}}$	1	$s_{\rho_{E\epsilon_f}}$	0.3
$\overline{\beta}_E^{\text{prior}}$	15	$\overline{\beta}_{\epsilon_f}^{\text{prior}}$	7		
s_{β_E}	5	$s_{\beta_{\epsilon_f}}$	2.3333		
$\overline{a}_{1E}^{\text{prior}}$ (GPa)	170	$\overline{a}_{1\epsilon_f}^{\text{prior}}$	0.0008		
$s_{a_{1E}}$ (GPa)	56.67	$s_{a_{1\epsilon_f}}$	2.6667×10^{-4}		
$\overline{a}_{2E}^{\text{prior}}$ (GPa)	270	$\overline{a}_{2\epsilon_f}^{\text{prior}}$	.0021		
$s_{a_{2E}}$ (GPa)	90	$s_{a_{2\epsilon_f}}$	7×10^{-4}		

By substituting the priors in Eqs. (5.21) and (5.23), the posterior is obtained. We use the adaptive Metropolis method [73] to draw samples from the posterior and hence, to obtain the statistical summaries such as the MAP. For each identification process 500×10^3 samples are drawn from the posterior whilst burning the first 30% of the samples. We have also imposed the constraint $a_1 < a_2$ in the sampling procedure. This entails that the samples that do not abide this constraint are rejected in the MCMC process.

The MAP estimates of the joint PDF are given in Table 5.2. Fig. 5-6 furthermore shows the true joint PDF and the identified joint PDF with and without correlation (i.e. with and without the copula) that correspond with these MAP estimates. One can observe that the identified joint PDF is somewhat wider than the true PDF, but substantially more accurate and less wide than the identified joint PDF without correlation.

Table 5.2: Damage: the true values and the identified MAP estimates.

α_E	β_E	a_{1E} (GPa)	a_{2E} (GPa)	α_{ϵ_f}	β_{ϵ_f}	$a_{1\epsilon_f}$	$a_{2\epsilon_f}$	$\rho_{E\epsilon_f}$
True values								
4	10	150	300	2	6	0.001	0.0019	0.7071
MAP estimates								
2.5786	8.3413	154.3811	365.6955	2.8056	7.3160	0.001	0.0021	0.6120

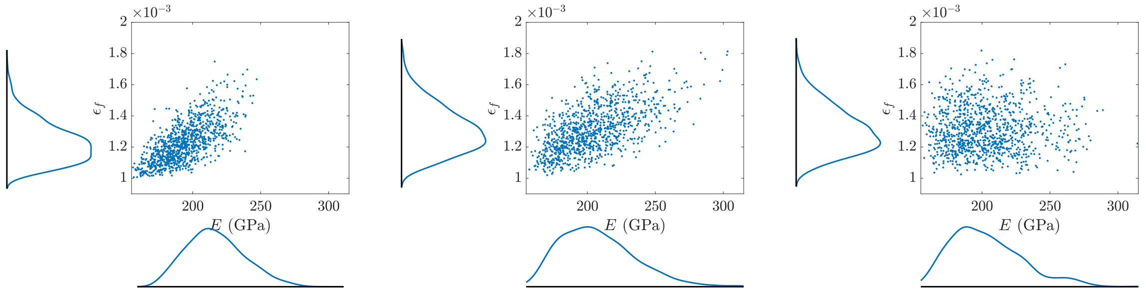

(a) True joint PDF

(b) Identified joint PDF

(c) Identified joint PDF without correlation

Figure 5-6: Damage: the scatter plots of the true joint PDF and the identified joint PDF with and without correlation. One can observe an increased scattering if the correlation is omitted, cf. (b) and (c).

Elastoplasticity

The same as for damage, we also assume for elastoplasticity that the true joint PDF consists of four-parameter beta distributions that are correlated via a Gaussian copula. For elastoplasticity, three univariate PDFs are required (for E, σ_0 and H) and a corresponding copula (consisting of a 3×3 covariance matrix with three independent parameters). The values selected for the true PDF are presented in Table 5.3.

Table 5.3: Elastoplasticity: the true values and the identified MAP estimates.

	True values	MAP estimates		True values	MAP estimates
α_E	4	2.1196	$\alpha_{\sigma_{y0}}$	2	2.7966
β_E	10	11.7261	$\beta_{\sigma_{y0}}$	6	5.5449
a_{1E} (GPa)	150	166.7861	$a_{1\sigma_{y0}}$ (GPa)	0.15	0.1420
a_{2E} (GPa)	300	344.4280	$a_{2\sigma_{y0}}$ (GPa)	0.5	0.4255
α_H	3	1.6400	$\rho_{E\sigma_{y0}}$	0.7071	0.6151
β_H	9	11.4085	ρ_{EH}	0.5	0.6063
a_{1H} (GPa)	30	32.8234	$\rho_{\sigma_{y0}H}$	0	0.0893
a_{2H} (GPa)	70	90.9644			

Also the same as for damage, we choose the same type of joint PDF to be identified. The priors are again chosen according to Eqs. (5.27) and (5.28), with their values shown in Table 5.4. We again obtain the MAP estimates by drawing 500×10^3 samples from the posterior, whilst burning the first 30% of them. Note that we again incorporate the constraint $a_1 < a_2$, but also that $\mathbf{\Gamma}_C$ must be positive semidefinite.

The true joint PDF is numerically presented in Table 5.3 and graphically in Fig. 5-7 together with the identified joint PDFs with and without correlation. Similar to the results for damage

Table 5.4: Elastoplasticity: the chosen values for the parameters that define the assigned priors.

$\overline{\alpha}_E^{\text{prior}}$	2	$\overline{\alpha}_{\sigma_{y0}}^{\text{prior}}$	3
s_{α_E}	1	$s_{\alpha_{\sigma_{y0}}}$	1
$\overline{\beta}_E^{\text{prior}}$	15	$\overline{\beta}_{\sigma_{y0}}^{\text{prior}}$	7
s_{β_E}	5	$s_{\beta_{\sigma_{y0}}}$	2.3333
$\overline{a}1_E^{\text{prior}}$ (GPa)	170	$\overline{a}1_{\sigma_{y0}}^{\text{prior}}$ (GPa)	0.2
s_{a1_E} (GPa)	56.67	$s_{a1_{\sigma_{y0}}}$ (GPa)	0.0667
$\overline{a}2_E^{\text{prior}}$ (GPa)	270	$\overline{a}2_{\sigma_{y0}}^{\text{prior}}$ (GPa)	.0.35
s_{a2_E} (GPa)	90	$s_{a2_{\sigma_{y0}}}$ (GPa)	0.1167
$\overline{\alpha}_H^{\text{prior}}$	2	$\overline{\rho}_{E\sigma_{y0}}^{\text{prior}}$	0.9
s_{α_H}	1	$s_{\rho_{E\sigma_{y0}}}$	0.3
$\overline{\beta}_H^{\text{prior}}$	12	$\overline{\rho}_{EH}^{\text{prior}}$	0.4
s_{β_H}	4	$s_{\rho_{EH}}$	0.1
$\overline{a}1_H^{\text{prior}}$ (GPa)	40	$\overline{\rho}_{\sigma_{y0}H}^{\text{prior}}$	0.1
s_{a1_H} (GPa)	13.3333	$s_{\rho_{\sigma_{y0}H}}$	0.0333
$\overline{a}2_H^{\text{prior}}$ (GPa)	80		
s_{a2_H} (GPa)	26.6667		

case, the identified joint PDF with correlation is more accurate and less wide than the identified joint PDF without correlation.

5.5.2 Propagating the material parameter PDFs in network models

In the previous subsection, we have clearly seen that the identified joint PDFs are relatively accurate representations of the true joint PDFs, regarding the limited number of data. We have also seen that the correlation is important to incorporate in order to achieve this accuracy. In the current subsection, we investigate how the differences between the true joint PDF and the identified joint PDF with and without correlation influences the macroscale responses of virtual fibre structures.

For the networks of type A (see Fig. 5-8), we investigate two configurations: one with $h = 0.1$ mm and one with $h = 0.025$ mm (where h denotes the horizontal distance between two adjacent constituents as mentioned in the previous section). Type A network with $h = 0.025$ mm thus contains 4 times more constituents than that with $h = 0.1$ mm and approximately 16 times more inter-constituent connections.

One may recall from the previous section that the networks of type B are the same as those of type A, except that the constituent length is finite and that their orientation is not the same. We investigate two different constituent lengths: one given by randomly sampling them from a uniform distribution with bounds 0.3 mm and 0.6 mm and one with bounds 1 mm and 1.5 mm. For both lengths, we also investigate different constituent densities: one given by $h = 0.1$ mm and one given by $h = 0.025$ mm. The remaining geometrical parameters for type B networks are $w_\theta = 15°$ and $h_c = 0.2h$. Some typical realisations can be seen in Figs. 5-9 and 5-10.

For the geometrically completely random networks (type C), we investigate two cases. In the first case we use 2000 constituents (Fig. 5-11) and in the second we use 5000 constituents. In both cases the constituent lengths are randomly taken from a uniform distribution with bounds 0.5 mm and 1 mm.

For each type of network, we simulate the mechanical responses of 1000 realisations. In

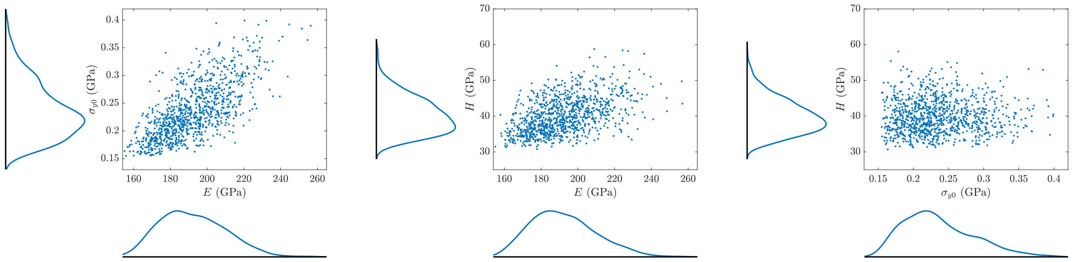

(a) (b) (c)

True joint PDF

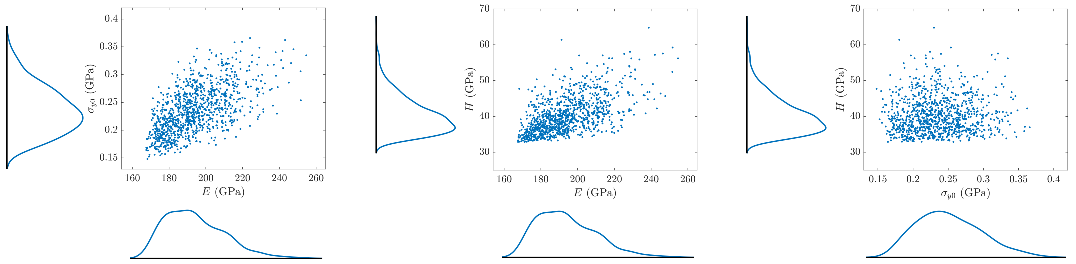

(d) (e) (f)

Identified joint PDF

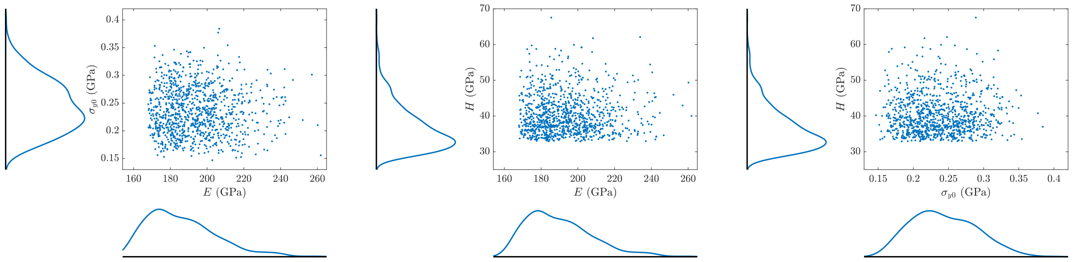

(g) (h) (i)

Identified joint PDF without correlation

Figure 5-7: Elastoplasticity: three views of the scatter plots of the true joint PDF (top row) and the identified joint PDF with correlation (centre row) and without correlation (bottom row). One can observe an increased scattering if the correlation is omitted, cf. (d,e,f) and (g,h,i).

case of damage, the stiffness matrix may become singular during a simulation, e.g. because the crack propagates through one of the domain edges to which boundary conditions are applied. In those cases, the predicted results are ignored for the analyses below.

Damage

Some typical damage patterns and force-displacements curves are presented in Figs. 5-8 to 5-11. For each response, we determine the maximum force ($F_{\max}$) and the dissipated energy (η) as measures for the macroscale response of the networks.

Fig. 5-12 shows the scatter plot of the maximum force and dissipated energy for the type A network with $h = 0.1$ mm. The first issue to observe, which can also be observed for the type A network with $h = 0.025$ mm, is that two domains seem to be present. We characterise the first domain in the results of the true PDF roughly by $0.08 < \eta < 0.13$ mJ, whereas the second domain roughly by $0.13 < \eta < 0.25$ mJ. The difference between these domains is caused by the damage pattern. We have observed that cracked beams remain present in the narrow

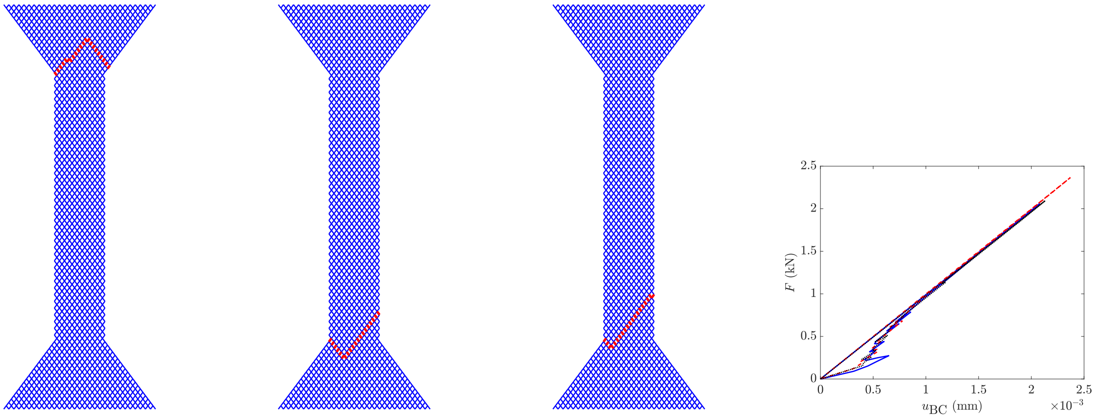

(a) (b) (c) (d)

Figure 5-8: Damage: some typical damage patterns for the type A networks with h = 0.1 mm (red: failed constituents) and some force-displacement curves.

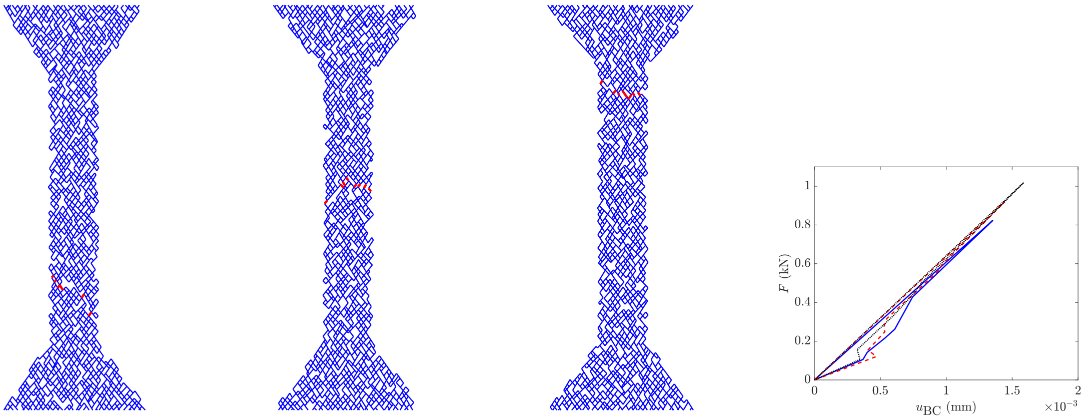

(a) (b) (c) (d)

Figure 5-9: Damage: some typical damage patterns for the type B networks with h = 0.1 mm and constituent lengths ranging between 0.3 mm and 0.6 mm (red: failed constituents), as well as some force-displacement curves.

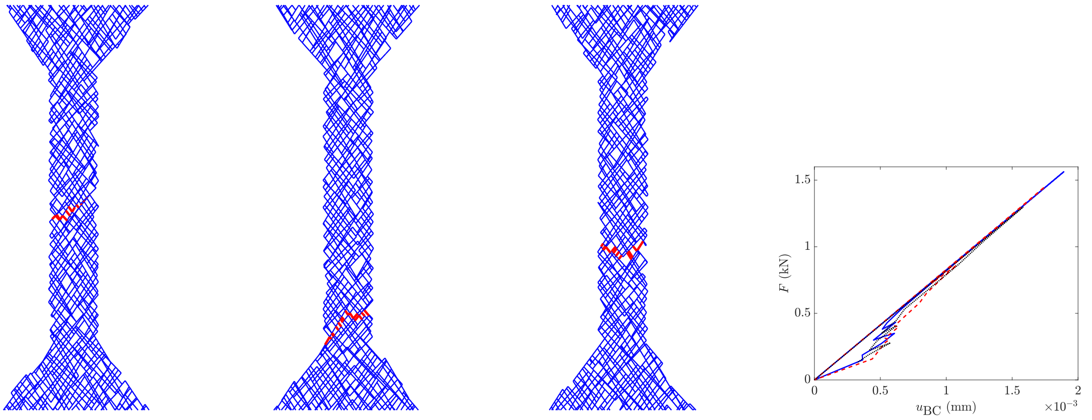

(a) (b) (c) (d)

Figure 5-10: Damage: some typical damage patterns for the type B networks with h = 0.1 mm and constituent lengths ranging between 1 mm and 1.5 mm (red: failed constituents), as well as some force-displacement curves.

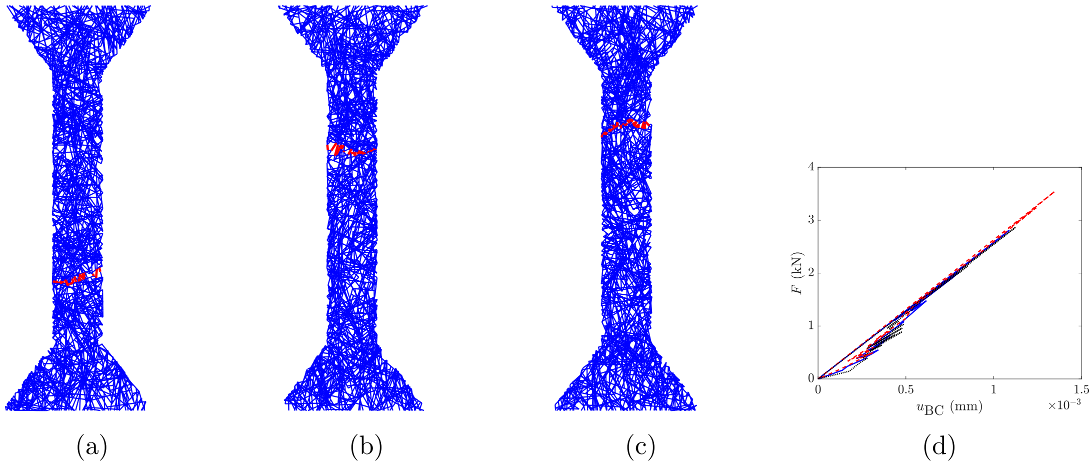

Figure 5-11: Damage: some typical damage patterns for the type C networks with 2000 constituents (red: failed constituents) and some force-displacement curves.

part of the dog-bone shaped specimens for the points in the first domain, whilst cracked beams also appear in the wider parts at the top and bottom of the dog-bone shaped specimens for points in the second domain. For the latter, longer crack lengths therefore occurr, explaining the increase in dissipation.

Comparing Figs. 5-12(a), 5-12(b) and 5-12(c), one can see that the marginal univariate PDFs for all three cases are similar, although the ones predicted using identified univariate marginal PDFs are clearly wider. The mean values of the maximum force and dissipated energy and the Pearson correlation coefficients are presented in Table 5.5. It can be observed that the mean values for both the maximum force and the dissipated energy are higher for the cases with the identified joint PDFs than for the cases with the true PDF. The difference in the results between whether or not incorporating the correlation is negligible.

Fig. 5-13 shows the same scatter plot, but with $h = 0.025$ mm, i.e. for an increased fibre density. The trends are similar as for the case of $h = 0.025$ mm. Even the relative difference between the means is very similar (Table 5.5).

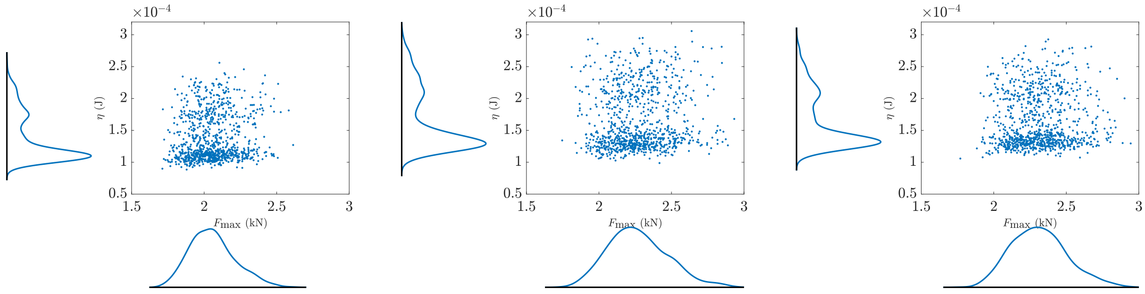

(a) True joint PDF (b) Identified joint PDF (c) Identified joint PDF without correlation

Figure 5-12: Damage: the scatter plots of the maximum force ($F_{\max}$) and dissipated energy (η) for the type A networks with $h = 0.1$ mm. One can see that the marginal univariate PDFs are similar in all the cases. One can also observe that the univariate marginal PDF for the dissipation consists of two domains. The first ($\eta < 0.13$ mJ) contains predictions with shorter crack paths than the second ($\eta > 0.13$ mJ), caused by crack path being present in the wide top and bottom regions of the dog-bone shaped specimens.

Next, we consider type B networks with constituent lengths randomly sampled from a uniform distribution with bounds 0.3 mm and 0.6 mm. Fig. 5-14 presents the scattered plot of

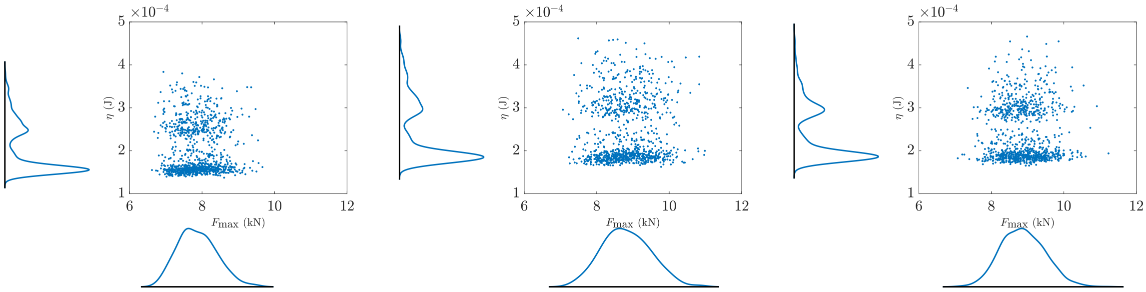

(a) True joint PDF (b) Identified joint PDF (c) Identified joint PDF without correlation

Figure 5-13: Damage: the scatter plots of the maximum force ($F_{\max}$) and dissipated energy (η) for the type A networks with $h = 0.025$ mm. One can see that the marginal univariate PDFs are similar in all the cases. Like the case with $h = 0.1$ mm and regardless of the used material parameter PDF, one can see that the univariate marginal PDF for the dissipation consists of two domains. This is caused by long fracture paths that propagate through the wide top and bottom regions of the dog-bone shaped specimens (see Fig. 5-8(a)), resulting in an increase of the dissipation.

Table 5.5: Damage: the mean values and Pearson correlation coefficient for the type A networks.

h (mm)	$F_{\max}^{\text{mean}}$ (kN)	η^{mean} (J)	$\rho_{F_{\max}\eta}$
True joint PDF			
0.1	2.0584	1.3703×10^{-4}	0.1067
0.025	7.8706	2.0107×10^{-4}	-0.0053
Identified joint PDF			
0.1	2.27014	1.647×10^{-4}	0.0734
0.025	8.8204	2.4216×10^{-4}	0.02069
Identified joint PDF without correlation			
0.1	2.3142	1.6342×10^{-4}	0.0402
0.025	8.8744	2.3866×10^{-4}	-5.5635×10^{-4}

the maximum force and dissipated energy for $h = 0.1$ mm and the mean values and correlation coefficient are given in Table 5.6. One can see that the mean values of the maximum force and dissipated energy are higher for both cases with the identified joint PDF than for the cases with the true joint PDF. However, this is not the case for correlation coefficient. The difference between the cases with the identified joint PDF with and without correlation is negligible.

If we now increase the fibre density (by setting $h = 0.025$ mm), we can see the same trend as for the type A networks (Fig. 5-15 and Table 5.6): although the mean of the maximum force and dissipated energy increase, the relative differences between the mean values of the cases with the true joint PDF and the identified joint PDFs remain similar. Increasing the constituent length ($l_{\min} = 1$ mm and $l_{\max} = 1.5$ mm) has practically no influence on the relative differences between the cases with the true PDF and the identified PDFs (Figs. 5-16 and 5-17).

Finally, we consider the results for the type C networks. Again, the same trends can be observed: increasing the fibre density causes a shift of the PDFs, the PDFs of the cases with the identified PDFs have larger means than those of the cases with the true PDF, but the relative differences between the means is again roughly 10%. Incorporating the correlation has a negligible effect on the results.

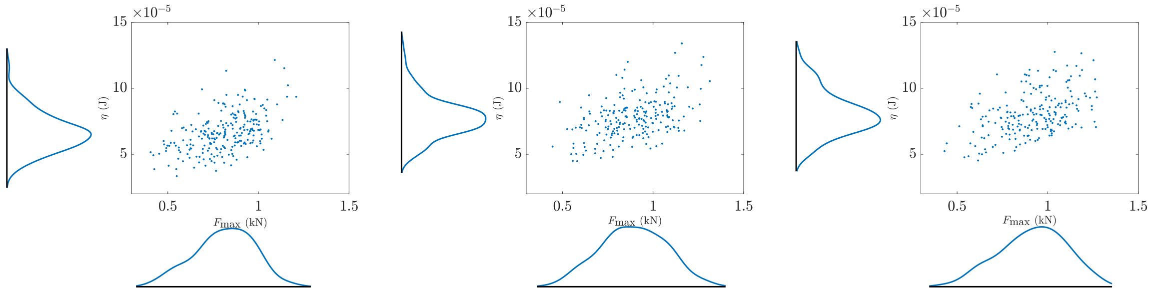

(a) True joint PDF (b) Identified joint PDF (c) Identified joint PDF without correlation

Figure 5-14: Damage: the scatter plots of the maximum force ($F_{\max}$) and dissipated energy (η) for the type B networks with constituent lengths randomly sampled from a uniform distribution with bounds 0.3 mm and 0.6 mm and $h = 0.1$ mm. One can observe similar trends for all cases. The means are larger for the cases with the identified PDFs than for the cases with the true PDF (also see Table 5.6).

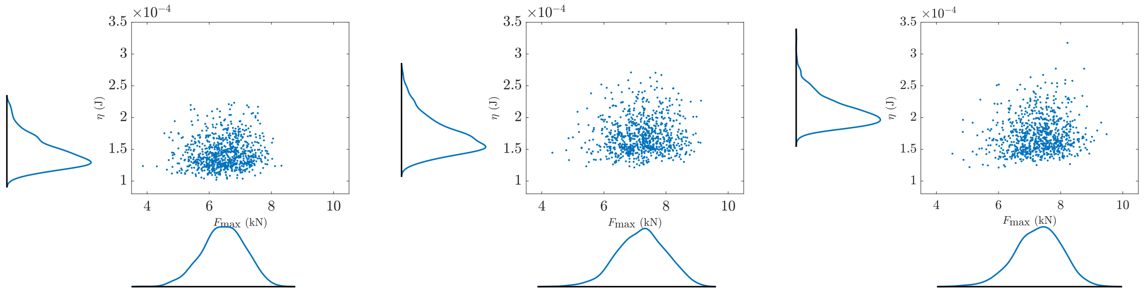

(a) True joint PDF (b) Identified joint PDF (c) Identified joint PDF without correlation

Figure 5-15: Damage: the scatter plots of the maximum force ($F_{\max}$) and dissipated energy (η) for the type B networks with constituent lengths randomly sampled from uniform distribution with bounds 0.3 mm and 0.6 mm and $h = 0.025$ mm. One can observe similar trends for all cases. The means are larger for the cases with the identified PDFs than for the cases with the true PDF (Table 5.6).

Table 5.6: Damage: the mean values and Pearson correlation coefficient for the type B networks with constituent lengths randomly sampled from a uniform distribution with bounds 0.3 mm and 0.6 mm.

h (mm)	$F_{\max}^{\text{mean}}$ (kN)	η^{mean} (J)	$\rho_{F_{\max}\eta}$
True joint PDF			
0.1	0.8103	6.6701×10^{-5}	0.4855
0.025	6.4519	1.4362×10^{-4}	0.0931
Identified joint PDF			
0.1	0.8900	7.7875×10^{-5}	0.4582
0.025	7.2117	1.7117×10^{-4}	0.0686
Identified joint PDF without correlation			
0.1	0.9184	8.0536×10^{-5}	0.4655
0.025	7.2788	1.7187×10^{-4}	0.1187

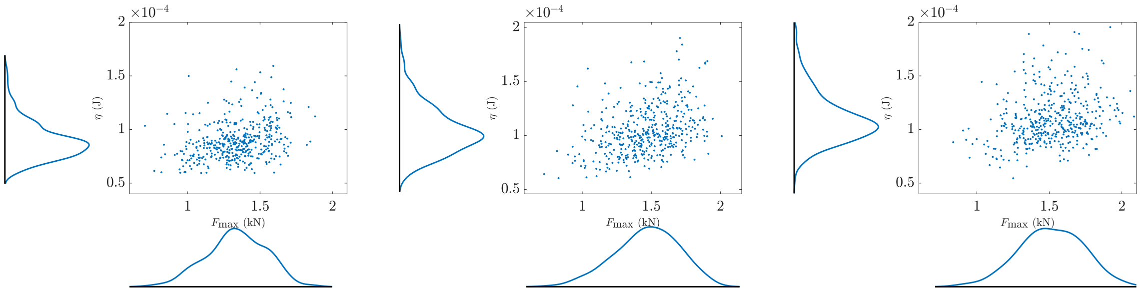

(a) True joint PDF (b) Identified joint PDF (c) Identified joint PDF without correlation

Figure 5-16: Damage: the scatter plots of the maximum force ($F_{\max}$) and dissipated energy (η) for the type B networks with constituent lengths randomly sampled from a uniform distribution with bounds 1 mm and 1.5 mm and $h = 0.1$ mm. One can observe similar trends for all cases. The means are larger for the cases with the identified PDFs than for the cases with the true PDF (Table 5.7).

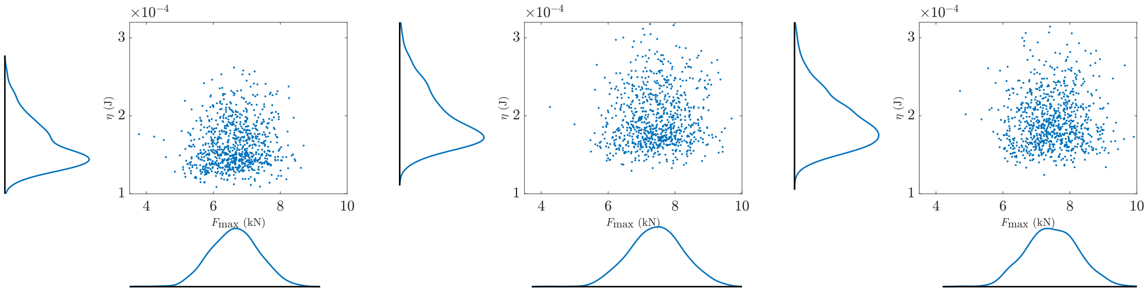

(a) True joint PDF (b) Identified joint PDF (c) Identified joint PDF without correlation

Figure 5-17: Damage: the scatter plots of the maximum force ($F_{\max}$) and dissipated energy (η) for the type B networks with constituent lengths randomly sampled from a uniform distribution with bounds 1 mm and 1.5 mm and $h = 0.025$ mm. One can observe similar trends for all cases. The means are larger for the cases with the identified PDFs than for the cases with the true PDF (Table 5.7).

Table 5.7: Damage: the mean values and Pearson correlation coefficient for the type B networks with constituent lengths randomly sampled from uniform distribution with bounds 1 mm and 1.5 mm.

h (mm)	$F_{\max}^{\text{mean}}$ (kN)	η^{mean} (J)	$\rho_{F_{\max}\eta}$
True joint PDF			
0.1	1.3353	8.9301×10^{-5}	0.2929
0.025	6.6424	1.6227×10^{-4}	0.1080
Identified joint PDF			
0.1	1.4664	1.0496×10^{-4}	0.3600
0.025	7.4416	1.9584×10^{-4}	0.0737
Identified joint PDF without correlation			
0.1	1.5131	1.0977×10^{-4}	0.2430
0.025	7.4673	1.9346×10^{-4}	0.0192

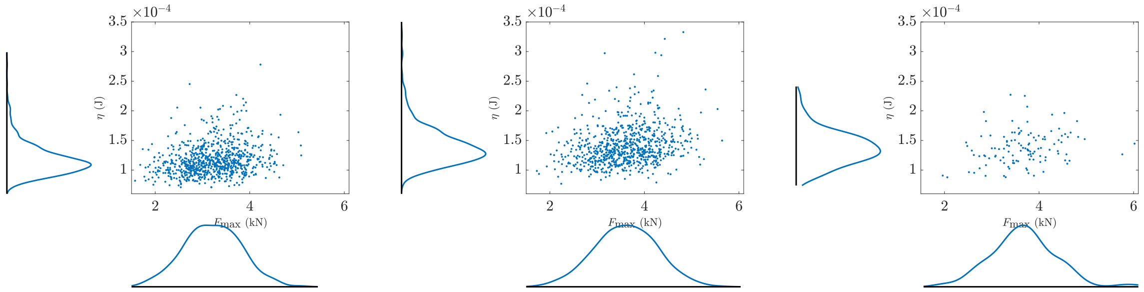

(a) True joint PDF (b) Identified joint PDF (c) Identified joint PDF without correlation

Figure 5-18: Damage: the scatter plots of the maximum force ($F_{\max}$) and dissipated energy (η) for the type C networks with 2000 constituents. The mean values of the maximum force, dissipated energy, as well as the correlation coefficient are shown in Table 5.8.

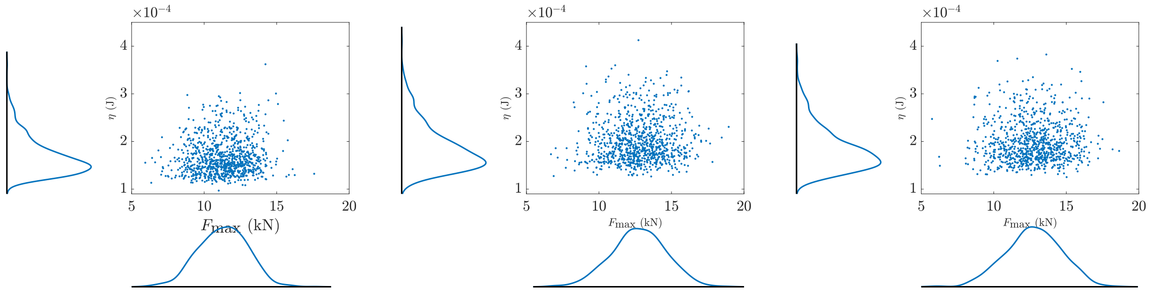

(a) True joint PDF (b) Identified joint PDF (c) Identified joint PDF without correlation

Figure 5-19: Damage: the scatter plots of the maximum force ($F_{\max}$) and dissipated energy (η) for the type C networks with 5000 constituents. The mean values of the maximum force, dissipated energy, as well as the correlation coefficient are shown in Table 5.8.

Table 5.8: Damage: the mean values and Pearson correlation coefficient for the type C networks.

Number of constituents	$F_{\max}^{\text{mean}}$ (kN)	η^{mean} (J)	$\rho_{F_{\max}\eta}$
True joint PDF			
2000	3.2110	1.1724×10^{-4}	0.2274
5000	11.2996	1.6765×10^{-4}	0.0775
Identified joint PDF			
2000	3.6055	1.4084×10^{-4}	0.2416
5000	12.7403	2.0117×10^{-4}	0.0498
Identified joint PDF without correlation			
2000	3.6680	1.3764×10^{-4}	0.2374
5000	12.7334	1.9868×10^{-4}	0.0215

Elastoplasticity

Some typical results of individual simulations for elastoplasticity are shown in Figs. 5-20 to 5-23. For the statistical analyses below, we describe the predicted force-displacement responses using the typical 1D expression of isotropic elastoplasticity with linear hardening for monotonically increasing, uniaxial tension, in which reaction force F is a function of prescribed displacement u_{BC} (see Fig. 5-2) as follows:

$$F = \begin{cases} k_E u_{\mathrm{BC}} & \text{if } u_{\mathrm{BC}} < \frac{F_{y0}}{k_E} \\ F_{y0} + \frac{k_E k_P}{k_E + k_P}\left(u_{\mathrm{BC}} - \frac{F_{y0}}{k_E}\right) & \text{if } u_{\mathrm{BC}} \geq \frac{F_{y0}}{k_E} \end{cases}, \tag{5.29}$$

where k_E, F_{y0} and k_P denote the system's equivalent elastic stiffness, initial yield force and hardening stiffness, respectively.

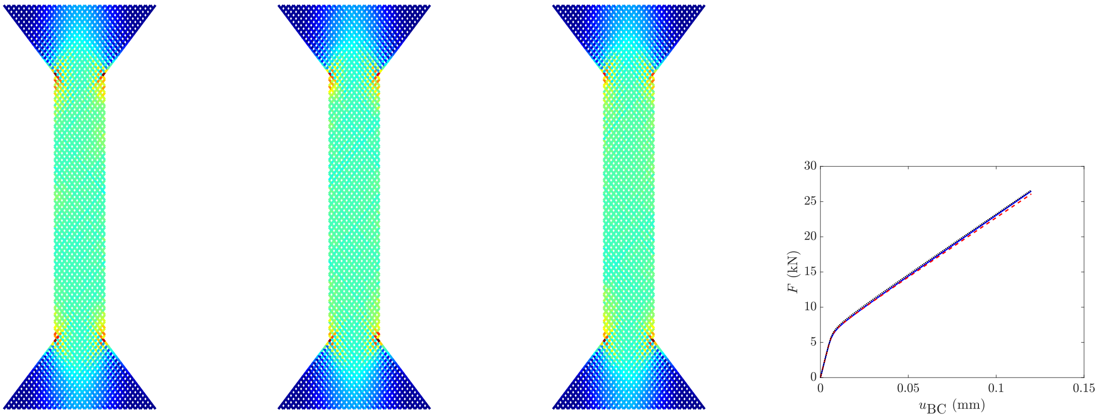

(a) (b) (c) (d)

Figure 5-20: Elastoplasticity: some typical patterns of the maximum cumulative plastic strain per beam element for the type A networks with $h = 0.1$ mm (blue: no cumulative plastic strain, red: maximum cumulative plastic strain), as well as some force-displacement curves.

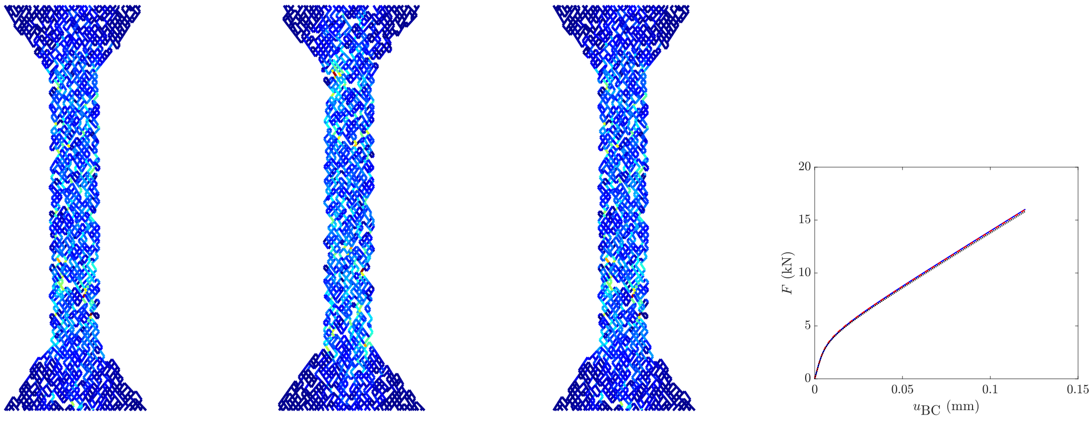

(a) (b) (c) (d)

Figure 5-21: Elastoplasticity: some typical patterns of the maximum cumulative plastic strain per beam element for the type B networks with $h = 0.1$ mm and constituent lengths ranging between 0.3 mm and 0.6 mm (blue: no cumulative plastic strain, red: maximum cumulative plastic strain), as well as some force-displacement curves.

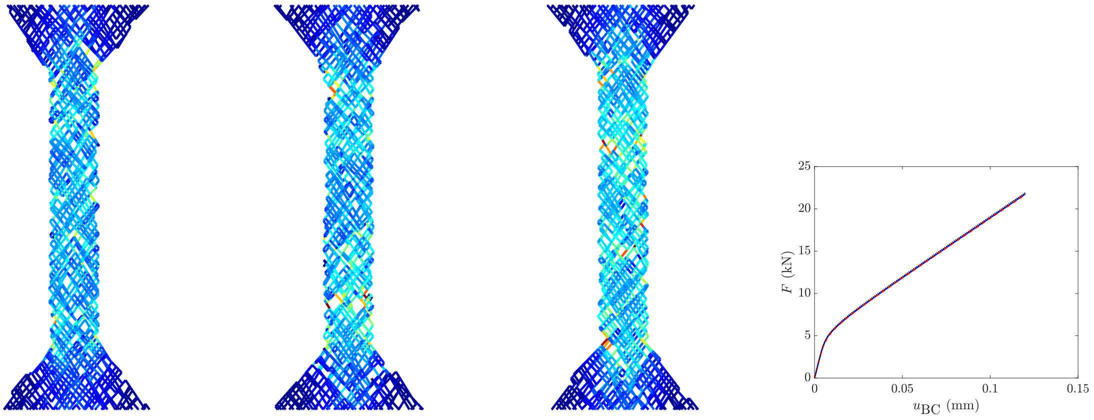

(a) (b) (c) (d)

Figure 5-22: Elastoplasticity: some typical patterns of the maximum cumulative plastic strain per beam element for the type B networks with $h = 0.1$ mm and constituent lengths ranging between 1 mm and 1.5 mm (blue: no cumulative plastic strain, red: maximum cumulative plastic strain), as well as some force-displacement curves.

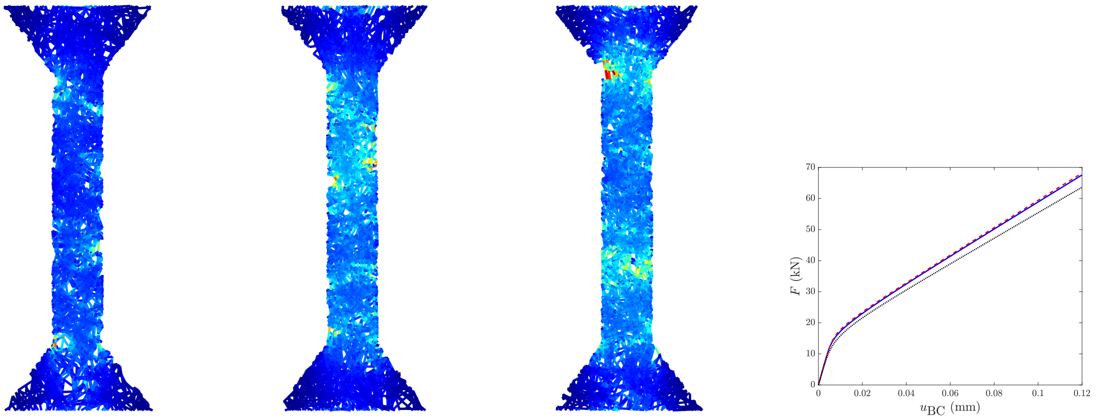

(a) (b) (c) (d)

Figure 5-23: Elastoplasticity: some typical patterns of the maximum cumulative plastic strain per beam element for the type C networks with 2000 constituents (blue: no cumulative plastic strain, red: maximum cumulative plastic strain), as well as some force-displacement curves.

We start again by discussing the scatter plots for the networks of type A with $h = 0.1$ mm, which are presented on three different planes in Fig. 5-24. The mean values of k_E and k_P are again somewhat larger for the cases with the identified PDFs than for the cases with the true PDF (Table 5.9), but a substantial difference can now be observed for the cases with the identified PDF with and without correlation: the PDF predicted with correlation is substantially closer to the PDF predicted with the true material parameter PDF than the PDF predicted without correlation.

If we increase the constituent density by reducing $h = 0.1$ mm to $h = 0.025$ mm, we see similar trends (Fig. 5-25 and Table 5.9). The mean values of k_E and k_P are again approximately 0.5% larger for the cases with the identified PDFs than for the cases with the true PDF and the correlation is significantly better predicted by the cases with the identified PDF with correlation than by the cases with the identified PDF without correlation.

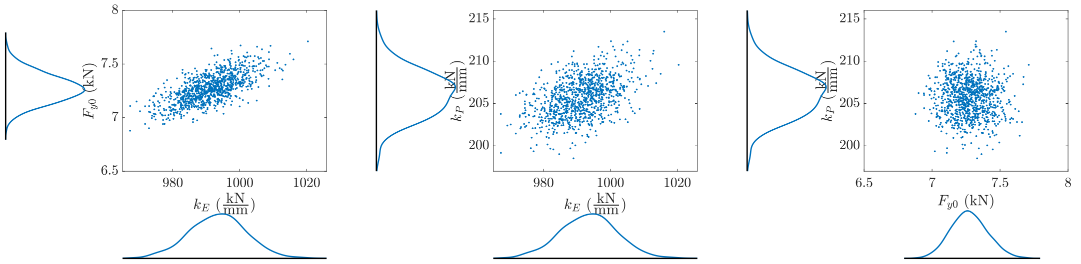

(a) (b) (c)

True joint PDF

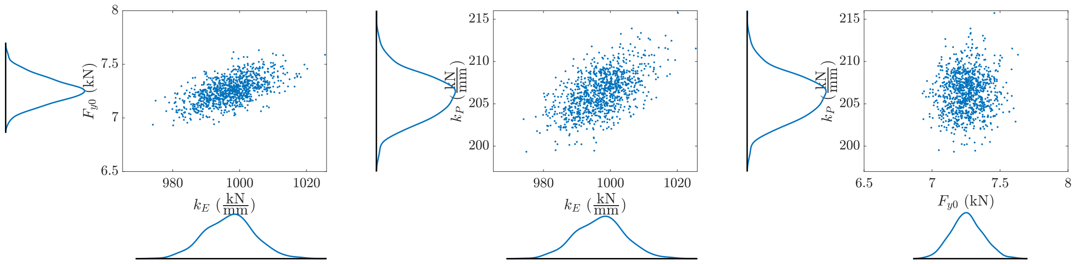

(d) (e) (f)

Identified joint PDF

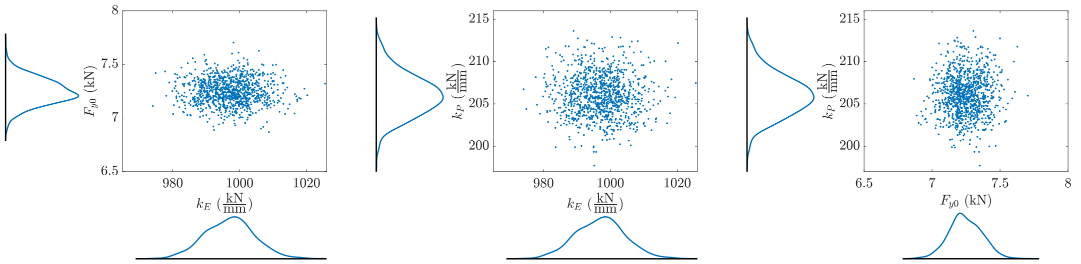

(g) (h) (i)

Identified joint PDF without correlation

Figure 5-24: Elastoplasticity: the scatter plots of the systems' equivalent elastic stiffness (k_E), initial yield force (F_{y0}) and plastic stiffness (k_P) for the type A networks with $h = 0.1$ mm. Comparing (a), (d) and (g) and (b), (e) and (h) shows that the correlation between system parameters is substantially better predicted by the cases with the identified PDF with correlation than by the cases with the identified PDF without correlation.

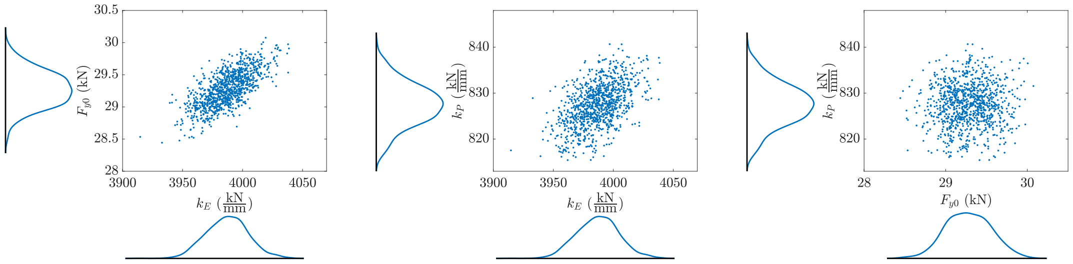

(a) (b) (c)

True joint PDF

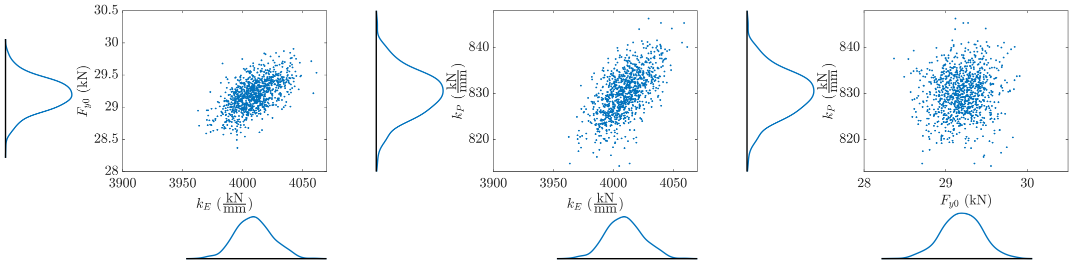

(d) (e) (f)

Identified joint PDF

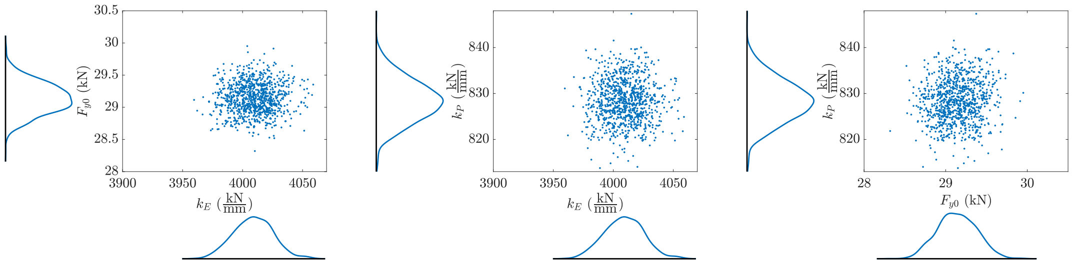

(g) (h) (i)

Identified joint PDF without correlation

Figure 5-25: Elastoplasticity: the scatter plots of the systems' equivalent elastic stiffness (k_E), initial yield force (F_{y0}) and plastic stiffness (k_P) for the type A networks with $h = 0.025$ mm. Similar as for the case with $h = 0.1$, the correlation between the system parameters is substantially better predicted by the cases with the identified PDF with correlation than by the cases with the identified PDF without correlation.

Table 5.9: Elastoplasticity: the mean values and Pearson correlation coefficients for the type A networks.

h (mm)	k_E^{mean} ($\frac{\text{kN}}{\text{mm}}$)	F_{y0}^{mean} (kN)	k_P^{mean} ($\frac{\text{kN}}{\text{mm}}$)	$\rho_{k_E F_{y0}}$	$\rho_{k_E k_P}$	$\rho_{F_{y0} k_P}$
			True joint PDF			
0.1	991.1905	7.2735	205.7121	0.6790	0.4605	-0.0257
0.025	3987.025	29.2798	827.4717	0.7057	0.5077	0.0502
			Identified joint PDF			
0.1	997.0578	7.2563	206.3549	0.5805	0.5535	0.0605
0.025	4009.4294	29.1966	830.0712	0.5793	0.6074	0.1056
			Identified joint PDF without correlation			
0.1	997.0578	7.2463	206.0329	-0.0228	-0.0249	0.0471
0.025	4008.8975	29.1396	828.4127	0.0439	0.0046	0.0948

If we now increase the geometrical randomness by considering the networks of type B characterised by $l_{\text{min}} = 0.3$ mm, $l_{\text{max}} = 0.3$ mm and $h = 0.1$ mm, we see that the correlation increases substantially (Fig. 5-26 and Table 5.10). Consequently, incorporating the correlation in the identified PDF seems of less influence than if type A networks are considered. We nevertheless still observe that the PDF predicted with the identified PDF with correlation is closer to the PDF predicted with the true PDF than the PDF predicted with the identified PDF without correlation. Increasing the fibre density (by setting $h = 0.025$ mm, instead of $h = 0.1$ mm) makes this difference grow (see Fig. 5-27 and Table 5.10).

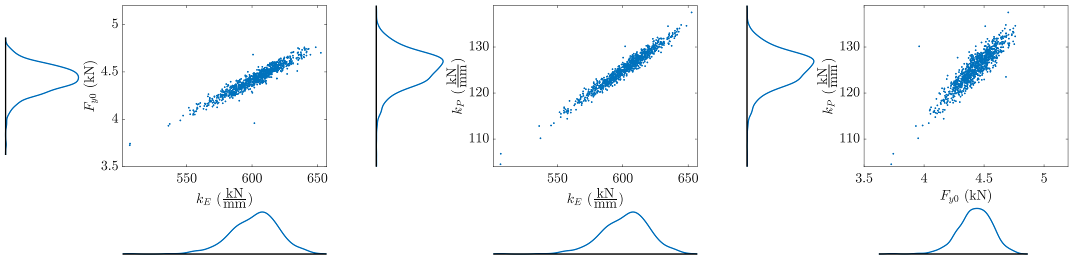

(a) (b) (c)

True joint PDF

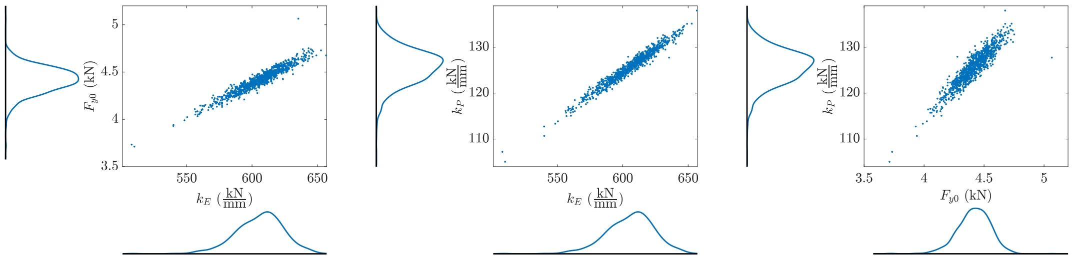

(d) (e) (f)

Identified joint PDF

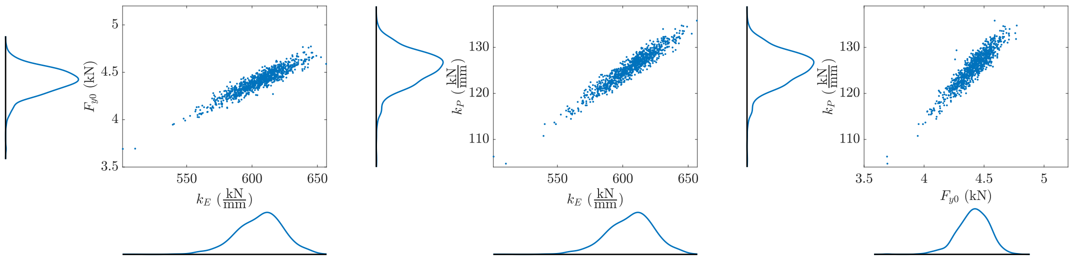

(g) (h) (i)

Identified joint PDF without correlation

Figure 5-26: Elastoplasticity: the scatter plots of the systems' equivalent elastic stiffness (k_E), initial yield force (F_{y0}) and plastic stiffness (k_P) for the type B networks with constituent lengths randomly sampled from a uniform distribution with bounds 0.3 mm and 0.6 mm and $h = 0.1$ mm. The results show that the effect of the correlation between the material parameters is smaller than for the type A networks, but remains to be present. The numerical values are presented in Table 5.10.

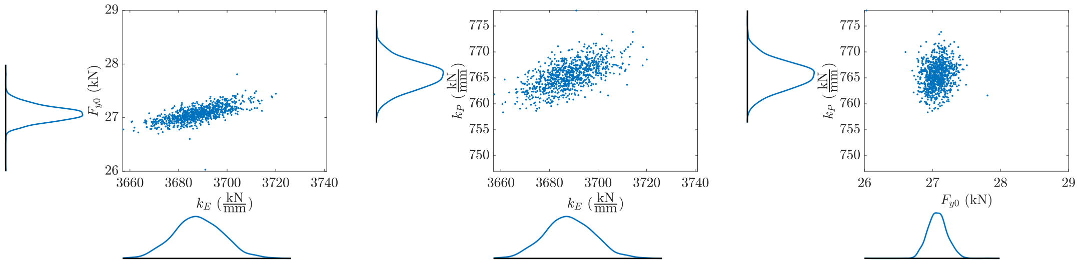

(a) (b) (c)

True joint PDF

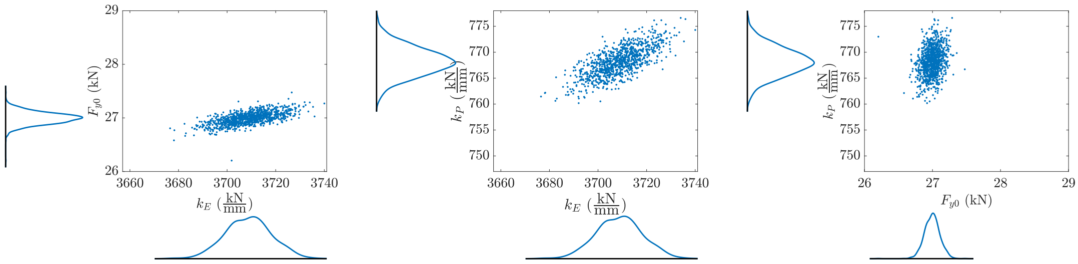

(d) (e) (f)

Identified joint PDF

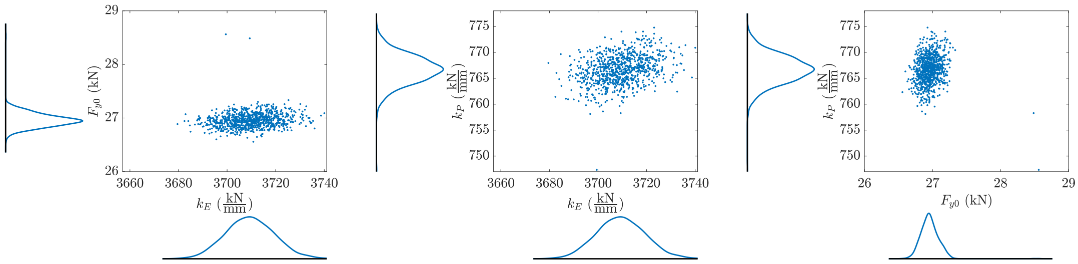

(g) (h) (i)

Identified joint PDF without correlation

Figure 5-27: Elastoplasticity: the scatter plots of the systems' equivalent elastic stiffness (k_E), initial yield force (F_{y0}) and plastic stiffness (k_P) for the type B networks with constituent lengths randomly sampled from a uniform distribution with bounds 0.3 mm and 0.6 mm and $h = 0.025$ mm. The influence of the correlation has increased due to the increased constituent density (cf. Fig. 5-26). The corresponding numerical values are given in Table 5.10.

Table 5.10: Elastoplasticity: the mean values and Pearson correlation coefficients for the type B networks with constituent lengths randomly sampled from a uniform distribution with bounds 0.3 mm and 0.6 mm.

h (mm)	k_E^{mean} $(\frac{\text{kN}}{\text{mm}})$	F_{y0}^{mean} (kN)	k_P^{mean} $(\frac{\text{kN}}{\text{mm}})$	$\rho_{k_E F_{y0}}$	$\rho_{k_E k_P}$	$\rho_{F_{y0} k_P}$
True joint PDF						
0.1	602.0250	4.4260	125.3475	0.9522	0.9773	0.9008
0.025	3688.1158	27.0729	765.4818	0.6984	0.6128	0.1191
Identified joint PDF						
0.1	605.7327	4.4164	125.7086	0.9593	0.9593	0.9251
0.025	3708.7848	26.9940	768.1752	0.6410	0.7212	0.2746
Identified joint PDF without correlation						
0.1	605.7224	4.4094	125.5335	0.9337	0.9572	0.9278
0.025	3709.4773	26.9600	766.6929	0.1778	0.3156	0.0694

If we now increase the length of the constituents by setting $l_{\min} = 1$ mm and $l_{\max} = 1.5$ mm, we also see that the correlation between the systems parameters is better captured if the correlation is incorporated in the identified PDF (see Fig. 5-28 and Table 5.11). We also see that if we increase the constituent density (by reducing $h = 0.1$ mm to $h = 0.025$ mm), the importance of incorporating the correlation increases (see Fig. 5-29 and Table 5.11). We can also conclude by comparing these results with the ones in which the constituent lengths is bound by $l_{\min} = 0.3$ mm and $l_{\max} = 0.6$ mm, that a reduction of the constituent length leads to an increase of the intrinsic correlation between system parameters (regardless of the material parameter PDF used).

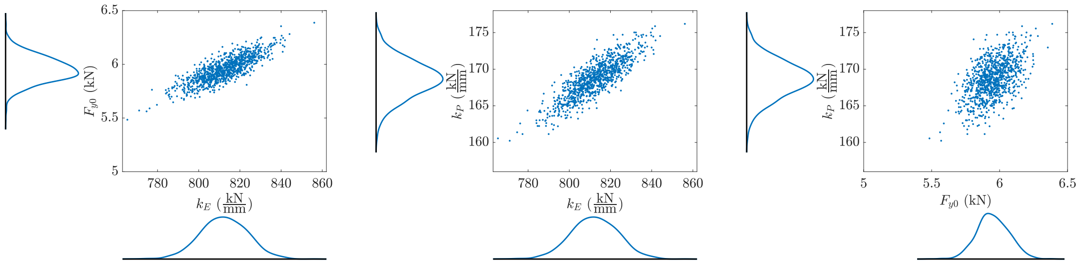

(a) (b) (c)

True joint PDF

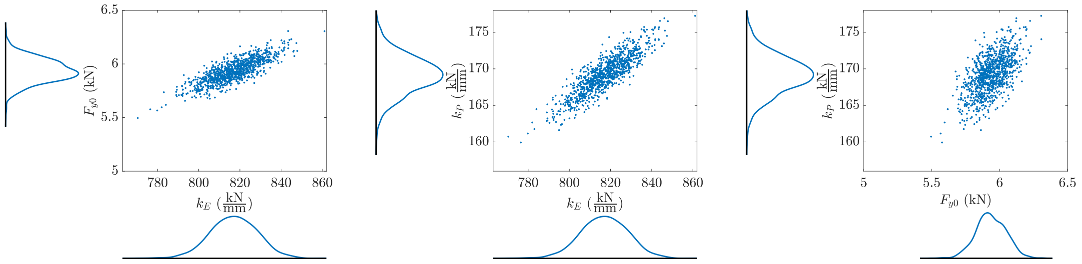

(d) (e) (f)

Identified joint PDF

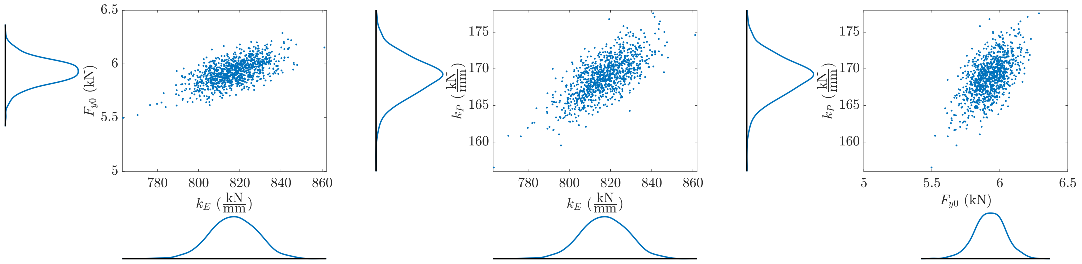

(g) (h) (i)

Identified joint PDF without correlation

Figure 5-28: Elastoplasticity: the scatter plots of the systems' equivalent elastic stiffness (k_E), initial yield force (F_{y0}) and plastic stiffness (k_P) for the type B networks with constituent lengths randomly sampled from uniform distribution with bounds 1 mm and 1.5 mm and $h = 0.1$ mm. The results show that the influence of the correlation is important to incorporate. The numerical values are presented in Table 5.11.

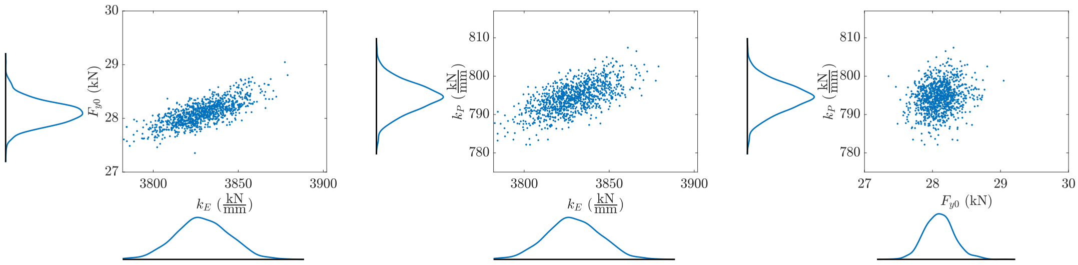

(a) (b) (c)

True joint PDF

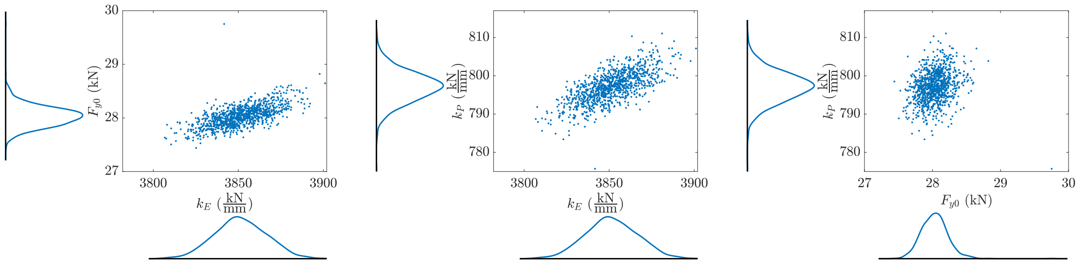

(d) (e) (f)

Identified joint PDF

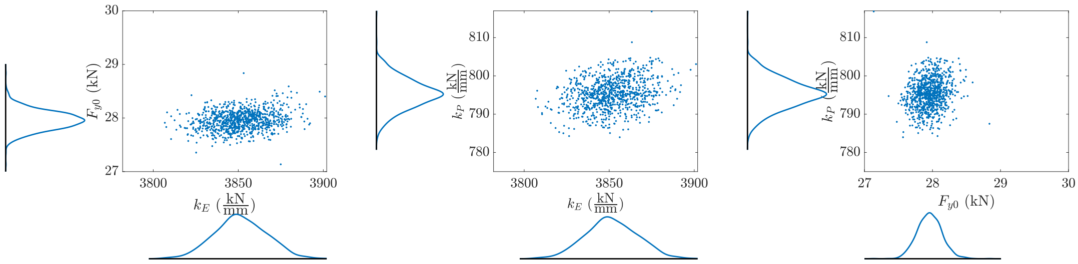

(g) (h) (i)

Identified joint PDF without correlation

Figure 5-29: Elastoplasticity: the scatter plots of the systems' equivalent elastic stiffness (k_E), initial yield force (F_{y0}) and plastic stiffness (k_P) for the type B networks with constituent lengths randomly drawn from a uniform distribution with bounds 1 mm and 1.5 mm and $h = 0.025$ mm. The results show that the influence of the correlation is more important to incorporate due to the increased fibre density (cf. Fig. 5-28). The numerical values are presented in Table 5.11.

Table 5.11: Elastoplasticity: the mean values and Pearson correlation coefficients for the type B networks with constituent lengths randomly sampled from a uniform distribution with bounds 1 mm and 1.5 mm.

h (mm)	k_E^{mean} $\left(\frac{\text{kN}}{\text{mm}}\right)$	F_{y0}^{mean} (kN)	k_P^{mean} $\left(\frac{\text{kN}}{\text{mm}}\right)$	$\rho_{k_E F_{y0}}$	$\rho_{k_E k_P}$	$\rho_{F_{y0} k_P}$
True joint PDF						
0.1	812.2191	5.9523	168.6532	0.8241	0.8488	0.5362
0.025	3828.9229	28.1010	794.4644	0.7389	0.6384	0.1997
Identified joint PDF						
0.1	817.0609	5.9371	169.2043	0.8165	0.8696	0.6005
0.025	3851.4226	28.0314	797.1486	0.6566	0.6957	0.2260
Identified joint PDF without correlation						
0.1	816.9840	5.9275	168.9104	0.6189	0.7018	0.5796
0.025	3851.4167	27.9573	795.3540	0.2157	0.2694	0.1635

Finally, we show the results for the type C networks (Figs. 5-30 and 5-31 and Table 5.12). We see that the intrinsic correlation between the system's parameters (regardless of the material parameter PDF used) becomes even more pronounced than was the case for the type B networks. Apparently, this is caused by the increased geometrical randomness. Consequently, the influence of incorporating the correlation in the identified PDF becomes less important, but the cases with the identified PDF with correlation still outperform those with the identified PDF without correlation.

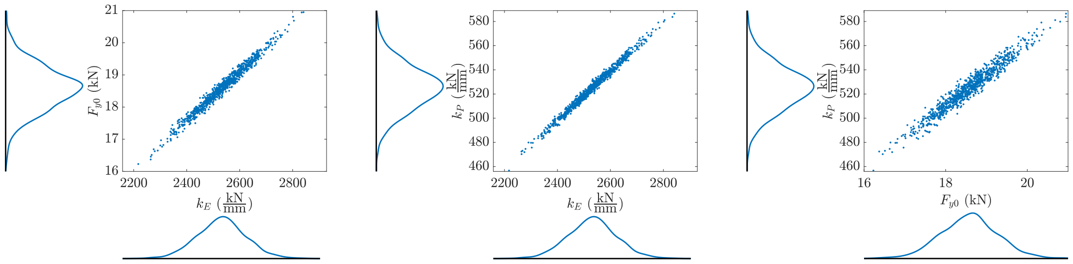

(a) (b) (c)

True joint PDF

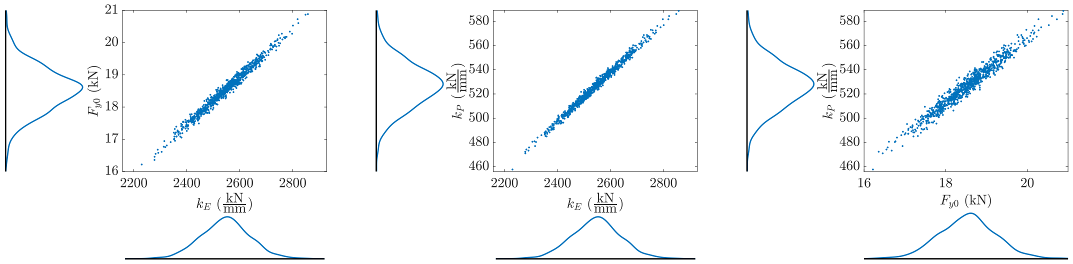

(d) (e) (f)

Identified joint PDF

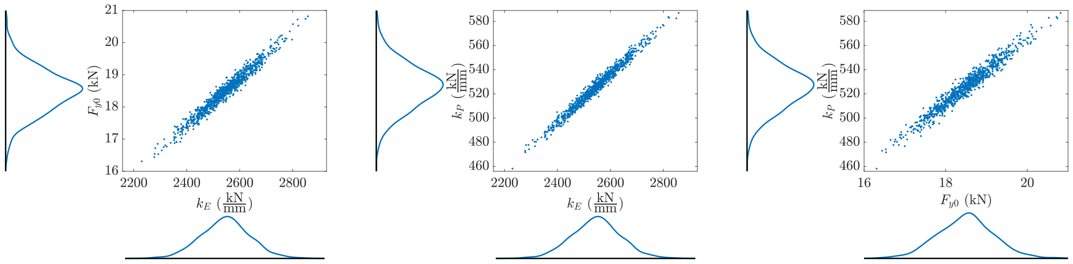

(g) (h) (i)

Identified joint PDF without correlation

Figure 5-30: Elastoplasticity: the scatter plots of the systems' equivalent elastic stiffness (k_E), initial yield force (F_{y0}) and plastic stiffness (k_P) for the type C networks with 2000 constituents. Due to the increased geometrical randomness relative to the type B networks, the correlation is also captured by the cases with the identified PDF without correlation, although they are still outperformed by the cases with the identified PDF with correlation. The corresponding numerical values are given in Table 5.12.

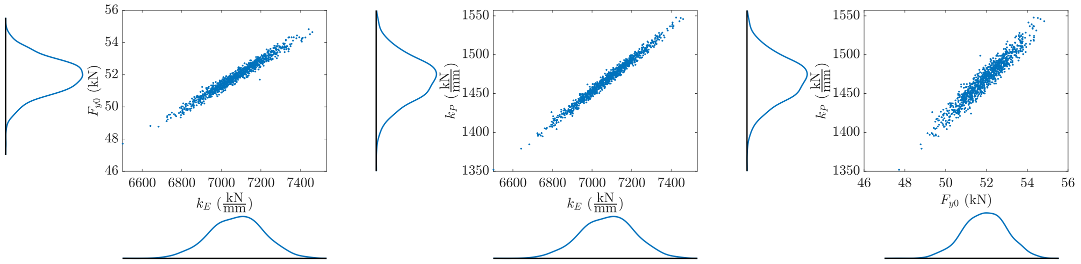

(a) (b) (c)

True joint PDF

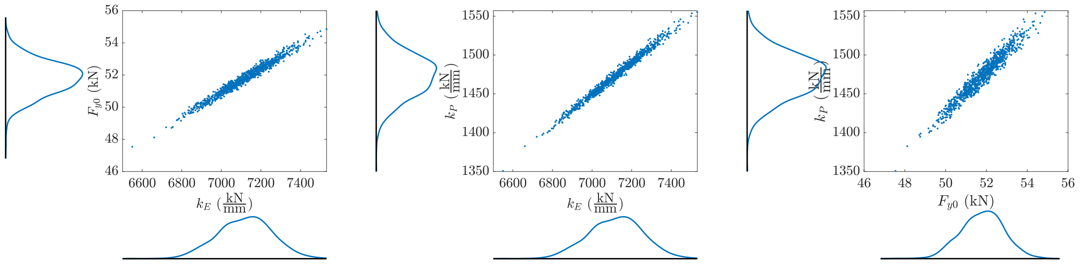

(d) (e) (f)

Identified joint PDF

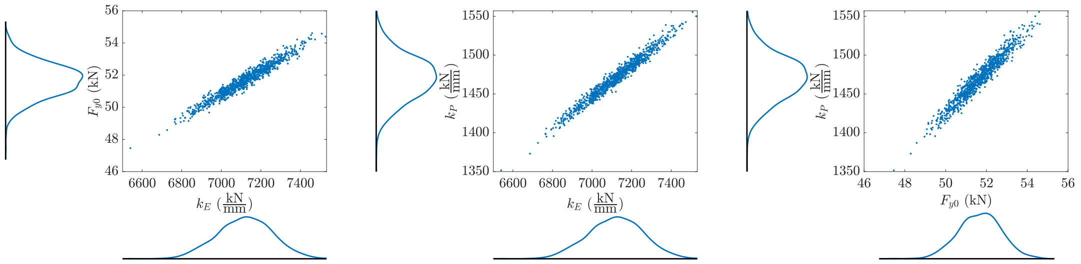

(g) (h) (i)

Identified joint PDF without correlation

Figure 5-31: Elastoplasticity: the scatter plots of the systems' equivalent elastic stiffness (k_E), initial yield force (F_{y0}) and plastic stiffness (k_P) for the type C networks with 5000 constituents. Due to the increased geometrical randomness relative to the type B networks, the correlation is also captured by the cases with the identified PDF without correlation, although they are still outperformed by the cases with the identified PDF with correlation. The corresponding numerical values are given in Table 5.12.

Table 5.12: Elastoplasticity: the mean values and Pearson correlation coefficients for the type C networks.

Number of constituents	k_E^{mean} ($\frac{\text{kN}}{\text{mm}}$)	F_{y0}^{mean} (kN)	k_P^{mean} ($\frac{\text{kN}}{\text{mm}}$)	$\rho_{k_E F_{y0}}$	$\rho_{k_E k_P}$	$\rho_{F_{y0} k_P}$
True joint PDF						
2000	2531.535	18.5793	525.0600	0.9879	0.9936	0.9726
5000	7077.5611	51.9244	1468.4445	0.9824	0.9908	0.9587
Identified joint PDF						
2000	2546.6575	18.5359	526.9446	0.9897	0.9943	0.9783
5000	7118.7663	51.7978	1473.4988	0.9857	0.9926	0.9700
Identified joint PDF without correlation						
2000	2546.6575	18.4928	525.7414	0.9806	0.9882	0.9763
5000	7118.3975	51.6759	1470.2447	0.9730	0.9834	0.9683

5.6 Conclusion

This chapter deals with the issue that different fibres, struts or yarns in fibrous and other discrete materials often have different material properties. We assume that the material properties of each fibre, strut or yarn are a realisation from some PDF. The question we try to answer is how the parameters of this PDF can be identified with limited experimental means; by testing only 20 constituents instead of hundreds.

We have proposed a four step identification scheme to determine the PDF's parameters. Bayesian inference plays an important role in the identification scheme as it regularises the individual identification problems. When the material parameters of each of the 20 constituents are identified, we first select a univariate PDF for each type of material parameter and identify the parameters of each univariate PDF using the regularisation offered by Bayesian inference. When the parameters of the univariate PDFs are identified, we join them in a single, joint PDF by the use of a copula function. The parameters of the copula need to be identified in turn, for which we again use Bayesian inference.

The presented identification results show that the identified PDFs are accurate representations of the true PDFs. The results also show that incorporating the correlation between the different types of material parameters (via copulas) improves the quality of the identified PDF.

Not only the material randomness is of influence on the macroscale responses of fibrous and other discrete materials however, but also the geometrical randomness. We have therefore also conducted a forward study using random network models in which the different PDFs are used to sample the material parameters of the constituents. These results have indicated that if a perfectly brittle damage model is used, the incorporation of the correlation between the Young's modulus and the failure strain has practically no influence on the accuracy of the predicted PDFs. We have also shown that the amount of geometrical randomness is of no influence. This story changes for elastoplasticity however. The correlation between the material parameters is important to incorporate and becomes more important if the fibre density increases or if the fibre length increases. We have also shown that the correlation's influence reduces for an increase of the geometrical randomness.

Chapter 6

Conclusions and outlook

6.1 Conclusions

In this thesis, Bayesian inference was developed to identify material parameters in solid mechanics. From a Bayesian perspective, uncertainties about values such as material parameters (e.g. uncertainties caused by measurement errors or model errors) are modelled as probability distributions. In Bayesian frameworks the prior choices for the probability distributions (i.e. the user's initial knowledge, represented by probability distributions) is updated by measurements through Bayes' theorem. The identification frameworks given here were mainly presented for uniaxial tests on elastoplastic and viscoelastic material models.

In Chapter 2, a gentle tutorial on Bayesian inference for the identification of parameters in elastoplasticity is presented. The results of this chapter have shown that the influence of prior knowledge on the posterior decreases as the number of measurements increases and that the posterior becomes narrower for an increase of the number of measurements (i.e. the uncertainty decreases). The results have also shown that as the number of measurements increases the point estimators of Bayesian inference (e.g. mean and MAP point, the point in which the posterior is maximum) tend to the values identified by the least squares method. It must be noted that the least squares method yielded a single set of identified values for the cases considered in this chapter.

In Chapter 3 a framework to identify viscoelastic materials was presented. The model of interest was the standard linear solid model and the experiments of interest were a relaxation test, a constant strain-rate test and a creep test in tension. One of the chapter's two objectives was to investigate the influence of the number of measurements and the influence of the prior on the identification results. The second aim was to investigate how the three different experiments affect the point estimators and their uncertainties. The results have shown that the prior in viscoelasticity has a larger effect on the point estimators (i.e. mean and MAP point), than the prior in elastoplasticity. Moreover, the results have shown that the uncertainty in the identified parameters resulting from the constant strain-rate test is substantially larger than those resulting from the relaxation test and the creep test. This can be due to the asymptotic behaviour in the relaxation and creep test, for which only one parameter is responsible. This entails that the uncertainty of this parameter is relatively small and, because of that, the uncertainties of the other parameters are also relatively small compared to those resulting from the constant strain-rate experiment.

In Chapter 4 a Bayesian framework to identify parameters in elasticity and elastoplasticity was formulated which not only considered the error in the output (error in the stress), but also the input error (the error in the strain), as well as the uncertainty in the model. Three different formulations are employed to describe the model uncertainty: (1) a random variable coming from a normal distribution with constant parameters, (2) a random variable coming from a normal distribution with an input-dependent mean and (3) a Gaussian process with a stationary covariance function.

The results have shown that incorporating any of the three model uncertainty formulations results in wider marginal posterior distributions of the Young's modulus. Consequently, the chance that the posterior distributions include the true value increases. Incorporating model uncertainty also results in wider posterior prediction intervals, which therefore contain more measurements.

If the error in the input (strain) was also considered, the resulting marginal posterior of the Young's modulus became even wider (with the exception of the Gaussian process as the model uncertainty). The posterior became narrower in this case, albeit the posterior at the true value was larger. This means that the true value has a higher chance to be realised from the posterior. Including the error in the input (strain) as well as model uncertainty also resulted in wider posterior prediction intervals. This increases the chance that these intervals contain the measurement data. If the model uncertainty is presented by a Gaussian process however, the prediction intervals did not become wider but did contain more measurements than if the input error was not included.

The results of this chapter have generally shown that incorporating both model uncertainty and the input error (besides the commonly incorporated output error) favourably influence the identified parameters and the posterior predictions, compared to only incorporating model uncertainty or only incorporating the input error (besides the commonly incorporated output error). As the difference between the true response and the response of the material model increases however, the added value of incorporating the input error as well reduces substantially.

Finally in Chapter 5, random fibre networks were considered for which it was assumed that the material parameter set of each fibre is a realisation of a probability density function (PDF). The aim was to identify the parameters of this PDF by testing a limited number of fibres (i.e. 20), instead of testing hundreds. Bayesian inference regularises this identification problem, because 20 parameter sets do not allow a deterministic identification of the PDF's parameters. The results have shown that the identified PDFs are sufficiently accurate approximations of the true PDFs.

The macroscale responses of random fibre networks are however also influenced by geometrical randomness. Chapter 5 therefore also aims to answer the question 'how precisely should the material randomness be identified, if geometrical randomness also exists?' The results of propagating the identified and true PDFs in random network models have shown that if a perfectly brittle damage model was considered, the incorporation of the correlation between the Young's modulus and the failure strain had practically no influence on the predicted PDFs. The opposite was observed for elastoplasticity however. The results for elastoplasticity have furthermore indicated that the correlation becomes less important to incorporate for an increase of the geometrical randomness and more important for an increase of the fibre density, as well as for an increase of the fibre length.

6.2 Future work

The following list details some possible future research directions based on the work and results of the presented thesis:

(1) Develop nonparametric formulations (e.g. Gaussian processes) for model uncertainty that incorporate the physical constraints of the identification problem at hand. Physical constraints have so far only been considered parametric formulations for model uncertainty

[135]. For example, incompressibility constraints for rubber-like and biological materials may be an interesting research direction [136].

(2) Model uncertainty may also be represented by random walks, which to the best of the author's knowledge were subject to very limited amounts of research [76]. Random walks may be convenient to describe model uncertainty thanks to their natural stochastic nature and the ease of implementation.

(3) In the case of random fibre networks, the material parameter set of each fibre was assumed to be a realisation from some probability density function. The material parameters may however spatially differ for each fibre, which may result in more accurate frameworks (provided that the spatial distributions can be identified). Spatial distributions may also be, and are currently, considered for continuous materials and the spatial characteristics of the distributions may be related to small-scale phenomena such as the underlying crystallographic structures of metals.

(4) Systematic studying the effect of boundary conditions on the uncertainty of the identified parameter values may also be considered an additional research direction. Results in Chapter 3 have shown that the type of experiment influences the uncertainty of the identified parameter values. This may also be true for boundary conditions.

(5) Develop an efficient Bayesian framework for parameter estimation in systems with large number of parameters [137], although this was performed in the study by Bui-Thanh et al. [137] for a linearised Bayesian formulation.

(6) Markov chain Monte Carlo methods may not be computationally efficient if data is gathered in real-time and online parameter identification is needed (e.g. for real-time identification of dynamic models[138]). The development of an efficient framework based on Bayesian inference can be a research direction [139].

6.3 Recommendations for new comers in Bayesian inference

Despite the fact that numerous research papers and text books exist for Bayesian inference and Bayesian theory, finding a proper starting point can be a challenge for new comers in the field. The book 'Bayesian Data Analysis' by Gelman et al. [17] may be perceived as useful because it covers the most essential topics in a simple way. The study 'Bayesian system identification based on probability logic' by Beck [16] furthermore provides a nice and relatively short illustration on system identification using Bayesian inference, as well as some useful concepts on probabilistic identification. More information about Markov chain Monte Carlo sampling techniques can be found in the books 'Markov chain Monte Carlo in practice' [23] and 'Handbook of Markov chain Monte Carlo' [24], whilst a gentle introduction on sampling and the Metropolis-Hastings algorithm is provided in [2]. Both JAGS [140] and Stan [141] furthermore are programmes that can be used for sampling.

Bibliography

[1] R. Mahnken, Encyclopedia of computational mechanics, Vol. 2, Wiley Online Library, 2004, Ch. Identification of material parameters for constitutive equations, pp. 637–655.

[2] D. Calvetti, E. Somersalo, An introduction to Bayesian scientific computing: Ten lectures on subjective computing, Vol. 2, Springer Science & Business Media, New York, 2007.

[3] B.S. Everitt, A. Skrondal, The Cambridge dictionary of statistics, Cambridge University Press, 2010.

[4] R.E. Walpole, R.H. Myers, S.L. Myers, K. Ye, Probability and statistics for engineers and scientists, Pearson custom library, Pearson, 2013.

[5] J. Mullins, S. Mahadevan, Bayesian uncertainty integration for model calibration, validation, and prediction, Journal of Verification, Validation and Uncertainty Quantification 1 (1) (2016) 011006.

[6] R. Mahnken, E. Stein, Parameter identification for viscoplastic models based on analytical derivatives of a least-squares functional and stability investigations, International Journal of Plasticity 12 (4) (1996) 451–479.

[7] M. Springmann, M. Kuna, Identification of material parameters of inelastic constitutive laws from displacement fields, WIT Transactions on Engineering Sciences 47 (2004) 13–23.

[8] L.A.A. Beex, C.W. Verberne, R.H.J. Peerlings, Experimental identification of a lattice model for woven fabrics: Application to electronic textile, Composites Part A: Applied Science and Manufacturing 48 (Supplement C) (2013) 82–92.

[9] J. Wakefield, Bayesian and frequentist regression methods, Springer Series in Statistics, Springer Science & Business Media, New York, 2013.

[10] H.E. Rauch, C.T. Striebel, F. Tung, Maximum likelihood estimates of linear dynamic systems, AIAA journal 3 (8) (1965) 1445–1450.

[11] R. Kashyap, Maximum likelihood identification of stochastic linear systems, IEEE Transactions on Automatic Control 15 (1) (1970) 25–34.

[12] J. Houssineau, S.S. Singh, A. Jasra, Identification of multi-object dynamical systems: Consistency and Fisher information, ArXiv e-prints.

[13] G.P. Sendeckyj, Fitting models to composite materials fatigue data, in: Test methods and design allowables for fibrous composites, ASTM International, 1981.

[14] A.D. Freed, K. Diethelm, Fractional calculus in biomechanics: A 3D viscoelastic model using regularized fractional derivative kernels with application to the human calcaneal fat pad, Biomechanics and Modeling in Mechanobiology 5 (4) (2006) 203–215.

[15] Y. Xiong, W. Chen, K.L. Tsui, D.W. Apley, A better understanding of model updating strategies in validating engineering models, Computer Methods in Applied Mechanics and Engineering 198 (15) (2009) 1327–1337.

[16] J.L. Beck, Bayesian system identification based on probability logic, Structural Control and Health Monitoring 17 (7) (2010) 825–847.

[17] A. Gelman, J.B. Carlin, H.S. Stern, D.B. Rubin, Bayesian data analysis, Chapman & Hall/CRC Texts in Statistical Science, Chapman & Hall/CRC, 2003.

[18] T.A. Catanach, Computational methods for Bayesian inference in complex systems, Ph.D. thesis, California Institute of Technology (2017).

[19] J.O. Berger, Statistical Decision Theory and Bayesian Analysis, Springer Series in Statistics, Springer Science & Business Media, New York, 1985.

[20] J.O. Berger, The case for objective Bayesian analysis, Bayesian Analysis 1 (3) (2006) 385–402.

[21] L. Wasserman, All of statistics: A concise course in statistical inference, Springer Texts in Statistics, Springer Science & Business Media, New York, 2004.

[22] C.M. Bishop, Pattern recognition and machine learning, Information Science and Statistics, Springer Science & Business Media, New York, 2006.

[23] W.R. Gilks, S. Richardson, D. Spiegelhalter, Markov chain Monte Carlo in practice, CRC press, 1995.

[24] S. Brooks, A. Gelman, G. Jones, X.L. Meng, Handbook of Markov chain Monte Carlo, CRC press, 2011.

[25] D. Higdon, H. Lee, Z. Bi, A Bayesian approach to characterizing uncertainty in inverse problems using coarse and fine scale information, IEEE Transactions on Signal Processing 50 (2002) 388–399.

[26] J. Wang, N. Zabaras, A Bayesian inference approach to the inverse heat conduction problem, International Journal of Heat and Mass Transfer 47 (17-18) (2004) 3927–3941.

[27] A. Solonen, Bayesian methods for estimation, optimization and experimental design, Ph.D. thesis, Lappeenranta University of Technology (2011).

[28] P. Risholm, F. Janoos, I. Norton, A.J. Golby, W.M. Wells, Bayesian characterization of uncertainty in intra-subject non-rigid registration, Medical image analysis 17 (5) (2013) 538–555.

[29] S. Lan, T. Bui-Thanh, M. Christie, M. Girolami, Emulation of higher-order tensors in manifold Monte Carlo methods for Bayesian inverse problems, Journal of Computational Physics 308 (2016) 81–101.

[30] H. Rappel, L.A.A. Beex, S.P.A. Bordas, Bayesian inference to identify parameters in viscoelasticity, Mechanics of Time-Dependent Materials 22 (2) (2018) 221–258.

[31] H. Rappel, L.A.A. Beex, J.S. Hale, L. Noels, S.P.A. Bordas, A tutorial on Bayesian inference to identify material parameters in solid mechanics, submitted for publication.

[32] H. Rappel, L.A.A. Beex, L. Noels, S.P.A. Bordas, Identifying elastoplastic parameters with Bayes' theorem considering double error sources and model uncertainty, Probabilistic Engineering Mechanics.

[33] H. Rappel, L.A.A. Beex, Estimating fibre material parameter distributions from limited data and their influence on the macroscopic behaviour of random network models, submitted for publication.

[34] N. Metropolis, A.W. Rosenbluth, M.N. Rosenbluth, A.H. Teller, E. Teller, Equation of state calculations by fast computing machines, The Journal of Chemical Physics 21 (1953) 1087–1092.

[35] N. Metropolis, S. Ulam, The Monte Carlo method, Journal of the American Statistical Association 44 (247) (1949) 335–341.

[36] C.P. Robert, G. Casella, Introducing Monte Carlo methods with R, Use R!, Springer Science & Business Media, New York, 2010.

[37] W.A. Link, M.J. Eaton, On thinning of chains in MCMC, Methods in ecology and evolution 3 (1) (2012) 112–115.

[38] B. Stephen, Markov chain Monte Carlo method and its application, Journal of the Royal Statistical Society: Series D (The Statistician) 47 (1) 69–100.

[39] S. Sandip, Assessing convergence of the Markov chain Monte Carlo algorithms: A review, ETS Research Report Series 2003 (1) (2003) i–52.

[40] S. Sarkar, D.S. Kosson, S. Mahadevan, J.C.L. Meeussen, H. van der Sloot, J.R. Arnold, K.G. Brown, Bayesian calibration of thermodynamic parameters for geochemical speciation modeling of cementitious materials, Cement and Concrete Research 42 (7) (2012) 889–902.

[41] J. Isenberg, Progressing from least squares to Bayesian estimation, in: Proceedings of the 1979 ASME design engineering technical conference, New York, 1979, pp. 1–11.

[42] K.F. Alvin, Finite element model update via Bayesian estimation and minimization of dynamic residuals, AIAA journal 35 (5) (1997) 879–886.

[43] J.L. Beck, L.S. Katafygiotis, Updating models and their uncertainties. I: Bayesian statistical framework, Journal of Engineering Mechanics 124 (4) (1998) 455–461.

[44] T. Marwala, S. Sibusiso, Finite element model updating using Bayesian framework and modal properties, Journal of Aircraft 42 (1) (2005) 275–278.

[45] C. Gogu, R. Haftka, R.L. Riche, J. Molimard, A. Vautrin, Introduction to the Bayesian approach applied to elastic constants identification, AIAA journal 48 (5) (2010) 893–903.

[46] C.K. Oh, J.L. Beck, M. Yamada, Bayesian learning using automatic relevance determination prior with an application to earthquake early warning, Journal of Engineering Mechanics 134 (12) (2008) 1013–1020.

[47] M.C. Kennedy, A. O'Hagan, Bayesian calibration of computer models, Journal of the Royal Statistical Society: Series B (Statistical Methodology) 63 (3) (2001) 425–464.

[48] J. Kaipio, E. Somersalo, Statistical and computational inverse problems, Vol. 160, Springer Science & Business Media, New York, 2006.

[49] T.C. Lai, K.H. Ip, Parameter estimation of orthotropic plates by Bayesian sensitivity analysis, Composite Structures 34 (1) (1996) 29–42.

[50] F. Daghia, S. de Miranda, F. Ubertini, E. Viola, Estimation of elastic constants of thick laminated plates within a Bayesian framework, Composite Structures 80 (3) (2007) 461–473.

[51] P.S. Koutsourelakis, A novel Bayesian strategy for the identification of spatially varying material properties and model validation: An application to static elastography, International Journal for Numerical Methods in Engineering 91 (3) (2012) 249–268.

[52] C. Gogu, W. Yin, R. Haftka, P. Ifju, J. Molimard, R. Le Riche, A. Vautrin, Bayesian identification of elastic constants in multi-directional laminate from moiré interferometry displacement fields, Experimental Mechanics 53 (4) (2013) 635–648.

[53] M. Muto, J.L. Beck, Bayesian updating and model class selection for hysteretic structural models using stochastic simulation, Journal of Vibration and Control 14 (1-2) (2008) 7–34.

[54] P. Liu, S.K. Au, Bayesian parameter identification of hysteretic behavior of composite walls, Probabilistic Engineering Mechanics 34 (2013) 101–109.

[55] D.D. Fitzenz, A. Jalobeanu, S.H. Hickman, Integrating laboratory creep compaction data with numerical fault models: A Bayesian framework, Journal of Geophysical Research: Solid Earth 112 (B8), B08410.

[56] T. Most, Identification of the parameters of complex constitutive models: Least squares minimization vs Bayesian updating, in: D. Straub (Ed.), Reliability and optimization of structural systems, CRC press, 2010, pp. 119–130.

[57] B.V. Rosić, A. Kčerová, J. Sýkora, O. Pajonk, A. Litvinenko, H.G. Matthies, Parameter identification in a probabilistic setting, Engineering Structures 50 (2013) 179–196, Engineering Structures: Modelling and Computations (special issue IASS-IACM 2012).

[58] W.P. Hernandez, F.C.L. Borges, D.A. Castello, N. Roitman, C. Magluta, Bayesian inference applied on model calibration of fractional derivative viscoelastic model, in: V. Steffen Jr, D.A. Rade, W.M. Bessa (Eds.), DINAME 2015-Proceedings of the XVII International symposium on dynamic problems of mechanics, Natal, 2015.

[59] J.M. Nichols, W.A. Link, K.D. Murphy, C.C. Olson, A Bayesian approach to identifying structural nonlinearity using free-decay response: Application to damage detection in composites, Journal of Sound and Vibration 329 (15) (2010) 2995–3007.

[60] S. Abhinav, C.S. Manohar, Bayesian parameter identification in dynamic state space models using modified measurement equations, International Journal of Non-Linear Mechanics 71 (2015) 89–103.

[61] S. Madireddy, B. Sista, K. Vemaganti, A Bayesian approach to selecting hyperelastic constitutive models of soft tissue, Computer Methods in Applied Mechanics and Engineering 291 (2015) 102–122.

[62] J.T. Oden, E.E. Prudencio, A. Hawkins-Daarud, Selection and assesment of phenomenological models of tumor growth, Mathematical Models and Methods in Applied Sciences 23 (7) (2013) 1309–1338.

[63] J. Chiachío, M. Chiachío, A. Saxena, S. Sankararaman, G. Rus, K. Goebel, Bayesian model selection and parameter estimation for fatigue damage progression models in composites, International Journal of Fatigue 70 (2015) 361–373.

[64] I. Babuška, Z. Sawlan, M. Scavino, B. Szabó, R. Tempone, Bayesian inference and model comparison for metallic fatigue data, Computer Methods in Applied Mechanics and Engineering 304 (2016) 171–196.

[65] S.L. Cotter, M. Dashti, J.C. Robinson, A.M. Stuart, Bayesian inverse problems for functions and applications to fluid mechanics, Inverse Problems 25 (11) (2009) 115008.

[66] J.C. Simo, T.J.R. Hughes, Computational inelasticity, Springer Science & Business Media, New York, 2000.

[67] T.J. Ulrych, M.D. Sacchi, A. Woodbury, A Bayes tour of inversion: A tutorial, GEOPHYSICS 66 (1) (2001) 55–69.

[68] J.L. Beck, S.K. Au, Bayesian updating of structural models and reliability using Markov chain Monte Carlo simulation, Journal of Engineering Mechanics 128 (4) (2002) 380–391.

[69] Y.M. Marzouk, H.N. Najm, L.A. Rahn, Stochastic spectral methods for efficient Bayesian solution of inverse problems, Journal of Computational Physics 224 (2) (2007) 560–586.

[70] J. Kristensen, N. Zabaras, Bayesian uncertainty quantification in the evaluation of alloy properties with the cluster expansion method, Computer Physics Communications 185 (11) (2014) 2885–2892.

[71] C. Andrieu, N. De Freitas, A. Doucet, M.I. Jordan, An introduction to MCMC for machine learning, Machine learning 50 (1-2) (2003) 5–43.

[72] A. Gelman, G.O. Roberts, W.R. Gilks, Efficient Metropolis jumping rules, in: J.M. Bernardo, J.O. Berger, A.P. Dawid, A.F.M. Smith (Eds.), Bayesian statistics, Vol. 5 of Oxford Science Publications, Oxford University Press, New York, 1996, pp. 599–607.

[73] H. Haario, E. Saksman, J. Tamminen, Adaptive proposal distribution for random walk Metropolis algorithm, Computational Statistics 14 (3) (1999) 375–396.

[74] S.J.D. Prince, Computer vision: Models learning and inference, Cambridge University Press, 2012.

[75] Y. Ling, J. Mullins, S. Mahadevan, Selection of model discrepancy priors in bayesian calibration, Journal of Computational Physics 276 (Supplement C) (2014) 665–680.

[76] G.B. Arhonditsis, D. Papantou, W. Zhang, G. Perhar, E. Massos, M. Shi, Bayesian calibration of mechanistic aquatic biogeochemical models and benefits for environmental management, Journal of Marine Systems 73 (1) (2008) 8–30.

[77] P.D. Arendt, D.W. Apley, W. Chen, Quantification of model uncertainty: Calibration, model discrepancy, and identifiability, Journal of Mechanical Design 134 (10) (2012) 100908.

[78] J. Brynjarsdóttir, A. O'Hagan, Learning about physical parameters: The importance of model discrepancy, Inverse Problems 30 (11) (2014) 114007.

[79] L.L. Magorou, F. Bos, F. Rouger, Identification of constitutive laws for wood-based panels by means of an inverse method, Composites Science and Technology 62 (4) (2002) 591–596.

[80] K. Genovese, L. Lamberti, C. Pappalettere, Improved global-local simulated annealing formulation for solving non-smooth engineering optimization problems, International Journal of Solids and Structures 42 (1) (2005) 203–237.

[81] C. Elster, G. Wübbeler, Bayesian regression versus application of least squares-an example, Metrologia 53 (1) (2016) S10.

[82] H. Rappel, L.A.A. Beex, J.S. Hale, S.P.A. Bordas, Bayesian inference for the stochastic identification of elastoplastic material parameters: Introduction, misconceptions and additional insight, ArXiv e-prints.

[83] E. Zhang, J. Chazot, J. Antoni, M. Hamdi, Bayesian characterization of Young's modulus of viscoelastic materials in laminated structures, Journal of Sound and Vibration 332 (16) (2013) 3654–3666.

[84] L. Mehrez, E. Kassem, E. Masad, D. Little, Stochastic Identification of linear-viscoelastic models of aged and unaged asphalt mixtures, Journal of Materials in Civil Engineering 27 (4).

[85] P. Miles, M. Hays, R. Smith, W. Oates, Bayesian uncertainty analysis of finite deformation viscoelasticity, Mechanics of Materials 91 (2015) 35–49.

[86] X. Zhao, A.A. Pelegri, A Bayesian approach for characterization of soft tissue viscoelasticity in acoustic radiation force imaging, International Journal for Numerical Methods in Biomedical Engineering 32 (4) e02741.

[87] Z.R. Kenz, H.T. Banks, R.C. Smith, Comparison of frequentist and Bayesian confidence analysis methods on a viscoelastic stenosis model, SIAM/ASA Journal on Uncertainty Quantification 1 (1) (2013) 348–369.

[88] H.T. Banks, S. Hu, Z.R. Kenz, A brief review of elasticity and viscoelasticity for solids, Advances in Applied Mathematics and Mechanics 3 (1) (2011) 151.

[89] M. Orosz, G. Molnarka, E. Monos, Curve fitting methods and mechanical models for identification of viscoelastic parameters of vascular wall-a comparative study, Medical Science Monitor 3 (4) (1997) MT599–MT604.

[90] X.Y. Liu, X.F. Chen, Y.H. Ren, Q.Y. Zhan, C. Wang, C. Yang, Alveolar type II cells escape stress failure caused by tonic stretch through transient focal adhesion disassembly, International journal of biological sciences 7 (5) (2011) 588–599.

[91] D.E. Goldberg, Genetic algorithms in search, optimization and machine learning, 1st Edition, Addison-Wesley Publishing Company, Boston, 1989.

[92] B.M. Chaparro, S. Thuillier, L.F. Menezes, P.Y. Manach, J.V. Fernandes, Material parameters identification: Gradient-based, genetic and hybrid optimization algorithms, Computational Materials Science 44 (2) (2008) 339–346.

[93] D. Higdon, J. Gattiker, B. Williams, M. Rightley, Computer model calibration using high-dimensional output, Journal of the American Statistical Association 103 (482) (2008) 570–583.

[94] J. McFarland, S. Mahadevan, Multivariate significance testing and model calibration under uncertainty, Computer Methods in Applied Mechanics and Engineering 197 (29) (2008) 2467–2479.

[95] S. Sankararaman, Y. Ling, C. Shantz, S. Mahadevan, Inference of equivalent initial flaw size under multiple sources of uncertainty, International Journal of Fatigue 33 (2) (2011) 75–89.

[96] K.V. Yuen, L.S. Katafygiotis, Bayesian modal updating using complete input and incomplete response noisy measurements, Journal of Engineering Mechanics 128 (3) (2002) 340–350.

[97] S.F. Gull, Bayesian data analysis: Straight-line fitting, in: J. Skilling (Ed.), Maximum entropy and Bayesian methods, Vol. 36 of Fundamental Theories of Physics, Springer Science & Business Media, Netherlands, 1989, pp. 511–518.

[98] P. Dellaportas, D.A. Stephens, Bayesian analysis of errors-in-variables regression models, Biometrics 51 (3) (1995) 1085–1095.

[99] R.J. Carroll, K. Roeder, L. Wasserman, Flexible parametric measurement error models, Biometrics 55 (1) (1999) 44–54.

[100] R. Scheines, H. Hoijtink, A. Boomsma, Bayesian estimation and testing of structural equation models, Psychometrika 64 (1) (1999) 37–52.

[101] B.C. Kelly, Some aspects of measurement error in linear regression of astronomical data, The Astrophysical Journal 665 (2) (2007) 1489.

[102] D.W. Hogg, J. Bovy, D. Lang, Data analysis recipes: Fitting a model to data, ArXiv e-prints.

[103] C.E. Rasmussen, C.K. Williams, Gaussian processes for machine learning, Vol. 1, MIT press Cambridge, 2006.

[104] S. Hassani, Mathematical methods: For students of physics and related fields, Springer Science & Business Media, New York, 2008.

[105] A. Kulachenko, T. Uesaka, Direct simulations of fiber network deformation and failure, Mechanics of Materials 51 (2012) 1–14.

[106] J. Persson, P. Isaksson, A particlebased method for mechanical analyses of planar fiber-based materials, International Journal for Numerical Methods in Engineering 93 (11) (2013) 1216–1234.

[107] D.V. Wilbrink, L.A.A. Beex, R.H.J. Peerlings, A discrete network model for bond failure and frictional sliding in fibrous materials, International Journal of Solids and Structures 50 (9) (2013) 1354–1363.

[108] L.A.A. Beex, R.H.J. Peerlings, M.G.D. Geers, A multiscale quasicontinuum method for lattice models with bond failure and fiber sliding, Computer Methods in Applied Mechanics and Engineering 269 (2014) 108–122.

[109] E. Bosco, R.H.J. Peerlings, M.G.D. Geers, Predicting hygro-elastic properties of paper sheets based on an idealized model of the underlying fibrous network, International Journal of Solids and Structures 56-57 (2015) 43–52.

[110] X. Badiche, S. Forest, T. Guibert, Y. Bienvenu, J.D. Bartout, P. Ienny, M. Croset, H. Bernet, Mechanical properties and non-homogeneous deformation of open-cell nickel foams: Application of the mechanics of cellular solids and of porous materials, Materials Science and Engineering: A 289 (1) (2000) 276–288.

[111] A. Jung, L.A.A. Beex, S. Diebels, S.P.A. Bordas, Open-cell aluminium foams with graded coatings as passively controllable energy absorbers, Materials & Design 87 (2015) 36–41.

[112] S. Gao, B. Liang, E. Vidal-Salle, Development of a new 3D beam element with section changes: The first step for large scale textile modelling, Finite Elements in Analysis and Design 104 (2015) 80–88.

[113] L.A.A. Beex, R.H.J. Peerlings, K. van Os, M.G.D. Geers, The mechanical reliability of an electronic textile investigated using the virtual-power-based quasicontinuum method, Mechanics of Materials 80 (2015) 52–66.

[114] G. Argento, M. Simonet, C.W.J. Oomens, F.P.T. Baaijens, Multi-scale mechanical characterization of scaffolds for heart valve tissue engineering, Journal of Biomechanics 45 (16) (2012) 2893–2898.

[115] A.M. Sastry, X. Cheng, C.W. Wang, Mechanics of stochastic fibrous networks, Journal of Thermoplastic Composite Materials 11 (3) (1998) 288–296.

[116] C.W. Wang, L. Berhan, A.M. Sastry, Structure, mechanics and failure of stochastic fibrous networks: Part I-microscale considerations, Journal of Engineering Materials and Technology, 122 (4) (2000) 450–459.

[117] C.A. Bronkhorst, Modelling paper as a two-dimensional elasticplastic stochastic network, International Journal of Solids and Structures 40 (20) (2003) 5441–5454.

[118] H. Hatami-Marbini, R.C. Picu, Scaling of nonaffine deformation in random semiflexible fiber networks, Physical Review E 77 (2008) 062103.

[119] R.C. Picu, Mechanics of random fiber networks-a review, Soft Matter 7 (2011) 6768–6785.

[120] A.S. Shahsavari, R.C. Picu, Size effect on mechanical behavior of random fiber networks, International Journal of Solids and Structures 50 (20) (2013) 3332–3338.

[121] E. Ban, V.H. Barocas, M.S. Shephard, C.R. Picu, Effect of fiber crimp on the elasticity of random fiber networks with and without embedding matrices, Journal of Applied Mechanics 83 (4) (2016) 041008–041008–7.

[122] T.H. Le, P.J.J. Dumont, L. Orgéas, D. Favier, L. Salvo, E. Boller, X-ray phase contrast microtomography for the analysis of the fibrous microstructure of SMC composites, Composites Part A: Applied Science and Manufacturing 39 (1) (2008) 91–103.

[123] P. Latil, L. Orgéas, C. Geindreau, P.J.J. Dumont, S.R. du Roscoat, Towards the 3D in situ characterisation of deformation micro-mechanisms within a compressed bundle of fibres, Composites Science and Technology 71 (4) (2011) 480–488.

[124] R.M. Sencu, Z. Yang, Y.C. Wang, P.J. Withers, C. Rau, A. Parson, C. Soutis, Generation of micro-scale finite element models from synchrotron X-ray CT images for multidirectional carbon fibre reinforced composites, Composites Part A: Applied Science and Manufacturing 91 (2016) 85–95.

[125] R.S. Seth, D.H. Page, The stress-strain curve of paper, in: J. Brander (Ed.), The role of fundamental research in paper making: Transactions of the symposium held at Cambridge, Mechanical Engineering Publications Ltd., London, 1983, pp. 421–452.

[126] A. Jung, S. Diebels, A. Koblischka-Veneva, J. Schmauch, A. Barnoush, M.R. Koblischka, Microstructural analysis of electrochemical coated open-cell metal foams by EBSD and nanoindentation, Advanced Engineering Materials 16 (1) (2013) 15–20.

[127] C. Genest, K. Ghoudi, L.P. Rivest, A semiparametric estimation procedure of dependence parameters in multivariate families of distributions, Biometrika 82 (3) (1995) 543–552.

[128] W. Hürlimann, Fitting bivariate cumulative returns with copulas, Computational Statistics & Data Analysis 45 (2) (2004) 355–372.

[129] O. Roch, A. Alegre, Testing the bivariate distribution of daily equity returns using copulas. An application to the Spanish stock market, Computational Statistics & Data Analysis 51 (2) (2006) 1312–1329.

[130] R.d.S. Silva, H.F. Lopes, Copula, marginal distributions and model selection: A Bayesian note, Statistics and Computing 18 (3) (2008) 313–320.

[131] R.B. Nelsen, An introduction to copulas, Springer Science & Business Media, New York, 2007.

[132] M. Sklar, Fonctions de répartition à n dimensions et leurs marges, Université Paris 8, 1959.

[133] Y. Noh, K.K. Choi, I. Lee, Identification of marginal and joint CDFs using Bayesian method for RBDO, Structural and Multidisciplinary Optimization 40 (1) (2009) 35.

[134] P.X. Song, Multivariate dispersion models generated from Gaussian copula, Scandinavian Journal of Statistics 27 (2) (2000) 305–320.

[135] E.C. DeCarlo, S. Mahadevan, B.P. Smarslok, Bayesian calibration of aerothermal models for hypersonic air vehicles, in: 54th AIAA/ASME/ASCE/AHS/ASC Structures, Structural Dynamics, and Materials Conference, 2013, p. 1683.

[136] B. Staber, Stochastic analysis, simulation and identification of hyperelastic constitutive equations, Ph.D. thesis, University of Paris-Est Marne-la-Vallée (2018).

[137] T. Bui-Thanh, O. Ghattas, J. Martin, G. Stadler, A computational framework for infinite-dimensional Bayesian inverse problems part I: The linearized case, with application to global seismic inversion, SIAM Journal on Scientific Computing 35 (6) (2013) A2494–A2523.

[138] E.A. Morelli, Real-time parameter estimation in the frequency domain, Journal of Guidance, Control, and Dynamics 23 (5) (2000) 812–818.

[139] R.C.H. Weng, D.S. Coad, Real-time Bayesian parameter estimation for Item response models, Bayesian Analysis 13 (1) (2018) 115–137.

[140] M. Plummer, JAGS: A program for analysis of Bayesian graphical models using Gibbs sampling, in: Proceedings of the 3rd international workshop on distributed statistical computing, Vol. 124, Vienna, Austria, 2003.

[141] B. Carpenter, A. Gelman, M.D. Hoffman, D. Lee, B. Goodrich, M. Betancourt, M. Brubaker, J. Guo, P. Li, A. Riddell, Stan: A probabilistic programming language, Journal of statistical software 76 (1).